National Library
of Canada

Acquisitions and
Bibliographic Services Branch

395 Wellington Street
Ottawa, Ontario
K1A 0N4

Bibliothèque nationale
du Canada

Direction des acquisitions et
des services bibliographiques

395, rue Wellington
Ottawa (Ontario)
K1A 0N4

Your file   Votre référence

Our file   Notre référence

NOTICE

The quality of this microform is heavily dependent upon the quality of the original thesis submitted for microfilming. Every effort has been made to ensure the highest quality of reproduction possible.

If pages are missing, contact the university which granted the degree.

Some pages may have indistinct print especially if the original pages were typed with a poor typewriter ribbon or if the university sent us an inferior photocopy.

Reproduction in full or in part of this microform is governed by the Canadian Copyright Act, R.S.C. 1970, c. C-30, and subsequent amendments.

AVIS

La qualité de cette microforme dépend grandement de la qualité de la thèse soumise au microfilmage. Nous avons tout fait pour assurer une qualité supérieure de reproduction.

S'il manque des pages, veuillez communiquer avec l'université qui a conféré le grade.

La qualité d'impression de certaines pages peut laisser à désirer, surtout si les pages originales ont été dactylographiées à l'aide d'un ruban usé ou si l'université nous a fait parvenir une photocopie de qualité inférieure.

La reproduction, même partielle, de cette microforme est soumise à la Loi canadienne sur le droit d'auteur, SRC 1970, c. C-30, et ses amendements subséquents.

Canada

UNIVERSITY OF ALBERTA

DISTANCE AND BANDWIDTH ENHANCEMENT OF FIBER OPTIC TRANSMISSION

BY

GREGORY DEAN MAY ©

A thesis submitted to the Faculty of Graduate Studies and Research in partial fulfillment of the requirements for the degree of **MASTER OF SCIENCE**.

DEPARTMENT OF ELECTRICAL ENGINEERING

Edmonton, Alberta
FALL, 1993

National Library of Canada
Acquisitions and Bibliographic Services Branch
395 Wellington Street
Ottawa, Ontario
K1A 0N4

Bibliothèque nationale du Canada
Direction des acquisitions et des services bibliographiques
395, rue Wellington
Ottawa (Ontario)
K1A 0N4

Your file Votre référence

Our file Notre référence

The author has granted an irrevocable non-exclusive licence allowing the National Library of Canada to reproduce, loan, distribute or sell copies of his/her thesis by any means and in any form or format, making this thesis available to interested persons.

L'auteur a accordé une licence irrévocable et non exclusive permettant à la Bibliothèque nationale du Canada de reproduire, prêter, distribuer ou vendre des copies de sa thèse de quelque manière et sous quelque forme que ce soit pour mettre des exemplaires de cette thèse à la disposition des personnes intéressées.

The author retains ownership of the copyright in his/her thesis. Neither the thesis nor substantial extracts from it may be printed or otherwise reproduced without his/her permission.

L'auteur conserve la propriété du droit d'auteur qui protège sa thèse. Ni la thèse ni des extraits substantiels de celle-ci ne doivent être imprimés ou autrement reproduits sans son autorisation.

ISBN 0-315-88182-8

Canada

UNIVERSITY OF ALBERTA
RELEASE FORM

NAME AUTHOR: **Gregory Dean May**

TITLE OF THESIS: **Distance and Bandwidth Enhancement of Fiber Optic Transmission**

DEGREE: **Master of Science**

YEAR THIS DEGREE GRANTED: **1993**

Permission is hereby granted to the University of Alberta Library to reproduce single copies of this thesis and to lend or sell such copies for private, scholarly or scientific research purposes only.

The author reserves all other publication and other rights in association with the copyright in the thesis, and except as hereinbefore provided neither the thesis nor any substantial portion may be printed or otherwise reproduced in any material form whatever without the author's prior written permission.

4711-40th Street
Lloydminster, Saskatchewan, Canada
S9V-OC1

DATE: September 16, 1993

UNIVERSITY OF ALBERTA

FACULTY OF GRADUATE STUDIES AND RESEARCH

The undersigned certify that they have read, and recommend to the Faculty of Graduate Studies and Research for acceptance, a thesis entitled **DISTANCE AND BANDWIDTH ENHANCEMENT OF FIBER OPTIC TRANSMISSION** submitted by **GREGORY DEAN MAY** in partial fulfillment of the requirements for the degree of **MASTER OF SCIENCE**.

J. Conradi

Dr. J. Conradi, Supervisor

Dr. R. I. MacDonald, Internal Examiner

Dr. W. Dobosiewicz, External Examiner

DATE: September 15, 1993

Dedication

To my parents, for their support and encouragement.

Abstract

The optical wavelength required to obtain gain from Erbium Doped Fiber Amplifiers is in the 1550 nm range. The vast majority of fiber links in place today have a chromatic dispersion minimum for a wavelength around 1300 nm. High bit rate transmission at 1550 nm through long sections of this fiber results in pulse broadening which ultimately corrupts the signal and therefore imposes a transmission distance limitation. Techniques that reduce the impact of chromatic dispersion are required to achieve further distances.

Duobinary coding to reduce transmission bandwidth, chirped transmission using a Mach-Zehnder external modulator, and optical multiplexing and demultiplexing based on signal polarization orientation are three techniques that are shown to significantly increase chromatic dispersion-limited transmission distance. Both electrical multiplexed and Optical Time Division Multiplexed (OTDM) externally modulated transmitters are experimentally studied to determine the impact of dispersion on eye closure and receiver sensitivity. The degradation of receiver sensitivity with distance is reported as a chromatic dispersion penalty. Simulations are also performed to compare the obtained waveform plots.

Electrically multiplexed transmitter studies focus on duobinary coding and chirped transmission. Compared to binary signaling over increasing distance, binary transmission with duobinary reception is shown to reduce dispersion penalties above 2.8 dB for zero chirp transmission, and above 0.6 dB for chirped transmission. For zero chirp transmission, duobinary reception increases transmission distance by 44 % (108 km versus 75 km) for a 5 dB penalty. For chirped transmission, it increases transmission distance by 13 % (156 km versus 138 km) for a 3 dB penalty.

OTDM transmitter studies focus on duobinary coding and polarization multiplexing and demultiplexing. A novel parallel duobinary encoder is presented. Receiver sensitivity data is not reported for duobinary coding because of performance limitations of components. Polarization multiplexing and demultiplexing are shown to at least double the maximum transmission distance of a 10 Gb/s OTDM transmitter (50 km with 4.5 dB penalty versus 100 km with maximum of 2.2 dB penalty). The maximum operation speed of any component in this polarization-based system is one half the speed required for electrical multiplexing and demultiplexing.

Acknowledgments

I would first of all like to thank Dr. Jan Conradi for providing the guidance and the excellent facilities that were so critical to successful completion of this work. Also, I would like to thank Alan Solheim and Jeff Stonos at Bell-Northern Research for helping me to set up the packaging for TRLab's collection of 10 Gb/s integrated circuits and their very important support of my early endeavors in the laboratory.

In addition, I would like to acknowledge Ken Benterud for his tremendous effort in packaging and characterizing many of the components that were used in the Optical Time Division Multiplexer experiments. I would also like to acknowledge David Clegg, Eric Cauchon, David Moore, and Sheldon Walklin for their assistance in the laboratory and for many useful discussions.

Finally, I would like to thank the Natural Sciences and Engineering Research Council, TRLabs, and the University of Alberta for the funding that made this all possible.

This work was supported by the Natural Sciences and Engineering Research Council of Canada, Bell-Northern Research, and TRLabs through the NSERC/BNR/TRLabs Industrial Research Chair in Fiber Optic Communications at the University of Alberta.

Table of Contents

1. Introduction 1
    1.1. Overview of High Speed Fiber Optic Technology 1
    1.2. Overview of Proposed Solutions for Chromatic Dispersion Problem 4
    1.3. Overview of Duobinary Coding to Reduce Chromatic Dispersion Effect 7
    1.4. Overview of Experimental Work 11
        1.4.1. Context of Research 11
        1.4.2. Bit Rates Studied 11
        1.4.3. Electrical Multiplexing Experiments 11
        1.4.4. Optical Time Division Multiplexing Experiments 12
        1.4.5. Thesis Organization 13

2. Simulation of Options 14
    2.1. Scope of Simulation Studies 14
    2.2. Simulator Models 14
        2.2.1. Mach-Zehnder Switch Model 15
        2.2.2. Fiber Model 16
        2.2.3. Transmitter and Receiver Component Models 19
    2.3. Electrical Multiplexing Options 20
        2.3.1. Models 20
        2.3.2. Binary Transmission with Binary Reception 21
        2.3.3. Binary Transmission with Duobinary Reception 21
        2.3.4. Duobinary Transmission 22
    2.4. OTDM Options 23
        2.4.1. Models 23
        2.4.2. Binary Transmission with Binary Reception 25
        2.4.3. Binary Transmission with Duobinary Reception 25
        2.4.3. Duobinary Transmission 26
    2.5. Conclusions 27

3. Receiver Modeling 28
    3.1. Power Penalty 28
    3.2. Receiver Model 28
    3.3. Noise Contributions 30
    3.4. Signal to Noise Ratio and Bit Error Rate 32

4. Electrical Multiplexing Experiments 37
    4.1. Scope of Experimental Work 37
    4.2. Receiver Layout 37
    4.3. Optical Link Layout 38
    4.4. Binary Transmission with Binary Reception 40
        4.4.1. Binary Transmitter 40
        4.4.2. Binary Receiver 42
        4.4.3. Predicted Receiver Sensitivity 46
        4.4.4. Experimental Receiver Sensitivity 48
    4.5. Binary Transmission with Duobinary Reception 50
        4.5.1. Binary Transmitter 50
        4.5.2. Duobinary Receiver 50
        4.5.3. Experimental Receiver Sensitivity 54
    4.6. Duobinary Transmission 56
        4.6.1. Trial 1 56
        4.6.2. Trial 2 59
    4.7. Evaluation of Results 61
        4.7.1. Binary Transmission with Binary Reception 61
        4.7.2. Binary Transmission with Duobinary Reception 62
        4.7.3. Comparison of Binary Reception with Duobinary Reception 63
        4.7.4. Duobinary Transmission 65

5. Optical Time Division Multiplexing Experiments 66
    5.1. Scope of Experimental Work 66
    5.2. Receiver Layout 66
    5.3. OTDM Layout 67
    5.4. Optical Link Layout 70
    5.5. Binary Transmission with Binary Reception 71

- 5.5.1. Scope of Experiments 71
- 5.5.2. 5 Gb/s Binary Signal Generation 73
- 5.5.3. Predicted Receiver Sensitivity 74
  - 5.5.3.1. Polarization-Sensitive Optical Demultiplexer 74
  - 5.5.3.2. Receiver Bandwidth 75
  - 5.5.3.3. EDFA Pre-Amplifier Characterization 78
  - 5.5.3.4. Predicted SNR and Receiver Sensitivity 78
- 5.5.4. Experimental Receiver Sensitivity 80
  - 5.5.4.1. 10 Gb/s NRZ Reception 80
  - 5.5.4.2. 5 Gb/s RZ Reception 84
  - 5.5.4.3. 10 Gb/s Polarization Demultiplexed Reception 87
  - 5.5.4.4. Active Recombination 90

5.6. Binary Transmission with Duobinary Reception 93
- 5.6.1. Scope of Experiments 93
- 5.6.2. Duobinary Receiver Design 93
- 5.6.3. 5 Gb/s Duobinary Reception 93
- 5.6.4. 10 Gb/s Duobinary Reception 95

5.7. Multilevel Transmission 97
- 5.7.1. Scope of Experiments 97
- 5.7.2. Duobinary Transmission 98
- 5.7.3. Pulsed Multilevel Transmission 100
- 5.7.4. Low Speed Multilevel Transmission 100

5.8. Evaluation of Results 105
- 5.8.1. Binary Transmission with Binary Reception 105
- 5.8.2. Binary Transmission with Duobinary Reception 107
- 5.8.3. Multilevel Transmission 107

6. Conclusion 108

6.1. Consolidated Overview of Results 108

6.2. System Improvements 110
- 6.2.1. Improved Frequency Response of Components 110
- 6.2.2. Automated Control 111
- 6.2.3. Duobinary Transmission using Mach-Zehnder Switches 112

6.3. Future Work 114

References 115

Appendix A: Bandwidth Reduction with Duobinary Coding 120
    A.1. Viewpoints 120
        A.1.1. Correlation Viewpoint 120
        A.1.2. Pulse Shape Viewpoint 123
Appendix B: Electro-optic Switch and Modulator Theory 125
Appendix C: Optical Time Division Multiplexer 129
Appendix D: BOSS Block Diagrams 130
Appendix E: Program to Generate Frequency Response of Fiber Transfer Function 135
Appendix F: Transmitter and Receiver Electronics 136
    F.1. Microwave Waveguides and Components 136
    F.2. Integrated Circuits 139
Appendix G: Binary Filter Selection 141
Appendix H: Duobinary Filter Implementation 143
    H.1. Practical options 143
    H.2. 6 dB Splitter / Combiner Implementation 143
    H.3. 6 dB Splitter / Wilkinson Power Combiner Implementation 144
Appendix I: Description of Components 145
    I.1. Amplifiers 145
    I.2. High Speed Integrated Circuits 146
    I.3. Optical Bandpass Filter 147
    I.4. Electro-Optic Components 148
        I.4.1. AT&T Mach-Zehnder Modulator 148
        I.4.2. ETEK and UTP Mach-Zehnder Switches 148
        I.4.3. BT&D Photodetector 152
    I.5. EDFA Data 153
        I.5.1. Amoco 1.5-AMP-18 EDFA 153
        I.5.2. TRLabs Prototype EDFA #303 154
Appendix J: Parallel Duobinary Code Generation 155
Appendix K: Receiver Sensitivity Theory for Binary and Duobinary Signaling 160
    K.1. Binary Receiver Sensitivity 160
    K.2. Duobinary Receiver Sensitivity 162

Appendix L: Clock Recovery Technique 167
Appendix M: Ternary Decision Circuit and Precoder 171
Appendix N: Comparison of PRBS and Precoded Sequence 173
Appendix O: Method for Tuning Duobinary Receiver 175
Appendix P: Polarization Technique for Characterizing an EDFA 177
Appendix Q: Parallel Precoding Technique 178

List of Tables

Table 4.1: Components Used in Optical Links at BNR 40
Table 5.1: Components Used in Optical Links at TRLabs 72
Table 5.2: Predicted Input Power Levels for 10^{-9} BER 80
Table 5.3: Comparison of 5 Gb/s RZ Reception and 10 Gb/s NRZ Polarization Demultiplexed Reception 106
Table I.1: Signal Amplifier Characteristics 145
Table I.2: Power Amplifier Characteristics 145
Table I.3: Integrated Circuit Characteristics 146

List of Figures

Figure 1.1: Conventional Fiber Optic Transmission System 1
Figure 1.2: External Modulation 3
Figure 1.3: General Model of an OTDM Transmitter 4
Figure 1.4: Output from Duobinary Transfer Function 9
Figure 1.5: Delay and Add Implementation 9
Figure 1.6: Location of Duobinary Transfer Function 10
Figure 1.7: Ternary Decision Circuit 10
Figure 1.8: Parallel Duobinary Encoding at the Inputs to an OTDM 13
Figure 2.1: Single Mode Fiber Model 19
Figure 2.2: Block Diagrams of Electrical Multiplexing Options 20
Figure 2.3: Binary Transmission with Binary Reception, Electrical Multiplexing 22
Figure 2.4: Binary Transmission with Duobinary Reception, Electrical Multiplexing 22
Figure 2.5: Duobinary Transmission, Electrical Multiplexing 23
Figure 2.6: OTDM Model 23
Figure 2.7: Block Diagrams of OTDM Options 24
Figure 2.8: Binary Transmission with Binary Reception, OTDM 25
Figure 2.9: Binary Transmission with Duobinary Reception, OTDM 26
Figure 2.10: Duobinary Transmission, OTDM 26
Figure 3.1: General Receiver Model 29
Figure 4.1: Receiver used for Electrical Multiplexing Trials 38
Figure 4.2: Two EDFA Optical Link 39
Figure 4.3: Three EDFA Optical Link 39
Figure 4.4: Binary Transmitter Arrangements 41
Figure 4.5: Binary Drive Signal Comparison 43
Figure 4.6: Binary Receiver 44
Figure 4.7: Zero Chirp Binary Eye Diagrams 45
Figure 4.8: Simulated Zero Chirp Binary Eye Diagrams 46
Figure 4.9: Negative Chirp Eye Diagram at 126 km 46
Figure 4.10: Predicted SNR 48
Figure 4.11: Binary Receiver BER Curves, Zero Chirp 49
Figure 4.12: Binary Receiver BER Curves, Negative Chirp 49
Figure 4.13: Duobinary Receiver 51

Figure 4.14: Duobinary Receiver with Modified Clock Recovery Circuit 52
Figure 4.15: Zero Chirp Duobinary Eye Diagram at 126 km 53
Figure 4.16: Simulated Zero Chirp Duobinary Eye Diagram at 125 km 54
Figure 4.17: Negative Chirp Duobinary Eye Diagram at 126 km 54
Figure 4.18: Duobinary Receiver BER Curves, Zero Chirp 55
Figure 4.19: Duobinary Receiver BER Curves, Negative Chirp 55
Figure 4.20: Trial 1 Duobinary Transmitter Configuration 56
Figure 4.21: Trial 1 Transmitted Duobinary Signal 57
Figure 4.22: Trial 1 Simulated Transmitted Duobinary Signal 58
Figure 4.23: Trial 2 Duobinary Transmitter Configuration 59
Figure 4.24: Trial 2 Transmitted Duobinary Signal 60
Figure 4.25: Simulated Trial 2 Transmitted Duobinary Signal 61
Figure 4.26: Binary Reception Comparisons 62
Figure 4.27: Duobinary Reception Comparisons 63
Figure 4.28: Binary Reception versus Duobinary Reception 64
Figure 5.1 Receiver Used for OTDM Trials 66
Figure 5.2: Optical Time Division Multiplexer 67
Figure 5.3: Optical Link for OTDM Trials 71
Figure 5.4: 5 Gb/s NRZ Signal Generator and Amplifiers 73
Figure 5.5: 5 Gb/s NRZ Signal from MiniCircuits Amplifiers 74
Figure 5.6: Polarization Demultiplexer 75
Figure 5.7: Binary Receiver Electronics for OTDM Trials 76
Figure 5.8: Frequency Response of Binary Receivers 77
Figure 5.9: Calculated Binary Receiver SNR 79
Figure 5.10: Simulated Intensity Coupling Between Time Slots at the Output of the OTDM 81
Figure 5.11: BER Curves for 10 Gb/s NRZ Reception 82
Figure 5.12: Actual 10 Gb/s NRZ Waveforms at 0 km and 75 km 83
Figure 5.13: Simulated 10 Gb/s NRZ Waveforms at 0 km and 75 km 84
Figure 5.14: Actual 5 Gb/s RZ Waveforms at 0 km and 125 km 85
Figure 5.15: Simulated Gb/s RZ Waveforms at 0 km and 125 km 85
Figure 5.16: BER Curves for 5 Gb/s RZ Reception, 5 GHz Receiver 86
Figure 5.17: BER Curves for 5 Gb/s RZ Reception, 10 GHz Receiver 86
Figure 5.18: BER Curves for 10 Gb/s NRZ Polarization Demultiplexed Reception, 5 GHz Receiver 88

Figure 5.19: BER Curves for 10 Gb/s Polarization Demultiplexed Reception, 10 GHz Receiver 88
Figure 5.20: BER Curves for Polarization Demultiplexed Reception with Overlapping Pulses 90
Figure 5.21: 5 Gb/s RZ Pulse Shapes Using Switch Recombination Stage in OTDM 92
Figure 5.22: Simulated Waveforms for Active Recombination OTDM 92
Figure 5.23: Duobinary Receiver 94
Figure 5.24: 5 Gb/s RZ Duobinary Reception Obtained Waveforms 96
Figure 5.25: 5 Gb/s RZ Duobinary Reception Simulated Waveforms 96
Figure 5.26: 10 Gb/s NRZ Duobinary Reception Obtained Waveforms 97
Figure 5.27: 10 Gb/s NRZ Duobinary Reception Simulated Waveforms 97
Figure 5.28: Two Channel Parallel Delay and Add Circuit Implementation 98
Figure 5.29: Inputs and Outputs of Parallel Duobinary Encoder 99
Figure 5.30: Optical Output from Parallel Duobinary OTDM Transmitter 101
Figure 5.31: Optical Output from Simulated Parallel Duobinary Transmitter 102
Figure 5.32: Pulsed Multilevel Transmission 103
Figure 5.34: Resulting Waveforms from Low Speed Multilevel Experiment 104
Figure 5.35: Comparison of Binary 10^{-9} BER Input Power Levels 105
Figure 6.1: Impact of Photodetector on 10 Gb/s OTDM 110
Figure 6.2: Ternary Drive Circuit using Limiting Amplifiers 113
Figure 6.3: Optical Ternary Signal Generator 113
Figure A.1: Comparison of Binary and Duobinary NRZ Power Spectrum 122
Figure A.2: Delay and Add Circuit 122
Figure A.3: Duobinary Transfer Function 123
Figure A.4: Pulse Spectrum Combined with Duobinary Filter Response 124
Figure B.1: Basic Structure of a Mach-Zehnder Section 125
Figure B.2: Output of Mach-Zehnder Modulator as a Function of Input 126
Figure C.1: Two Channel OTDM 129
Figure D.1: Mach-Zehnder Switch Model 130
Figure D.2: Binary Transmission with Binary Reception, Electrical Multiplexing 130
Figure D.3: Drive Circuit for Binary Transmitter, Electrical Multiplexing and OTDM 131

Figure D.4: Duobinary Receiver for Binary Transmission, Electrical Multiplexing 131
Figure D.5: Drive Circuit for Duobinary Transmitter, Electrical Multiplexing 132
Figure D.6: Binary Transmission with Binary Reception, OTDM 132
Figure D.7: Two Input OTDM 133
Figure D.8: Duobinary Receiver for Binary Transmission, OTDM 133
Figure D.9: Duobinary Transmission, OTDM 133
Figure D.10: Parallel Duobinary Drive Circuit for OTDM 134
Figure F.1: 6 dB Resistive Splitter 137
Figure F.2: A Simple Wilkinson Power Divider Implementation 138
Figure F.3: S-Parameters of a Simple Wilkinson Power Divider 138
Figure F.4: 10 Gb/s Integrated Circuit Packaging 139
Figure H.1: Delay and Add Circuit Implementations 144
Figure I.1: Monochromator Scan of EDFA Pre-Amplifier Filter 147
Figure I.2: Representative Frequency Response Plot for AT&T Modulator 148
Figure I.3: Frequency Response of BT&D Photodetector 152
Figure I.4: Gain Bandwidth of Amoco EDFA 153
Figure I.5: System Noise Figure versus Input Power for Amoco EDFA 153
Figure I.6: Filtered ASE from EDFA #303 as a Function of Input Power 154
Figure I.7: Gain of EDFA #303 as a Function of Input Power 154
Figure J.1: General Model of an OTDM Transmitter 155
Figure J.2: Bit Interleaved Multiplexer 156
Figure J.3: Parallel Duobinary Encoder 157
Figure J.4: Parallel Delay and Add Implementation 159
Figure K.1: Probability Density Functions of Gaussian Noise 160
Figure K.2: Duobinary Transfer Function 162
Figure K.3: Ternary Signal Probability Density Function 164
Figure L.1: Basic Components of a 9.952 GHz Clock Recovery Circuit 168
Figure L.2: Computation of Clock Tone Magnitude 169
Figure M.1: Ternary Decision Circuit Implementation 171
Figure M.2: Precoding Stage for Serial Duobinary Filter 172
Figure M.3: Precoding Stage using Toggle Flip-Flop 172
Figure N.1: PRBS Shift Registers Followed by Precoder 173
Figure O.1: Ternary Decision Circuit 175

Figure P.1: EDFA Characterization Setup.. 177
Figure Q.1: Parallel Precoder Circuit.. 178

List of Abbreviations

ASE	Amplified Spontaneous Emission
ASIC	Application Specific Integrated Circuit
APD	Avalanche Photodiode
BER	Bit Error Rate
BERT	Bit Error Rate Test set
BNR	Bell-Northern Research
BOSS	Block Oriented System Simulator
cw	continuous wave
D-FF	D Flip-Flop
DC	Direct Current
EDFA	Erbium Doped Fiber Amplifier
FWHM	Full Width, Half Maximum
NOI	National Optics Institute
NRZ	Non-Return to Zero
NSERC	Natural Sciences and Engineering Research Council
OTDM	Optical Time Division Multiplexing
PRBS	Pseudo-Random Bit Sequence
QAM	Quadrature Amplitude Modulation
RF	Radio Frequency
RIN	Relative Intensity Noise
RZ	Return to Zero
SNR	Signal to Noise Ratio
SONET	Synchronous Optical NETwork
TRLabs	Telecommunication Research Laboratories (University of Alberta)
VOA	Variable Optical Attenuator
XOR	Exclusive-OR

1. Introduction

1.1. Overview of High Speed Fiber Optic Technology

Fiber systems are continually evolving towards higher bit rates in order to reduce overall costs to network providers and to permit new service capabilities. With each new increase in bit rate comes new technology limitations that must be overcome. Currently 2.5 Gb/s fiber systems are available from a number of suppliers. The next generation of high speed fiber systems will almost certainly operate at 10 Gb/s. Most high speed fiber system research is now geared towards overcoming the obstacles which will then permit the transition from 2.5 Gb/s to 10 Gb/s.

The vast majority of fiber systems available today have the same fundamental architecture. As shown in Figure 1.1, the laser source is modulated directly and its output is coupled to a fiber. A receiver at the other end of the fiber converts the optical signal back into electrical form. This conventional approach to fiber optic communication has made great strides over the past decade, from commercially available multi-mode systems that operated at 44.736 Mb/s in the early 1980s to the single-mode systems that run at 2.5 Gb/s today. However, it is questionable whether this approach will be able to allow this trend towards increasing bandwidth to continue since fundamental physical limits are now being reached.

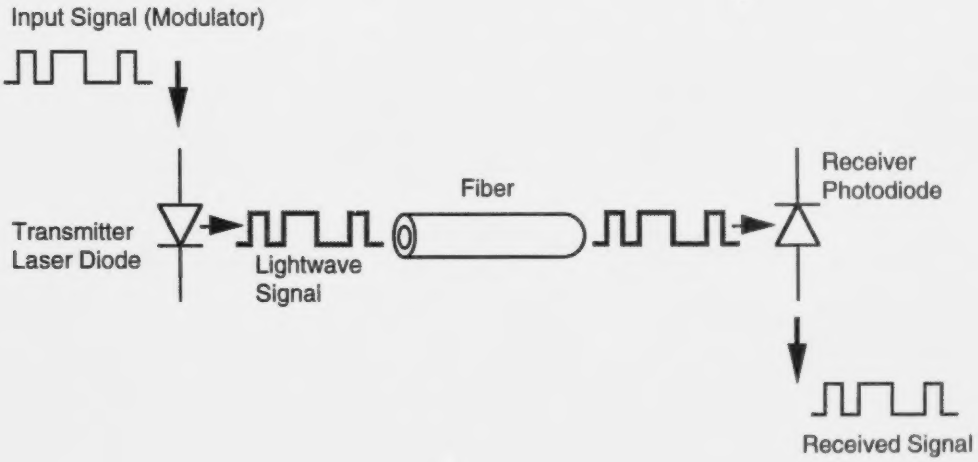

Figure 1.1: Conventional Fiber Optic Transmission System

There are four major limitations to the transmission rate of any single mode fiber optic system. These are:

- **Attenuation:** optical power in a signal is lost by scattering and absorption as it passes through fiber and optical devices. The length of the transmission path and the insertion loss of devices in the fiber path are therefore limited because the receiver requires a minimum amount of signal power to overcome noise.

- **Laser Transient Characteristics:** a laser with a time varying current applied to it has dynamic frequency shift (chirp) effects which broaden the frequency content of the signal.

- **Electronics speed:** currently available electronics technology has a speed ceiling in the Gb/s range because of limits in the available fabrication materials and because of stray inductance and capacitance effects in the devices and connections.

- **Chromatic Dispersion:** the group velocity of a narrow optical pulse down a fiber is sensitive to the frequency content within the pulse. This causes a transmitted digital pulse to broaden as it travels down a fiber, potentially resulting in high intersymbol interference. Most fiber installed today has a dispersion minimum at an operating wavelength of 1310 nm. Fiber systems not operating at 1310 nm are subject to high dispersion.

Methods for increasing performance bounds due to these limitations have been proposed and experimentally verified:

Attenuation

Erbium Doped Fiber Amplifier (EDFA) technology has provided a means to combat the fiber attenuation problem and lengthen the distance between a fiber transmitter and receiver. These devices are capable of directly amplifying a signal without the addition of a large amount of noise power. Signal power can therefore be boosted to compensate for loss. The technology is maturing rapidly, and is expected to reduce or eliminate attenuation problems in some fiber systems. It also permits the use of novel transmitter and receiver designs despite their insertion loss. For example, optical switches can now be incorporated into transmitters and receivers, even though they introduce significant attenuation. The primary disadvantage of EDFA technology is that its operating wavelength is in the 1550 nm wavelength window, where the effect of chromatic dispersion in conventional fiber is very high.

Laser Transient Characteristics

Optical switches and modulators allow the external modulation of continuous wave (cw) laser light. As shown in Figure 1.2, the laser itself is not modulated and therefore it does not introduce chirp. Instead, its light output is passed through the switch device, which can be controlled by the modulation signal to change the distribution of light intensity at its output ports. These optical switch devices can be operated in a zero chirp regime, or can be used to introduce a controlled amount of chirp [1]. The result of zero chirp external modulation is a very narrow transmitted power spectrum. Its width is essentially the minimum value determined by the information bandwidth impressed onto it by modulation, provided that the optical linewidth of the laser source is much less than the information bandwidth.

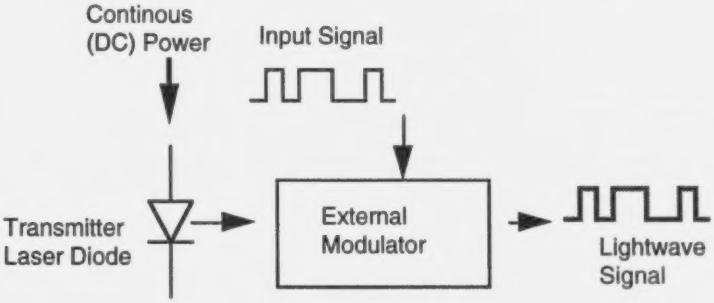

Figure 1.2: External Modulation

Electronics Speed

Optical Time Division Multiplexing (OTDM) technology has shown promise in multiplexing low speed streams into a high speed stream without the need for high speed electronics, and has already been evaluated to some extent at TRLabs [2]. With this approach, the final stage of multiplexing is performed optically with optical switches. The first stage of demultiplexing at the receiver can also be performed optically. With both optical time division multiplexing and demultiplexing in place, electronic digital signals need only be supported at the tributary (low speed channel) rates. This reduces the need for high speed digital electronics. A general model of an OTDM transmitter is shown in Figure 1.3. Multiple stages of optical switches can be used to modulate the pulses and interleave them together. Optical time division demultiplexing at the receiver reverses the interleaving stage and outputs N parallel optical pulses.

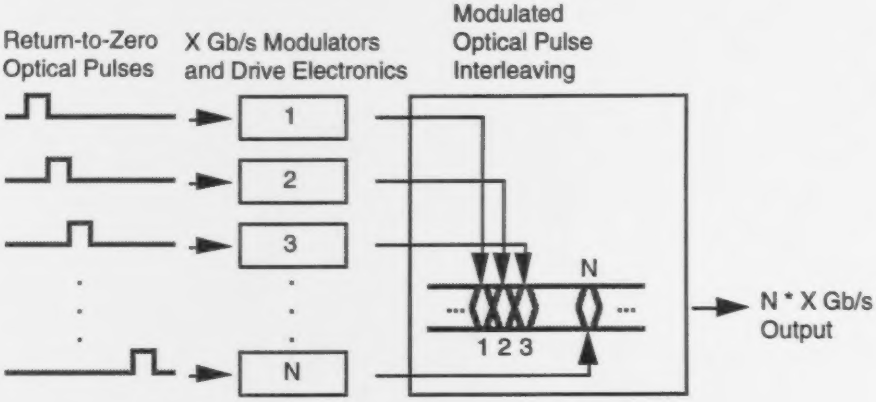
Return-to-Zero Optical Pulses
X Gb/s Modulators and Drive Electronics
Modulated Optical Pulse Interleaving
1
2
3
N
N
1 2 3
N * X Gb/s Output

Figure 1.3: General Model of an OTDM Transmitter

Chromatic Dispersion

To date, the impact of chromatic dispersion on transmission systems has been low for two reasons: the first is that most current systems operate at 1310 nm, where chromatic dispersion is minimal. The second is that most operate at a relatively low bit rate. This situation is rapidly changing due to increased bit rates and increased interest in transmission using the 1550 nm wavelength window to take advantage of EDFAs. Chromatic dispersion is currently a very active research area. Although many solutions have been proposed, no really effective solution with the exception of wholesale replacement of conventional fiber with dispersion shifted fiber has yet emerged. This option represents prohibitive expense to network providers, so obviously they are interested in practical alternatives.

1.2. Overview of Proposed Solutions for Chromatic Dispersion Problem

A search of current literature indicates that dispersion reduction is only now attracting attention because of the development of EDFAs. Three general approaches have been commonly proposed to reduce dispersion penalties:

- The first approach is to use signal processing to reverse the impact of the signal distortion caused by the fiber. Three electronic techniques are commonly proposed for direct detection lightwave systems: linear equalization with transversal filters, nonlinear cancellation, and maximum likelihood detection [3-7]. Transversal filters are used to correct for linear distortion using a weighted tap approach to implement an arbitrary magnitude and frequency response. Nonlinear cancellation reduces the impact of intersymbol interference by using previous bit decisions to determine the threshold level and sampling time for the current bit. Maximum likelihood detection considers a sequence of bits together to make reliable decisions. Optical signal processing is also a possibility. In this case, the optical signal is passed through a device or through fiber with the opposite dispersion characteristic of conventional fiber before it is converted into electrical form at the receiver. This optical technique has received considerable attention lately, as demonstrated by the number of recent papers published on the topic [8-23]. It is also possible to use spectral inversion to have conventional fiber act as its own equalizer, if the spectral content of the signal is reversed in mid-span [24][25].

- The second approach is chirped transmission. External modulators can be used to introduce frequency shifts onto the rising and falling edges of a pulse which can cause a chromatic dispersion effect that acts to compress the pulse. Over a range of fiber lengths, this offsets the natural tendency of the pulse to broaden because of chromatic dispersion [26-30]. Another technique is to use the inherent wavelength shift of a laser to frequency modulate the signal at the transmitter and use chromatic dispersion to convert this frequency modulation into amplitude modulation for the receiver [31].

- The third approach is line coding. This can be used to insert extra overhead into symbol blocks in order to introduce error correction [32][33] or to avoid bit sequences with high intersymbol interference [34]. Multilevel line coding at the transmitter or receiver is also a possibility [35][36]. This acts to narrow the transmission bandwidth of the signal, either by coding multiple bits into multiple signal amplitudes, or by introducing controlled intersymbol interference. Since chromatic dispersion is wavelength (frequency) dependent, it is also optical transmission bandwidth dependent. A reduction in transmission bandwidth should therefore reduce the impact of dispersion on the signal.

A fourth possible approach to reduce the impact of chromatic dispersion which has not appeared in literature as such is polarization multiplexing. This involves the combination of multiple signals with different states of polarization at the transmit end with polarization-sensitive separation at the receive end [37-40]. Polarization multiplexing has been typically proposed as a technique to improve optical system throughput. However, such a system features lower bit rate transmission than a serial system and therefore should have a longer dispersion-limited transmission distance.

No clear winning solution has emerged yet because all of the previously mentioned approaches have disadvantages which would impede their use in an actual product. Electrical signal processing techniques in general are poorly suited to 10 Gb/s applications because of the limited availability and capability of devices with Gb/s operation speeds. Also, a single bit period delay occupies at most 3 cm of waveguide length. This imposes a severe restriction on the layout and complexity of any electrical signal processor, especially if discrete components are used. Optical signal processing techniques are more popular in literature because they avoid the speed and layout problems associated with electronics. However, they also have some disadvantages. Dispersion compensating fiber introduces more path loss and also requires housing for the additional spools of fiber introduced in the path. Dispersion compensating devices require tuning to the specific transmission wavelength that is used [14]. Spectral inversion is also wavelength specific.

The use of chirped modulation restricts the transmitter to using a device which supports the appropriate chirp regime and may introduce further control complexity into the transmitter design. Also, chirped transmission in a multi-vendor environment may require further standardization of the optical signal format for mid-span meet purposes.

Line coding using block codes requires additional overhead, and therefore the loss of transmission capacity. Also, block codes designed to avoid high intersymbol interference sequences are specific to particular fiber spans. A new block code would have to be designed each time a system is installed into a fiber span.

Polarization multiplexing has not been investigated in great detail yet. However, the stability of states of polarization within a long section of fiber is a real concern. Polarization states are sensitive to the geometry of the fiber waveguide. This geometry inevitably changes as different mechanical stresses are imposed on the fiber by acoustic or thermal effects. Further work is required before polarization multiplexing becomes viable.

One remaining option which has not been explored in great depth is multilevel coding. There as two basic multilevel coding schemes that can be implemented: The first is simply the coding of a block of binary symbols into a multilevel code. For example, in a four level code, the group of bits 00 is represented as level "0", 01 is level "1", 10 is level "2" and 11 is level "3". In general, a set of N levels can encode $\log_2(N)$ bits, with a corresponding reduction in symbol rate and overall system bandwidth. The trade-off required is that the decision spacing at the receiver is reduced by a factor of N-1, making the receiver more susceptible to distortion and noise. The second multilevel scheme is Partial Response Signaling, originally proposed by Lender [41] [42]. This scheme correlates bits by using a specific filter shape to combine them together. For example, two bits are encoded into a three level symbol. Unlike the first option, transmission bandwidth reduction is not accomplished by a lower symbol rate, but by the correlation introduced into the signal stream. This could result in more noise immunity than the first option because the decision spacing is larger for approximately the same transmission bandwidth.

1.3. Overview of Duobinary Coding to Reduce Chromatic Dispersion Effect

A look into the past at techniques to reduce the impact of dispersion indicates that the Partial Response class of multilevel codes has been used successfully. This coding was used in Northern Telecom's FD-135 multi-mode fiber optic transmission system. The actual scheme used was Duobinary coding, a member of the Partial Response code set. In the FD-135, a Duobinary filter at the receiver converted the incoming distorted binary optical signal into a multi-level form, and at the same time reduced the transmission bandwidth of the signal. The result was improved receiver sensitivity compared to the binary system for long distance transmission.

The Duobinary receiver in the FD-135 was developed as a solution to multimode dispersion. However, it serves as a starting point to test multilevel coding in the single-mode dispersion context because it reduces transmission bandwidth, which appears to be an important parameter to control.

Duobinary codes have less transmission bandwidth than binary codes with the same throughput for two reasons: the first is that the code is multilevel. The second is that the symbols are now correlated because of controlled intersymbol interference [43]. Duobinary codes relate to Nyquist's Second Criteria for band-limited error free transmission: controlled intersymbol interference can be used in a constructive manner if the symbols are interpreted correctly. Appendix A presents the fundamental theory explaining the bandwidth reduction caused by duobinary coding. In general terms, a duobinary code is created when a binary impulse stream is passed through a filter with the frequency response:

$$\cos(\pi f / f_o)\, \Pi(f / f_o) \qquad (1.1)$$

where: f_o = the bit rate frequency

the gate function $\Pi(x) = 1$ for $|x| \leq 0.5$

$= 0$ for $|x| > 0.5$

This creates a ternary signal which can be decoded by sampling between the original symbols, as shown in Figure 1.4 (after [43]).

A duobinary stream with the symbols ("-1", "0", and "1") that is produced from a random binary sequence has the following properties:

- A change between the symbols "-1" and "1" (or "1" and "-1") in a sequence is always separated by an odd number of "0"s.
- A sequence of constant "-1" or "1" symbols is always separated by no "0"s or an even number of "0"s.

This amounts to correlation in the stream, and ultimately a reduction in information bandwidth.

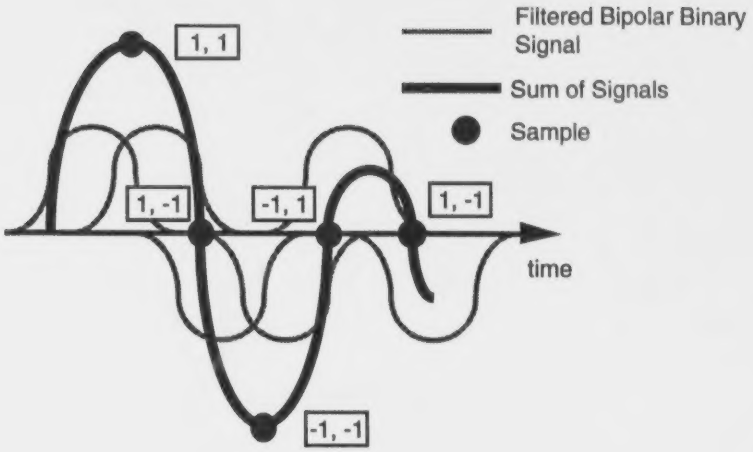

Figure 1.4: Output from Duobinary Transfer Function

The cosine shaped response in (1.1) can be exactly realized with a simple delay and add circuit followed by an ideal low-pass filter, as shown in Figure 1.5. The delay used is one bit period. This results in a spectral null at one half the bit frequency. In reality, pulses input to the duobinary transfer function will not be impulse shaped. They generally will be either in Return to Zero (RZ) or Non-Return to Zero (NRZ) form. Thus, the delay and add filter realization will result in a distorted output. The ideal solution to this problem is to introduce an additional transfer function which factors out the spectral shape of the incoming pulses. The actual amount of distortion without this additional transfer function is highly dependent on the incoming pulse shape, and in some cases may be acceptable.

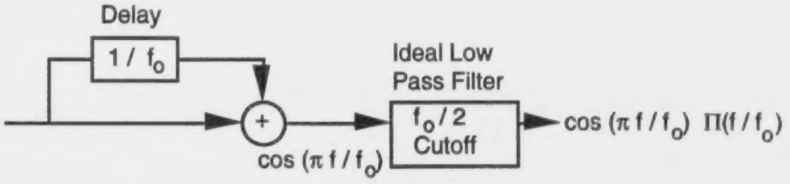

Figure 1.5: Delay and Add Implementation

Since duobinary encoding is accomplished with a transfer function, it can conceivably be located at either the system transmitter or the system receiver, as shown in Figure 1.6. If all transfer functions were linear, the same performance could be expected for either location of the duobinary transfer function. In fact, the transmitter and fiber transfer functions are nonlinear. This will have some impact on the performance of the two options. Both options are legitimate approaches which should be and are explored in following chapters. The source of the transmitter and fiber nonlinearity will also be discussed later.

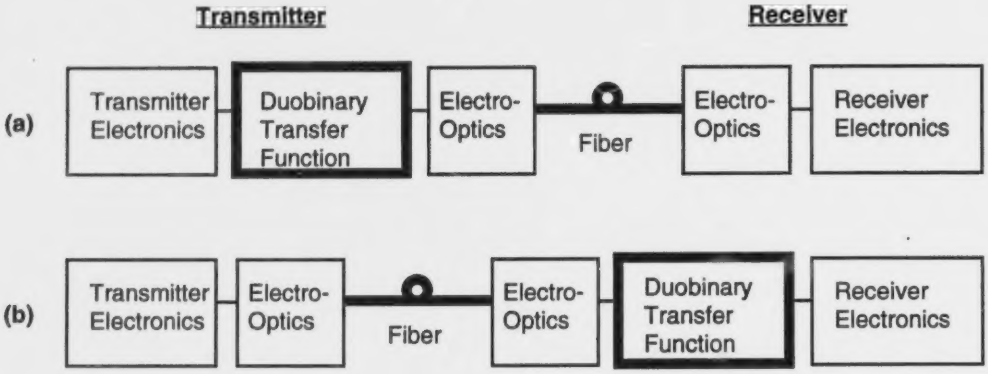
Transmitter
Receiver
(a)
Transmitter Electronics
Duobinary Transfer Function
Electro-Optics
Fiber
Electro-Optics
Receiver Electronics
(b)
Transmitter Electronics
Electro-Optics
Fiber
Electro-Optics
Duobinary Transfer Function
Receiver Electronics

Figure 1.6: Location of Duobinary Transfer Function

Since the symbols produced by the duobinary transfer function are three-level, a ternary decision circuit is required to convert the incoming signal back into binary form. The general block diagram of this decision circuit is shown in Figure 1.7. The original binary sequence can be retrieved by using combinational logic at the transmitter and receiver, as will be shown in following chapters.

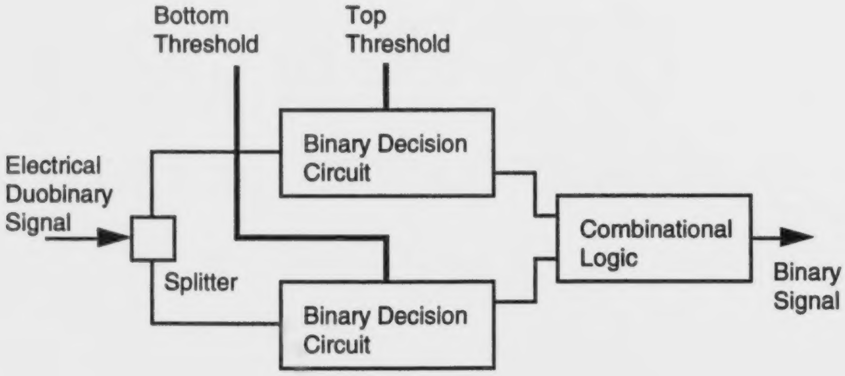
Bottom Threshold
Top Threshold
Electrical Duobinary Signal
Binary Decision Circuit
Splitter
Binary Decision Circuit
Combinational Logic
Binary Signal

Figure 1.7: Ternary Decision Circuit

1.4. Overview of Experimental Work

1.4.1. Context of Research

Rapid progress has been made in overcoming the obstacles which block the realization of high performance fiber systems that operate at bit rates of 10 Gb/s and higher. Chromatic dispersion remains a significant problem which has not been completely addressed. Many options to reduce the impact of chromatic dispersion have not yet been fully investigated. In particular, Duobinary coding appears to be a promising technology which has not been considered at all for use in a high bit rate single mode fiber system despite its proven success in a multi-mode product. Other techniques which also warrant further study are chirped transmission and polarization multiplexing. The following sections outline experiments that were performed to measure the relative benefits of these techniques.

1.4.2. Bit Rates Studied

All techniques explored are of most interest for fiber optic transmission applications complying with Synchronous Optical NETwork (SONET) transmission standards. The bit rates used were therefore binary multiples of the OC-48 standard rate of 2.48832 Gb/s (i.e. 2.48832 Gb/s, 4.97664 Gb/s, and 9.95328 Gb/s). All results reported in the following chapters were for these bit rates. For clarity they have been rounded up to 2.5 Gb/s, 5 Gb/s, and 10 Gb/s.

1.4.3. Electrical Multiplexing Experiments

The use of 10 Gb/s electrical multiplexing coupled to an external modulator with a cw optical input allows comparison of two different techniques to reduce the impact of dispersion at the same time: zero chirp versus chirped binary transmission with and without duobinary reception. Duobinary transmission can also be tested.

External modulation experiments at 10 Gb/s were of interest to the Fiber Systems Group at Bell-Northern Research (BNR) in Ottawa. Cooperation from this group and funding from the NSERC/BNR/TRLabs Industrial Research Chair in Fiber Optic Communications at the University of Alberta made it possible for these options to be explored in detail on site at BNR over the course of a four month work term [44]. This was advantageous because of the wide array of 10 Gb/s test equipment and piece components that were available at BNR and not at TRLabs.

1.4.4. Optical Time Division Multiplexing Experiments

As with the electrical multiplexing case, the duobinary transfer function for an OTDM system can be placed at either the transmitter or the receiver. The exact implementation of the duobinary transfer function depends on the configuration of the OTDM, because the duobinary transfer function works on the entire 10 Gb/s symbol stream and this may only be available in optical form in the OTDM. The same ternary decision circuit used for the external modulation case (shown earlier in Figure 1.7) still applies. It can operate on the entire high speed stream produced by the OTDM, or on low speed optically demultiplexed channels.

Duobinary coding at the OTDM transmitter definitely requires a different duobinary encoder than the serial delay and add transfer function proposed earlier because the final stage of multiplexing is performed optically. In its place, a parallel implementation that works across the input electrical channels can be envisioned. As shown in Figure 1.8, this could work at the low speed tributary rate to sum and correlate the incoming channels. The resulting optical output has the duobinary polarity properties discussed in Section 1.3. This form of parallel encoding is advantageous because it operates at the low speed tributary rates. Therefore, the OTDM's advantage of requiring only tributary rate electronics is not compromised.

Duobinary coding at the receiver depends on the implementation of the receiver. If optical time division demultiplexing is performed then the entire binary stream is not available for signal processing. If the stream is not optically demultiplexed, then it is available in electrical form and the standard electrical duobinary transfer function can be used. This receiver would have the same basic design as the receiver for electrically multiplexed signals. This requires higher speed electronics than would be required for optical time division demultiplexing, but can be used to compare the relative benefits of duobinary coding at the transmitter and receiver in the OTDM context.

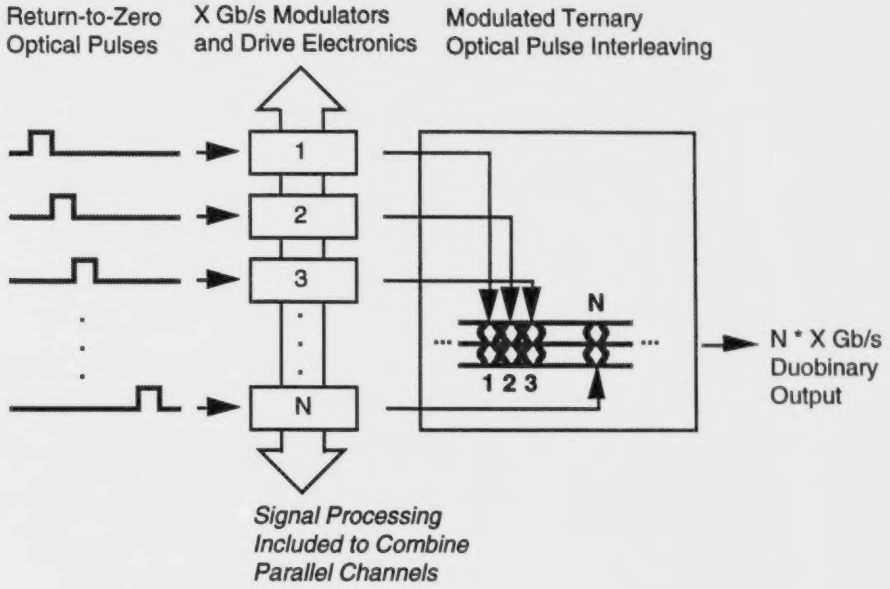
Return-to-Zero
Optical Pulses
X Gb/s Modulators
and Drive Electronics
Modulated Ternary
Optical Pulse Interleaving
1
2
3
N
N
1 2 3
N * X Gb/s
Duobinary
Output
Signal Processing
Included to Combine
Parallel Channels

Figure 1.8: Parallel Duobinary Encoding at the Inputs to an OTDM

The OTDM architecture allows polarization-sensitive devices to be incorporated easily. Therefore, polarization multiplexing and demultiplexing can also be evaluated at the same time as duobinary coding is tested.

1.4.5. Thesis Organization

This Chapter has described the current state of the art for high bit rate fiber systems and has identified chromatic dispersion as an area warranting further investigation. An overview of the experiments which can be performed to provide a comprehensive study of duobinary coding, and at the same time to gain insight into polarization multiplexing and chirped transmission has also been presented. Chapter 2 will now present an overview of computer simulations of various options to illustrate the severity of the chromatic dispersion problem and the potential for duobinary coding to reduce its impact. This is followed by a presentation of theoretical considerations related to measuring the impact chromatic of dispersion in Chapter 3. Chapters 4 and 5 will present results from the experiments that were briefly described above. Finally, Chapter 6 concludes this work with a short review and points to future research directions.

2. Simulation of Options

2.1. Scope of Simulation Studies

Simulation of a fiber optic system can be performed to varying degrees of accuracy, depending on the complexity of the model. The approach taken was to use waveform based simulations to obtain an initial view of how well an option would work with a relatively simple model, and then to incorporate additional accuracy into the model to compare with experimental results. Correspondence between simulated and actual waveforms increased confidence in the experimental procedure and at the same time validated the simulated models.

The scope of simulations covered noise-free zero chirp transmission. This was sufficient to describe the majority of experiments that were performed. The only experimental trials that could not be tested directly were chirped transmission because of the complexity involved in accurately modeling frequency shifts at the transmitter. Zero chirp results are useful even for this case because they demonstrate the minimum benefit of that could be realized with chirped transmission. Further extensions also could be included to allow for noise, gain from EDFAs and electrical amplifiers, and attenuation for bit error rate projections. However, reasonable expectations for these can be found from signal to noise ratio predictions without the need for simulations.

This chapter will overview the validated simulation models that were used and will present best case simulation results to demonstrate the full potential of duobinary coding to reduce dispersion penalties within electrical multiplexing and OTDM systems. More detailed simulations in which the properties of actual laboratory components are include in the simulations are presented along side experimentally obtained waveforms in Chapter 4 and Chapter 5.

2.2. Simulator Models

Block Oriented System Simulator (BOSS) is a waveform-oriented simulator on the Sun SPARC 2 Unix work stations at TRLabs. This software package was used to model various options over the course of the research and experimentation work. It is based on block descriptions of important elements within a transmission system. The connections between these blocks determines the flow of signals. BOSS performs discrete-time signal processing operations based on the descriptions of these blocks. A standard library is provided with BOSS to model common functions (e.g. adders, delays, Butterworth filters). Arbitrary mathematical functions can be built from these library primitives. Also, arbitrary filter shapes can be defined by using Frequency Domain Filter blocks in BOSS to input representative data points from real frequency response plots. These newly defined blocks form the basis for defining simulated electrical multiplexing and OTDM systems. Important blocks are described below.

2.2.1. Mach-Zehnder Switch Model

All optical switches and modulators used in the experiments were Mach-Zehnder devices. A comprehensive description of the operation of these devices is presented in Appendix B. The types of devices used in the actual OTDM (described in Appendix C and Chapter 5) were 1x2 (one input, two output) switches and balanced-bridge (two input, two output) interferometers. Both devices have identical input / output characteristics if only one input of the balanced bridge interferometer is used. The balanced bridge model also suffices to describe the operation of a modulator if only one input and one output is used. The model designed and validated in [2] was used here. One fundamental equation is sufficient to describe its overall operation. This is similar to that developed in Appendix B, with extensions to model the frequency response of the electro-optic switch and its extinction ratio. The coupling of optical power from the input of the switch to one of its outputs in response to an applied voltage V is:

$$\eta = \chi + (1-2\chi)\cos^2\left[\frac{\pi V}{2V_{\pi DC}} H(f)\right] \tag{2.1}$$

where: η is the intensity magnitude of one output ($1-\eta$ is the other output)

χ is the maximum extinction level of the switch

V is the applied signal voltage (DC bias and RF components)

$V_{\pi DC}$ is the V_π of the switch at DC

H(f) is a frequency domain description representing the reduction of effective drive voltage at high frequencies

The extinction ratio of the switch is related to χ by:

$$\text{Extinction Ratio} = 10\log_{10}\left[\frac{1-\chi}{\chi}\right] \tag{2.2}$$

A Frequency Domain Filter block can be used for H(f) to model the real frequency response of the switches. Representative sample points for each of the switches were simply typed into a file for use in the models.

The block diagram for this switch is shown in Figure D.1 in Appendix D. The transfer function H(f) is excluded from this diagram. It is incorporated into the switch drive models that will be described later.

Obviously the electro-optic switch can not be represented by a simple transfer function, and therefore represents a nonlinear element within the model. Time domain convolution (frequency domain multiplication) does not apply to the switch model. The effect of a transfer function placed before the switch may be different than the effect of a transfer function located after the switch. BOSS takes this into account automatically by converting back and forth between the time domain and frequency domain where necessary. The nonlinear behavior of the switch means that the performance of a duobinary transfer function located at a transmitter (before the switch) will differ from the performance of a duobinary transfer function located at a receiver (after the switch).

The input "optical" power for this model is simply a constant value of "1", or in the case of the OTDM it can be the output from another switch model. The simulations do not consider the line width of the true optical source, nor does it include any phase shift or chirp on the optical signal. In all experimental cases, the line width of the optical source was much less than information bandwidth that was impressed on it, so excluding line width from the simulations does not have a significant impact.

2.2.2. Fiber Model

The fiber transfer function is based on a low pass equivalent chromatic dispersion model. The transmission bandwidth of the signal is narrow compared to its carrier frequency. Therefore, a single mode fiber can be modeled in terms of electric field as a band pass filter with a flat amplitude response and linear group delay within the signal bandwidth [45]. The slope of the group delay relative to wavelength is as follows:

$$\frac{d\tau}{d\upsilon}=\frac{d\tau}{d\lambda}\cdot\frac{d\lambda}{d\upsilon}=\left(\frac{-1d\tau}{L\,d\lambda}\right)\left(\frac{\lambda^2}{c}\right)L \qquad (2.3)$$

where: υ is the optical frequency
L is the fiber length
c is the speed of light in free space

The fiber dispersion parameter $D(\lambda)$ is defined as:

$$D(\lambda)=\frac{-1}{L}\cdot\frac{d\tau}{d\lambda} \qquad (2.4)$$

Representative values for $D(\lambda)$ vary. However, a figure of 17 ps / (nm km) at 1550 nm wavelength is commonly quoted (e.g. [2][26][46] for conventional single mode fiber with a dispersion minimum at 1310 nm) and will be used for the purposes of these simulations. The group delay of the fiber can be approximated by a Taylor series expansion which is truncated to the first two terms:

$$\tau(\upsilon)\approx\tau(\upsilon_c)+(\upsilon-\upsilon_c)\left.\frac{d\tau}{d\upsilon}\right|_{\upsilon=\nu_c} \qquad (2.5)$$

where: υ_c is the optical carrier frequency

The phase is now given by:

$$\phi(\upsilon)=\int_0^{\upsilon}\tau(\upsilon')d\upsilon'=2\pi\upsilon\,\tau(\upsilon_c)-\frac{2\pi\upsilon_c^2}{2}\left.\frac{d\tau}{d\upsilon}\right|_{\upsilon=\upsilon_c}+\frac{2\pi(\upsilon-\upsilon_c)^2}{2}\left.\frac{d\tau}{d\upsilon}\right|_{\upsilon=\upsilon_c} \qquad (2.6)$$

The first two terms within (2.6) are constant and therefore cause a linear phase shift which corresponds to a constant time delay. Excluding these, the transfer function of the fiber can be written in terms of a low pass equivalent model in terms of base band frequency f as:

$$H(f) = e^{-j\phi(f)} = e^{-j\alpha f^2} \tag{2.7}$$

$$\alpha = \pi D(\lambda)\frac{\lambda^2}{c}L \tag{2.8}$$

$$f = \upsilon - \upsilon_c \tag{2.9}$$

Representative data points for this transfer function were generated for BOSS using the program included in Appendix E. This enables simulation of the entire base band fiber optic system without requiring consideration of the light carrier frequency.

The electric field of the output of the fiber can now be expressed as:

$$X_{out}(f) = X_{in}(f)H(f) \tag{2.10}$$

where: $X_{in}(f)$ is the Fourier Transform of the input signal
$X_{out}(f)$ is the Fourier Transform of the output signal

The time domain electric field is recovered using an inverse Fourier Transform.

$$x_{out}(t) = \int_{-\infty}^{\infty} X_{out}(f)e^{j2\pi f t}\,df \tag{2.11}$$

A direct detection receiver converts intensity into photocurrent. This corresponds to the squared magnitude of the resultant time domain signal.

$$y_{out}(t) = [\mathrm{Re}[x_{out}(t)]]^2 + [\mathrm{Im}[x_{out}(t)]]^2 \tag{2.12}$$

The BOSS model for this fiber transfer function is shown in Figure 2.1.

This fiber model is nonlinear in terms of optical intensity because of the square root at the head end and magnitude squared detection of the time domain signal at the tail end. The effect of a transfer function located before the fiber therefore may be different than the effect of a transfer function after the fiber. This, like the electro-optic switch transfer function, impacts the relative performance of duobinary reception and duobinary transmission. BOSS takes it into account automatically.

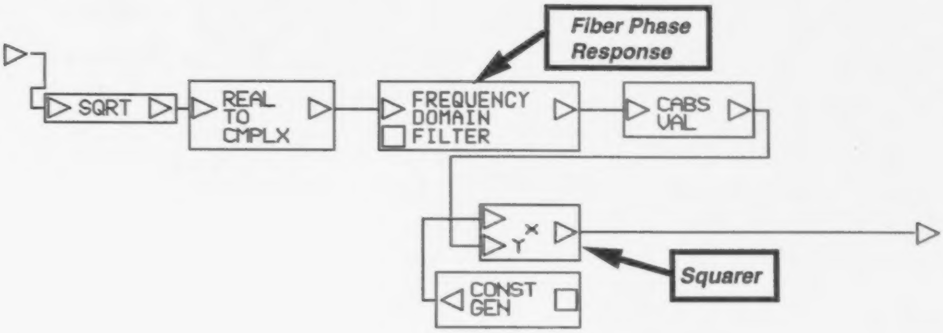

Figure 2.1: Single Mode Fiber Model

2.2.3. Transmitter and Receiver Component Models

Appendices F, G, and H provide a general description of the components that were used in the various experimental transmitters and receivers, and some of the design guidelines used to realized binary and duobinary filters. Accurate modeling of the frequency response of these components is required to obtain representative simulation results. All of these components have linear transfer functions, which allows either the frequency response of individual components to be modeled as individual simulation blocks, or the concatenated frequency response of many components to be lumped together into one block. The required frequency response plots were collected by using a network analyzer to measure S-parameters of individual components and the concatenated response of many components. Representative points from these frequency response plots were entered manually for use by BOSS within Frequency Domain Filter blocks.

All components except for the amplifiers have a flat frequency response down to almost DC. To simplify the models, the low end frequency response of the amplifiers was also assumed to be flat down to DC. This is a valid assumption providing that the simulations model actual systems that use short repetitive pattern strings with little low frequency content. This is true of all systems described in Chapter 4 and Chapter 5, which use 2^7-1 (127 bit) Pseudo-Random Bit Sequences (PRBS). Group delay response was also omitted as a further simplification. These simplifications result in simulations which can be slightly optimistic about signal quality.

2.3. Electrical Multiplexing Options

2.3.1. Models

These models correspond to the real 10 Gb/s systems that are evaluated in Chapter 4. Three transmitter and receiver combinations are modeled. These combinations are binary transmission with binary reception, binary transmission with duobinary reception, and duobinary transmission with duobinary reception. Figure 2.2 presents simplified block diagrams of these options. Each Model block contains frequency or time domain descriptions of the components that appear in the real systems. More detailed block diagrams from BOSS can be found in Appendix D.

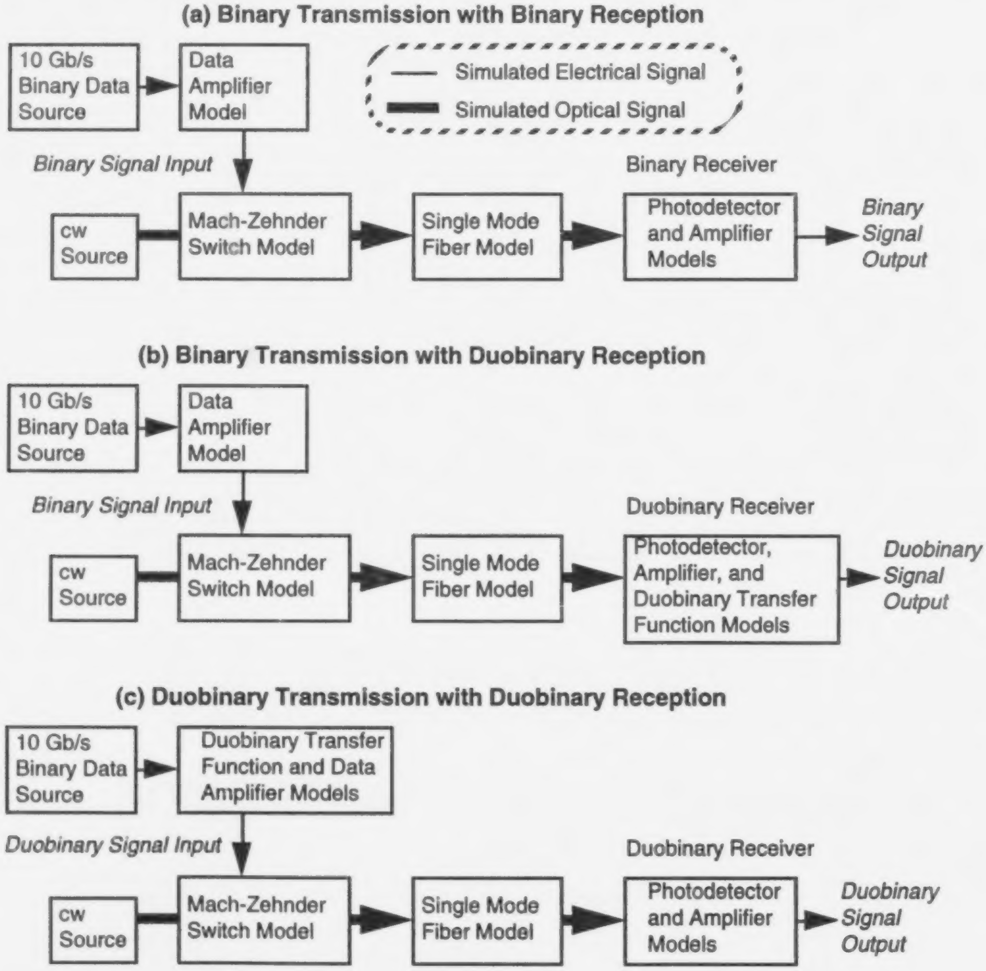
(a) Binary Transmission with Binary Reception
10 Gb/s Binary Data Source
Data Amplifier Model
Simulated Electrical Signal
Simulated Optical Signal
Binary Signal Input
Binary Receiver
cw Source
Mach-Zehnder Switch Model
Single Mode Fiber Model
Photodetector and Amplifier Models
Binary Signal Output
(b) Binary Transmission with Duobinary Reception
10 Gb/s Binary Data Source
Data Amplifier Model
Binary Signal Input
Duobinary Receiver
cw Source
Mach-Zehnder Switch Model
Single Mode Fiber Model
Photodetector, Amplifier, and Duobinary Transfer Function Models
Duobinary Signal Output
(c) Duobinary Transmission with Duobinary Reception
10 Gb/s Binary Data Source
Duobinary Transfer Function and Data Amplifier Models
Duobinary Signal Input
Duobinary Receiver
cw Source
Mach-Zehnder Switch Model
Single Mode Fiber Model
Photodetector and Amplifier Models
Duobinary Signal Output

Figure 2.2: Block Diagrams of Electrical Multiplexing Options

2.3.2. Binary Transmission with Binary Reception

The BOSS model for binary transmission with binary reception is presented in Figure D.2. Annotations have been overlaid on top of the block diagrams to describe important features of the model. The modulator (electro-optic switch) at the transmit end is driven by the circuit in Figure D.3, which also includes a block for modeling the modulator frequency response H(f).

The ideal system would use components that have a flat amplitude and group delay frequency response out to infinity. A scenario which is more representative of the best achievable case (given an unlimited budget and unlimited time to fine tune transmitter and receiver frequency responses) is to model the systems using the frequency response the some of the highest quality components that are currently available. This is somewhat arbitrary, but is sufficient to demonstrate the potential for each option to reduce the signal distortion impact of dispersion.

Figure 2.3 shows eye diagrams for the binary case, assuming only the frequency response of the actual modulator that was used at the transmitter (described in Chapter 4 and Appendix I), and SHF90P amplifiers at the transmitter and receiver. The SHF90P amplifier has a pass band ranging from 10 kHz to 15 GHz with a ±1 dB gain ripple, so it is representative of premium quality high power amplifiers. The frequency response of the photodetector and all passive microwave components has been assumed to be flat beyond the pass band of the amplifier. A 15 dB extinction ratio has been used for all simulations, which is a realistic figure to achieve in practice. The binary eye diagram resulting from these assumptions is very clean at 0 km and is almost completely closed at 100 km because of chromatic dispersion-induced intersymbol interference.

2.3.3. Binary Transmission with Duobinary Reception

The BOSS model for binary transmission with duobinary reception is virtually identical to the previous model, with the exception of the duobinary receiver (shown in Figure D.4) which replaces the binary receiver. Figure 2.4 shows eye diagrams using the same assumptions used to generate the eye diagrams for Figure 2.3. Duobinary coding at the receiver is able to maintain eye openings beyond 125 km.

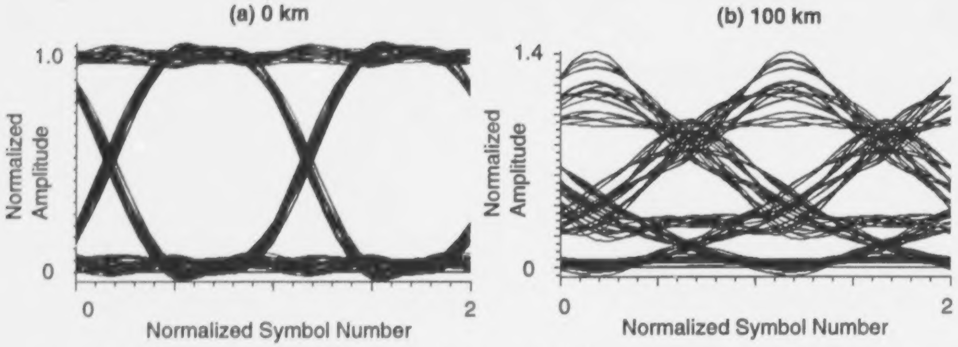

Figure 2.3: Binary Transmission with Binary Reception, Electrical Multiplexing

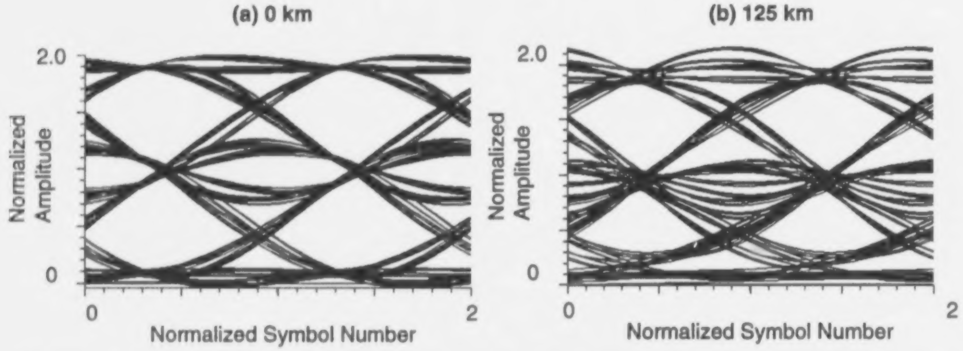

Figure 2.4: Binary Transmission with Duobinary Reception, Electrical Multiplexing

2.3.4. Duobinary Transmission

The BOSS model for duobinary transmission with duobinary reception is very similar to the binary transmission with binary reception model, with exception of the duobinary drive circuit for the modulator (Figure D.5). Figure 2.5 shows eye diagrams using the same assumptions used to generate the eye diagrams for Figure 2.3 and Figure 2.4. Duobinary transmission has comparable performance to binary transmission with duobinary reception. Some additional distortion is apparent on the duobinary signal (compared to Figure 2.4) because of the impact of the nonlinear modulator transfer function. Like duobinary encoding at the receiver, duobinary encoding at the transmitter is able to maintain eye openings beyond 125 km.

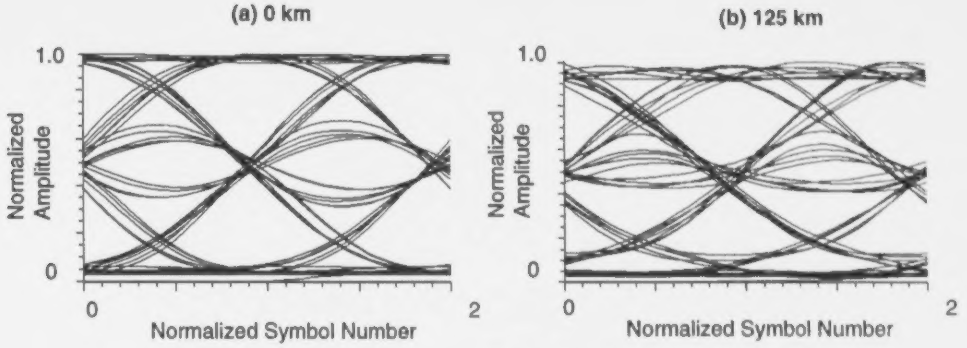

Figure 2.5: Duobinary Transmission, Electrical Multiplexing

2.4. OTDM Options

2.4.1. Models

These models correspond to the 10 Gb/s systems evaluated in Chapter 5. The block diagram of the OTDM is shown in Figure 2.6. Three Mach-Zehnder switching stages are included. The first stage (point A) is driven by a 5 GHz tone signal. The output of this switch stage are 5 Gb/s Return to Zero (RZ) pulses which alternate between the two outputs of the switch. These pulses are then modulated by the second stage of switches (points B and C) which are driven by two separate 5 Gb/s Non Return to Zero (NRZ) signals. The modulated 5 Gb/s RZ pulses are then interleaved into a 10 Gb/s NRZ signal by summing them together at point D. More information

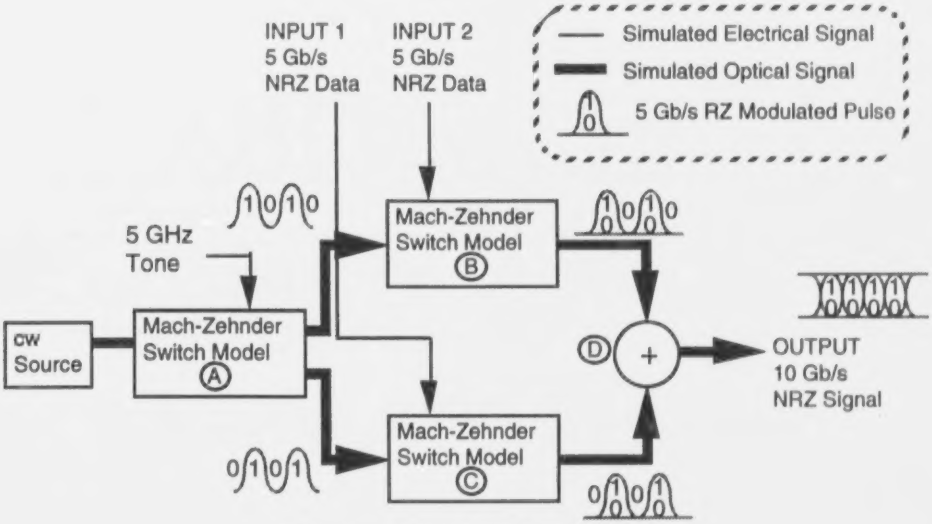
INPUT 1
5 Gb/s
NRZ Data
INPUT 2
5 Gb/s
NRZ Data
Simulated Electrical Signal
Simulated Optical Signal
5 Gb/s RZ Modulated Pulse
5 GHz
Tone
CW
Source
Mach-Zehnder
Switch Model
A
Mach-Zehnder
Switch Model
B
Mach-Zehnder
Switch Model
C
D
+
OUTPUT
10 Gb/s
NRZ Signal
1 0 1 0
0 1 0 1

Figure 2.6: OTDM Model

information about this OTDM architecture appears in Appendix C. The options that were modeled match the electrical multiplexing options and are shown in Figure 2.7.

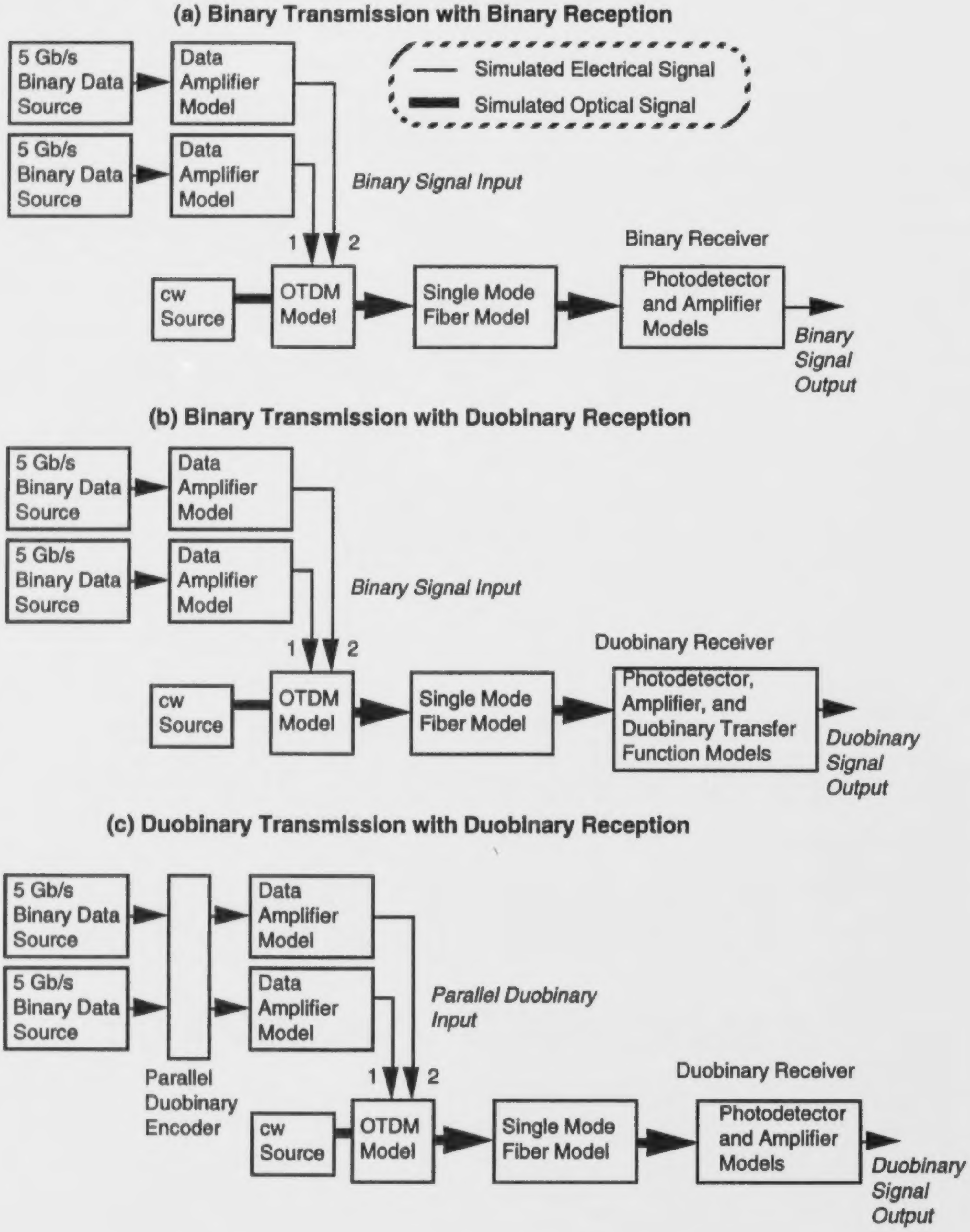
(a) Binary Transmission with Binary Reception
5 Gb/s Binary Data Source
Data Amplifier Model
Simulated Electrical Signal
Simulated Optical Signal
5 Gb/s Binary Data Source
Data Amplifier Model
Binary Signal Input
1
2
Binary Receiver
cw Source
OTDM Model
Single Mode Fiber Model
Photodetector and Amplifier Models
Binary Signal Output
(b) Binary Transmission with Duobinary Reception
5 Gb/s Binary Data Source
Data Amplifier Model
5 Gb/s Binary Data Source
Data Amplifier Model
Binary Signal Input
1
2
Duobinary Receiver
cw Source
OTDM Model
Single Mode Fiber Model
Photodetector, Amplifier, and Duobinary Transfer Function Models
Duobinary Signal Output
(c) Duobinary Transmission with Duobinary Reception
5 Gb/s Binary Data Source
5 Gb/s Binary Data Source
Data Amplifier Model
Data Amplifier Model
Parallel Duobinary Input
Parallel Duobinary Encoder
1
2
Duobinary Receiver
cw Source
OTDM Model
Single Mode Fiber Model
Photodetector and Amplifier Models
Duobinary Signal Output

Figure 2.7: Block Diagrams of OTDM Options

2.4.2. Binary Transmission with Binary Reception

Figure D.6 presents the binary OTDM system model. The internal switch blocks of the OTDM are shown in Figure D.7, and the drive circuit for the binary modulators is shown in Figure D.3. 5 Gb/s RZ versions of these systems are created by tying only one output of the OTDM in Figure D.6 to the fiber model and connecting the other to a SINK block. 5 Gb/s simulations are useful for comparison with the experimental results presented in Chapter 5.

Simulations of the OTDM options are more complicated than the electrical multiplexing options because of the large number of components involved and the settings required to properly phase and amplitude adjust the interleaved signals. An arbitrary "high quality" scenario can be established by modeling only perfect phasing and amplitudes, and including only the frequency response of the actual switch devices that were used (described in Chapter 5 and Appendix I) and SHF90P amplifiers in the transmitter and receiver. All other components are assumed to have a flat frequency response beyond the pass band of the amplifiers. Representative eye diagrams are shown in Figure 2.8. Note that the eye closure present at 100 km is similar to that present with the electrical multiplexed transmitter.

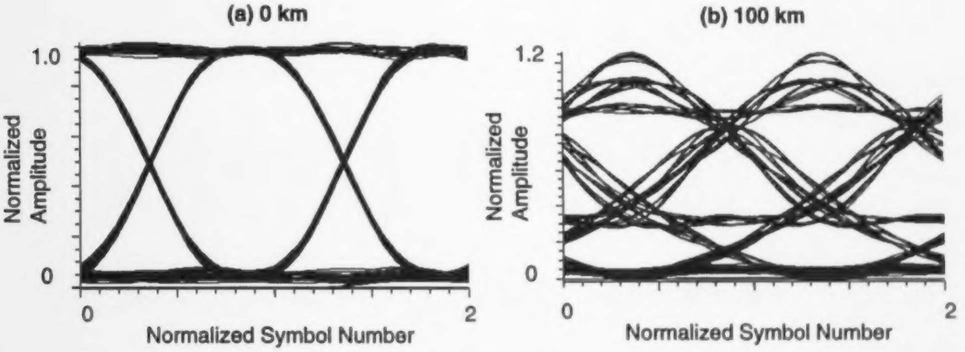

Figure 2.8: Binary Transmission with Binary Reception, OTDM

2.4.3. Binary Transmission with Duobinary Reception

This model uses the same binary transmitter as the binary reception case. The receiver has been reconfigured to include a duobinary transfer function, as shown in Figure D.8. Representative eye diagrams for this case are shown in Figure 2.9. These were generated using the same assumptions that were used to generate the eye diagrams in Figure 2.8. Eye closure at 125 km is more pronounced than the electrical multiplexing case, but clear openings are still present.

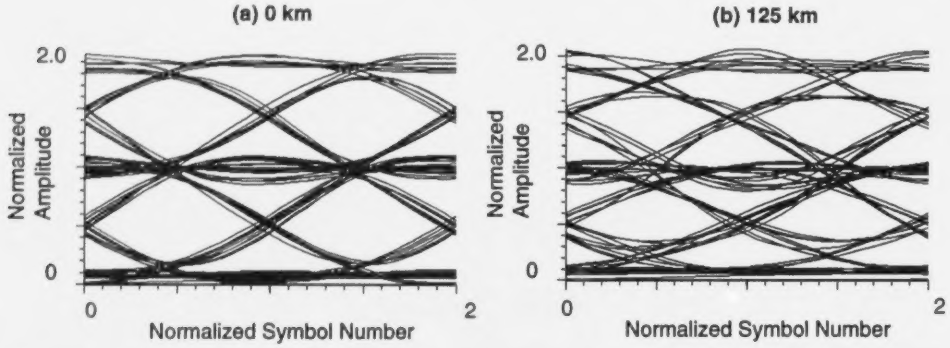

Figure 2.9: Binary Transmission with Duobinary Reception, OTDM

2.4.3. Duobinary Transmission

The duobinary OTDM system is shown in Figure D.9. The same basic optical OTDM model (Figure D.7) was again used. As discussed in Chapter 1, this OTDM duobinary transmitter requires a parallel duobinary encoder overlay. The operation of this overlay is presented in Appendix J. A model of a two input version of the parallel duobinary encoder is shown in Figure D.10. Figure 2.10 shows representative eye diagrams using the same assumptions as the other cases. The 5 GHz low pass filter required to band limit the duobinary signal was placed at the receiver for this case. This differs from the electrical multiplexing case, where it was placed at the transmitter. The duobinary eye openings at 125 km are narrower than the electrical multiplexing case, but are still relatively clear.

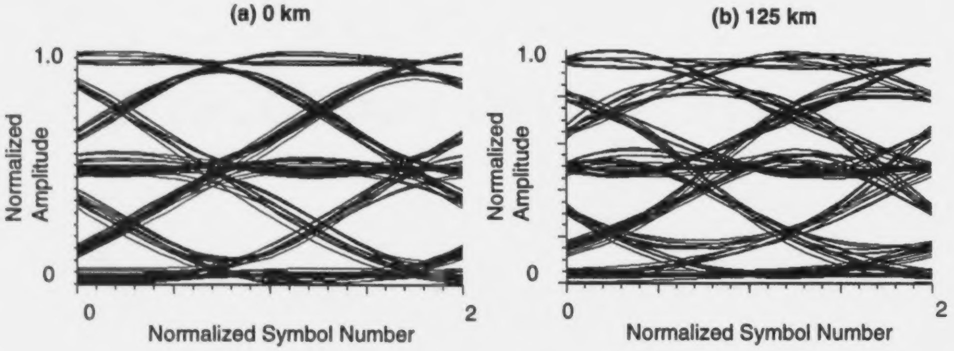

Figure 2.10: Duobinary Transmission, OTDM

2.5. Conclusions

Computer simulations were used to obtain an initial view of the effectiveness of duobinary coding and to validate experimental procedure. Optimistic simulations using low distortion components provide compelling evidence that duobinary encoding either at the transmitter or the receiver will reduce the impact of chromatic dispersion on eye closure compared to a binary system. Chapter 4 and 5 will study this from an experimental viewpoint, and also from additional simulations which include the limitations of actual laboratory components.

3. Receiver Modeling

3.1. Power Penalty

Chapter 2 showed that chromatic dispersion can result in significant distortion and intersymbol interference in a signal stream after it passes through a long section of fiber. A qualitative assessment of the impact of dispersion is available from plotting the received eye diagram at various fiber lengths and examining the resulting eye closure. A quantitative measure of the impact of dispersion is obtained from obtaining bit error rate (BER) data as a function of input power. This is known as receiver sensitivity.

BER data provides the most meaningful measure of dispersion since it indicates dispersion penalty as a function of distance. This dispersion penalty is conventionally defined as the increment in receiver power required to maintain a given bit error rate at the receiver (usually 10^{-9}) for a given distance compared to the power level required for 0 km. This increment in power is related to the amount of eye closure present at the receiver. BER data for other input power levels also can be collected in order to gain confidence in the experimental procedure and the 10^{-9} BER points. Another related penalty figure that can be obtained from BER data is a measure of the increased power above and beyond the dispersion penalty that is required to maintain a 10^{-9} BER for a system with polarization multiplexing and demultiplexing. This is useful for determining the amount of intersymbol interference caused by crosstalk between different polarization states.

This chapter describes the relevant theory behind the bit error rate measurement and shows how dispersion penalty is related to eye closure.

3.2. Receiver Model

Figure 3.1 shows the receiver layout that was used for bit error rate measurements. It includes an EDFA pre-amplifier stage, an optical bandpass filter, a photodetector, and receiver electronics. The receiver input is defined to be the input to the EDFA. A variable optical attenuator (VOA) was used to control the input power to the EDFA. Another VOA followed the EDFA pre-amplifier to act as a gain control mechanism to maintain the same power level on the photodiode. The optical splitter and tap were used to monitor this power. In some experiments, gain control was not implemented and both VOA 2 and the optical splitter were omitted from the receiver.

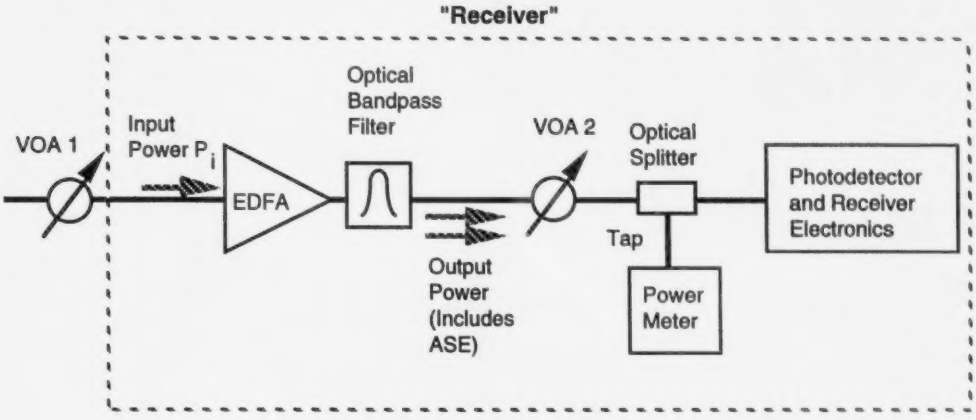
"Receiver"
VOA 1
Input
Power P_i
EDFA
Optical
Bandpass
Filter
VOA 2
Optical
Splitter
Tap
Photodetector
and Receiver
Electronics
Output
Power
(Includes
ASE)
Power
Meter

Figure 3.1: General Receiver Model

The input power of the receiver is measured at the input of the EDFA. The EDFA amplifies this input power and also adds Amplified Spontaneous Emission (ASE). This ASE contribution generally has a broader bandwidth than the signal, and therefore can be reduced by locating an optical bandpass filter with a pass band centered on the signal wavelength at the output of the EDFA. The input power of the receiver may also have an ASE component that has been accumulated from other EDFAs which precede the EDFA pre-amplifier. This has been assumed to be negligible in the following discussion. Referring to Figure 3.1, the total optical power into the photodetector is as follows:

$$P_{tot} = P_i \eta_i G \eta_o L_f A_2 L_s + P_{ASE} \eta_o L_f A_2 L_s \tag{3.1}$$

where: P_i is the receiver (EDFA) input power

η_i is the input coupling efficiency of the EDFA

G is the internal EDFA gain

η_o is the output coupling efficiency of the EDFA

L_f is the loss of the optical bandpass filter

A_2 is the attenuation factor for VOA 2

L_s is the loss of the splitter

P_{ASE} is filtered (in-band) ASE output power from the EDFA

If VOA 2 and the splitter are not included in the receiver, the factors A_2 and L_s in (3.1) are set to 1.

To simplify the following expressions, let:

$$G_{ff} = \eta_i G \eta_o \tag{3.2}$$

where: G_{ff} is the fiber-to-fiber gain

The total amplified input power that is incident on the photodetector is found by eliminating the ASE component from P_{tot}:

$$P_d = P_i G_{ff} L_f A_2 L_S = P_{tot} - P_{ASE} \eta_O L_f A_2 L_s \tag{3.3}$$

3.3. Noise Contributions

The ASE power into the receiver depends on the loss between the EDFA and the photodetector, the gain of the EDFA, and the bandwidth of the optical bandpass filter. It can be modeled as [47][48]:

$$P_{ASE} = m_t h\upsilon N_{sp} (G-1) B_o \tag{3.4}$$

where: m_t is the number of polarization states ($m_t = 2$ for unpolarized light)
N_{sp} is the spontaneous emission factor of the EDFA
$h = 6.6262 * 10^{-34}$ J-s is Planck's constant
υ is the light frequency
B_o is the bandwidth of the optical bandpass filter in Hz

The gain of an EDFA decreases with increasing input power because its output power tends to saturate. ASE power also decreases with increasing input power because from (3.4) it is approximately directly proportional to gain for $G >> 1$.

The average photocurrent due to ASE is:

$$I_{ASE} = r P_{ASE} \eta_O L_f A_2 L_s \tag{3.5}$$

where: r is the photodetector responsivity

The average photocurrent due to amplified input power is:

$$I_d = r\,P_d = r\,P_i\,G_{ff}\,L_f\,A_2\,L_S \tag{3.6}$$

The total receiver noise can be predicted knowing the specifications of the electrical amplifiers, the noise bandwidths of the receiver optical bandpass filters and the receiver electronics, and having at hand ASE data for the EDFA pre-amplifier. Receiver noise sources include thermal noise, relative intensity noise (RIN) from the laser, shot noise in the photodetector, and noise resulting from ASE in the optical link. All noise terms below are expressed as mean square current at the photodetector.

Overall thermal noise is dominated by resistor noise produced at the photodetector output and increased by the noise factor of the first amplifier stage [49]. This noise factor dominates over other receiver amplifier noise factors.

$$N_{th} = \frac{4kTF}{R} B_e \tag{3.7}$$

where: $k = 1.3807 * 10^{-23}$ J / K is Boltzmann's constant

T is the temperature at the input of the amplifier

F is the noise factor of the first electronic amplifier stage

R is the resistance at the input to the amplifier

B_e is the electrical noise bandwidth of the receiver in Hz

The noise current due to the RIN of the optical source is:

$$N_{RIN} = RIN\, I_d^2\, B_e \tag{3.8}$$

where: RIN is the relative intensity noise of the source laser

Shot noise from the photodetector is a function of amplified input power and ASE [47]:

$$N_{shot} = 2q[I_{ASE} + I_d]B_e \tag{3.9}$$

where: $q = 1.6 * 10^{-19}$ C is the charge of an electron

ASE results in spontaneous-spontaneous beat noise at the photodetector. This is [47]:

$$N_{sp-sp} = I_{ASE}^2 \frac{B_e[2B_o - B_e]}{B_o^2} \quad \text{if } B_e \le B_o \tag{3.10}$$

ASE also results in signal-spontaneous beat noise at the photodetector. The input power to the EDFA for all cases studied was highly polarized. Only the component of ASE that has polarization aligned with the source will contribute to this noise term. The expression for signal-spontaneous beat noise therefore depends on the value for m_t, which determines whether the receiver is polarization sensitive or not. From (3.4) and (3.5), this is reflected in the definition of a new polarized ASE photocurrent parameter:

$$I'_{ASE} = r[N_{sp} h\upsilon(G-1)B_o]\eta_o L_f A_2 L_s \tag{3.11}$$

where: I'_{ASE} is the average photocurrent resulting from polarized ASE

Obviously:

$$I'_{ASE} = I_{ASE} / m_t \tag{3.12}$$

Signal-spontaneous beat noise now can be expressed in general terms as [47]:

$$N_{s-sp} = 4[I_d I'_{ASE}]\frac{B_e}{B_o} \quad \text{if } B_e \le B_o / 2 \tag{3.13}$$

This noise term can also be written in the same form as the other noise terms.

$$N_{s-sp} = \frac{4}{m_t}[I_d I_{ASE}]\frac{B_e}{B_o} \quad \text{if } B_e \le B_o / 2 \tag{3.14}$$

3.4. Signal to Noise Ratio and Bit Error Rate

Signal to noise ratio (SNR) can be directly related to BER if the statistical properties of the noise are known. This section will show the relationship between receiver input power, SNR, and ultimately BER. An interpretation of dispersion penalty also will be provided.

The following discussion assumes binary transmission in a Gaussian noise environment with the same noise associated with binary "0" and "1" symbols and the same 0.5 probability for each. Appendix K provides more detail on the relationship between SNR and BER for a binary receiver and also a binary receiver equipped with a duobinary filter when these assumptions are used.

A tail probability parameter Q determines BER. Assuming that noise associated with a "1" level is identical to the noise associated with a "0" level, it can be calculated from [47]:

$$Q = \frac{I(1) - I(0)}{\sqrt{N_{tot}(1)} + \sqrt{N_{tot}(0)}} = \frac{I(1) - I(0)}{2\sqrt{N}} \qquad (3.15)$$

where: I(1) and I(0) are the mean photocurrent for "1" and "0" symbols

$N_{tot}(1) = N_{tot}(0) = N$ are the total mean square noise current associated with each symbol

A Q value of 6 yields a BER of 10^{-9}.

Average signal current can be defined from (3.15) as:

$$I_{sig} = \frac{I(1) - I(0)}{2} \qquad (3.16)$$

From (3.15) and (3.16):

$$Q = \frac{I_{sig}}{\sqrt{N}} \qquad (3.17)$$

Q is equivalent to the ratio of average signal current to average noise current. In power terms, Q^2 is equivalent to SNR. An SNR value of 15.5 dB (6^2) results in a BER of 10^{-9}.

Average optical signal power at the input of the EDFA (P_{sig}) can be related to signal photocurrent as follows:

$$I_{sig} = r\, P_{sig}\, G_{ff}\, L_f\, A_2\, L_S \tag{3.18}$$

It is now important to make the distinction between receiver input power (P_i) and signal power (P_{sig}) since most experiments were performed in a regime where signal corruption due to chromatic dispersion was high. From (3.16) and (3.18), signal power is a measure of the average power sampled by the decision circuit to distinguish one symbol from another. On the other hand, receiver input power is an all-inclusive long term average measurement of the total power incident on the EDFA. These two terms are not always equivalent.

Receiver input power and signal power can be directly related for a transmission system with no distortion. Assuming an equal probability of "1" and "0" symbols, the signal power associated with optical bits of an NRZ on-off signaling format is:

$$P_{sig} = \frac{P_1 - P_0}{2} = \frac{P_1(1-\delta)}{2} \tag{3.19}$$

where: P_1 and P_0 are the sampled optical power levels of "1" and "0" symbols
$\delta = P_0/P_1$ is the signal extinction ratio (δ=0 for an ideal on-off format)

This signal power is constant across the entire bit period of all symbols. Therefore signal power and input power are identical:

$$P_i = P_{sig} \tag{3.20}$$

Since the two power levels are the same, from (3.6) and (3.18) the normalized signal power in receiver photocurrent is:

$$I_{sig}^2 = I_d^2 \tag{3.21}$$

Similarly, input power can be related to signal power for an optical RZ on-off signaling format with pulses that occupy one half of the bit period and have an equal probability of "1" and "0" symbols. The signal spacing and resulting power P_{sig} is identical to that for the NRZ format, so (3.19) still applies. However, the relationship with input power changes because only one half of the bit period is occupied and the other half has no signal. This means that:

$$P_i = \frac{P_{sig}}{2} \tag{3.22}$$

For a given input power P_i, the optical signal power associated with RZ signaling (3.22) is twice that associated with NRZ signaling (3.20). Note that signal power for RZ signaling is actually higher than receiver input power because signal power is an average of sampled power and input power is a long term average.

From (3.6), (3.18) and (3.22), the normalized signal power in receiver photocurrent is:

$$I_{sig}^2 = (2I_d)^2 = 4I_d^2 \tag{3.23}$$

For a distortion-free transmission system, signal photocurrent can now be expressed as:

$$I_{sig}^2 = k_f I_d^2 \tag{3.24}$$

where: k_f is a signal format constant = 1 for NRZ and 4 for half-width RZ

The equations (3.18) through (3.23) have all assumed an ideal distortion-free transmission system with perfect on-off signaling. The relationship between input power and signal power becomes less defined in the case of high signal distortion. This can be thought of in terms of a non-calculable dispersion factor η_d which models the amount of eye closure that is present. An all-inclusive normalized signal power in receiver photocurrent for each case now becomes:

$$I_{sig}^2 = \eta_d k_f I_d^2 \tag{3.25}$$

The factor η_d is exactly 1 for a distortion-free system. Since chromatic dispersion often results in eye closure, decision spacing can become narrower and the signal power component within input power is reduced. Therefore η_d decreases for increasing dispersion and has a minimum value of 0 when the signal is completely corrupted. In a system with polarization multiplexing and demultiplexing, crosstalk between polarization states can also reduce η_d.

SNR can now be related to receiver input power. From (3.17) it is simply the ratio of signal power to the sum of all noise powers:

$$\mathrm{SNR} = \frac{I_{sig}^2}{N_{th} + N_{RIN} + N_{shot} + N_{sp-sp} + N_{s-sp}} \tag{3.26}$$

Substituting in (3.6) and (3.25) results in SNR as a function of input power:

$$\mathrm{SNR} = \frac{\eta_d k_f [P_i G_{ff} L_f A_2 L_s r]^2}{N_{th} + N_{RIN} + N_{shot} + N_{sp-sp} + N_{s-sp}} \tag{3.27}$$

The dispersion factor η_d decreases with increasing distance due to an accompanying increase in dispersion. Therefore, to maintain the same SNR (and consequently the same BER), the receiver input power must be increased. This impacts the operating conditions of the EDFA and the setting of A_2, which in turn affect the net signal power. With the exception of thermal noise, all of the noise terms are also affected by these changes. As long as the increase in signal power for an increase in receiver input power is larger than the corresponding increase in noise power, the original 0 km SNR and BER can be obtained. For a particular distance, then, the increase in input power required to maintain a particular SNR for a 10^{-9} BER compared to the required input power at 0 km now provides a dispersion penalty measurement since it indicates the increase in power required at the receiver to compensate for increased signal distortion. Once this measurement has been made, polarization multiplexing and demultiplexing can be introduced to measure the incremental power required to overcome additional intersymbol interference introduced by crosstalk between the polarization states.

4. Electrical Multiplexing Experiments

4.1. Scope of Experimental Work

This chapter outlines the results of experimental work that was done at BNR in Ottawa over the course of a four month internship which began in September 1992. The following discussion focuses on the most complete set of trials that were performed. Further information about these experiments and about other trials can be found in [44]. Detailed component information can be found in Appendix I.

This work centered on comparing the chromatic dispersion penalty of duobinary systems against binary systems in a 10 Gb/s electrical multiplexing environment. Chirped binary transmission was also evaluated at the same time for both binary receivers and duobinary receivers. Duobinary encoding at the receiver was of considerably more interest to BNR than duobinary encoding at the transmitter. This is because binary optical transmission formats are much easier to standardize than duobinary optical formats. Most laboratory time was therefore dedicated to binary transmission experiments that compared the relative performance of duobinary and binary receivers.

Simulations and noise analysis were completed after the term to compare results. Insufficient time was available in the laboratory to characterize the frequency response of the SHF75 amplifier, EDFAs, photodetectors, and modulator that were used. This incomplete information causes simulations results to be optimistic because the frequency response of some components has been excluded. Also, only an estimate of the predicted 10^{-9} BER input power of the receiver can be made.

4.2. Receiver Layout

Figure 4.1 shows the receiver layout that was used. It is identical to the general receiver model shown in Chapter 3, so all of the signal and noise equations defined in that Chapter directly apply. Optical gain control was used to maintain photodetector input power at a typical value around 0 dBm. The input power of the receiver is defined to be at the input of the EDFA pre-amplifier.

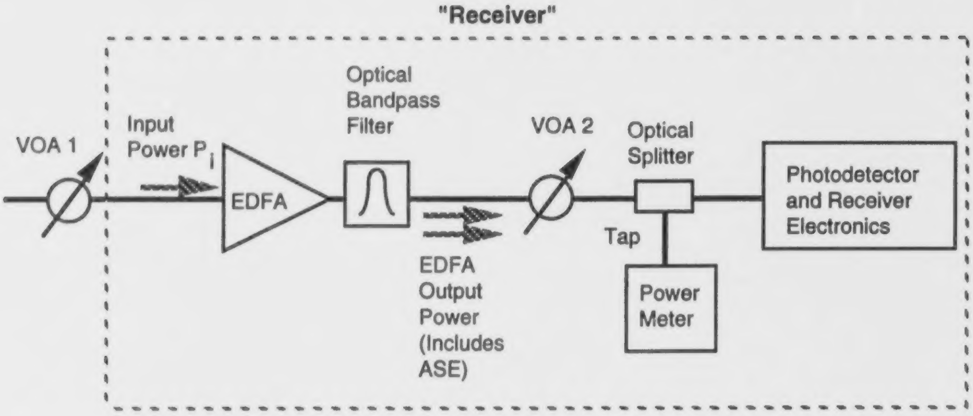
"Receiver"
VOA 1
Input
Power P_i
EDFA
Optical
Bandpass
Filter
EDFA
Output
Power
(Includes
ASE)
VOA 2
Optical
Splitter
Tap
Power
Meter
Photodetector
and Receiver
Electronics

Figure 4.1: Receiver used for Electrical Multiplexing Trials

4.3. Optical Link Layout

The optical link layouts are shown in Figure 4.2 and 4.3, while the components used within the link are shown in Table 4.1. Two EDFAs were sufficient for relatively short distance trials. Three EDFAs were required for long distance trials to overcome the attenuation caused by the extra fiber. Prototype EDFAs were used at locations EDFA 1 and EDFA 2. No characterization of these EDFAs was performed, therefore little information about their gain or noise characteristics is available. Path attenuation ensured that the EDFA pre-amplifier (EDFA 3) dominated the receiver noise. Some information is available for EDFA 3 so checks on baseline (0 km) receiver 10^{-9} BER power levels can be performed. All EDFAs used were equipped with optical isolators at their inputs and outputs to eliminate problems with back scattered ASE.

In the two EDFA links, the VOA controlling the EDFA pre-amplifier input power was placed before the fiber spool to minimize the effect of scattering caused by high power into the fiber. Only two optical filters were available for the three EDFA links. To minimize ASE into the receiver, these were located after the second EDFA and after the receiver pre-amplifier.

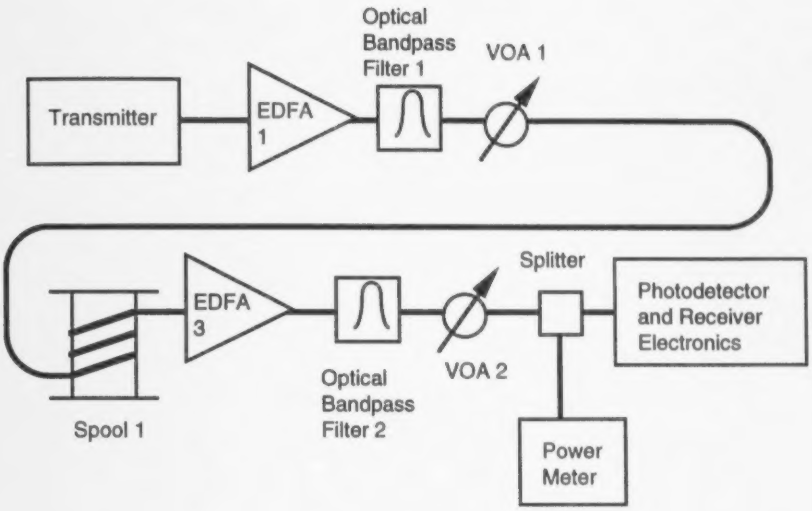
Optical
Bandpass
Filter 1
VOA 1
Transmitter
EDFA
1
EDFA
3
Splitter
Photodetector
and Receiver
Electronics
Spool 1
Optical
Bandpass
Filter 2
VOA 2
Power
Meter

Figure 4.2: Two EDFA Optical Link

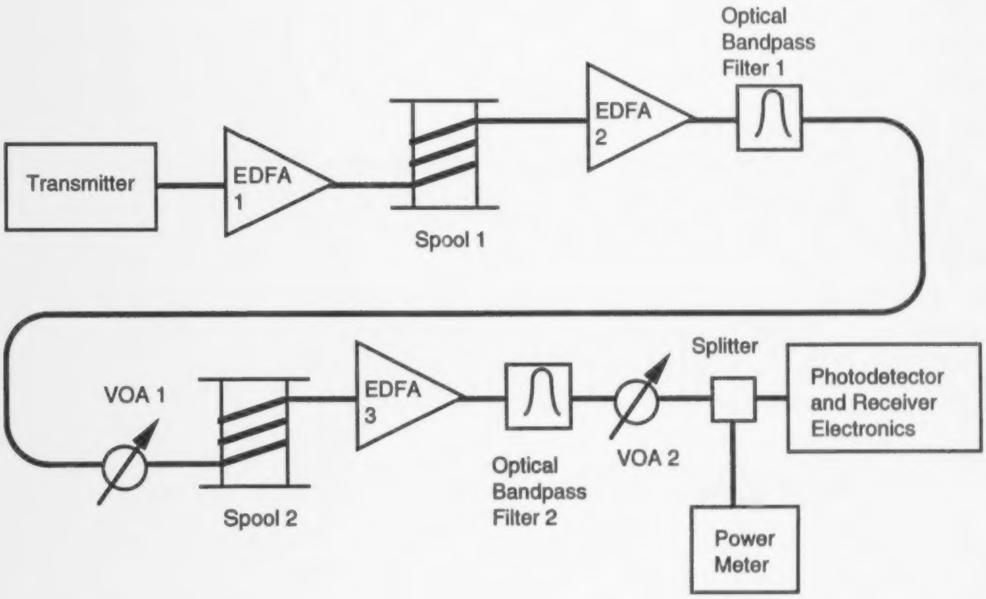
Optical
Bandpass
Filter 1
EDFA
2
Transmitter
EDFA
1
Spool 1
Splitter
VOA 1
EDFA
3
Photodetector
and Receiver
Electronics
Spool 2
Optical
Bandpass
Filter 2
VOA 2
Power
Meter

Figure 4.3: Three EDFA Optical Link

Component	Description
EDFA 1 (Post Amplifier)	Corning 2 Pump Prototype 20 dB Gain at 1538 nm
EDFA 2	Corning 1 Pump Prototype 17 dB Gain at 1538 nm
EDFA 3 (Pre-Amplifier)	Amoco 1.5-AMP-18 35 dB Gain at 1538 nm 18 dBm Max Output Power
Optical Bandpass Filter 1	JDS TB1562 1.3 nm Bandwidth
Optical Bandpass Filter 2	JDS TB3500 Scanning Optical Bandpass Filter, 1.3 nm Bandwidth
Spool 1	Up to 92 km
Spool 2	Up to 54 km

Table 4.1: Components Used in Optical Links at BNR

For long distance data points beyond the Spool 1 and Spool 2 lengths listed above, fiber spools were distributed before the pre-amplifier and after the post-amplifier. This extracted further gain out of the system by pulling the input signal below the gain saturation of the post amplifier and by replacing some of the gain control attenuation after the pre-amplifier (A_2) with fiber attenuation.

4.4. Binary Transmission with Binary Reception

4.4.1. Binary Transmitter

Figure 4.4 shows the two transmitter configurations that were used in the trials. The first was zero chirp, the second was negative chirp. A source wavelength of 1538 nm was used to capitalize on the maximum gain wavelength regime of the EDFAs. A 10 Gb/s NRZ 2^7-1 pseudo-random bit sequence (PRBS) was provided by a high speed bit error rate test set (BERT). The external modulator used at the transmitter was an AT&T m2123AB-2 Mach-Zehnder modulator with a nominal 8 GHz bandwidth. This modulator has two radio frequency (RF) inputs so that either one or two drive signals could be applied to compare zero chirp transmission with negative chirp transmission.

As discussed in Appendix B, zero chirp transmission is achieved by applying two equal and opposite drive signals to the external modulator and applying a DC bias level. A chirp parameter of -1 can be achieved by driving only one RF input of the external modulator and setting the DC bias of this signal within the negative chirp operating region of the modulator [1].

A 2^7-1 PRBS was used to evaluate the systems in all cases discussed in this Chapter. The BER of each system degraded sharply when tested with longer pattern strings. This indicated that the low frequency cut-off of some of the components was at a relatively high frequency compared to the pattern string (i.e. cutoff above 80 MHz). The prime suspects for this cut-off are the microstrip waveguides in the integrated circuits since the frequency response of most of the other components were known. There is no way to get an accurate measurement of the frequency response of these waveguides since they are connected directly to integrated circuit pins.

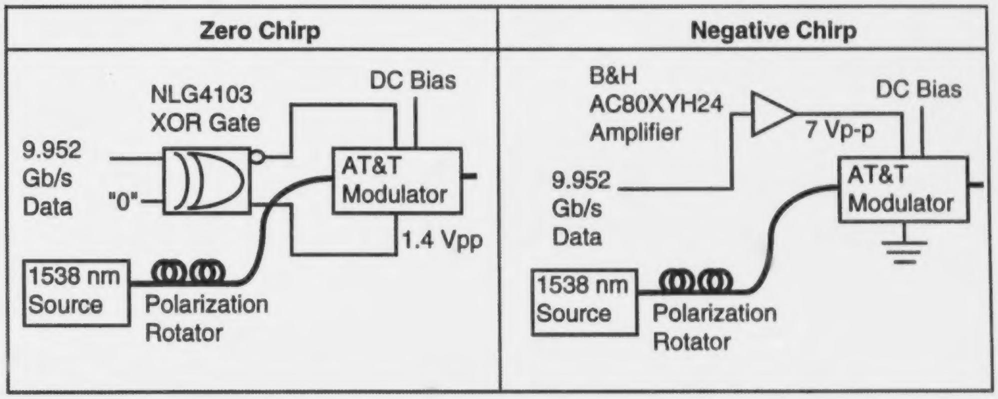
Zero Chirp
Negative Chirp
NLG4103
XOR Gate
DC Bias
9.952
Gb/s
Data
"0"
AT&T
Modulator
1.4 Vpp
1538 nm
Source
Polarization
Rotator
B&H
AC80XYH24
Amplifier
DC Bias
7 Vp-p
9.952
Gb/s
Data
AT&T
Modulator
1538 nm
Source
Polarization
Rotator

Figure 4.4: Binary Transmitter Arrangements

The zero chirp transmitter configuration used the normal and complementary outputs of an NTT Electronics (NEL) 4103 Exclusive-OR (XOR) gate. One of these 10 Gb/s (100 ps bit period) outputs is shown in Figure 4.5(a). This gate acted as an inverter and distributor since its second input was at 0 Volts (a logical "1" level for the gate). This gate produces a clean digital signal but had a peak-to-peak output voltage that was lower than the full voltage range of the modulator. The sum of the XOR gate complementary output levels was at most 2.8 Vp-p. A peak-to-peak voltage of around

7 V was required to drive the modulator fully to extinction voltage V_π and to minimize digital signal distortion. The typical extinction ratio which could be expected from this XOR gate arrangement is 4.0, providing that the drive signal is DC biased at the center of the modulator's transfer function. A higher extinction ratio was obtained by setting the DC bias point off the center of the modulator's transfer function. In general, zero chirp extinction ratios were above 9 dB. The relatively poor extinction ratios obtained from the XOR gate drive result in a DC optical power component on measuring instruments and additional noise associated with the transmitted logical "0" level.

The normal and complementary outputs from the XOR gate were not completely symmetric in amplitude nor perfectly in-phase. This slight difference results in residual chirp in the modulator which was not quantified. This is a significant problem for double drive modulator designs. Although they allow arbitrary chirp to be impressed on the signal, zero chirp transmission is not easily accomplished because it is difficult to generate two perfectly complementary RF signals.

The negative chirp configuration used a B&H amplifier with a pass band ranging from 1 kHz to around 7.6 GHz. The output of this amplifier is shown in Figure 4.5(b). The band-limiting of the B&H amplifiers caused significant signal degradation. A chirp value of +1 or -1 was achieved by driving only one RF input of the external modulator, depending on the DC bias point. It was readily apparent from observing the eye opening of the signal after any significant length of fiber whether positive chirp or negative chirp had been realized. Negative chirp causes the leading edge of the pulse to propagate through the fiber at a slower rate than the trailing edge of the pulse. This results in pulse compression and increased eye openings. Positive chirp has the opposite effect.

4.4.2. Binary Receiver

The binary receiver and its components is shown in Figure 4.6. The binary receiver was composed of a photodetector and amplifier followed by two paths: a clock recovery path and a signal path. The clock recovery path includes amplification, signal processing, and clock distribution. This extracts clock using the method discussed in Appendix L. The signal path includes amplification, signal processing, and a binary decision circuit (D flip-flop). The photodetector power levels were selected to maintain a 2 Vp-p input signal level on the D flip-flops. A DC block was located before the D flip-flop to allow a negative DC voltage to be applied to the RF signal to pull it down to the input range of the D flip-flop. The decision threshold and timing were set manually for this receiver and for all others described in this Chapter as well.

(a) XOR Gate Ouput

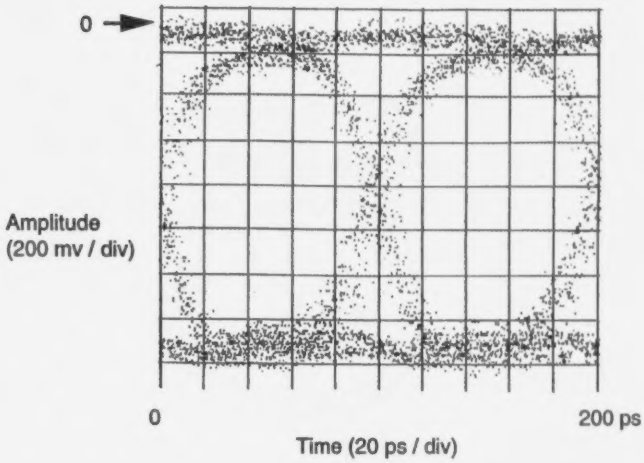

(b) B&H Amplifier Output

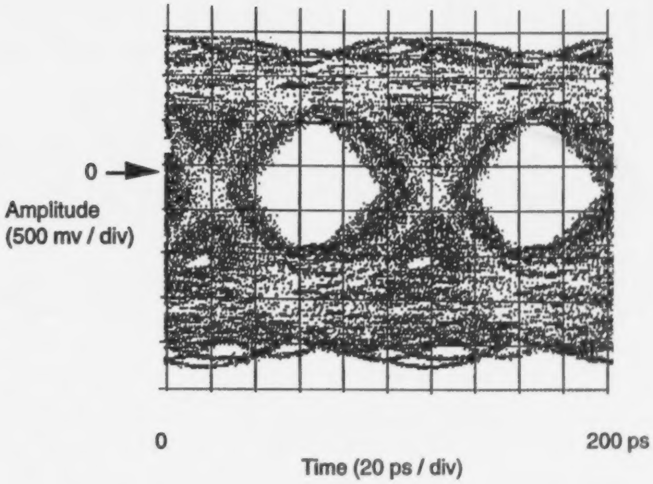

Figure 4.5: Binary Drive Signal Comparison

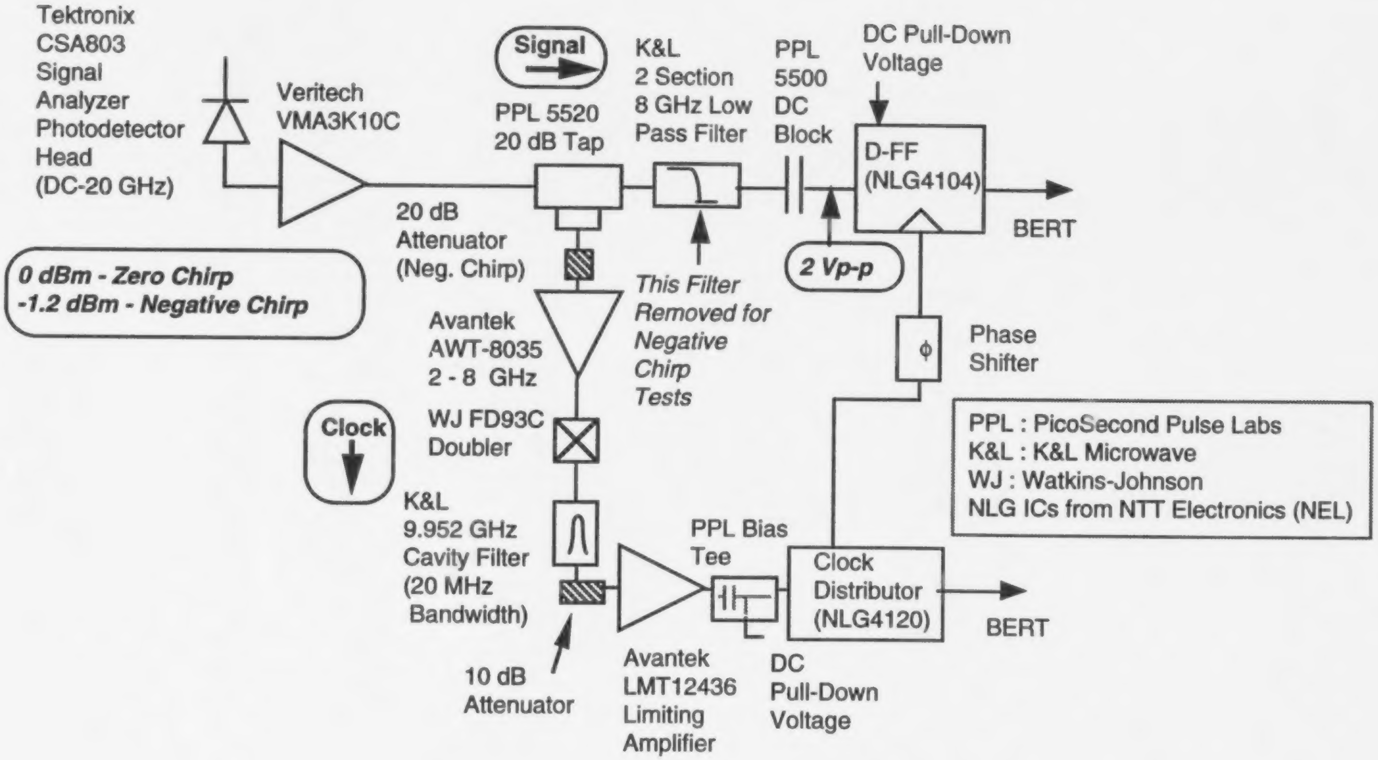
Tektronix
CSA803
Signal
Analyzer
Photodetector
Head
(DC-20 GHz)
Veritech
VMA3K10C
0 dBm - Zero Chirp
-1.2 dBm - Negative Chirp
Signal
PPL 5520
20 dB Tap
20 dB
Attenuator
(Neg. Chirp)
Avantek
AWT-8035
2 - 8 GHz
Clock
WJ FD93C
Doubler
K&L
9.952 GHz
Cavity Filter
(20 MHz
Bandwidth)
10 dB
Attenuator
K&L
2 Section
8 GHz Low
Pass Filter
This Filter
Removed for
Negative
Chirp
Tests
PPL
5500
DC
Block
2 Vp-p
DC Pull-Down
Voltage
D-FF
(NLG4104)
BERT
Phase
Shifter
ϕ
PPL : PicoSecond Pulse Labs
K&L : K&L Microwave
WJ : Watkins-Johnson
NLG ICs from NTT Electronics (NEL)
PPL Bias
Tee
Avantek
LMT12436
Limiting
Amplifier
DC
Pull-Down
Voltage
Clock
Distributor
(NLG4120)
BERT

Figure 4.6: Binary Receiver

Figure 4.7 shows zero chirp binary eye diagrams at the input to the decision circuit at 0 km and 126 km. The 126 km eye diagram was obtained from the photodetector in Figure 4.6 followed by a 6 dB attenuator and an SHF90P amplifier. This receiver path was used for the 126 km scope plot because the 15 GHz bandwidth of the SHF amplifier resulted in a larger eye opening than the 10 GHz bandwidth of the Veritech amplifier. It was not used for BER data collection because the full 32 dB gain of the Veritech amplifier was required (the SHF amplifier has only 23 dB gain). Figure 4.8 show simulated zero chirp binary eye diagrams at these distances. Figure 4.9 shows a negative chirp binary eye diagram from the same receiver used to obtain the 126 km zero chirp eye diagram. The negative chirp binary eye is more open than the zero chirp binary eye.

(a) 0 km

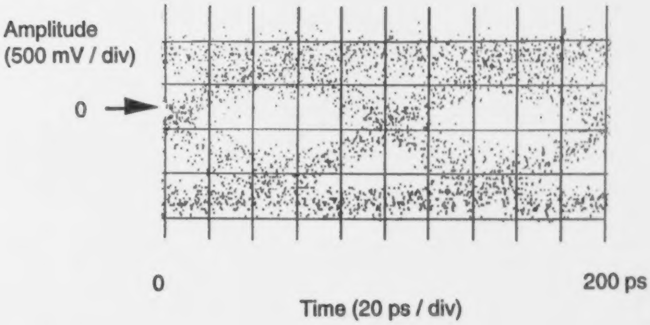

(b) 126 km (SHF90P Amplifier Output)

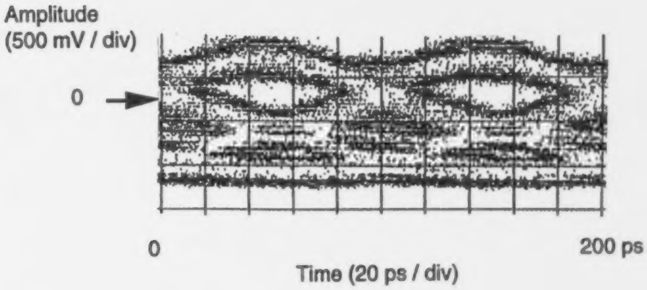

Figure 4.7: Zero Chirp Binary Eye Diagrams

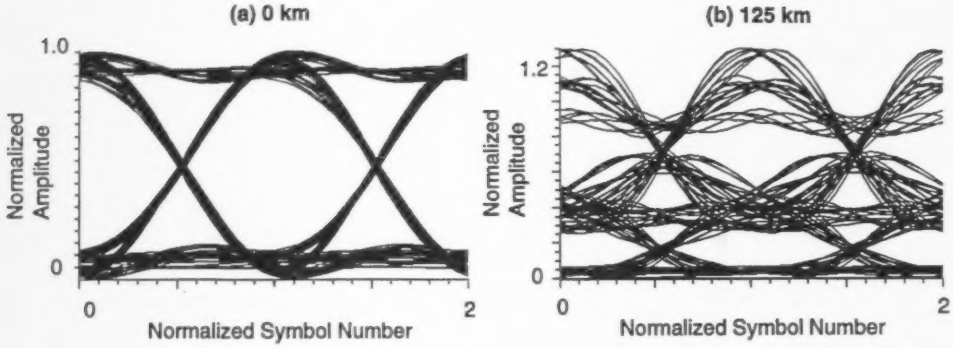

Figure 4.8: Simulated Zero Chirp Binary Eye Diagrams

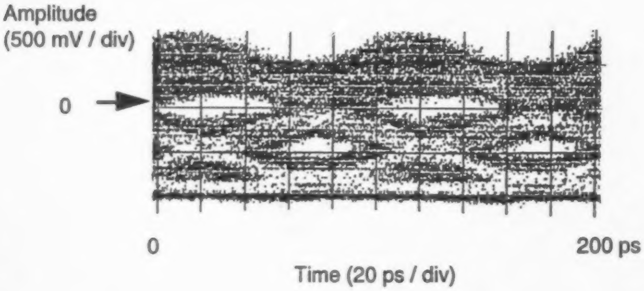

Figure 4.9: Negative Chirp Eye Diagram at 126 km

4.4.3. Predicted Receiver Sensitivity

The expected 10^{-9} BER input power can be predicted using the theory from Chapter 3. This requires ASE data for the EDFA pre-amplifier, the noise specifications of the electrical amplifiers, as well as the noise bandwidths of the receiver optical bandpass filters and the receiver electronics. Unfortunately, there was insufficient time in the laboratory at BNR to obtain data on all the parameters required in the above noise equations. However, some estimates can be made with available data to determine whether obtained baseline (0 km) receiver 10^{-9} BER power levels are reasonable. For the purposes of this calculation, the input power to the receiver can be assumed to be equivalent to the signal power at the input of the receiver. This is equivalent to assuming that the system introduced no distortion to the 10 Gb/s NRZ transmission format.

No measurements on the receiver EDFA are available, so an estimate will be made using data provided with the EDFA by the supplier (Amoco). These are presented in Appendix I. This particular amplifier has a noise figure above 9 dB for an input power less than -5 dBm. This can be approximately related to N_{sp} by [50][51]:

$$F_o \approx 2N_{sp} \tag{4.1}$$

where: F_o is the noise factor of the EDFA

This indicates that N_{sp} is greater than or equal to 4 for input powers below -5 dBm. The curve shape relating noise figure to input power indicates that N_{sp} will be much greater than 4 for input powers around -20 dBm. Also, the maximum ASE for the EDFA is 14.3 dBm for an optical bandwidth of approximately 30 nm. The bulk of this ASE at low input power is in the high gain wavelength operating region of the EDFA. This can arbitrarily be selected to be the wavelength region with a gain above 25 dB for -40 dBm input, which is has an optical bandwidth of approximately 16 nm and is centered at 1540 nm. In this region, the gain of the EDFA is on average around 35 dB. Substituting this information into (3.4) provides an N_{sp} figure of 16. An N_{sp} of 10 is therefore a reasonable estimate for the purposes of determining whether receiver 10^{-9} BER input power is in line with expectations.

The following parameters are reasonable estimates for parameters required for the noise equations in Chapter 3: T=300 K, N_{sp} = 10, r = 0.9, B_o = 165 GHz (corresponding to 1.3 nm optical bandwidth centered at 1538 nm), B_e = 8 GHz, R = 50 Ω, F= 5 (the noise factor of the SHF90P amplifier), L_f= 2 dB, and RIN = -134.5 dB/ Hz (corresponding to a real 1551 laser source at TRLabs [2]). The parameters η_i, η_o , and L_s are assumed to have a value of 1.0 (i.e. negligible loss). Figure 4.10 shows a SNR plot as a function of pre-amplifier input power using these assumptions.

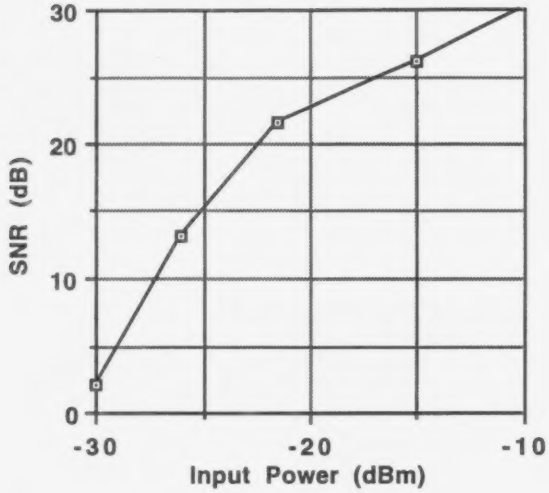

Figure 4.10: Predicted SNR

If the statistics of the noise are Gaussian and the same amount of noise is associated with a "1" as a "0", then an SNR of 15.5 dB is required at the sampling interval to achieve a BER of 10^{-9} for binary NRZ transmission and reception (see Appendix K). This point occurs in the above plot at around -25 dBm input.

4.4.4. Experimental Receiver Sensitivity

The curves showing experimental BER as a function of input power for the binary receiver are presented in Figure 4.11 and 4.12. Power limitations prohibited a full range of BER measurements for the zero chirp case at 91 km. However, a 10^{-9} BER at -15.4 dBm input power was recorded. The 0 km 10^{-9} BER power level was -24.2 dBm for zero chirp and -22.5 dBm for negative chirp. This agrees well with a predicted 10^{-9} BER input power of -25 dBm.

The data collected for negative chirp binary transmission and reception was partially for a two EDFA path and a three EDFA path. Once the third amplifier was introduced into the path, a number of measurements were repeated to check the consistency of the additional power penalty due to the extra amplifier noise. This penalty was found to be approximately 1.5 dB. The cause of this penalty is suspected to be high power-induced fiber nonlinearities at the transmit end. The output power from the EDFA post-amplifier was 7.5 dBm. This is within a power regime which results in increased noise from optical nonlinearities [52]. This 1.5 dB penalty was added to all data points collected for the two EDFA path (marked with a "*" in Figure 4.12). All data points reported in Figure 4.12 are therefore for the three EDFA configuration.

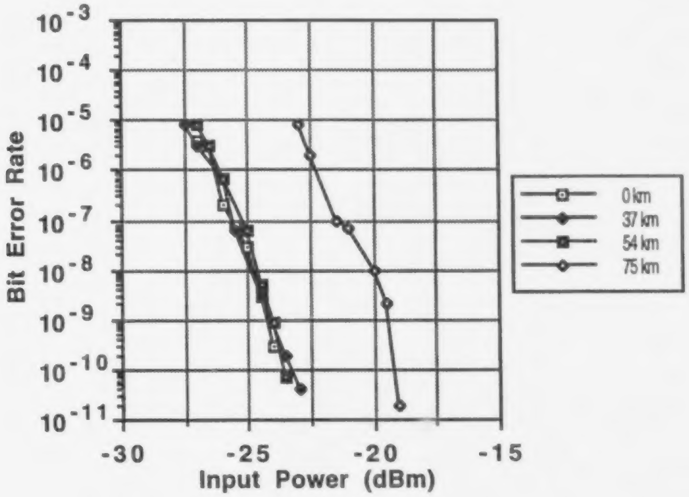

Figure 4.11: Binary Receiver BER Curves, Zero Chirp

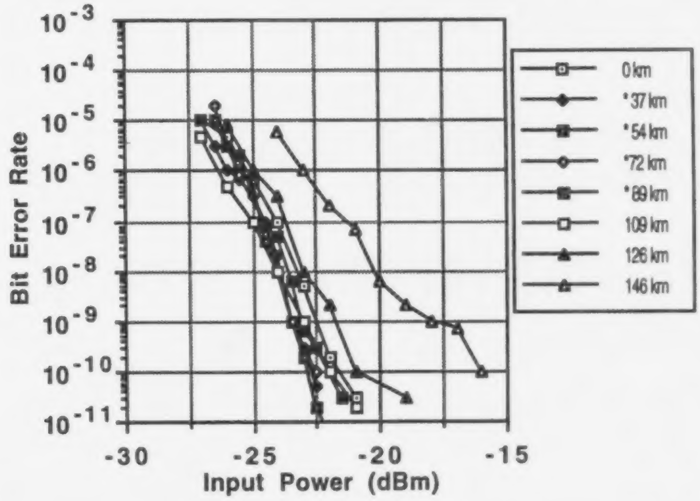

Figure 4.12: Binary Receiver BER Curves, Negative Chirp

4.5. Binary Transmission with Duobinary Reception

4.5.1. Binary Transmitter

The zero chirp and negative chirp transmitters used for the binary reception experiments were also used for these experiments.

4.5.2. Duobinary Receiver

The duobinary receiver is shown in Figure 4.13. A 6 dB splitter / combiner implementation of the duobinary delay and add circuit was used because of better lower-band performance than a Wilkinson combiner implementation and because the power budget of the receiver could compensate for the additional loss (an overview of possible implementations is presented in Appendix H). A broadband coaxial line stretcher was added into the circuit to allow the spectral null of the delay and add circuit to be shifted. Typically it was located around 5.2 GHz. Small decreases (up to 15 - 20 ps) in the delay had little appreciable effect on the duobinary eye openings. The photodetector power levels were selected to maintain a 2 Vp-p signal level on the D flip-flops.

The combination of the two D flip-flops and the XOR gate make up a ternary decision circuit which allows the duobinary symbols to be converted back into binary information, provided it is precoded in advance (Appendix M). Fortunately, a 2^7-1 PRBS is identical to a precoded sequence shifted by 6 positions, so precoding was not required (a proof for this property can be found in Appendix N).

It was necessary to modify the clock recovery path for negative chirp transmission beyond 120 km. At these distances, the standard clock recovery circuit produced a noisy tone which adversely affected BER. This was most likely a result of a reduction in the frequency content of the signal used by the clock recovery circuit because of dispersion-induced pulse broadening. As discussed in Appendix L, the clock tone amplitude is proportional to the frequency content of the signal around 5 GHz. This frequency content is reduced as the signal pulses broaden. The duobinary receiver with a modified clock recovery path is shown in Figure 4.14.

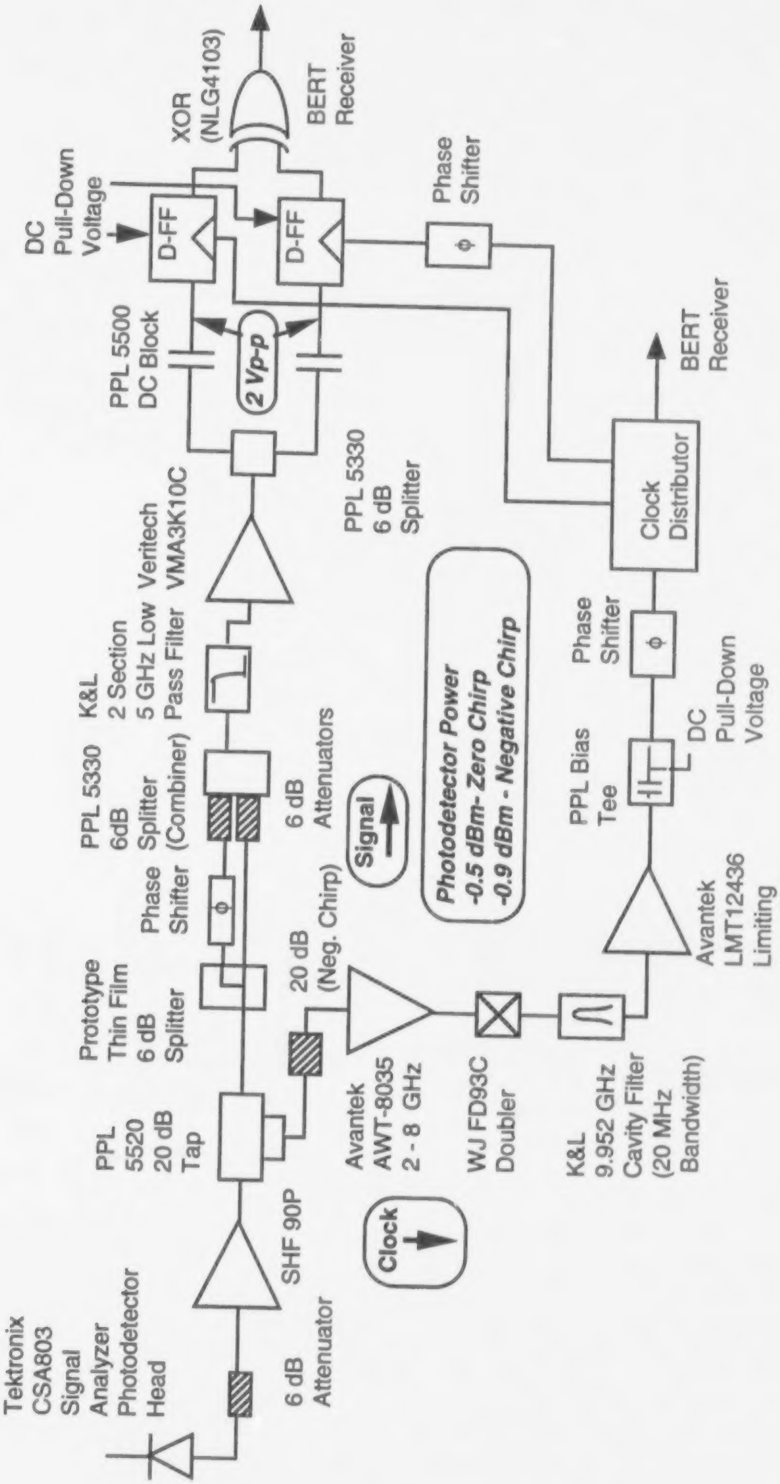
Tektronix CSA803 Signal Analyzer Photodetector Head
6 dB Attenuator
SHF 90P
PPL 5520 20 dB Tap
Prototype Thin Film 6 dB Splitter
Phase Shifter
PPL 5330 6dB Splitter (Combiner)
6 dB Attenuators
K&L 2 Section 5 GHz Low Pass Filter
Veritech VMA3K10C
PPL 5330 6 dB Splitter
PPL 5500 DC Block
2 Vp-p
DC Pull-Down Voltage
D-FF
D-FF
XOR (NLG4103)
BERT Receiver
Phase Shifter
Clock
Avantek AWT-8035 2 - 8 GHz
20 dB (Neg. Chirp)
Signal
Photodetector Power
-0.5 dBm- Zero Chirp
-0.9 dBm - Negative Chirp
WJ FD93C Doubler
K&L 9.952 GHz Cavity Filter (20 MHz Bandwidth)
Avantek LMT12436 Limiting Amplifier
PPL Bias Tee
DC Pull-Down Voltage
Phase Shifter
Clock Distributor
BERT Receiver

Figure 4.13: Duobinary Receiver

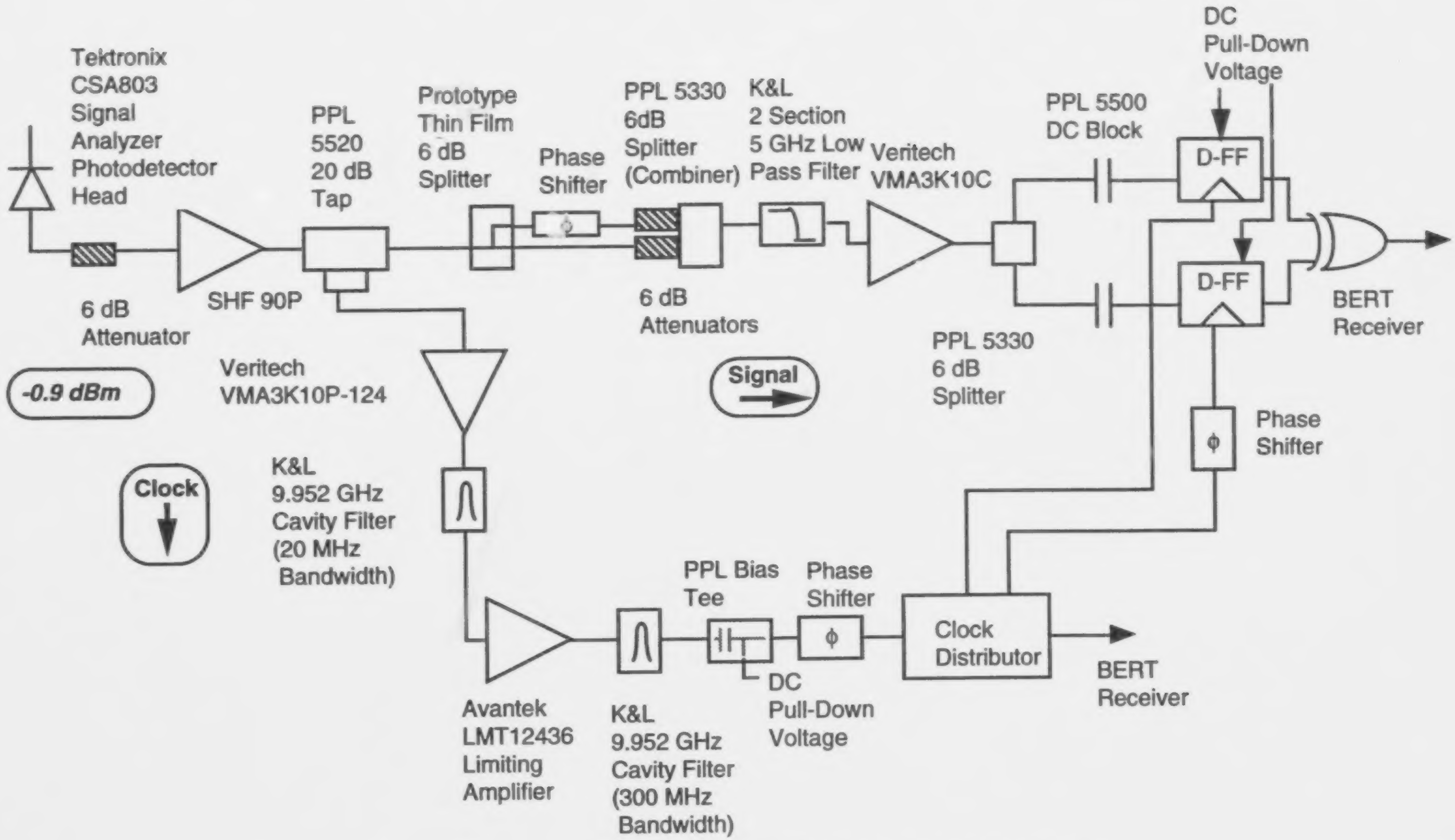
Tektronix
CSA803
Signal
Analyzer
Photodetector
Head
6 dB
Attenuator
-0.9 dBm
SHF 90P
PPL
5520
20 dB
Tap
Veritech
VMA3K10P-124
Clock
K&L
9.952 GHz
Cavity Filter
(20 MHz
Bandwidth)
Prototype
Thin Film
6 dB
Splitter
Phase
Shifter
PPL 5330
6dB
Splitter
(Combiner)
6 dB
Attenuators
K&L
2 Section
5 GHz Low
Pass Filter
Signal
Veritech
VMA3K10C
PPL 5330
6 dB
Splitter
PPL 5500
DC Block
DC
Pull-Down
Voltage
D-FF
D-FF
BERT
Receiver
Phase
Shifter
ϕ
Avantek
LMT12436
Limiting
Amplifier
K&L
9.952 GHz
Cavity Filter
(300 MHz
Bandwidth)
PPL Bias
Tee
DC
Pull-Down
Voltage
Phase
Shifter
ϕ
Clock
Distributor
BERT
Receiver

Figure 4.14: Duobinary Receiver with Modified Clock Recovery Circuit

The modified clock recovery path extracted the inherent 10 GHz tone in the received signal by passing the signal through successive stages of amplification and band pass filters. Note that no modification to the clock recovery circuit was required for zero chirp transmission. This is due to the difference in transmitter bandwidth. The output from the negative chirp transmitter (B&H amplifier) had less frequency content above 5 GHz than the output from the zero chirp transmitter (XOR gate).

Tuning the duobinary receiver was complex due to the numerous parameters involved. The appropriate sampling time for the individual decision circuits must be set. The clock tone must be high quality, or it will affect sampling points and BER. Also, DC offsets must be applied to the signal and then each decision threshold must be set. Because all of these variables can affect the receiver BER performance, multiple tuning iterations were required to ensure that the BER versus input power corresponded to the absolute minimum power into the receiver. Data points were repeated and the receiver was re-tuned at intervals to increase confidence in readings. Also, the shape of the obtained BER curve was checked for consistency with other BER curves for the duobinary receiver. The procedure used to tune the duobinary receiver is described in detail in Appendix O.

Figure 4.15 shows the 126 km zero chirp duobinary eye diagram at the output of the Veritech amplifier. Figure 4.16 shows simulated eye diagrams for the zero chirp duobinary case. Figure 4.17 shows the 126 km negative chirp duobinary eye diagram at the output of the Veritech amplifier.

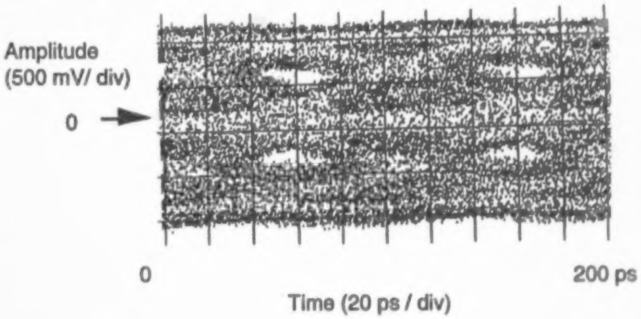

Figure 4.15: Zero Chirp Duobinary Eye Diagram at 126 km

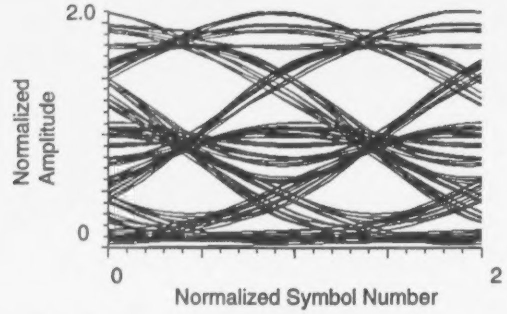

Figure 4.16: Simulated Zero Chirp Duobinary Eye Diagram at 125 km

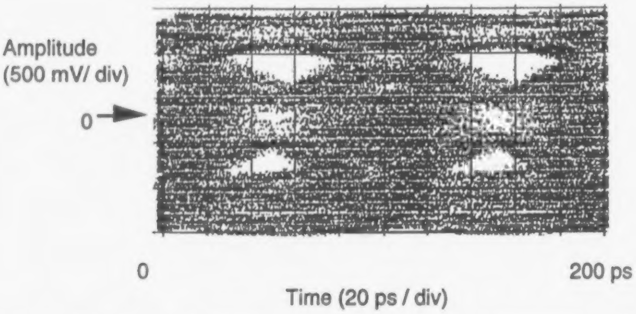

Figure 4.17: Negative Chirp Duobinary Eye Diagram at 126 km

4.5.3. Experimental Receiver Sensitivity

The BER curves for the zero chirp and negative chirp trials are shown in Figures 4.18 and 4.19 respectively. The input power for 10^{-9} BER was -22.5 dBm for zero chirp transmission and -20.3 dBm for negative chirp transmission. These 10^{-9} BER power levels differ from their corresponding binary receiver power levels by a factor of about 2 dB. This is in line with the factor between 1.5 dB and 3 dB that was expected (Appendix K).

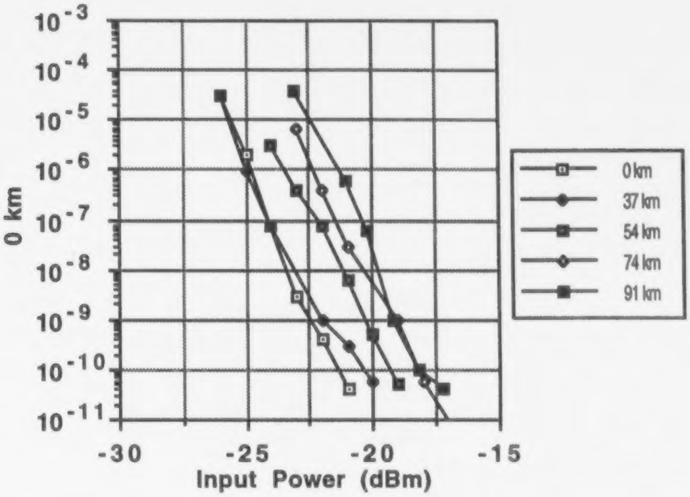

Figure 4.18: Duobinary Receiver BER Curves, Zero Chirp

Power budget limitations in the zero chirp case prohibited collection of a BER curve at 126 km. However, an $8 * 10^{-8}$ BER point was recorded at an input power of -18.7 dBm. A good estimate of the 10^{-9} BER input power is around -16 dBm, considering the typical shape of the BER curves in Figure 4.18.

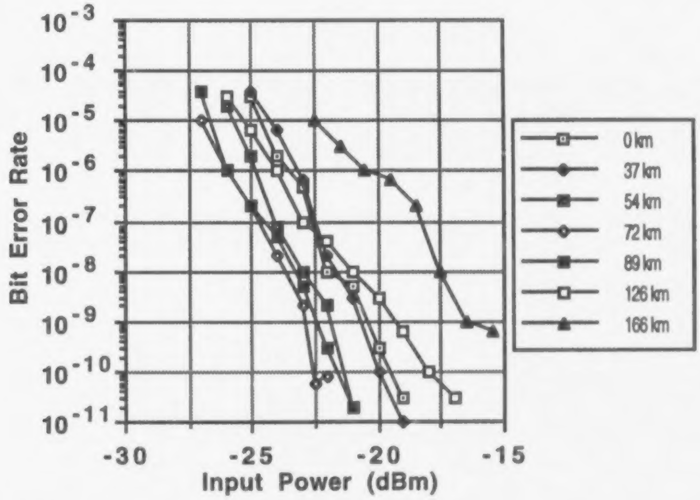

Figure 4.19: Duobinary Receiver BER Curves, Negative Chirp

4.6. Duobinary Transmission

Duobinary transmission experiments were a lower priority over the course of the work term. The systems could not be fine-tuned well enough to collect BER data in the time that was available. Therefore, only qualitative results were obtained. Two trials were performed and are described below.

4.6.1. Trial 1

The transmitter was configured as shown in Figure 4.20. The duobinary filter implementation was a 6 dB splitter / Wilkinson combiner arrangement (described in Appendix H). This filter had a sufficiently clean frequency response to be used successfully for other 10 Gb/s duobinary reception trials that are reported in [44]. The receiver consisted of an HP 83440C DC-20 GHz photodetector followed by a PPL 5520 scope probe, a Veritech VMA3K10C amplifier, and a PPL 5330 6 dB splitter. The receiver output was monitored at one output of the 6 dB splitter while the other output was terminated with a matched impedance load to prevent reflections. The received optical signal was so distorted that BER measurements could not be made, even for a back-to-back optical path.

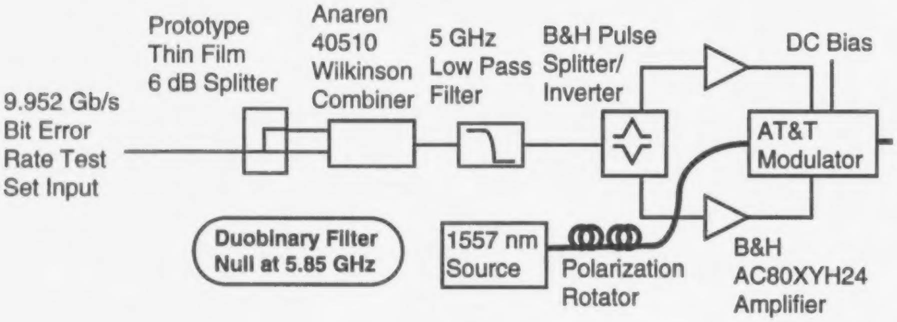
9.952 Gb/s
Bit Error
Rate Test
Set Input
Prototype
Thin Film
6 dB Splitter
Anaren
40510
Wilkinson
Combiner
5 GHz
Low Pass
Filter
B&H Pulse
Splitter/
Inverter
DC Bias
AT&T
Modulator
Duobinary Filter
Null at 5.85 GHz
1557 nm
Source
Polarization
Rotator
B&H
AC80XYH24
Amplifier

Figure 4.20: Trial 1 Duobinary Transmitter Configuration

Even the electrical driving signal of the modulator was highly distorted. An eye diagram of this driving signal is shown in Figure 4.21 for 9.6 Gb/s, which was the bit rate which produced the best quality output. Its quality was only marginally better than 10 Gb/s transmitted signal. It was not possible to register a BER at the receiver, even at 9.6 Gb/s.

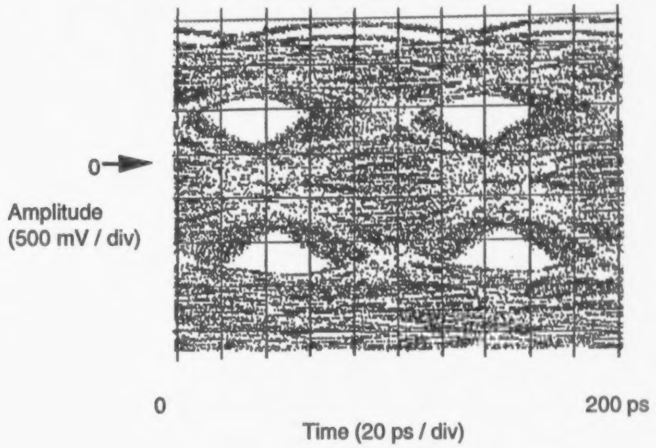
(a) B&H Amplifier Ouput

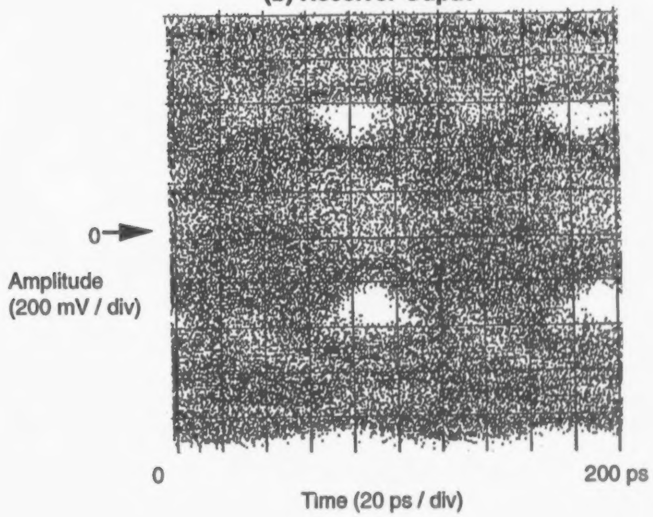
(b) Receiver Ouput

Figure 4.21: Trial 1 Transmitted Duobinary Signal

Figure 4.22 shows a simulated eye diagram for the same setup at 10 Gb/s. The eye openings in the simulated waveform are larger than found in the real results. This discrepancy occurs because the modulator frequency response roll-off was not perfectly modeled. Also, the quality of the signal from the output of the B&H amplifier is higher in the simulation that in the real case, possibly because the simulator did not account for group delay variations. The simulator worked with almost a perfect extinction ratio which cause significant pulse compression at the signal edges. This is not evident in the actual waveform, which may also partially account for the quality difference.

The simulator output and the oscilloscope trace are in agreement on the amount of pattern sensitivity shown in the eye diagram. In both, there are very apparent individual traces in the signal. This shows up as single lines in the simulated waveforms, and a fuzzier eye diagram on the oscilloscope (since this trace is sampled by the oscilloscope less often than others).

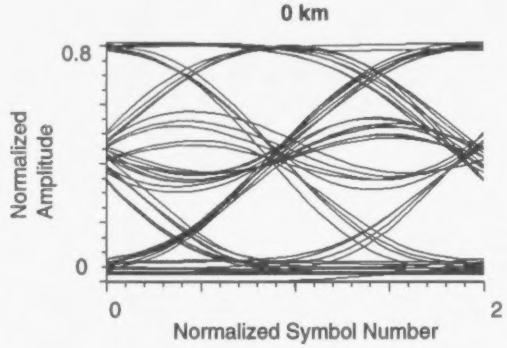

Figure 4.22: Trial 1 Simulated Transmitted Duobinary Signal

The clock recovery circuit used for the majority of trials was designed for binary transmission. It was uncertain whether it would work for duobinary transmission, because 10 Gb/s duobinary signals have a null at 5 GHz, not at 10 GHz as the binary signal does. The existence of clock tone was checked at various distance intervals in this trial. It was found that a clean tone existed up to 126 km. This indicates that there was a high degree of spectral content in the baseband signal above 5 GHz, contrary to what should have been there after the signal was filtered and band limited at the transmitter.

4.6.2. Trial 2

It was suspected that the poor results from Trial 1 were caused by high distortion in the combination of the B&H amplifiers and the duobinary filter. Attempts were made to clean up this driving signal by using a custom SHF75 amplifier, which has a broader bandwidth (a 9 GHz high frequency cut off compared to 7.6 GHz for the B&H amplifiers). Since only one of these amplifiers was available, the modulator was driven in a negative chirp configuration. Figure 4.23 shows the driving circuit. The receiver that was used consisted only of the DC - 20 GHz photodetector head from a Tektronix CSA803 Signal Analyzer.

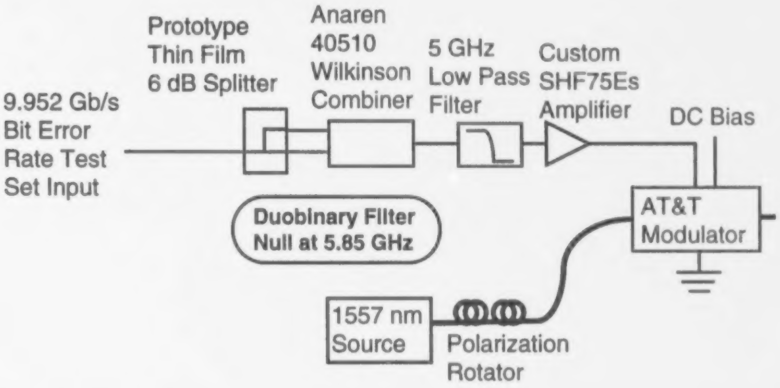
9.952 Gb/s
Bit Error
Rate Test
Set Input
Prototype
Thin Film
6 dB Splitter
Anaren
40510
Wilkinson
Combiner
5 GHz
Low Pass
Filter
Custom
SHF75Es
Amplifier
DC Bias
Duobinary Filter
Null at 5.85 GHz
AT&T
Modulator
1557 nm
Source
Polarization
Rotator

Figure 4.23: Trial 2 Duobinary Transmitter Configuration

Again, the optical duobinary eye was considerably distorted. Changes to modulator drive levels and DC bias points within the operating region of the modulator did not have an appreciable affect on the modulator's performance. Figure 4.24 shows typical eye diagrams. Because of time constraints, no attempts were made to input this signal into a duobinary receiver. Figure 4.25 shows simulated eye diagrams for the same setup. As with Trial 1, the simulator was very optimistic about signal quality.

(a) SHF75 Amplifier Output

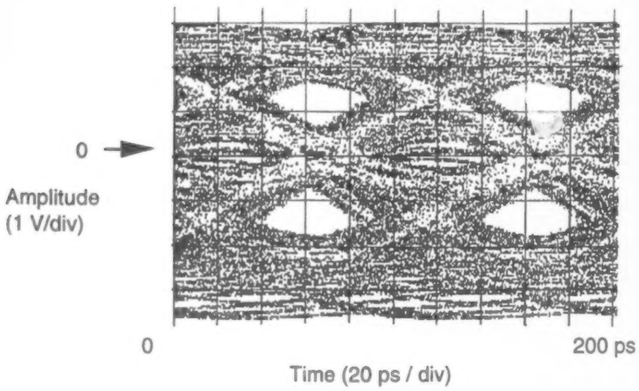

(b) Photodetector Ouput

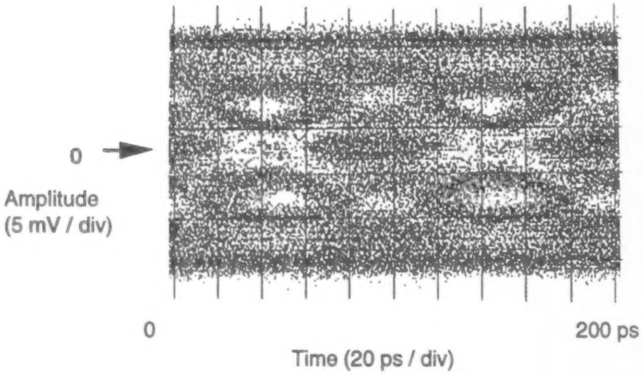

Figure 4.24: Trial 2 Transmitted Duobinary Signal

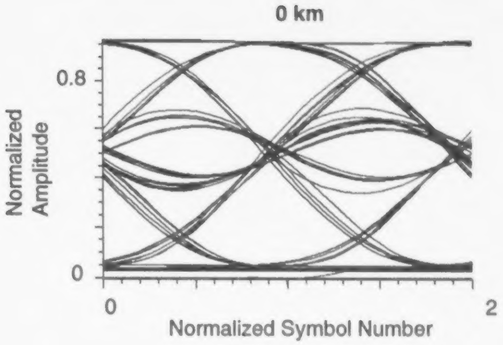

Figure 4.25: Simulated Trial 2 Transmitted Duobinary Signal

4.7. Evaluation of Results

BER data were only collected for binary transmission. Both binary reception and duobinary reception were tested extensively. The most meaningful way to interpret all of the data is to plot the required 10^{-9} BER input power as a chromatic dispersion penalty, starting with a 0 dB baseline at 0 km. The fixed differences in 10^{-9} BER input power levels between the options are less important because the EDFAs provide ample power. The increase in power required to maintain a 10^{-9} BER is more important because it provides a quantitative measure of the severity of intersymbol interference.

4.7.1. Binary Transmission with Binary Reception

The dispersion penalty as a function of distance for zero chirp and negative chirp binary transmission are shown in Figure 4.26. Negative chirp transmission provided a substantial increase in transmission distance. Baseline 10^{-9} BER receiver power levels were -24.2 dBm for the zero chirp binary receiver and -22.5 dBm for the negative chirp binary receiver. Negative chirp transmission clearly reduces the impact of chromatic dispersion compared to zero chirp transmission. For example, it results in about twice the transmission distance when 3 dB dispersion penalty points are compared (66 km distance for zero chirp transmission compared to 138 km for negative chirp transmission).

For comparison, results from [28] for a simulated Avalanche Photodiode (APD) receiver have also been included in Figure 4.26. Since the simulated receiver configuration is different from the experimental receiver, fixed offsets in 10^{-9} BER input power are expected and are present. The 10^{-9} BER receiver power for the simulated zero chirp receiver and the simulated negative chirp receiver is around -30.2 dBm. The zero chirp binary dispersion penalty agrees well with the simulated results up to 60 km. Beyond 60 km, the binary experimental data are significantly more dispersion limited than the simulated data. This performance degradation is likely caused by residual positive chirp in the modulator due to the off-center bias setting of the modulator as well as imbalances in the modulator drive signal. This could unfavorably broaden the spectrum of the signal and result in additional chromatic dispersion-induced eye closure. The negative chirp results agree well with the simulated results. Only one input to the modulator is driven in this case, so modulator drive asymmetries are not an issue. Therefore similar operating conditions to the simulated case were ensured.

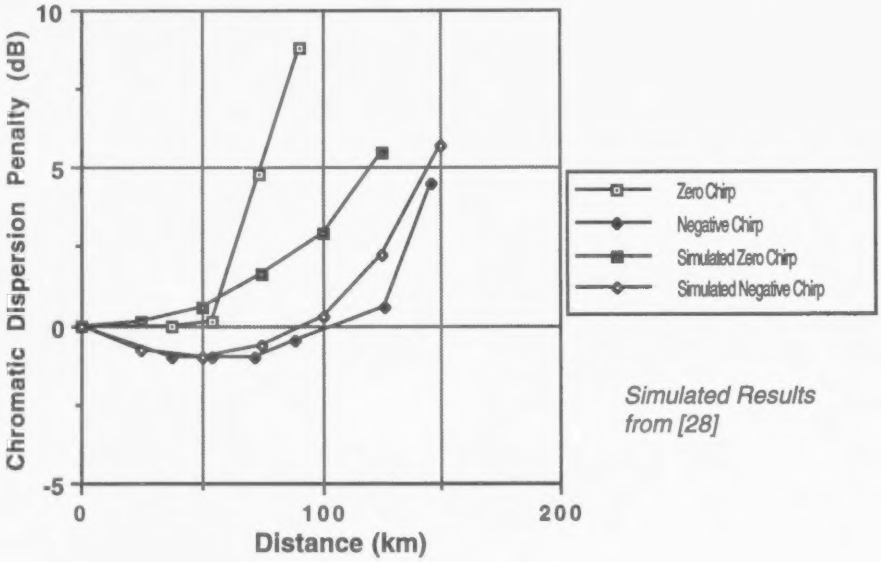

Figure 4.26: Binary Reception Comparisons

4.7.2. Binary Transmission with Duobinary Reception

Plots of duobinary receiver dispersion penalty for a 10^{-9} BER are presented in Figure 4.27. 0 km 10^{-9} BER input power levels were -22.5 dBm for the zero chirp duobinary case and -20.3 dBm for the negative chirp duobinary case. Negative chirp transmission results in more than double the transmission distance compared to zero chirp transmission when 3 dB dispersion penalties are used as a benchmark (68 km distance for zero chirp transmission compared to 156 km for negative chirp transmission).

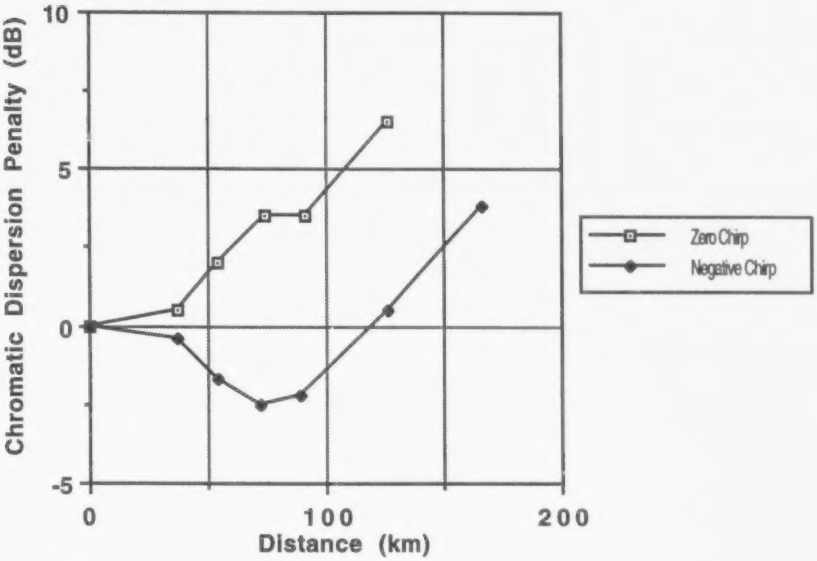

Figure 4.27: Duobinary Reception Comparisons

4.7.3. Comparison of Binary Reception with Duobinary Reception

A plot of all binary transmission results is shown in Figure 4.28. The change in chromatic dispersion penalty with distance is comparable when the binary and duobinary receivers are compared on a zero chirp basis and then on a negative chirp basis. The key difference is the rate of increase of the penalty at extreme distances. The duobinary receivers consistently have a slower growth in dispersion penalty with distance at these extremes. This is evident at a dispersion penalty higher than 2.8 dB for zero chirp transmission and higher than 0.6 dB for negative chirp transmission. The zero chirp transmission distances at the 3 dB dispersion penalty point for each receiver are essentially the same. If a 5 dB dispersion penalty point is compared, then the zero chirp transmission distance for the duobinary receiver (108 km) is significantly further than the zero chirp transmission distance (75 km) for the binary receiver. This represents a 44 % gain in transmission distance. A comparison of 3 dB dispersion penalty distances for negative chirp transmission shows a meaningful increase in achievable distance for the duobinary receiver. Its transmission distance is 18 km or 13 % further than the negative chirp transmission distance for the binary receiver.

This more rapid increase in dispersion penalty with increasing distance for a binary receiver indicates that it will have a signal that is completely corrupted by intersymbol interference at a shorter distance than the identical signal processed by a duobinary receiver. This agrees with numerous scope traces and simulation plots which show eye closure in binary received signals at long distances and eye openings in duobinary received signals for the same distance. This is an important result, since EDFAs usually can provide the gain necessary to improve SNR, but can not be used to overcome complete signal corruption caused by high intersymbol interference.

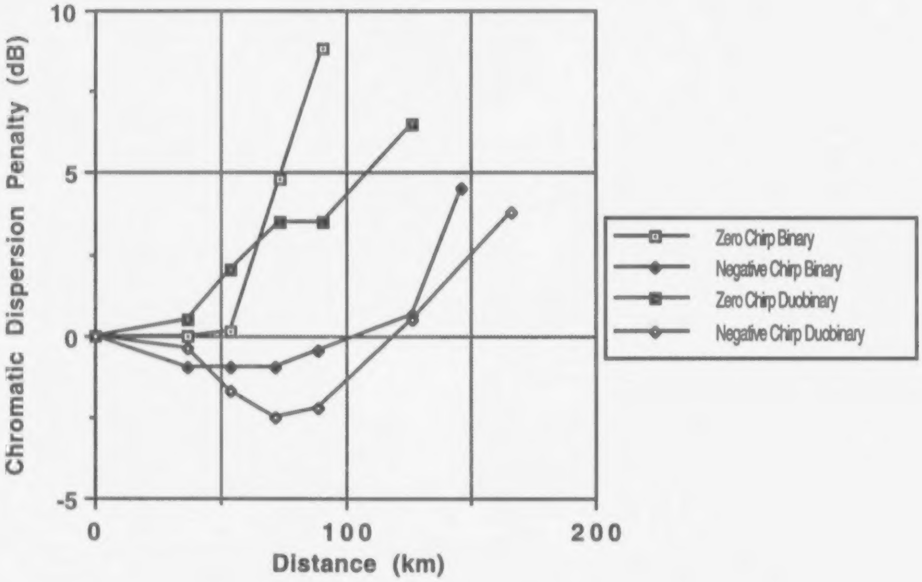

Figure 4.28: Binary Reception versus Duobinary Reception

4.7.4. Duobinary Transmission

Duobinary transmission of sufficient quality to make BER readings was not accomplished. There was simply too much distortion in the transmitter path to provide clean ternary symbols for the duobinary decision circuit. The major contributor of distortion is suspected to be the nonlinear (squared cosine) transfer function of the modulator. This tends to compress signal variation at the extreme limits of the modulator and increase it in the center driving range of the modulator. This problem will be studied in more depth in Chapter 5.

5. Optical Time Division Multiplexing Experiments

5.1. Scope of Experimental Work

This Chapter focuses on OTDM techniques that can reduce the impact of chromatic dispersion. This work was performed at TRLabs so many of the components that were used differ from those used in the electrical multiplexing experiments described in Chapter 4. As with the electrical multiplexing trials, three principal transmitter and receiver configurations were tested: binary transmission with binary reception, binary transmission with duobinary reception, and duobinary transmission with duobinary reception. The change in receiver power required for a 10^{-9} BER provides a quantitative measure of chromatic dispersion penalty. The OTDM architecture also permitted polarization multiplexing and demultiplexing to be evaluated.

5.2. Receiver Layout

The receiver arrangement that was used is shown in Figure 5.1. The photodetector and receiver electronics could perform signal processing on the entire signal stream generated by the OTDM. Another option presented by this receiver was to include an optical demultiplexing stage before the photodetector and receiver electronics to evaluate the benefits of optical demultiplexing and lower speed signal processing. This optical demultiplexing stage will be described in more detail in Section 5.5.

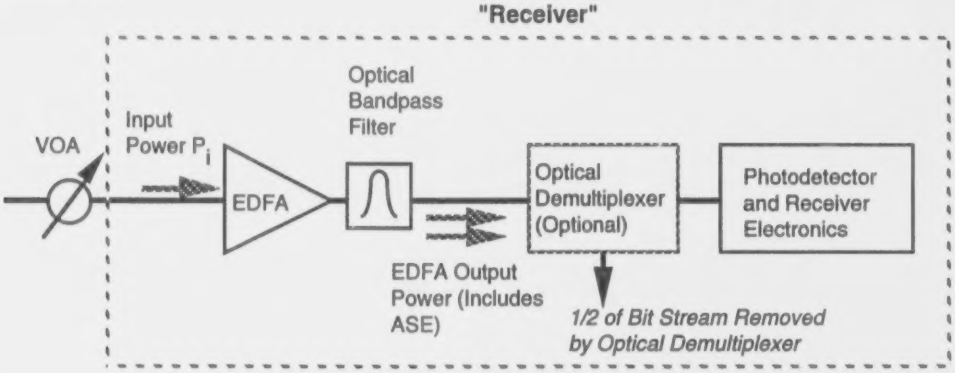
"Receiver"
VOA
Input Power P_i
EDFA
Optical Bandpass Filter
Optical Demultiplexer (Optional)
Photodetector and Receiver Electronics
EDFA Output Power (Includes ASE)
1/2 of Bit Stream Removed by Optical Demultiplexer

Figure 5.1 Receiver Used for OTDM Trials

This receiver is similar to that used for electrical multiplexing experiments. A key difference was that a VOA for gain control was not included between the EDFA pre-amplifier and the photodetector, therefore the signal amplitude varied with changing input power. The EDFA was operated with constant pump power. This resulted in its gain ranging from a small signal to a saturated regime, depending on the input power level. Changes in input power also changed the SNR and corresponding BER at the receiver. This configuration was used because the optical signal and ASE power levels from the EDFA pre-amplifier were sufficiently low that they did not require attenuation before the photodetector. The interpretation of chromatic dispersion penalty does not change with this procedure. Thermal noise in the receiver is now more significant because of the lower optical power level at the photodetector.

5.3. OTDM Layout

The basic operation of the OTDM is discussed in Appendix C. Figure 5.2 presents this OTDM with the components that were used. Component descriptions are provided in Appendix I.

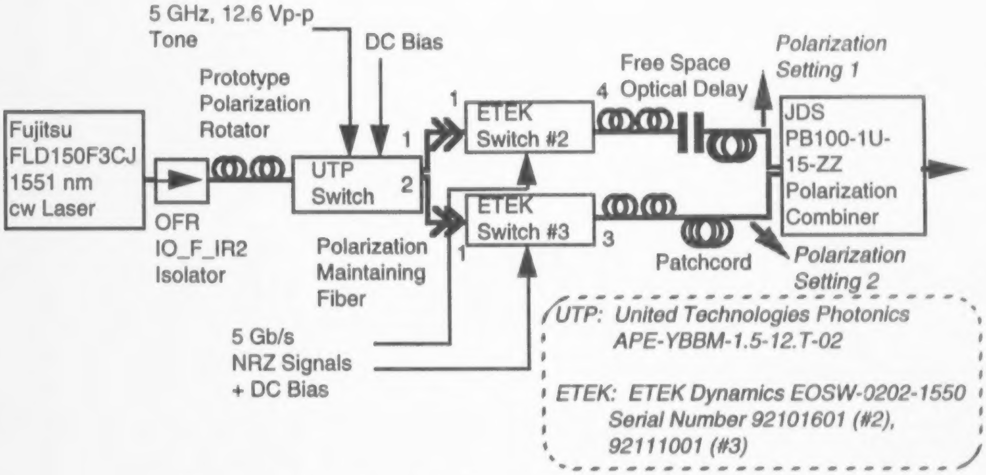
5 GHz, 12.6 Vp-p
Tone
DC Bias
Prototype
Polarization
Rotator
Fujitsu
FLD150F3CJ
1551 nm
cw Laser
OFR
IO_F_IR2
Isolator
UTP
Switch
1
2
Polarization
Maintaining
Fiber
1
ETEK
Switch #2
1
ETEK
Switch #3
4
3
Free Space
Optical Delay
Patchcord
Polarization
Setting 1
Polarization
Setting 2
JDS
PB100-1U-
15-ZZ
Polarization
Combiner
5 Gb/s
NRZ Signals
+ DC Bias
UTP: United Technologies Photonics
APE-YBBM-1.5-12.T-02
ETEK: ETEK Dynamics EOSW-0202-1550
Serial Number 92101601 (#2),
92111001 (#3)

Figure 5.2: Optical Time Division Multiplexer

The continuous 1551 nm light source was a Fujitsu distributed feedback laser with an output power of +6 dBm. This laser source was followed by an OFR polarization independent isolator to minimize linewidth broadening due to reflections. The linewidth of the laser when followed by the isolator was measured to be approximately 150 MHz [2]. This was well below the ultimate information bandwidth that was impressed on this carrier. A polarization rotator followed the isolator to set the light polarization to the axis required by the electro-optic switches for maximum extinction. The insertion loss of the isolator was around 2 dB and the insertion loss of the polarization rotator was around 1 dB. The continuous optical power into the first switching stage was therefore 3 dBm.

The next stage of the OTDM was an electro-optic switch which was used to distribute alternating light pulses between its outputs. A United Technology Photonics (UTP) 1x2 Switch was used for this application. A 5 GHz sinusoidal tone near the maximum input power of the switch (27 dBm) was used to drive the switch close to maximum extinction. This drive signal resulted in an on-off waveform that resembled 5 Gb/s RZ optical pulses at each switch output. The insertion loss of the switch at DC was 4.5 dB for the top output (Output 1) and 5.0 dB for the bottom output (Output 2) [2]. This switch was connected directly to the adjacent switches with the polarization maintaining fiber pigtails of the devices.

The 5 Gb/s RZ pulses were then modulated using ETEK Dynamics 2x2 electro-optic switches. The DC insertion loss through the ports used in ETEK switch #2 is 5.6 dB and through the ports used in ETEK switch #3 is 7.1 dB [2]. The drive signals on the switches were around 8 Vp-p to drive them close to maximum extinction. These switches were followed by polarization rotators that align the signals into the orthogonal states of a polarization multiplexer.

Phasing of the two independent 5 Gb/s RZ pulse streams was then set so that they could be interleaved. Fiber patchcords followed the rotators to act as coarse optical delay adjustment. Since it is difficult to cut fiber precisely to length to perfectly phase the pulses, a variable optical delay adjustment was also included in the path through ETEK switch #2. This consisted of pigtailed SELFOC® lenses mounted on precision axis rotators and XYZ positioners. This free space optical delay was also used as a variable optical attenuator by introducing slight misalignment between the lenses. A minimum through loss of 1 dB could be achieved with this arrangement.

The two 5 Gb/s modulated RZ pulse streams were then interleaved with a polarization multiplexer. The polarization multiplexer combined two orthogonal polarized signals with an insertion loss of around 0.4 dB. Other coupling methods could be envisioned here. One is to introduce another electro-optic switch driven by a 5 GHz sinusoid to reverse the function of the UTP switch (active recombination). Another option is to use a passive coupler that is not polarization sensitive. Polarization multiplexing has three main advantages over these other methods. The first advantage is that the polarization multiplexer has a relatively low insertion loss. Secondly, the optical signals are in orthogonal polarization states that present an opportunity to use polarization-sensitive optical demultiplexing at the receiver. Finally, polarization multiplexing effectively eliminates random fluctuations in the signal caused by quasi-coherent addition of two pulses originating from the same optical source.

Quasi-coherent addition occurs when light originating from the same source is recombined with a path length difference between the two signals that is not within the source's coherence length. If this difference in path length is not significantly longer than the coherence length, then the phase components fluctuate over relatively long time periods. This results in fluctuating interference effects in the between the two electric fields from the light source when they are combined, and a corresponding fluctuation in optical signal intensity. This phase fluctuation problem is increased and perhaps dominated by thermal changes in the length and the refractive index of the path. The coherence length of the source is inversely proportional to its linewidth. Using the relation of coherence length to Full Width Half Maximum (FWHM) linewidth for a Lorentzian profile [56]:

$$l_c = \frac{0.32c}{\Delta\upsilon_{FWHM}} \tag{5.1}$$

where: l_c is the coherence length
$\Delta\upsilon_{FWHM}$ is the linewidth of the source in Hz

The source that was used has a Lorentzian profile with a line width of around 150 MHz [2]. This corresponds to a coherence length of around 0.64 m.

A passive coupler without polarization sensitivity was tested with the OTDM at the combiner location in Figure 5.2. The difference in optical path lengths into the coupler was increased from the fixed 0.25 m difference between the path lengths to around 20 m and then to 10 km by inserting lengths of fiber between the UTP switch and ETEK switch #3. A polarization rotator was also included to realign polarization into the ETEK switch. Power fluctuations were very apparent in the 0.25 m and 20 m cases because of the coherency problem. No fluctuations were observed when the polarization combiner was used, even when the difference between the path lengths was only 0.25 m.

The losses associated with the OTDM transmitter can be estimated by summing the DC insertion losses in the path through ETEK switch #3 and the polarization combiner, as shown in Figure 5.2. The minimum insertion loss for this path was 13.5 dB. The minimum insertion loss of the path through ETEK switch #2 was less than this. To compensate for this mismatch, the attenuation in the free space optical delay was increased by changing the alignment between the SELFOC® lenses. The power input to the UTP switch was 3 dBm. The resulting modulated optical output from the OTDM therefore could be at best -13.5 dBm. A maximum power output of around -17 dBm was realized in the laboratory largely due to additional RF losses in the ETEK switches.

All of the optical switches available at TRLabs were designed for chirp-free operation. No residual chirp was found to be present in earlier characterization work [2]. Therefore, all work in conjunction with the OTDM transmitter was zero chirp. Negative chirp trials could not be attempted to provide comparisons with the electrical multiplexing results.

The signal quality out of the OTDM transmitter was highly unstable because of polarization and DC bias point drift. The switch devices have maximum extinction with a particular polarization orientation. Polarization orientation changed slightly over time because of physical changes in the fiber waveguide shape caused by thermal effects. The more chronic problem, however, was the tendency for the DC bias points of the UTP switch and the two ETEK switches to change over time. The ETEK and UTP devices are fabricated out of $LiNb0_3$ material. This material has an inherent DC bias point drift problem [53]. These required continuous monitoring and adjustment to avoid extra signal distortion that could have an unfavorable impact on the BER at the receiver. Extreme caution was required to ensure that all OTDM settings were appropriate before data were collected.

5.4. Optical Link Layout

The optical link used for all experiments is shown in Figure 5.3 and its components are listed in Table 5.1. In cases where sufficient power was available, only two EDFAs were used. For measurements at 75 km and beyond, three EDFAs were required to overcome the additional loss of the fiber. The attenuation provided by the combination of fiber spools and VOAs preceding EDFA 3 ensured that its noise characteristics dominated over noise produced by the other EDFAs. This was verified by repeating receiver sensitivity measurements with and without the third EDFA in the path.

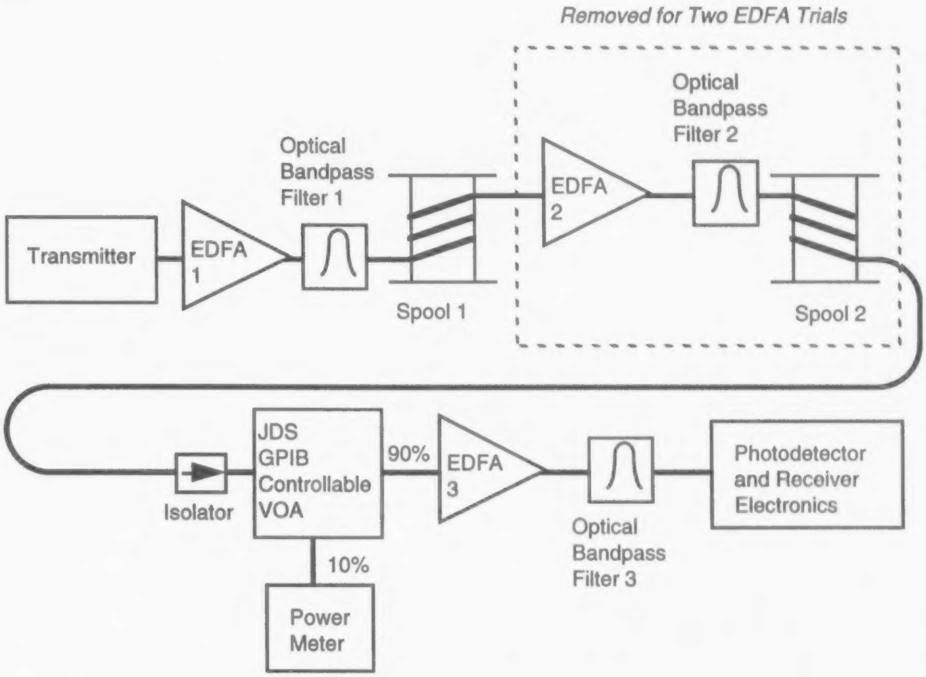
Removed for Two EDFA Trials
Transmitter
EDFA 1
Optical Bandpass Filter 1
Spool 1
EDFA 2
Optical Bandpass Filter 2
Spool 2
Isolator
JDS GPIB Controllable VOA
90%
10%
Power Meter
EDFA 3
Optical Bandpass Filter 3
Photodetector and Receiver Electronics

Figure 5.3: Optical Link for OTDM Trials

A polarization independent isolator was inserted before the VOA in order to reduce the impact of back scattered backward ASE into EDFA 3. Additional optical noise was clearly visible on the signal without this isolator, especially for the longer distance trials.

5.5. Binary Transmission with Binary Reception

5.5.1. Scope of Experiments

Power penalty data for the binary transmission with binary reception case provide a baseline for which duobinary reception and transmission can be compared. It also allows polarization-based techniques to be evaluated.

Component	Description (1551 nm Inputs)
EDFA 1 (Post-amplifier)	Packaged TRLabs EDFA #302 18 dB Small Signal Gain
EDFA 2	EG&G 980 nm Pump Source #003 Coupled to 22 m of NOI-3 Fiber 15 dB Small Signal Gain
EDFA 3 (Pre-amplifier)	Packaged TRLabs EDFA #303 20.5 dB Small Signal Gain
Optical Bandpass Filter 1	JDS Model TB1570 2.9 nm Bandwidth 1.8 dB Insertion Loss
Optical Bandpass Filter 2	JDS Model TB1500B 1.4 nm Bandwidth 2.5 dB Insertion Loss
Optical Bandpass Filter 3	JDS Model TB1500B 1.4 nm Bandwidth 1.7 dB Insertion Loss
Isolator	Hoechst-Celanese YE-35-1590 Polarization Independent 2 dB Insertion Loss
Spool 1	Up to 100 km fiber
Spool 2	Up to 25 km fiber

Table 5.1: Components Used in Optical Links at TRLabs

The OTDM generates a full 10 Gb/s binary NRZ signal. This signal can be processed directly by the receiver electronics if optical demultiplexing is excluded. 5 Gb/s RZ transmission and reception without optical demultiplexing is also possible by obstructing the passage of light through the free space optical delay in the OTDM (Figure 5.2) to remove one of the two interleaved 5 Gb/s RZ streams that make up the 10 Gb/s NRZ signal. Alternatively, polarization-sensitive optical demultiplexing can be included before the receiver electronics (Figure 5.1) to extract one of the two polarization multiplexed 5 Gb/s RZ streams from the complete 10 Gb/s NRZ stream. The resulting BER data demonstrate the merits of polarization demultiplexing compared to full 10 Gb/s NRZ reception, and the additional penalty associated with polarization demultiplexing beyond the chromatic dispersion penalty associated with 5 Gb/s RZ transmission and reception.

5.5.2. 5 Gb/s Binary Signal Generation

The bit error rate test set at TRLabs has a maximum bit rate of 3 Gb/s. The OTDM required two 5 Gb/s NRZ signals to generate a full 10 Gb/s pseudo-random signal. Another electrical multiplexing stage was therefore required in order to generate this 5 Gb/s signal for the OTDM. Figure 5.4 shows the 5 Gb/s multiplexer arrangement, along with the required amplifiers. The 5 Gb/s multiplexer that was used is an NTT Electronics (NEL) NLG4115 2:1 selector. This device transmits one input on the rising edge of the clock and the other input on the falling edge of the clock. Therefore, a 5 Gb/s signal can be generated with a 2.5 GHz clock and two 2.5 Gb/s inputs. An additional delay of 1.2 ns for the BERT $\overline{Q}$ output was added which corresponds to three 2.5 Gb/s bits. This delay and the inversion at the output of the BERT transmitter acted to scramble the two 2.5 Gb/s signals. A second delay of 400 ps (two 5 Gb/s bits) was introduced between the two outputs of the 2:1 selector to scramble the 5 Gb/s channels before being optically multiplexed into a 10 Gb/s stream. Some additional correlation is inherently present in this form of signal generation since it is effectively interleaving copies of sequences. This can potentially have an impact on the power spectrum and pattern sensitivity of the transmitted signal which in turn may affect its dispersion penalty. This was checked by changing both delays and repeating selected data points. The results from these tests are discussed later.

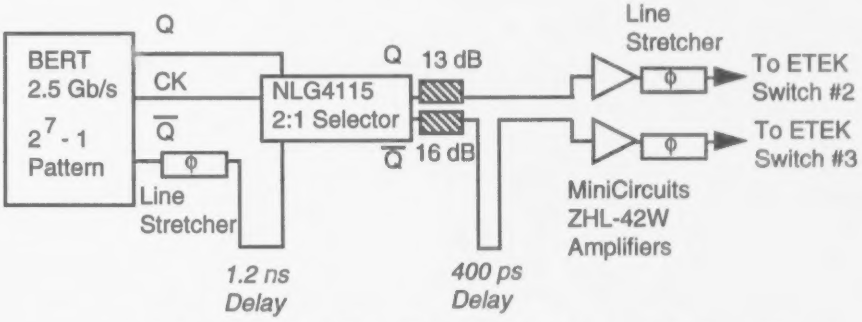

Figure 5.4: 5 Gb/s NRZ Signal Generator and Amplifiers

The attenuation at the outputs of the multiplexer was required to compensate for the gains of the MiniCircuits amplifiers that were used. These attenuators were unequal because the gain of the two amplifiers differed by around 3 dB. The amplified output signal was around 8 Volts peak-to-peak. The amplifiers have a high frequency cutoff at 4.2 GHz and therefore are marginal for use in a 5 Gb/s application. They exhibited poor rise and fall times, along with some ringing behavior, as shown in Figure 5.5. Fortunately their outputs were used to modulate RZ optical pulses. The spurious features of the drive signal introduced by the MiniCircuits amplifiers appear to a lesser extent in the optical signal because the optical pulses are centered on the peak or minimum output from the drive signal. Also, the transfer function of the switch tended to compress the extremes seen by the RZ pulses (as discussed in Appendix B).

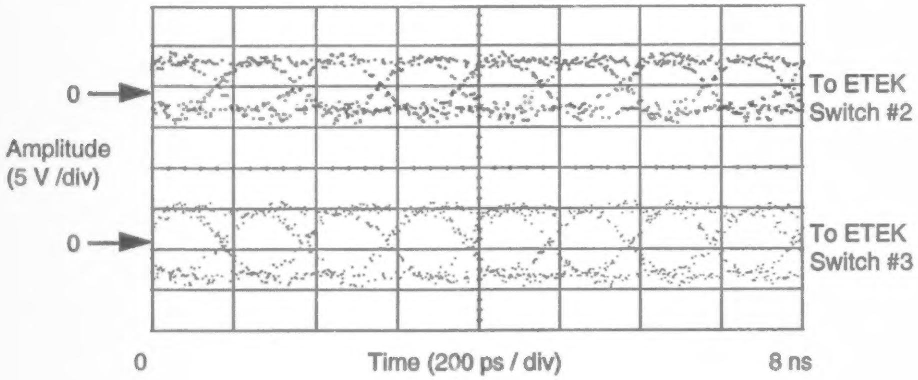

Figure 5.5: 5 Gb/s NRZ Signal from MiniCircuits Amplifiers

5.5.3. Predicted Receiver Sensitivity

5.5.3.1. Polarization-Sensitive Optical Demultiplexer

The 10 Gb/s polarization demultiplexed receiver incorporated a polarization rotator and polarization splitter between the optical bandpass filter and the photodetector in the receiver, as shown in Figure 5.6. This arrangement had a 1.4 dB through loss. Since the 5 Gb/s RZ signals at the transmitter were combined with orthogonal states of polarization, it was possible to separate the two streams at the receiver with the polarization demultiplexer.

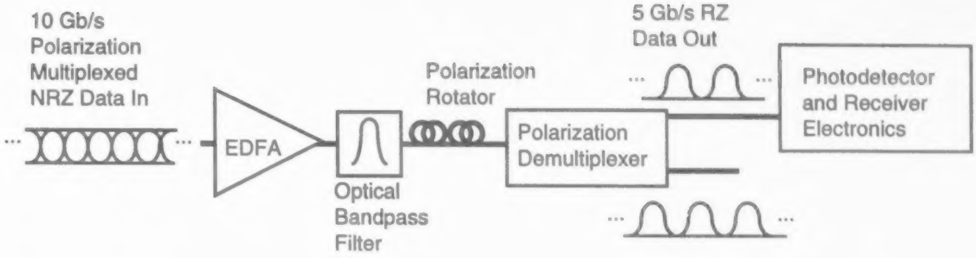

Figure 5.6: Polarization Demultiplexer

5.5.3.2. Receiver Bandwidth

The electronics within the binary receiver was common to all trials, and is shown in Figure 5.7. It consists of a BT&D photodetector followed by SHF and Veritech broadband amplifiers. These two amplifiers were followed by a 6 dB attenuator with a flat frequency response from DC to 26.5 GHz. This was required to maintain a signal level within the acceptable drive limits of the decision circuit (D flip-flop) without significantly affecting the SNR. This attenuator was followed by a 20 dB broadband scope probe (tap) which was used to monitor the signal quality. 5 Gb/s reception (5 Gb/s RZ and 10 Gb/s polarization demultiplexed) was evaluated with and without a 5 GHz low pass filter preceding the scope probe to determine whether increased sensitivity could be gained by reducing noise bandwidth. A DC block allowed the D flip-flop to apply a negative DC offset to the signal. This pulled the incoming binary signal down to within the rated input limits of the flip-flop.

A 2.5 GHz clock from the bit error rate test set transmitter was used to time the decision circuit. In the case of 10 Gb/s reception, the D flip-flop sampled every fourth bit and passed its decision on to the bit error rate test set receiver. In the case of 5 Gb/s reception, it sampled every second bit. The D flip-flop therefore acted as a demultiplexer as well as a decision circuit. This scheme was used because the bandwidth of the bit error rate test set was insufficient for bit rates higher than 3 Gb/s. A clock recovery circuit was not used because it would have introduced considerably more complexity into the receiver and because the transmission distances tested were relatively short (less than). Longer distance tests would have warranted a 10 GHz clock recovery circuit and a 10 Gb/s 1:4 demultiplexer to remove the effects of clock jitter caused by thermal effects in the fiber.

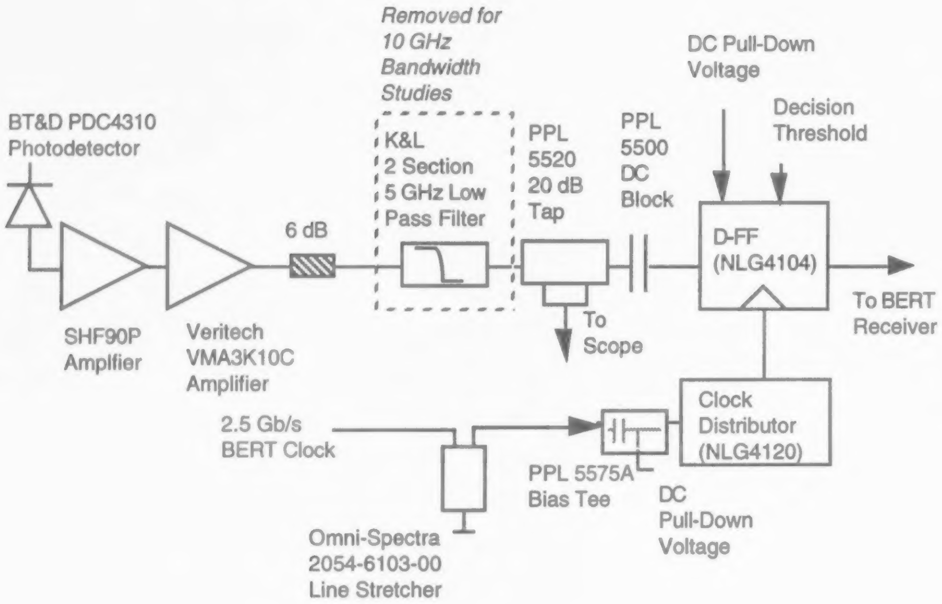
Removed for 10 GHz Bandwidth Studies
BT&D PDC4310 Photodetector
K&L 2 Section 5 GHz Low Pass Filter
PPL 5520 20 dB Tap
PPL 5500 DC Block
DC Pull-Down Voltage
Decision Threshold
6 dB
D-FF (NLG4104)
To BERT Receiver
SHF90P Amplfier
Veritech VMA3K10C Amplifier
To Scope
2.5 Gb/s BERT Clock
Clock Distributor (NLG4120)
PPL 5575A Bias Tee
DC Pull-Down Voltage
Omni-Spectra 2054-6103-00 Line Stretcher

Figure 5.7: Binary Receiver Electronics for OTDM Trials

The concatenated frequency response of the receiver components is an important consideration in determining the bandwidth of the receiver and for modeling it accurately within a simulation. The measured responses are shown in Figure 5.8. This does not include the frequency response of the photodetector, which was measured in [2] and is included in Appendix A. This photodetector has a relatively sharp roll off in its frequency response (down 3 dB at 4 GHz) which significantly reduces the bandwidth of either receiver configuration.

The noise equivalent bandwidth of the receiver can be obtained by performing a normalized integral on the frequency response of the binary receivers, assuming that the noise power spectral density is uniform across the pass band of the receiver. A numerical integration technique can be readily performed using a spreadsheet, once sufficient data points from the frequency response have been entered. The peak output from the receiver is normalized to 1 (0 dB). Then, the power response is obtained from a rectangle rule numerical integration:

$$B_e = \sum_{i=0}^{n} H(i\,\Delta f)\,\Delta f \tag{5.2}$$

where: $H(f)$ is the magnitude of the frequency response
B_e is the noise equivalent bandwidth of the receiver
n is the number of samples
Δf is the frequency step between the samples

This integration was performed for both the binary receiver responses in Figure 5.8 for 31 data points with 0.5 GHz spacing (i.e. from 0 GHz to 15 GHz) to provide good approximations for noise equivalent bandwidth. The resulting bandwidth for the 5 GHz band limited receiver is 4.78 GHz and for the 10 GHz receiver is 8.48 GHz.

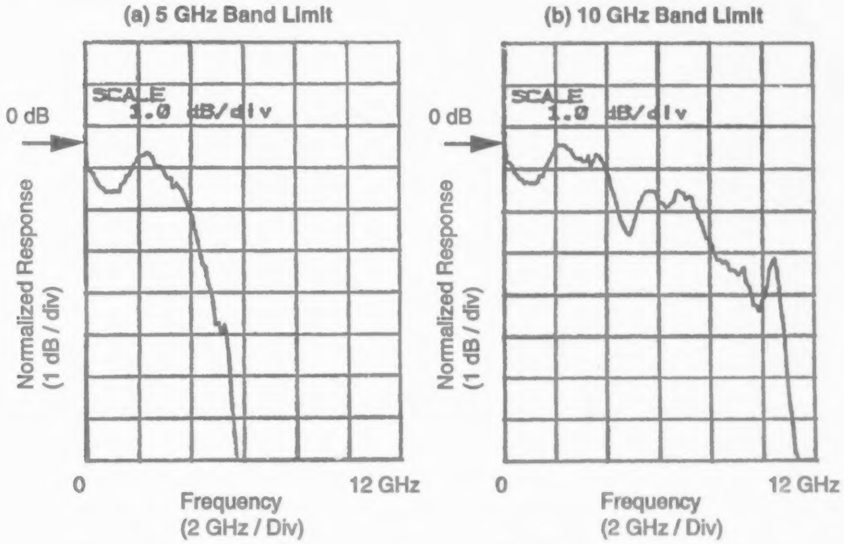

Figure 5.8: Frequency Response of Binary Receivers

A similar technique yields the noise equivalent bandwidth B_o of the JDS TB1500B optical bandpass filter following the EDFA pre-amplifier. The results from a monochromator scan of filtered ASE centered at 1551 nm is shown in Appendix I. This data were numerically integrated to produce an approximate bandwidth of 181 GHz (1.45 nm).

5.5.3.3. EDFA Pre-Amplifier Characterization

The ASE output of the EDFA as a function of input power can be measured using a polarization demultiplexed method (Appendix P). This results in the characteristics shown in Appendix I for the EDFA pre-amplifier used at maximum pump current (160 mA), which was the setting for all experiments.

The EDFA noise factor Nsp can be calculated from the filtered ASE power as follows:

$$N_{sp} = \frac{P_{sp}}{m_t h\upsilon B_o (G-1)} \qquad (5.3)$$

where: $m_t = 2$ is the number of polarization states

P_{sp} is the ASE power out of the EDFA, excluding filter loss

G is the operating gain of the EDFA

Using data with the EDFA input at -40.5 dBm (unsaturated conditions), P_{sp} = -20.3 dBm and G = 20.4 dB. This results in a realistic N_{sp} figure of 1.86 for input power below -15 dBm.

5.5.3.4. Predicted SNR and Receiver Sensitivity

With the above EDFA and bandwidth data, it is now possible to use the equations in Chapter 3 to plot SNR as a function of EDFA input power. The parameters η_i, η_o, A_2 and L_s are all set to 1.0 for this calculation. The other parameters required for the calculations are T=300K, r = 0.7 Amps / Watt, F = 5 (SHF90P amplifier noise factor) and R = 50 Ω (SHF90P amplifier input resistance). These plots are shown in Figure 5.9 for the 10 Gb/s NRZ, 5 Gb/s RZ, and 10 Gb/s polarization demultiplexed cases.

The bandwidth of the receiver (Figure 5.7) is limited to around 10 GHz by the stop band of the Veritech amplifier. When configured for 5 Gb/s signals, this receiver can have its bandwidth reduced without introducing a large amount of signal distortion by inserting a 5 GHz low pass filter into the path. This applies to the 5 Gb/s RZ case. It also applies to the polarization demultiplexed case, since the receiver sees only one output from the polarization demultiplexer after it has split the 10 Gb/s NRZ stream into two 5 Gb/s RZ streams. According to the results plotted in Figure 5.9, the lower noise bandwidth of the 5 GHz receiver compared to the receiver without a low pass filter (10 GHz bandwidth) results in about a 3 dB improvement in SNR at a given input power. Another offset in the SNR curves occur because of signaling format. As discussed in Chapter 3, RZ signaling has a 6 dB increase in SNR over NRZ signaling for a given input power because of the 50 % duty cycle of RZ signaling.

The 10 Gb/s NRZ and polarization demultiplexed cases have the same receiver input power and also have identical receiver arrangements if no low pass filter is included. Intuitively one would expect identical SNR curves for these cases. This does not occur because of the insertion loss of the polarization rotator and splitter devices required for polarization demultiplexing. This loss is partially compensated for by a reduction in total ASE relative to signal at the output of the polarization demultiplexer, and subsequently a reduction in spontaneous-spontaneous beat noise and shot noise.

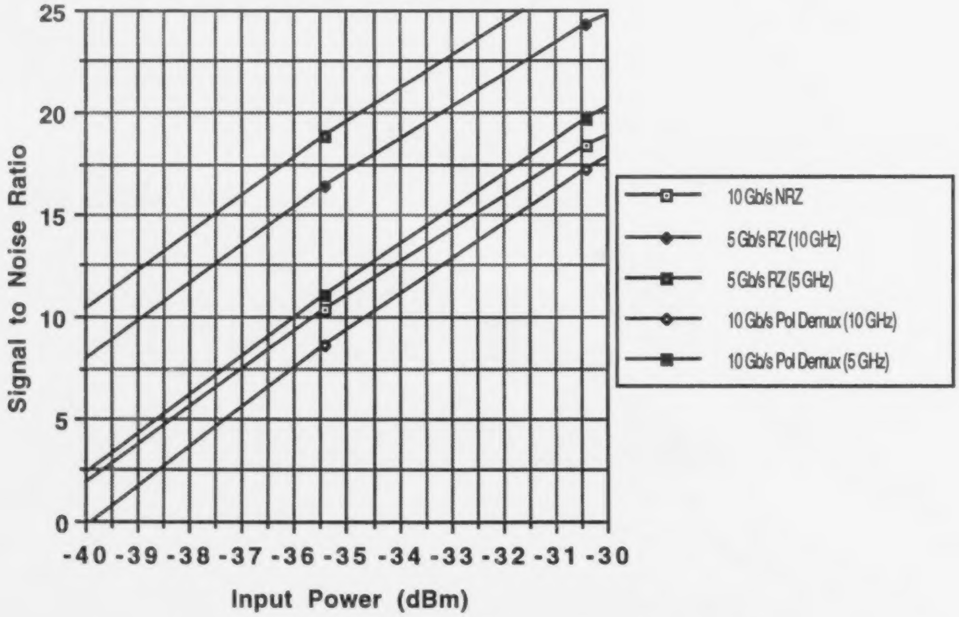

Figure 5.9: Calculated Binary Receiver SNR

If the statistics of the noise are Gaussian and the same amount of noise is associated with a "1" as a "0", then an SNR of 15.5 dB is required at the sampling point to achieve a BER of 10^{-9} (see Appendix K). This Gaussian model is sufficiently accurate to obtain a reasonable estimate of receiver sensitivity. Table 5.2 shows the theoretical input powers required for a 10^{-9} BER.

Received Format	10^{-9} BER Power (dBm)
10 Gb/s NRZ	-32.2
5 Gb/s RZ (10 GHz)	-35.8
5 Gb/s RZ (5 GHz)	-37.2
10 Gb/s Pol. Demux (10 GHz)	-31.4
10 Gb/s Pol. Demux (5 GHz)	-32.8

Table 5.2: Predicted Input Power Levels for 10^{-9} BER

5.5.4. Experimental Receiver Sensitivity

5.5.4.1. 10 Gb/s NRZ Reception

This option is extremely susceptible to transmitter bias points, polarization states, and relative channel levels. This is especially true because the adjacent time slots are not perfectly isolated from each other. A considerable amount of power from one pulse spills over into adjacent time slots because of the sinusoidal drive at the first stage (UTP switch), as shown in Figure 5.10. In terms of intensity, intersymbol interference affects at least 70 percent of the time slot in a transmitter with a perfect extinction ratio. Therefore, intersymbol interference affects this system even with no fiber between its transmitter and receiver. The channel output levels and extinction ratios must be well balanced in order to ensure uniform eye openings for each time slot at the input to the receiver.

Tuning the OTDM transmitter for optimal 10 Gb/s NRZ transmission required a delicate balancing act in order to obtain a symmetric eye pattern. The UTP switch bias point was an especially important parameter which influenced sensitivity. By adjusting this, it was possible to reduce the BER (and increase the relative width) of one time slot at the expense of increasing the BER (and reducing the relative width) of the other. Therefore, care was taken to ensure that the BER was uniform in all channels before a BER reading was made. The obtained 10^{-9} BER receiver sensitivity differs from the predicted sensitivity by approximately 5 dB at 0 km. This can be attributed to severe eye closure caused by the high degree of intersymbol interference between the channels and distortion introduced by transmitter and receiver components.

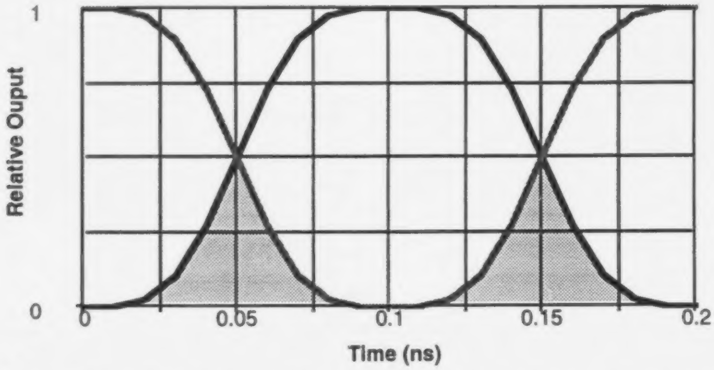

Figure 5.10: Simulated Intensity Coupling Between Time Slots at the Output of the OTDM

Figure 5.11 shows BER as a function input power from 0 km to 50 km. The receiver sensitivity at 0 km was better than the receiver tested for comparable electrical multiplexing trials because of the lower noise contribution of the EDFA pre-amplifier that was used. A BER floor of 10^{-6} was observed at 60 km, indicating that the signal was highly corrupted by dispersion. This is not surprising considering the high degree of intersymbol interference inherent in the 10 Gb/s transmitter even at 0 km. Any pulse broadening at all results in considerable eye closure. Even small drifts in switch bias points were responsible for increased signal distortion and changes in receiver sensitivity. Data points were repeated with an increased 2 ns delay (five 2.5 Gb/s bits) between the inputs of the 2:1 selector and increased 2 ns (ten 5 Gb/s bits) between the outputs of the 2:1 selector. No significant difference in receiver sensitivity was observed. From this, it can be concluded that the intersymbol interference associated with this signaling method was the dominant controller of the BER.

The input powers into the receiver for the 10 Gb/s NRZ were extremely high. This resulted in gain saturation in the Veritech amplifier, since its 1 dB gain compression point occurs at an output power of 17 dBm (approximately 3.2 Vp-p for a square wave input). Visible gain compression occurred at an optical input power of approximately -25 dBm. The output signal becomes distorted, and the top and bottom parts of the waveform flatten because of clipping in the amplifier. This was very beneficial because it helped protect the decision circuit and removed some variation at the high and low signal levels.

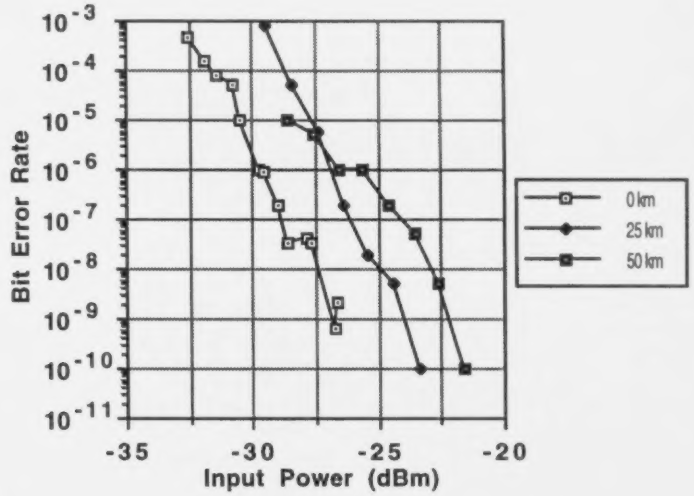

Figure 5.11: BER Curves for 10 Gb/s NRZ Reception

For further trials, an HP 8494 DC-18 GHz variable attenuator with 1 dB increments was placed between the SHF and Veritech amplifiers to avoid the Veritech amplifier's gain compression problem. 10^{-9} BER receiver sensitivity was at least 3 dB worse than the gain saturated case. This difference shows that the clipping effect of the saturated Veritech amplifier can be useful. There was also a marginal (10 to 20 %) increase in receiver thermal noise relative to signal when high attenuation was located between the SHF and Veritech amplifiers because the Veritech amplifier's noise contribution now becomes significant.

Figure 5.12 shows the best received binary eye diagrams and time plots at 0 km and 75 km for the case where the variable attenuator was placed between the SHF and Veritech amplifiers, and therefore for the operating condition where the Veritech amplifier was not saturated. Note that the features of the waveforms are more rounded than the theoretical pulse shapes at the output of the OTDM transmitter (Figure 5.10) because of the concatenated frequency response of the components in the receiver. These waveforms correspond well with simulated results which model the frequency response of all components (Figure 5.13). The simulated time plot shows the same signal features, and the eye diagram shows the same severe eye closure present in the signal at 75 km. Figure 5.12 also shows the waveforms for the gain saturated case at 0 km to demonstrate the effect of amplifier gain compression.

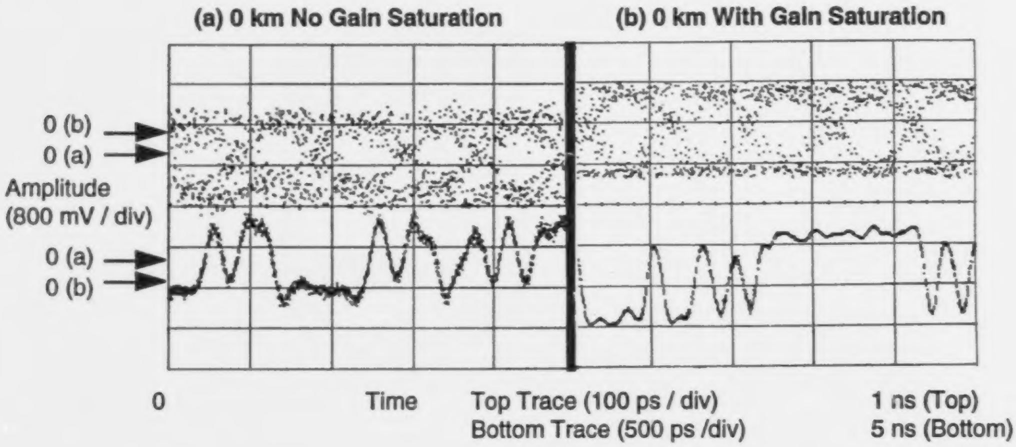
(a) 0 km No Gain Saturation

(b) 0 km With Gain Saturation

(C) 75 km No Gain Saturation

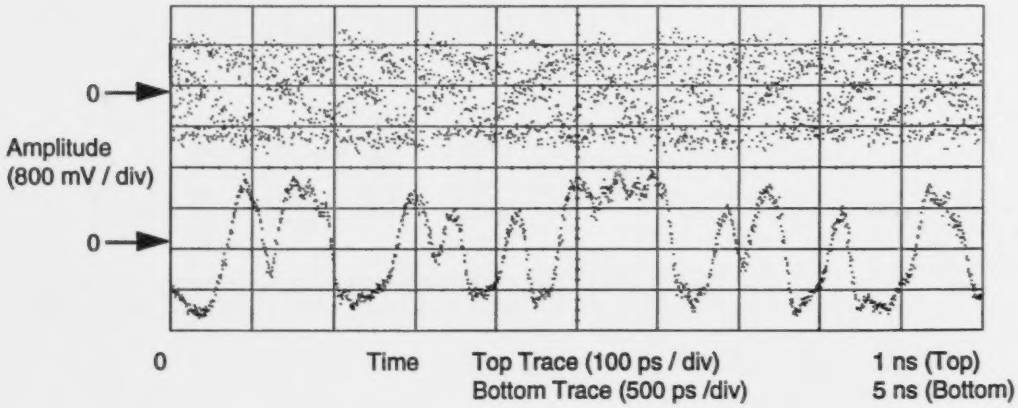

Figure 5.12: Actual 10 Gb/s NRZ Waveforms at 0 km and 75 km

(a) 0 km Eye Diagram

(b) 0 km Time Plot

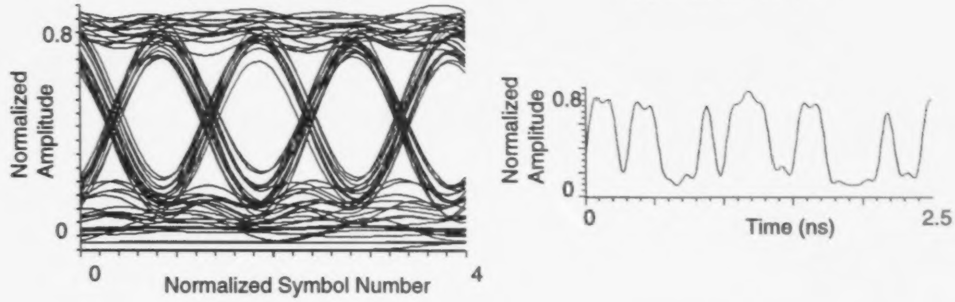

(c) 75 km Eye Diagram

(d) 75 km Time Plot

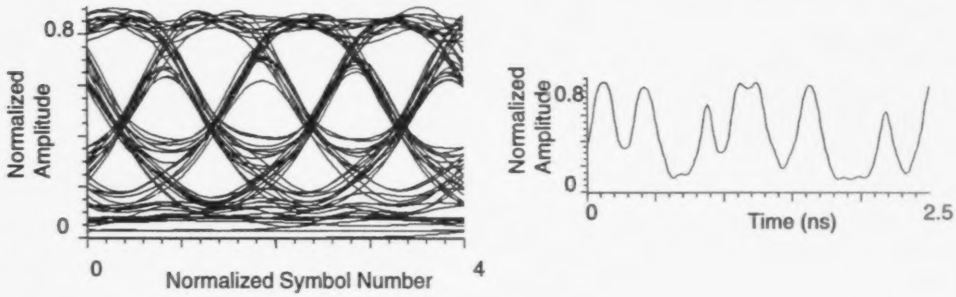

Figure 5.13: Simulated 10 Gb/s NRZ Waveforms at 0 km and 75 km

5.5.4.2. 5 Gb/s RZ Reception

A 5 Gb/s RZ signal was produced by simply obstructing the free space optical delay in the transmitter. The resulting signal can be detected with the binary receiver presented earlier in Figure 5.7 with or without the 5 GHz filter in place. Figure 5.14 shows typical waveforms obtained in the 5 Gb/s trials as seen at the output of the binary receiver. The output from the receiver with the low pass filter is similar. Figure 5.15 shows simulated versions of these waveforms when the low pass filter is excluded. The simulated time plots have the same features as the experimental time plots and the simulated eye diagrams have good agreement with experimental eye diagrams. Signal distortion caused by chromatic dispersion broadened the 5 Gb/s RZ waveforms into almost NRZ form by 125 km. This reduced the amplitude of the signal at the sampling point. This reduced the SNR corresponding to a particular receiver input power and therefore increased the dispersion penalty. Note that pulse broadening is not quite as severe in the simulated waveforms. The simulator appears to be underestimating the impact of dispersion on the signal.

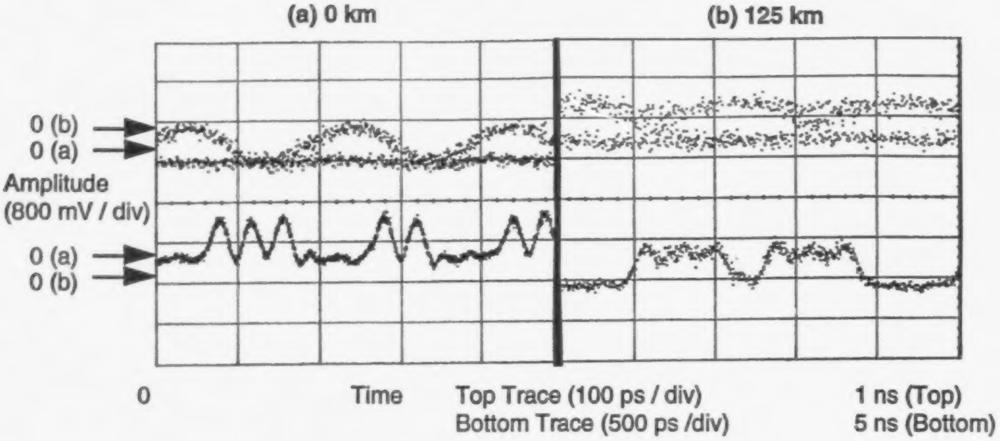

Figure 5.14: Actual 5 Gb/s RZ Waveforms at 0 km and 125 km

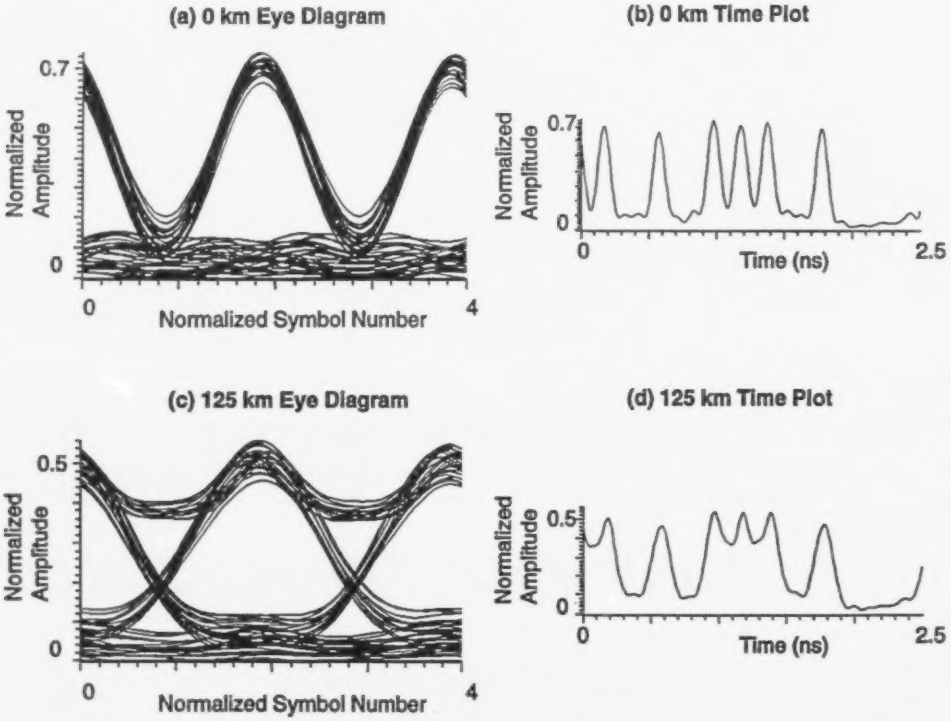

Figure 5.15: Simulated Gb/s RZ Waveforms at 0 km and 125 km

BER curves for 5 Gb/s RZ reception are presented in Figure 5.16 and 5.17. The 0 km 10^{-9} BER power for the 5 GHz receiver was -34.2 dBm (-37.2 dBm predicted) and for the 10 GHz case was -33.2 dBm (-35.8 dBm predicted).

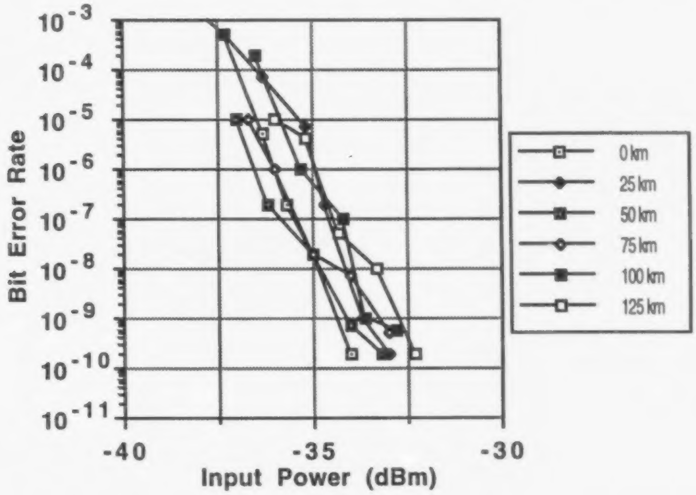

Figure 5.16: BER Curves for 5 Gb/s RZ Reception, 5 GHz Receiver

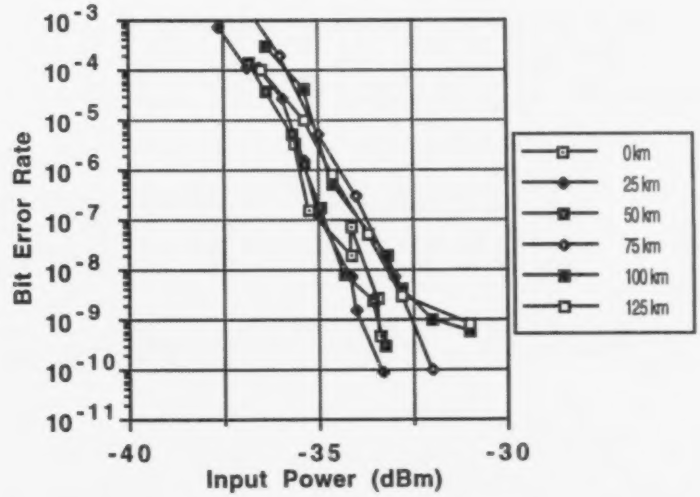

Figure 5.17: BER Curves for 5 Gb/s RZ Reception, 10 GHz Receiver

Selected data points were repeated with a delay between the inputs of the 2:1 selector (5 Gb/s multiplexer) of 2 ns (five 2.5 Gb/s bits). No apparent change in receiver sensitivity was observed. No change was expected because the bits were well spaced and therefore insensitive to pattern changes and slight differences in dispersion-induced pulse broadening.

5.5.4.3. 10 Gb/s Polarization Demultiplexed Reception

The resulting BER curves for polarization demultiplexed reception are plotted in Figure 5.18 and Figure 5.19. Obtained eye diagrams and time plots are identical to those obtained from 5 Gb/s RZ tests. The 0 km 10^{-9} BER power for the 5 GHz receiver was -30 dBm (-32.8 dBm predicted) and for the 10 GHz receiver was -29 dBm (-31.4 dBm predicted). The increase in required power compared the 5 Gb/s RZ cases at 0 km are around 4.4 dB for both receivers, of which 3 dB can be accounted for in a doubling of signal power due to detecting twice as many bits per second at 10 Gb/s relative to 5 Gb/s. The remaining 1.4 dB can be attributed to the insertion loss of the polarization rotator and demultiplexer in the receiver. Both receiver configurations had virtually identical measured receiver sensitivities beyond 25 km. Obtained scope traces were identical to those obtained from the 5 Gb/s RZ trials.

The polarization orientation at the receiver was continually adjusted in order to ensure the best possible isolation between the signal channel and the orthogonal channel. This was accomplished by obstructing the free space delay in the transmitter. The polarization rotator in the receiver was then set so that the remaining 5 Gb/s RZ signal was not visible on the monitoring oscilloscope and the photodetector current was at a minimum. The obstruction was then removed, with the result that the previously obstructed 5 Gb/s RZ channel alone was visible on the oscilloscope. Minimum crosstalk could be achieved using this technique.

With the free space delay obstructed, the minimum achievable photocurrent was 1.6 μA, corresponding to one half the filtered ASE output of the EDFA after the attenuation of the polarization rotator and demultiplexer. This was observed at all receiver input power levels for distances up to 50 km. At 75 km, the minimum photocurrent associated with ASE and cross talk from the isolated signal for a -30 dBm 5 Gb/s RZ signal was 2 μA and by 125 km it was 2.5 μA. This degree of isolation was extremely difficult to achieve and at long distances required continual checking and resetting from the minutes time frame at short distances to under a minute at 125 km.

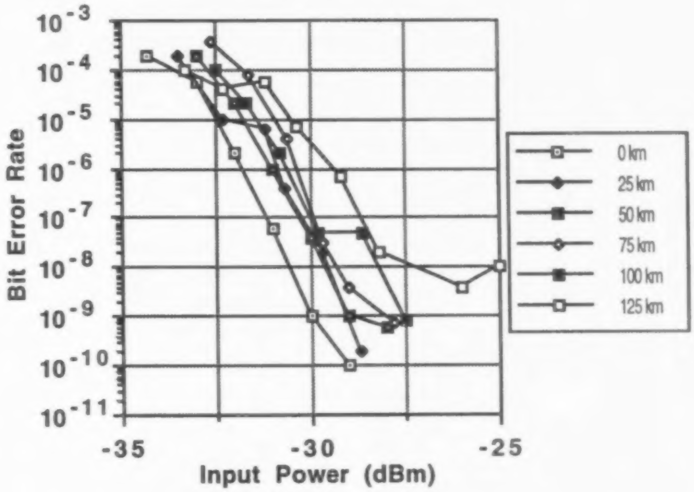

Figure 5.18: BER Curves for 10 Gb/s NRZ Polarization Demultiplexed Reception, 5 GHz Receiver

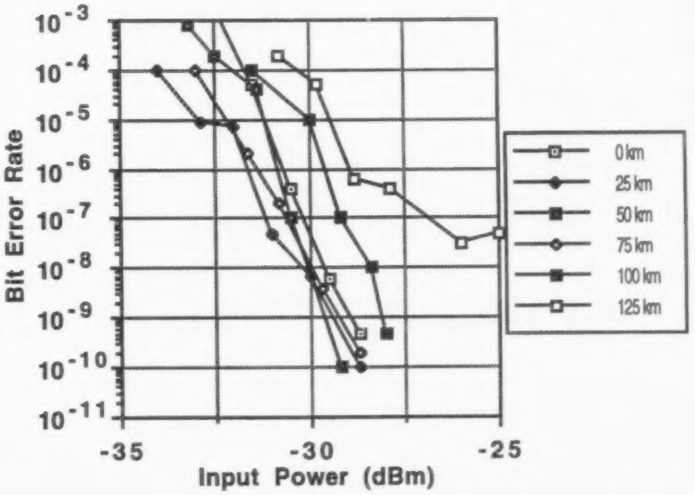

Figure 5.19: BER Curves for 10 Gb/s Polarization Demultiplexed Reception, 10 GHz Receiver

Some of the penalty associated with polarization demultiplexing may be associated with the method used to take BER readings. The decision circuit threshold and timing required manual optimization which for long distance trials took in the order of the same time to accomplish as it took for the polarization state of the receiver to change. Also, bit errors were often bursty at optimum polarization settings. In general, the amount of fluctuation observed was directly correlated to the amount of polarization crosstalk present and therefore indicated how well isolation was achieved. For low BERs the gating feature on the bit error rate test set receiver was required to average the BER over several minutes. The 10^{-8} BER floor observed at 125 km was caused by the combined effects of clock jitter, poor polarization isolation, and fluctuations in polarization orientation. Repeated efforts could not yield a reduced BER. This floor occurs at a slightly lower input power for the 5 GHz receiver because of its reduced noise bandwidth. As with the 5 Gb/s RZ case, no apparent change in receiver sensitivity was observed when the delay between the inputs of the 2:1 selector was increased a further 2 ns.

Both polarization mode coupling and changes in polarization orientation were significant problems for long distance transmission. These are a result of birefringence in the fiber (a different group velocity in each of the two states of polarization caused by the lack of circular symmetry) caused by stress imposed on the fiber. This lack of symmetry causes polarization dispersion, which results in the polarization orientation of the fiber being spread over a continuum of states [54]. This increases crosstalk at the output of the polarization demultiplexer. Birefringence continually changes because of changing stresses imposed on the fiber. This changes the characteristics of polarization dispersion and also acts to rotate the orientation of the polarization of the signal.

Although many fiber patchcords were exposed to air movement within the laboratory and therefore could move around slightly, thermal effects on the lengths of spooled fiber appeared to be the dominant source of polarization fluctuations. This fiber was significantly longer than the patch cords and it was under considerable stress because it was tightly wound on spools. Therefore, its polarization stability was highly susceptible to small temperature variations. Previous measurements [55] indicate a similar problem with tightly wound fiber.

The available fiber spools in the laboratory were compared to gain insight into their polarization stability. A 50 km link over two 15 cm diameter Corning fiber spools was compared with a 50 km link over a 30 cm diameter Northern Telecom fiber spool. No appreciable difference in receiver sensitivity or BER fluctuation was observed.

Polarization multiplexing and demultiplexing was also evaluated for the same system with a 5 GHZ receiver but with the free space optical delay at the transmitter changed so that the RZ pulses were not interleaved, but were overlapping. This provided insight to how well polarization multiplexing and demultiplexing would work outside of an OTDM arrangement. The resulting BER curves are shown in Figure 5.20. The upper bound on the penalty of using this technique compared to interleaving the polarization multiplexed time slots is about 1.5 dB.

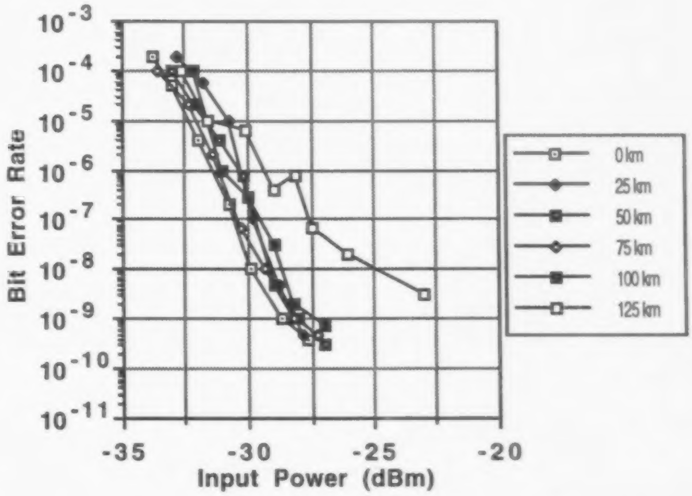

Figure 5.20: BER Curves for Polarization Demultiplexed Reception with Overlapping Pulses

5.5.4.4. Active Recombination

The use of an active recombination stage was also studied. Unfortunately, BER data could not be collected because of limitations in the components that were available. In this case, the polarization multiplexer was replaced with another ETEK switch, driven by a 5 GHz sinusoidal signal with sufficient power to achieve around a 10 dB extinction ratio (5 Vp-p, using the output of an Avantek AWT-8035 amplifier at its distortion limit). Large signal fluctuations due to quasi-coherent addition was very apparent. Removal of this problem required the insertion of a length of fiber in one of the optical paths. This was inserted between the UTP switch and ETEK switch #3 so that it did not upset the alignment of the modulated time slots. A polarization rotator was also inserted to realign polarization into the ETEK switch. The coherency problem was still apparent when a section of 20 m of patch cord was used. A 10 km spool of fiber was then tried. This apparently removed the visible fluctuation problem, but also introduced another 2.2 dB of loss on top of the 1 dB loss due to the polarization rotator.

Ignoring the poor extinction ratio of the recombination stage, and including 1 dB polarization rotator loss and the 8 dB through loss of another ETEK switch, the net power output of the actively recombined transmitter could be at most -26 dBm, or 9 dB below the maximum output of the polarization multiplexed OTDM. In reality, it was at least 3 dB lower depending on the length of fiber used to remove coherency problems. The post-amplifier used for the other binary transmitter experiments (followed by a 3 nm optical bandpass filter) had a gain of 16 dB and an unsaturated output ASE level of -16.4 dBm. Using it resulted in a highly ASE corrupted signal before other EDFAs were even included in the path. The 0 km 10 Gb/s BER curve in Figure 5.11 provides a good approximation of the BER that can be expected if the best quality amplifier and filter combination available in the laboratory (the EDFA pre-amplifier set-up normally used in the binary receiver) was used. The minimum BER that could be expected is 10^{-6}, assuming that -29 dBm output power could be achieved from the transmitter. Good quality transmission for this OTDM arrangement clearly requires amplification before the final switch stage or a higher gain low noise EDFA post-amplifier to keep ASE low relative to signal. Because of this power limitation, the active recombination transmitter was not investigated in great detail in the laboratory.

Plots of the single channel 5 Gb/s RZ waveforms were taken at 0 km (Figure 5.21), and observed at 100 km. These had the same shape the polarization multiplexed waveforms, and a comparable dispersion penalty. Further simulation work confirmed that the effect of dispersion would be not be significantly less in a 10 Gb/s NRZ system (Figure 5.22). Spill over between time slots is still a problem, although now only about 40 percent of the time slot width is affected. This option has no apparent difference in dispersion penalty for considerable additional transmitter complexity.

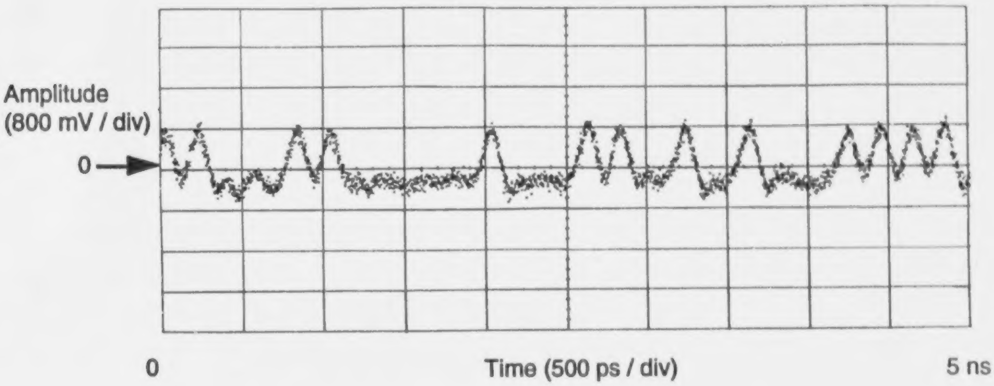

Figure 5.21: 5 Gb/s RZ Pulse Shapes Using Switch Recombination Stage in OTDM

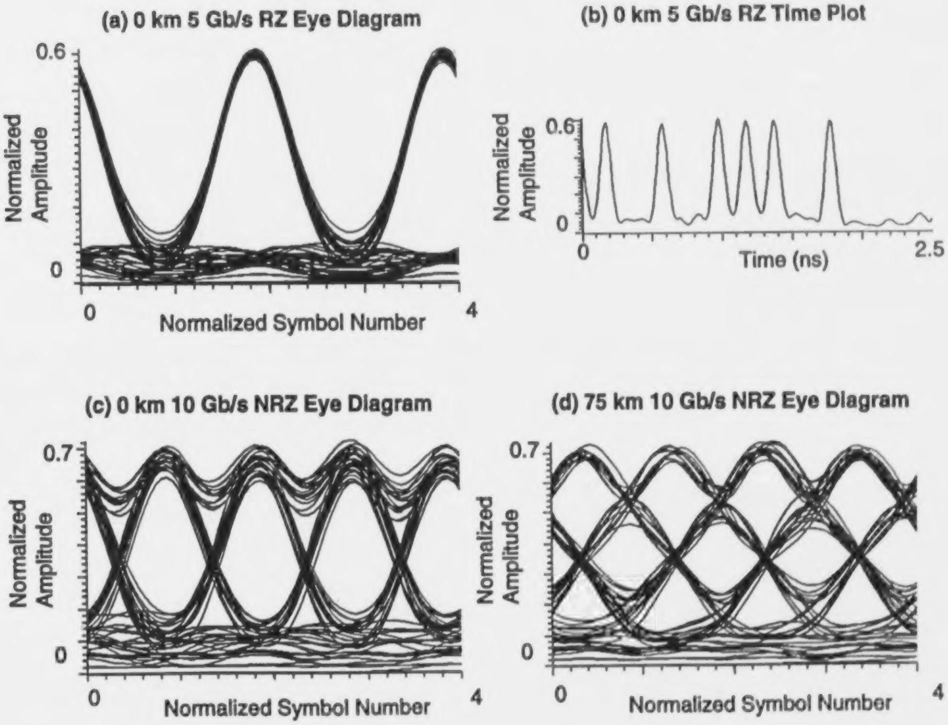

Figure 5.22: Simulated Waveforms for Active Recombination OTDM

5.6. Binary Transmission with Duobinary Reception

5.6.1. Scope of Experiments

The binary transmitter used was identical to the polarization multiplexed transmitter used for binary reception BER data collection. A duobinary receiver similar to the one used for electrical multiplexing experiments was used in conjunction with the OTDM transmitter. This receiver could work with the full 10 Gb/s NRZ binary stream generated by the OTDM, or with a 5 Gb/s RZ binary stream resulting from polarization demultiplexing the 10 Gb/s NRZ output from the OTDM. As a starting point in evaluating polarization demultiplexing, 5 Gb/s RZ duobinary reception can also be performed without polarization multiplexing by obstructing the free space delay in the OTDM transmitter. Experiments were performed in an attempt to obtain BER data for 5 Gb/s RZ binary reception without polarization demultiplexing, and also 10 Gb/s NRZ reception.

5.6.2. Duobinary Receiver Design

The design of the delay and add circuit was similar to the Wilkinson Combiner arrangement used for electrical multiplexing duobinary transmission experiments. This time a line stretcher was used to implement the delay. This component had a plunger on the outside of its package to set a delay, unlike other line stretchers used previously which required that the coaxial line be physically stretched. This was a much more versatile arrangement since a relative delay setting did not require semi-rigid coaxial cable to be bent to accommodate it. Also, a delay between 0 ps and 240 ps could be set. This allowed the same delay and add circuit to be used for 5 Gb/s (200 ps delay) and 10 Gb/s (100 ps delay). The optimal delay was set by observing the duobinary eye openings when the appropriate signal was being received by the photodetector. The through loss of this arrangement was approximately 4 dB, including the loss of the lowpass filter. Figure 5.23 shows the duobinary receiver complete with this new delay and add circuit and a ternary decision circuit.

5.6.3. 5 Gb/s Duobinary Reception

It was expected that the bit error rate test set receiver would have to be programmed to accommodate the bit sequence produced by the duobinary decision circuit because of the interleaving performed by the transmitter multiplexing stages. A program was written to generate this so that the sequence could be typed in. After the sequence was programmed into the bit error rate test set receiver, it was found to be unnecessary because this sequence matched a 2^7-1 PRBS shifted by 63 positions. This was an unexpected result, considering that the received sequence was the sum of two interleaved and added PRBS sequences.

Clear eye openings were apparent in the duobinary signal when the delay and add circuit was not followed by a low pass filter. In this case, a 10^{-9} BER could be obtained at an input power around -25 dBm for an optimally tuned duobinary receiver (Appendix O).

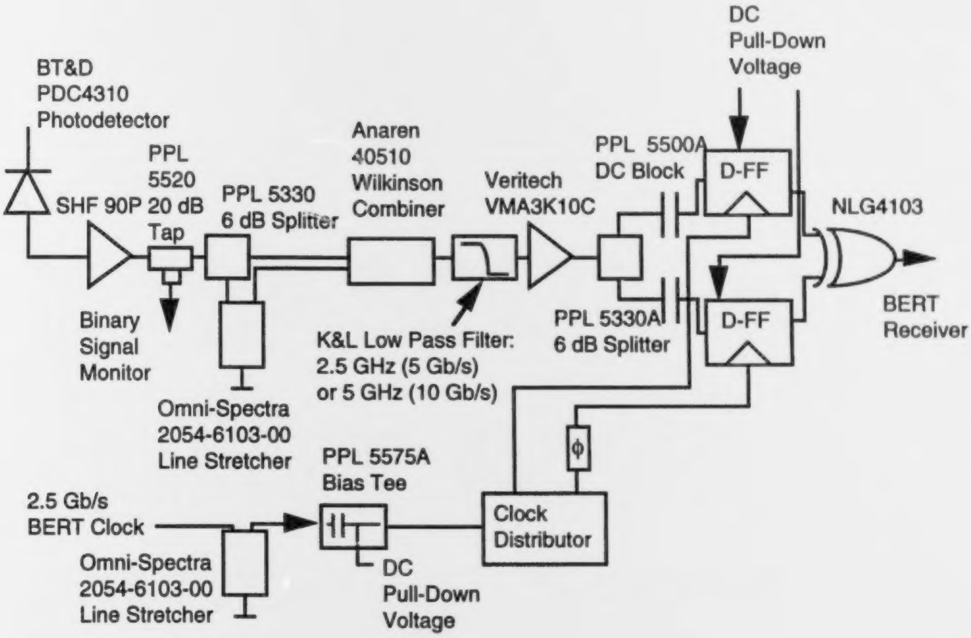

DC Pull-Down Voltage
BT&D PDC4310 Photodetector
PPL 5520 20 dB Tap
SHF 90P
PPL 5330 6 dB Splitter
Anaren 40510 Wilkinson Combiner
Veritech VMA3K10C
PPL 5500A DC Block
D-FF
NLG4103
D-FF
BERT Receiver
Binary Signal Monitor
Omni-Spectra 2054-6103-00 Line Stretcher
K&L Low Pass Filter: 2.5 GHz (5 Gb/s) or 5 GHz (10 Gb/s)
PPL 5330A 6 dB Splitter
ϕ
PPL 5575A Bias Tee
2.5 Gb/s BERT Clock
Omni-Spectra 2054-6103-00 Line Stretcher
DC Pull-Down Voltage
Clock Distributor

Figure 5.23: Duobinary Receiver

Eye openings were narrower when a 2.5 GHz low pass filter for 5 Gb/s signals was inserted after the delay and add circuit. The lowpass filter distorted the signal considerably and also acted to lower the peak to peak signal at the decision circuit by broadening it across the full 5 Gb/s time slot. A BER floor of 10^{-6} was observed at an input power of -21 dBm. The receiver sensitivity was expected to be within 3 dB of the 5 Gb/s RZ binary receiver sensitivity, or -30 dBm. Signal distortion is partly responsible for this difference. Attenuation is the major source of the problem. Compared to a binary receiver, the duobinary receiver had an additional 10 dB electrical path loss due to its duobinary filter and the 6 dB splitter located before the decision circuit.

Figure 5.24 show the obtained waveforms for 0 km with and without the 2.5 GHz low pass filter. Figure 5.25 shows simulated waveforms. The simulated waveforms have a reasonable match to the actual waveforms.

5.6.4. 10 Gb/s Duobinary Reception

Duobinary reception was also attempted for 10 Gb/s NRZ signals. Eye openings were barely discernible (Figure 5.26), making it pointless to attempt a BER measurement. Simulations point to high distortion as well (Figure 5.27), although they do produce a marginal eye opening. This indicates that duobinary reception is not viable for 10 Gb/s NRZ signal generated by the OTDM. This result is contrary to the externally modulated transmitter results which show that duobinary reception provides a considerable reduction in dispersion penalty. The difference lies in the quality of signal produced at the transmitter. The OTDM tested had a high degree of intersymbol interference between time slots that was not present in the externally modulated transmitter.

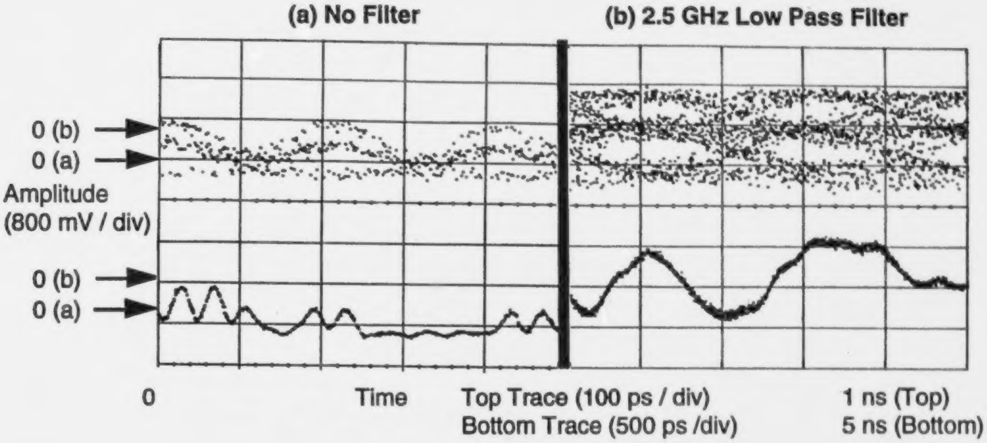
(a) No Filter

(b) 2.5 GHz Low Pass Filter

Figure 5.24: 5 Gb/s RZ Duobinary Reception Obtained Waveforms

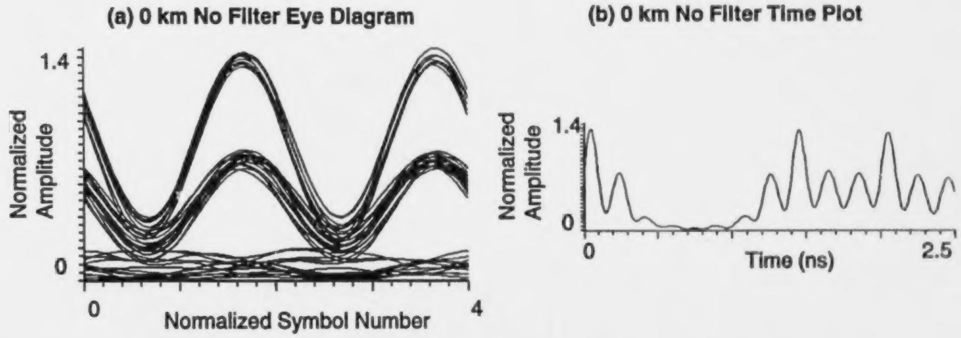
(a) 0 km No Filter Eye Diagram

(b) 0 km No Filter Time Plot

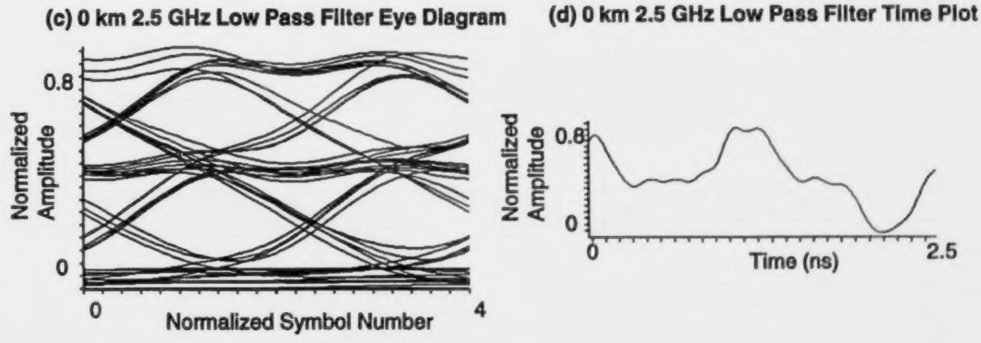
(c) 0 km 2.5 GHz Low Pass Filter Eye Diagram

(d) 0 km 2.5 GHz Low Pass Filter Time Plot

Figure 5.25: 5 Gb/s RZ Duobinary Reception Simulated Waveforms

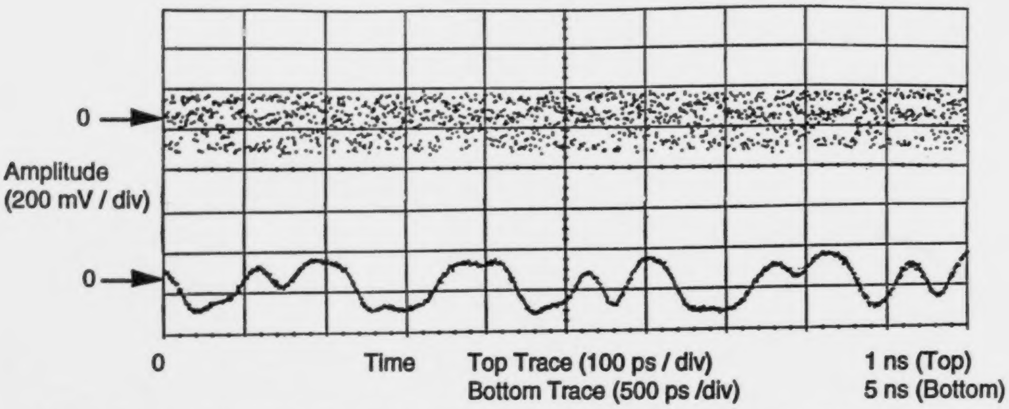

Figure 5.26: 10 Gb/s NRZ Duobinary Reception Obtained Waveforms

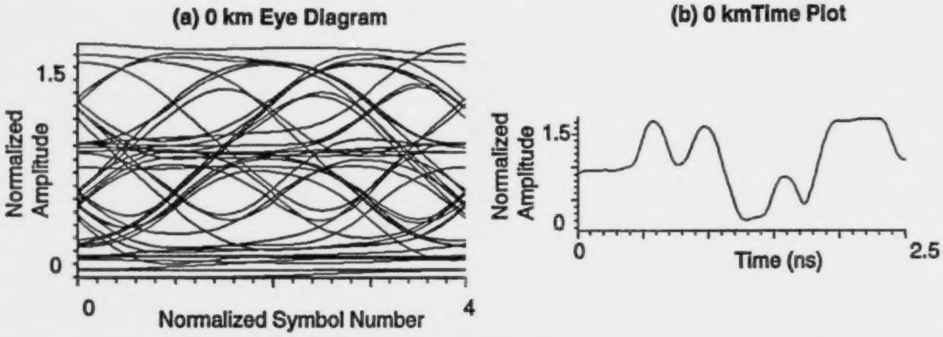

Figure 5.27: 10 Gb/s NRZ Duobinary Reception Simulated Waveforms

5.7. Multilevel Transmission

5.7.1. Scope of Experiments

Many options are available for implementing multilevel transmission with the OTDM transmitter. Duobinary transmission is of most interest because it proves that the parallel duobinary code generation technique outlined in Appendix J is viable. This in turn may eventually lead to a promising technique to reduce intersymbol interference, as shown by simulation results presented in Chapter 2. Other experiments are also of interest to study in more depth the multilevel transmission distortion problem that was identified in Chapter 4. In particular, it is interesting to study the effect of modulating pulses with a multilevel signal at the transmitter, and also to study the impact of reducing the system symbol rate to reduce distortion in the transmitter.

5.7.2. Duobinary Transmission

The entire transmitted signal is not available in electrical form. Therefore, the parallel duobinary coding implementation discussed in Appendix J must be used to obtain transmitted duobinary symbols. A two input parallel duobinary encoder is shown in Figure 5.28 (a). This can be implemented using coaxial components, as shown in Figure 5.28 (b). Additional detail of the coaxial connections is provided to show how proper phasing can be achieved given the physical layout of the coaxial components used and the additional 200 ps (around 4 cm) delay required in the feedback path. 10 dB attenuators are included in each path to isolate outputs from inputs. For example, power that is coupled indirectly from input 2 to output 3 (via the splitter associated with output 4 and combiner associated with input 1) is attenuated 32 dB more than power that is coupled directly from input 2 to output 3. This eliminates visible ripple in the outputs due to the unwanted power coupling.

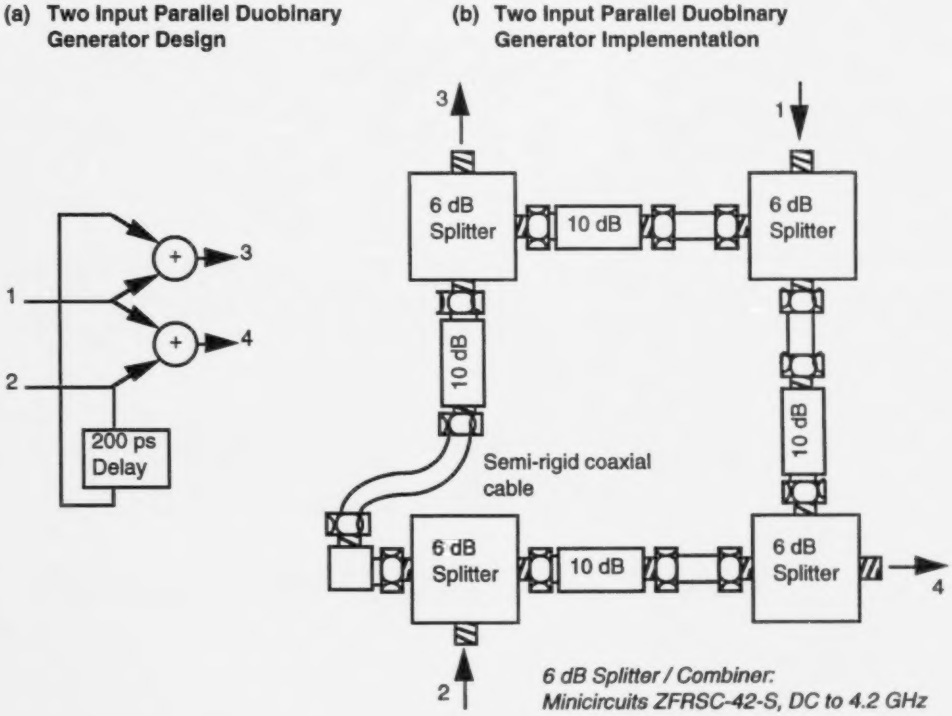
(a) Two Input Parallel Duobinary Generator Design

(b) Two Input Parallel Duobinary Generator Implementation

1
2
+
+
3
4
200 ps Delay
3
1
6 dB Splitter
10 dB
6 dB Splitter
10 dB
10 dB
Semi-rigid coaxial cable
6 dB Splitter
10 dB
6 dB Splitter
4
2
6 dB Splitter / Combiner: Minicircuits ZFRSC-42-S, DC to 4.2 GHz

Figure 5.28: Two Channel Parallel Delay and Add Circuit Implementation

The inputs and outputs for this circuit are shown in Figure 5.29. The amplifier gain was sufficient to overcome the additional 10 dB loss introduced by the parallel delay and add circuit. The same amplifiers used for the binary transmission case are also used for this case. An additional 3 dB attenuator was required in the bottom amplifier input in order to compensate for a 3 dB gain mismatch between the amplifiers. The same polarization multiplexed OTDM transmitter used for the binary trials was also used in conjunction with this drive circuit.

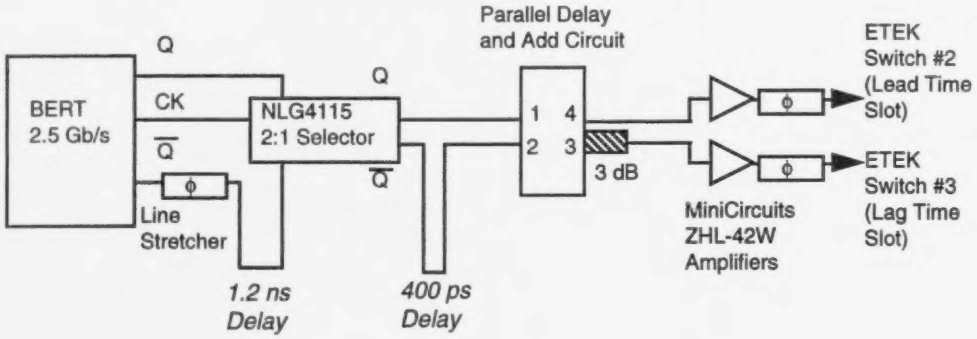
BERT
2.5 Gb/s
Q
CK
$\overline{Q}$
Line Stretcher
ϕ
NLG4115
2:1 Selector
Q
$\overline{Q}$
1.2 ns Delay
400 ps Delay
Parallel Delay and Add Circuit
1
2
3
4
3 dB
MiniCircuits ZHL-42W Amplifiers
ϕ
ϕ
ETEK Switch #2 (Lead Time Slot)
ETEK Switch #3 (Lag Time Slot)

Figure 5.29: Inputs and Outputs of Parallel Duobinary Encoder

Careful phasing of the electrical and optical signals was required to ensure that the duobinary coded output from the parallel duobinary encoder was interleaved properly. This was achieved by equalizing optical path lengths as much as possible with fiber patch cords. Then, additional sections of coaxial cable were added before the input of ETEK switch #2 to ultimately interleave the symbols. Fine delay adjustments were performed with coax line stretchers and the free space optical delay. The signal modulated by ETEK switch #2 was in the time slot directly in front of the signal modulated by ETEK switch #3. It was connected to output 4 of the parallel delay and add circuit, since the signal from output 4 needed to precede the signal from output 3 to realize the correct duobinary sequence.

Figure 5.30 shows the output 5 Gb/s optical signals from the duobinary transmitter before they are combined with the polarization multiplexer. Note that the interleaved symbols have the duobinary polarity property (i.e. an odd number of "1"s separates a transition from a "0" to "2" or a "2" to a "0", and an even number of "1"s separates a transition from a "0" to a "0" or a "2" to a "2"). Eye openings were clearly visible in the individual 5 Gb/s RZ streams.

Figure 5.30 also shows the 10 Gb/s NRZ resulting output from the duobinary transmitter when the two 5 Gb/s RZ channels are combined. This signal is highly distorted and results in no eye openings at the best settings. It was clear that a receiver would not be able to make reliable decisions. Results from simulation of this option appear in Figure 5.31. The simulations generated similar 5 Gb/s RZ outputs, but were optimistic on the 10 Gb/s signal quality.

5.7.3. Pulsed Multilevel Transmission

The nonlinear transfer function of the switch created the same multilevel transmission problem identified in Chapter 4. The switch's output tends to compress extreme level signals ("0" and "2" symbols), but broadens the center level of the signal (the "1" symbol). Figure 5.32 shows a 5 Gb/s ternary signal that was generated by the Wilkinson delay and add circuit and amplified by one of the MiniCircuits amplifiers as it appeared electrically and optically at the output of ETEK switch #3. Although the optical signal produced by modulating a cw 1551 nm laser source was severely distorted, clear eye openings were achievable by modulating the 5 Gb/s RZ pulses generated by the UTP switch when driven by a 5 GHz sinusoidal source from the OTDM setup.

5.7.4. Low Speed Multilevel Transmission

Further experimental work was performed to study the impact of a cleaner switch drive signal. A 2.5 Gb/s rate was used instead of a 5 Gb/s rate. This NRZ signal was passed through a delay and add circuit and then amplified by one of the Mini-Circuits amplifiers, as shown in Figure 5.33. This amplifier has a high frequency cut-off at 4.2 GHz and therefore could amplify the signal with little distortion. Note that the Wilkinson Combiner was not used for this test because the 6 dB combiner with 10 dB input attenuators had a flatter frequency response and sufficient amplifier gain was available to overcome the extra loss.

(a) 5 Gb/s RZ Eye Diagrams

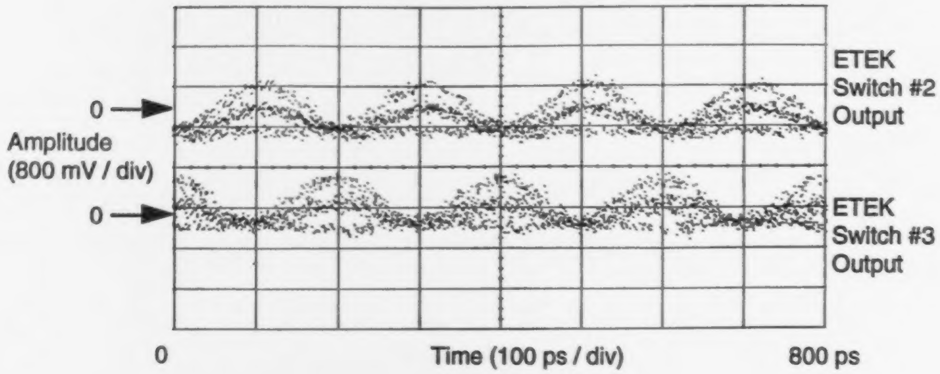

(b) 5 Gb/s RZ Time Plot

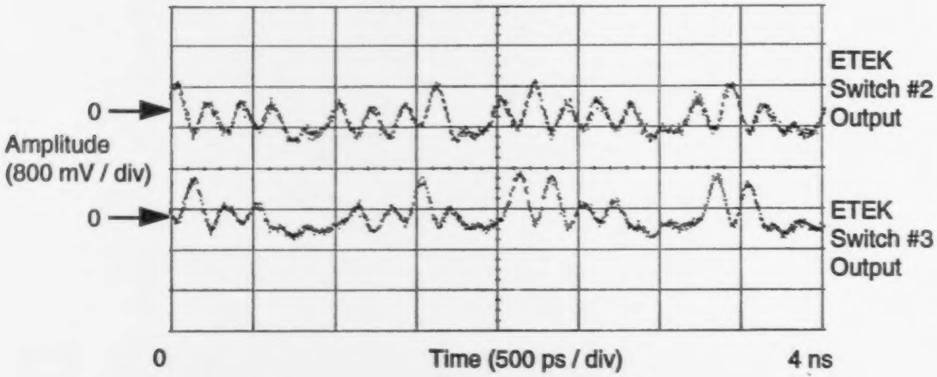

(c) 10 Gb/s NRZ Time Plot (Eyes Closed)

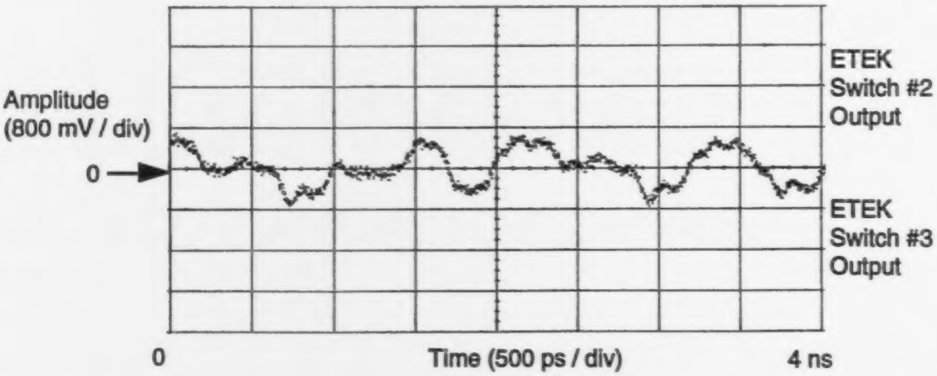

Figure 5.30: Optical Output from Parallel Duobinary OTDM Transmitter

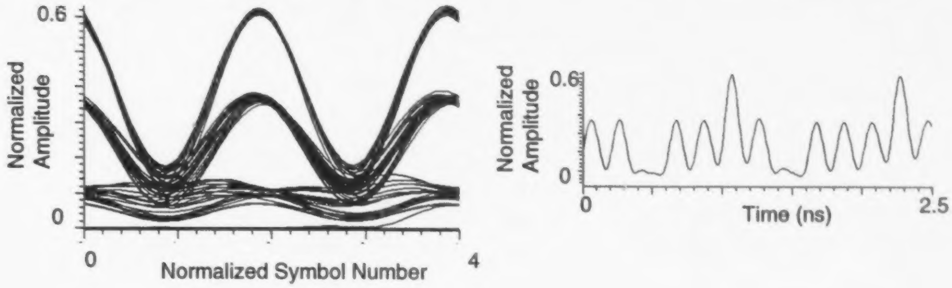
(a) 5 Gb/s RZ Eye Diagram

(b) 5 Gb/s RZ Time Plot

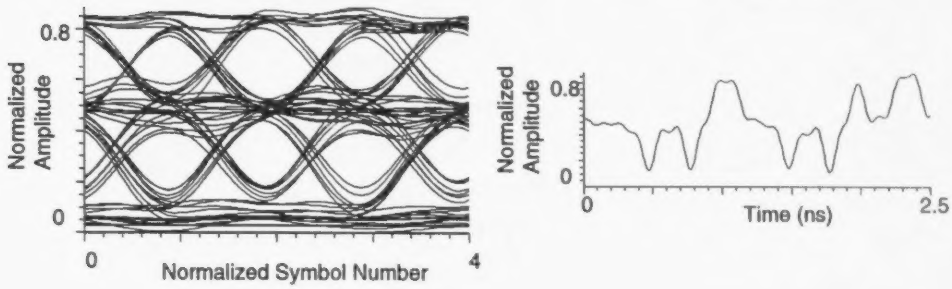
(c) 10 Gb/s NRZ Eye Diagram

(d) 10 Gb/s NRZ Time Plot

Figure 5.31: Optical Output from Simulated Parallel Duobinary Transmitter

The amplified ternary 2.5 Gb/s signal resulted in a very clean electrical signal, and under proper biasing and input signal level conditions, a reasonably clean optical signal as well (Figure 5.34). Higher drive voltages (closer to full switch extinction) resulted in a plot with increased eye closure because of broadening of the center drive level. Also, the eye diagrams had a fuzzier appearance, indicating the presence of more pattern sensitivity (traces that were sampled by the oscilloscope less often than others). This indicates that multilevel transmission is feasible if very high quality transmission amplifiers are used and if the drive signal level is kept low to reduce amplitude swings in the middle level of the signal. Some benefit in middle level swing can be realized by reducing the drive signal amplitude and therefore the full on-full off extinction ratio.

(a) Drive Signal

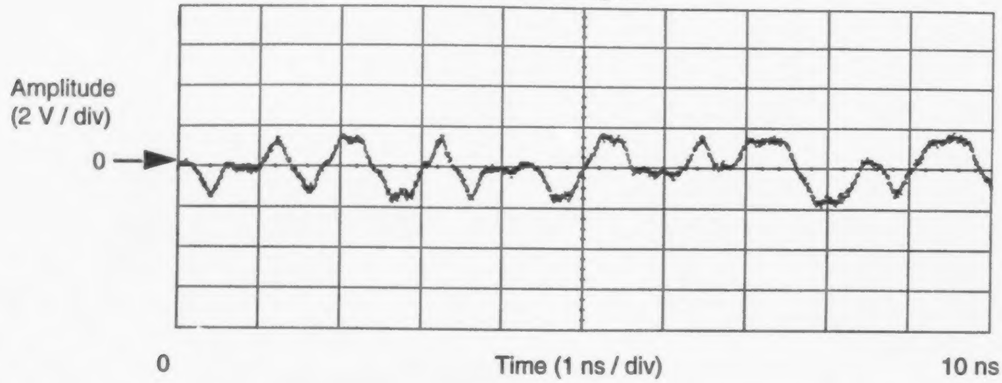

(b) Corresponding Optical Signal With cw Input (Eyes Closed)

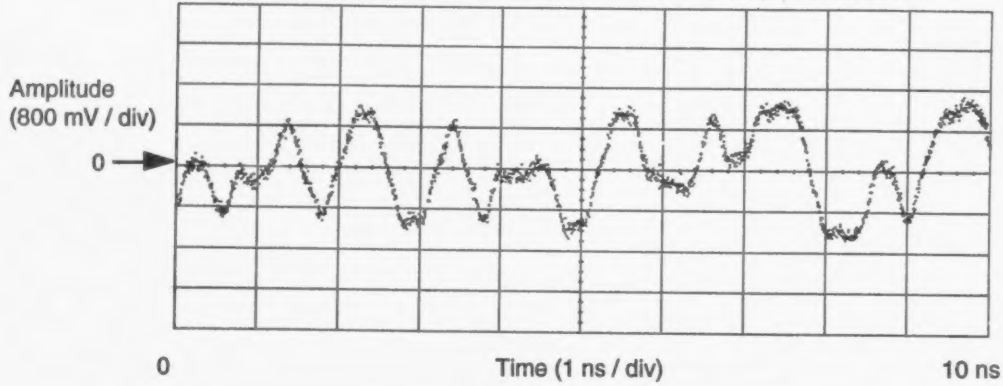

(c) Corresponding Optical Signal with Pulsed Input (Eyes Open)

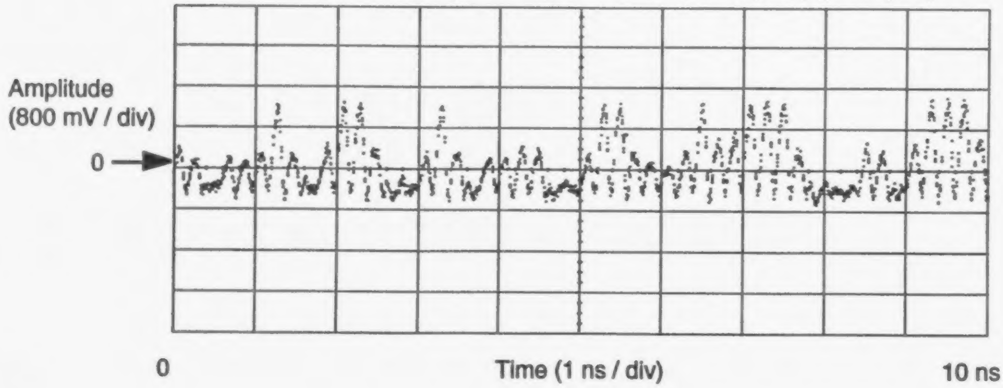

Figure 5.32: Pulsed Multilevel Transmission

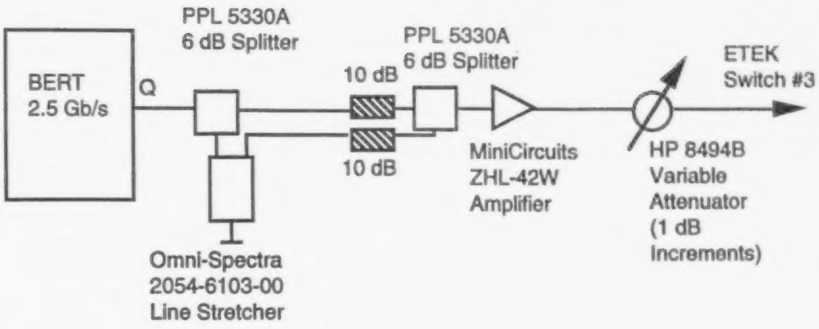
BERT
2.5 Gb/s
Q
PPL 5330A
6 dB Splitter
10 dB
10 dB
PPL 5330A
6 dB Splitter
MiniCircuits
ZHL-42W
Amplifier
HP 8494B
Variable
Attenuator
(1 dB
Increments)
ETEK
Switch #3
Omni-Spectra
2054-6103-00
Line Stretcher

Figure 5.33: Low Speed Multilevel Signaling Setup

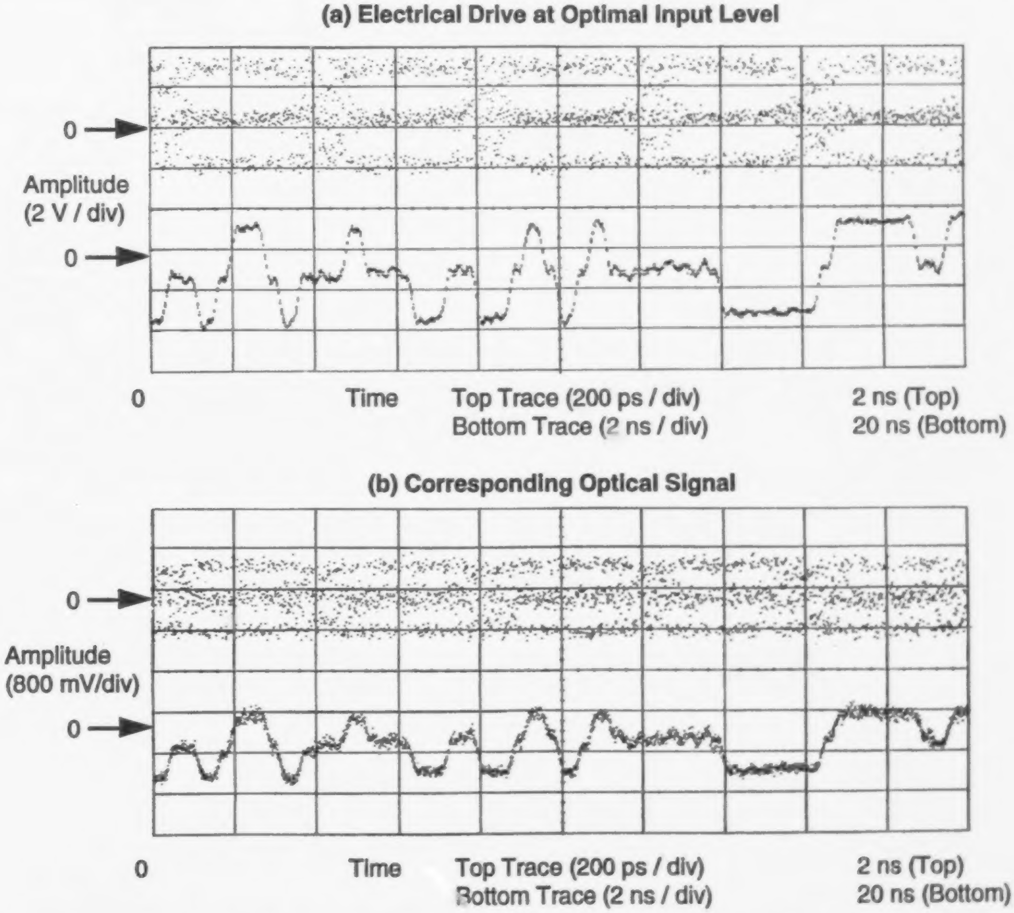

Figure 5.34: Resulting Waveforms from Low Speed Multilevel Experiment

5.8. Evaluation of Results

The OTDM arrangement tested was obviously highly distortion and chromatic dispersion limited. The broad width of the modulated pulses causes a high degree of overlap between adjacent time slots. In terms of intensity, at least 70 percent of a time slot was affected by coupling with its neighbor. Minimal additional distortion beyond that introduced by the receiver and photodetector was required to cause a high intersymbol interference penalty. For this reason, only binary BER data collection was feasible.

5.8.1. Binary Transmission with Binary Reception

A comparison of the 10^{-9} BER input power levels for the different binary transmission and reception options is presented in Figure 5.35. 10 Gb/s NRZ transmission was highly dispersion limited and reached an ultimate transmission limit just beyond 50 km. 5 Gb/s RZ transmission is not affected by chromatic dispersion to the same degree, with a 1.6 dB penalty at 125 km for the 5 GHz receiver and a 1.9 dB penalty at 125 km for the 10 GHz receiver. On average the 5 GHz receiver had about a 1 dB sensitivity improvement over the 10 GHz receiver.

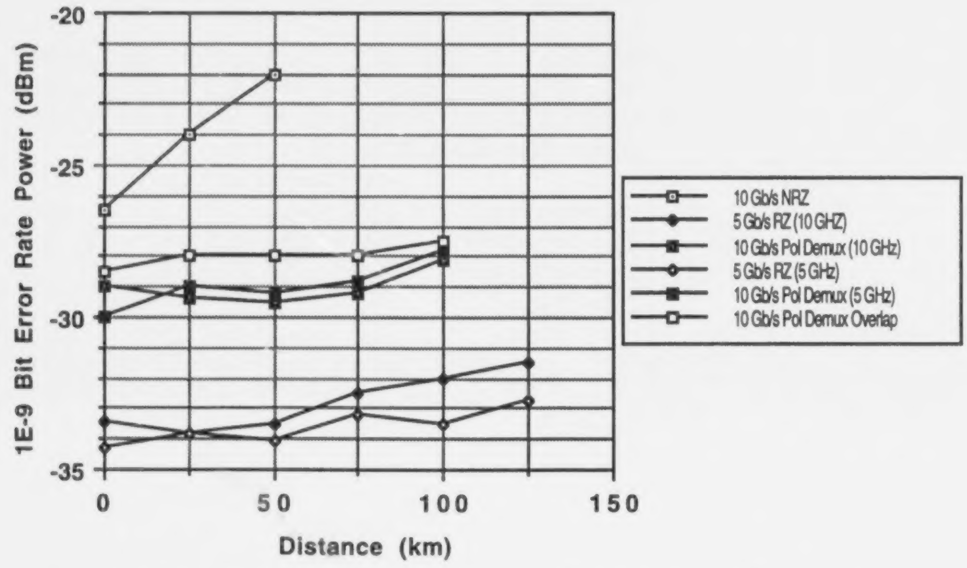

Figure 5.35: Comparison of Binary 10^{-9} BER Input Power Levels

The polarization demultiplexing technique that was used was effective up to and beyond 100 km with a 10 Gb/s throughput and, when compared to 0 km 10^{-9} BER power levels, had a combined chromatic dispersion and polarization crosstalk penalty at 100 km of 0.9 dB for the 10 GHz receiver and 2.2 dB for the 5 GHz receiver. With consideration to experimental error, the 0 km polarization demultiplexing results indicate that the 5 GHz low pass filter could improve receiver sensitivity. The maximum penalty associated with overlapping the pulses is found by comparing the results for this trial with the polarization demultiplexed results for interleaved pulses (5 GHz receiver). The maximum penalty found was 1.5 dB. This indicates that other signaling formats such as NRZ should be feasible over distances up to and beyond 100 km with polarization multiplexing and demultiplexing in place.

Table 5.3 shows the 10^{-9} BER power level differences between 5 Gb/s RZ reception and 10 Gb/s polarization demultiplexed reception as a function of distance. A factor of 3 dB has been removed from this difference to account for the fact that the polarization demultiplexed receiver requires twice the input power for the same decision spacing as the 5 Gb/s RZ receiver. The power required for polarization demultiplexing is consistently higher than the power required for 5 Gb/s reception, even with this factor taken into account. The residual difference between the two formats is at most 2.7 dB, of which 1.4 dB can be accounted for by the insertion loss of the polarization rotator and polarization splitter in the polarization demultiplexed receiver. Therefore, the upper bound on the penalty associated with polarization crosstalk is 1.3 dB. This occurs at 100 km. Other data in the Table indicate that the polarization crosstalk penalty is not significant.

Distance (km)	5 GHz Receiver Difference (dB)	10 GHz Receiver Difference (dB)
0	1.3	1.4
25	1.8	1.4
50	1.9	1.0
75	1.4	0.3
100	2.7	0.9

Table 5.3: Comparison of 5 Gb/s RZ Reception and 10 Gb/s NRZ Polarization Demultiplexed Reception

These polarization demultiplexing results are perhaps the most important findings from the OTDM work. By using this technique, full 10 Gb/s throughput has been achieved over 100 km with a combined chromatic dispersion and polarization crosstalk penalty that does not exceed 2.2 dB. This outperforms even the simulated 10 Gb/s zero chirp binary system in [28] which has a chromatic dispersion penalty of 3 dB at 100 km. This has been accomplished despite the fact that distortion in the transmitter and receiver components prohibited low BER 10 Gb/s reception beyond 50 km without the polarization demultiplexer in place. This polarization demultiplexing technique has the additional benefit that it complements the low electronics speed philosophy of the OTDM transmitter. With the polarization demultiplexer in place, there is no component anywhere in the transmitter or receiver of the 10 Gb/s system that requires an operation speed above 5 Gb/s.

5.8.2. Binary Transmission with Duobinary Reception

Meaningful BER data could not be collected for any of the receivers that convert binary optical signals into electrical duobinary signals. The duobinary receivers had severe power and distortion constraints, especially when a band limit was imposed. A different OTDM system with lower distortion transmitter and receiver components may rectify this problem.

5.8.3. Multilevel Transmission

10 Gb/s multilevel transmission was distortion limited. Despite the lack of BER data, the generation of 10 Gb/s duobinary symbols with the OTDM has demonstrated that the parallel duobinary encoder concept is viable. Further work into cleaning up ternary transmission could result in a parallel coding concept that can reduce dispersion penalties. Preliminary results indicate that a pulsed transmission and a cleaner drive signal will improve transmission quality considerably. Some options for doing this are discussed in Chapter 6.

6. Conclusion

6.1. Consolidated Overview of Results

This work has resulted in the first demonstration of full 10 Gb/s throughput at the University of Alberta, and one of the first 10 Gb/s systems operating anywhere in North America. The chromatic dispersion problem in high bit rate 1550 nm fiber systems using conventional fiber has been studied from a number of viewpoints in both an external modulated system and an OTDM system. Three techniques have been experimentally proven to increase transmission distance substantially beyond the capabilities of conventional binary systems. These are:

a) Converting a binary signal to a duobinary format at the receiver of a system using a simple duobinary transfer function.

b) Introducing negative chirp on the optical signal at the transmitter by applying an RF drive voltage to only one RF input of a Mach-Zehnder modulator.

c) Multiplexing the signal over orthogonal polarization states and performing the first stage of demultiplexing optically using a polarization-sensitive splitter.

These techniques can be combined to increase transmission distance even further.

Also, a novel parallel duobinary encoding method has been developed and implemented. This is an overlay for an OTDM, and therefore allows a new coding method to be incorporated into the transmitter without requiring higher speed electronics than normally required by the OTDM.

Many of the components that were used introduced a significant distortion into either the transmitter path or the receiver path. These in many cases were some of the highest quality components available at the time. This distortion must be expected since 10 Gb/s technology is far from being mature. Further design iterations would result in improved baseline receiver sensitivity, less overall distortion, and potentially could result in BER data to be collected for some of the trials that were distortion limited. This is evident in the results from computer simulations (Chapter 2) which point to significantly improved eye openings when lower distortion components are used.

Electrical multiplexing experiments (Chapter 4) focused on studying zero chirp transmission versus negative chirp transmission, and also compared binary transmission with binary reception to binary transmission with duobinary reception. Using a 3 dB dispersion penalty as a benchmark, negative chirp binary transmission increased the dispersion-limited distance of binary and duobinary reception by over 100 %. Also, the increase in dispersion penalty with increasing distance was more gradual with duobinary reception after about a 2.8 dB penalty for zero chirp transmission and about a 0.6 dB penalty for negative chirp transmission. Simulated results and experimental eye diagrams provide evidence that a wider gap between binary and duobinary reception would be present with an improved design.

Simulated zero chirp electrical multiplexing dispersion penalty results from [28] are better than the experimental results, which likely indicates that residual chirp was present in the modulator and further zero chirp transmission distances could be obtained with a higher quality transmitter drive circuit. Duobinary transmission was also attempted, but signals of sufficient quality to obtain BER data could not be realized due to the nonlinear nature of the modulator and the distortion introduced by the drive components.

OTDM experiments (Chapter 5) focused on studying duobinary coding and polarization multiplexing. Distortion introduced by the OTDM components caused severe eye closure and prohibited BER data from being collected for either duobinary coding at the transmitter or duobinary coding at the receiver. Despite this problem, the parallel duobinary encoding technique developed in Appendix J was implemented and demonstrated to be viable. Another design iteration is definitely required to generate signals of sufficient quality to obtain BER data.

More success was had with binary transmission and reception, and also with incorporating polarization multiplexing and demultiplexing into the OTDM. Two 5 Gb/s polarization multiplexed signals (10 Gb/s throughput) were transmitted over 100 km with less than a 1.5 dB additional penalty compared to an independent 5 Gb/s RZ stream. Full 10 Gb/s transmission was dispersion limited to only 50 km when polarization diversity at the receiver was not exploited. The potential for this polarization multiplexing technique to transmit even further was also demonstrated with BER curves that had a 10^{-8} floor at 125 km. Given the time varying nature of the transmitted signal, a lower BER at this distance could almost certainly be achieved by introducing a clock recovery circuit and a control system to follow changes in polarization state. Polarization multiplexing and demultiplexing was found to be highly susceptible to environmental conditions due to thermal effects on fiber birefringence.

6.2. System Improvements

All dispersion reduction techniques tested showed some advantages compared to conventional approaches and all have their share of limitations. Potential solutions which could be applied to overcome these limitations are presented below.

6.2.1. Improved Frequency Response of Components

The concatenated frequency response of the RF and electro-optic components was a major contributor to determining the quality of the transmitted and received signals. More accurate simulations in advance of building up the actual experiments could target components that would cause the highest signal corruption. When possible, they should be replaced. For example, Figure 6.1 shows the simulated output of the binary OTDM studied in Chapter 5 at 0 km when the frequency response of the actual photodetector that was used has been included and when it has been excluded. A significant improvement in eye opening could be obtained by simply replacing the photodetector that was used with one with a flatter frequency response up to and beyond 10 GHz.

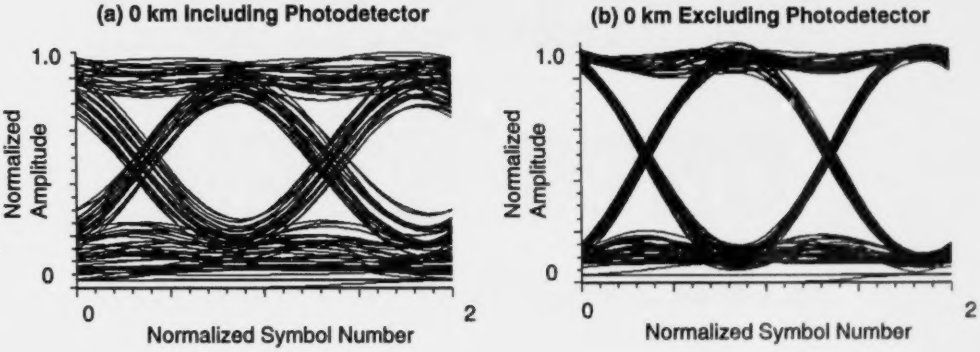

Figure 6.1: Impact of Photodetector on 10 Gb/s OTDM

Also, suppliers are continually upgrading their products to meet the growing market for high frequency RF components. New designs should take advantage of the newest technology.

6.2.2. Automated Control

The DC bias points of all the transmitter Mach-Zehnder devices continually drifted over time frames of less than an hour. This drift results in additional signal distortion and eye closure. Manual adjustment of the bias point was sufficient in laboratory prototypes to keep this under control. A system intended for extended unsupervised operation requires a feedback control system to continually monitor and adjust this bias point. This should be feasible at least for a binary transmitter. From Appendix B, the output intensity of the Mach-Zehnder switch as a function of input voltage has a squared cosine characteristic. If the peak-to-peak amplitude of the drive signal is less than the full extinction voltage V_π and the bias point is set to position the drive signal in the center of this characteristic, then the squared cosine response is approximately linear and few harmonics in the optical signal should result. However, if the bias point is off-center, then one of the extremes of the drive signal will be distorted and more harmonic content in the signal will result. A feedback control system could potentially monitor these harmonics and position the bias point accordingly.

Fluctuations were also present in polarization dispersion and polarization orientation. Laboratory experience has provided evidence that changes in polarization state occur in a time frame in the order of tens of seconds for lengths of spooled fiber at least up to 125 km. This may be different depending on circumstances. For example, fiber deployed in conduit may have characteristics which vary over longer periods because of there may be less stress on it than tightly wound fiber on spools. Given that this time frame appears to be at least into seconds, an active control system to follow changes should be feasible. One possible method that could be used would be to impress a low frequency (kHz) tone on the polarized signal. A simple feedback control system at the receiver should be sufficient to monitor this tone at the orthogonal (isolated) polarization demultiplexer output. This information could be used to allow the polarization orientation of the incoming signal to be continually adjusted for minimum crosstalk. Solutions for polarization problems may be available from wireless technology, where similar time changing transmission medium behavior has always been a problem.

The receiver decision circuit also requires some automation to continually optimize decision threshold and timing. This is already in place for many existing fiber systems, so current designs should be adaptable for new 10 Gb/s designs. Two such control systems could likely be modified for use with a ternary decision circuit in a duobinary receiver.

6.2.3. Duobinary Transmission using Mach-Zehnder Switches

One problem which arose continually in both the electrical multiplexing and the OTDM cases was distortion introduced by the Mach-Zehnder switches when a ternary signal was applied. Although the frequency response of the modulator is important, the main contributor to this problem appears to be its squared cosine voltage-intensity relationship; a large voltage swing tends to result in a small output intensity swing at extreme drive levels (near V_π) and large output intensity swings at the center drive level ($V_\pi / 2$). This characteristic also distorts the transition between levels.

Chapter 5 presented a brief investigation into improving ternary transmission. Two parameters affect the overall ternary signal quality. The first the bandwidth of the RF components relative to the symbol rate. In general, a larger bandwidth reduces the amount of distortion in the signal at the output. The second parameter is input power. The amount of swing in the center level can be reduced considerably by simply reducing the peak-to-peak voltage of the RF signal applied to the modulator. This operates the modulator in a more linear regime. A trade-off in modulator extinction ratio is required because the peak-to-peak signal will be less than V_π.

More sophisticated solutions for this modulator problem can also be envisioned. Since the modulator tends to accentuate voltage swings in the center of its transfer function, high power device which has discrete transitions between levels should result in better quality ternary signals when inserted between the drive amplifier and the modulator electrodes. One possibility is to split the ternary signal between two saturated high speed limiting amplifiers (Figure 6.2). These amplifiers could produce "railed" output which when summed together produce clean high power ternary signals. Diode clamping circuits in a similar configuration may also be a possibility if sufficient high frequency analog components can be found.

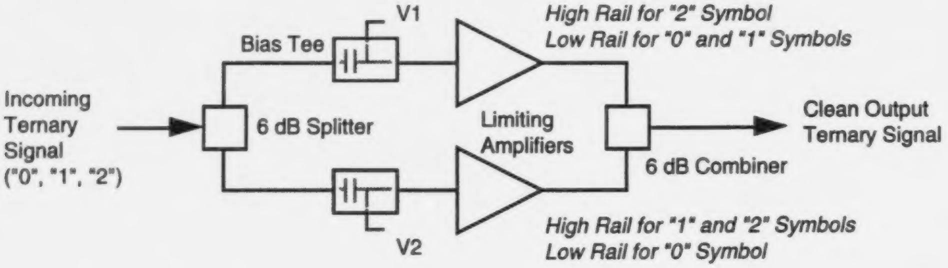
V1
Bias Tee
High Rail for "2" Symbol
Low Rail for "0" and "1" Symbols
Incoming
Ternary
Signal
("0", "1", "2")
6 dB Splitter
Limiting
Amplifiers
Clean Output
Ternary Signal
6 dB Combiner
High Rail for "1" and "2" Symbols
Low Rail for "0" Symbol
V2

Figure 6.2: Ternary Drive Circuit using Limiting Amplifiers

Another approach which looks promising is to perform the addition of the signal optically. Two binary modulators could be used in parallel, followed by an optical addition stage. This is shown in Figure 6.3. Note its similarity to the OTDM system investigated in Chapter 5. Another solution following this theme is to avoid ternary transmitter electronics all together and implement the delay and add function optically. Optical coherency is an important issue for either implementation. It can be avoided by using polarization multiplexing to combine the signals, multiple incoherent sources, or optical delays which separate the added pulses beyond the coherence time of the source.

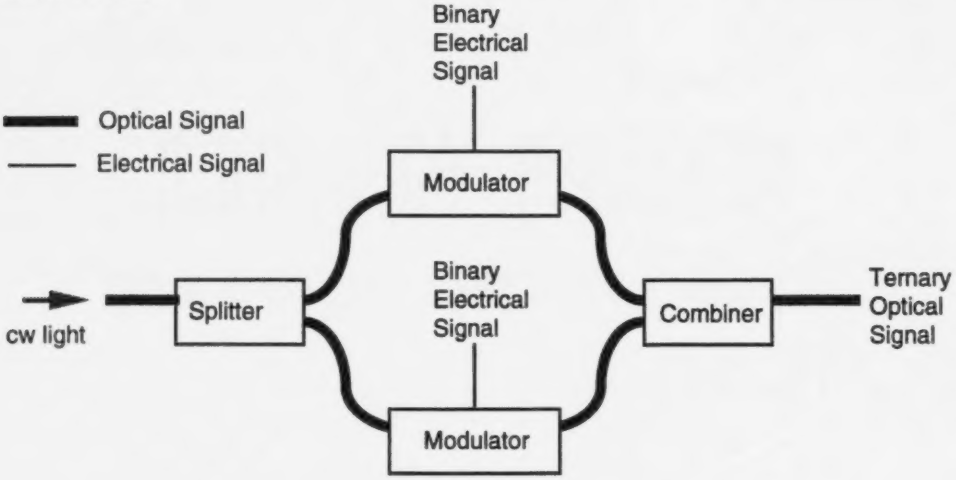
Binary
Electrical
Signal
Optical Signal
Electrical Signal
Modulator
cw light
Splitter
Binary
Electrical
Signal
Combiner
Ternary
Optical
Signal
Modulator

Figure 6.3: Optical Ternary Signal Generator

6.3. Future Work

This work has built on previous OTDM investigations at TRLabs [2] and has also explored new possibilities using electrical multiplexing on its own. Three different approaches to reduce the impact of dispersion have been identified. Each has limitations which partly can be addressed with the solutions presented in this chapter. In particular, using superior components and active control systems should result in a truly robust fiber system capable of long term operation.

Although some investigation into combining two of these three techniques (negative chirped transmission and duobinary reception) has been performed, further work is warranted into combining these with polarization multiplexing and demultiplexing. Given that 10 Gb/s throughput has been demonstrated over at least 160 km of conventional fiber by using a negative chirped binary transmitter coupled to a duobinary receiver, and that polarization multiplexing and demultiplexing has been demonstrated for conventional fiber lengths up to 125 km, there is some logic to the argument that 20 Gb/s throughput over at least 160 km of conventional fiber could be accomplished by combining negative chirp binary transmission, duobinary reception, and polarization multiplexing and demultiplexing. More research into the properties of fiber longer than 125 km would be the first step towards achieving this objective.

Clean multilevel transmission using external modulators remains an elusive goal. Further investigation into combating the nonlinear effects of the modulator transfer function is definitely required in order to use this option to increase transmission system throughput. A study into other modulator configurations is also warranted to see if others have a more linear response.

Polarization multiplexing and demultiplexing has been demonstrated to be feasible, even with optical pulses that are overlapped instead of being interleaved. This opens up the possibility of polarization being another dimension in a signal constellation, just as phase is within a Quadrature Amplitude Modulation (QAM) transmission system. Multilevel signaling creates the other dimension in the constellation. The foundation research work has now been completed to overcome many obstacles that in the past have prohibited multi-gigabit transmission over long distances. Further work could result in a system that can be moved out of the laboratory and deployed in a real network.

References

[1] F. Koyama , K. Iga, "Frequency Chirping in External Modulators", Journal of Lightwave Technology, vol. 6, no. 1, January 1988, pp. 87-93

[2] K. Benterud, Fiber Optic Transmission using Optical Time Division Multiplexing, M.Sc. Thesis, University of Alberta, Fall 1993

[3] J.H. Winters, R.D. Gitlin, S. Kasturia, "Reducing the Effects of Transmission Impairments in Digital Fiber Optic Systems", IEEE Communications Magazine, June 1993, pp. 68-76

[4] J.H. Winters, R.D. Gitlin, "Electrical Signal Processing Techniques in Long-Haul Fiber-Optic Systems", IEEE Transactions on Communications, vol. 28, no. 9, September 1990, pp. 1439-1453

[5] N.L. Swenson, J.M. Cioffi, "Precluding Nonlinear ISI in Direct Detection Long-Haul Fiber Optic Systems", IEEE Photonics Letters, vol. 3, no. 2, February 1991, pp. 182-184

[6] J.H. Winters, S. Kasturia, "Adaptive Nonlinear Cancellation for High-Speed Fiber Optic Systems", Journal of Lightwave Technology, vol. 10, no. 7, July 1992, pp. 971-977

[7] S. Kasturia, J.H. Winters, "Techniques for High-Speed Implementation of Nonlinear Cancellation", IEEE Journal on Selected Areas in Communications, vol. 9, no. 5, June 1991, pp. 711-717

[8] H. Izadpanah et al., "Dispersion Compensation for Upgrading Interoffice Networks Built with 1310 nm Optimized SMFs Using an Equalizer Fiber, EDFAs, and 1310/1550 nm WDM", Post-deadline paper no. PD15, OFC 1992, pp. 369-372

[9] H. Izadpanah, et al, "Dispersion Compensation in 1310 nm-Optimised SMFs Using Optical Equalizer Fibre, EDFAs and 1310 / 1550 nm WDM", Electronics Letters, vol. 28, no. 15, July 16, 1992, pp. 1469-1471

[10] H. Izadpanah, E. Goldstein, C. Lin, "Broadband Multiwavelength Simultaneous Dispersion Compensation Near 1550 nm Through Singlemode Fibers Optimized for 1310 nm", Electronics Letters, vol. 29, no. 4, February 18, 1993, pp. 364-365

[11] C.D. Poole, J.M. Wiesenfeld, D.J. DiGiovanni, "Elliptical-Core Dual-Mode Fiber Dispersion Compensator", IEEE Photonics Technology Letters, vol. 5, no. 2, February 1993, pp. 194-197

[12] J.M. Dugan et al., "All-Optical, Fiber-Based 1550 nm Dispersion Compensation in a 10 Gbit/s, 150 km Transmission Experiment over 1310 nm Optimized Fiber", Post-deadline paper no. PD14, OFC 1992 , pp. 367-370

[13] A.H. Gnauck et al., "Optical Equalization of Fiber Chromatic Dispersion in a 5-Gb/s Transmission System", IEEE Photonics Technology Letters, vol. 2, no. 8, August 1990, pp. 585-587

[14] A.H. Gnauck et al., "8 Gb/s - 130 km Transmission Experiment Using Er-Doped Fiber Preamplifier and Optical Dispersion Equalization", IEEE Photonics Technology Letters, vol. 3, no. 12, December 1991, pp. 1147-1149

[15] L.J. Cimini, L.J. Greenstein, A.A.M. Saleh, "Optical Equalization to Combat the Effects of Laser Chirp and Fiber Dispersion", Journal of Lightwave Technology, vol. 8, no. 5, May 1990, pp. 649-659

[16] L.J. Cimini, L.J. Greenstein, A.A.M. Saleh, "Optical Equalization for High-Bit-Rate Fiber-Optic Communications", IEEE Photonics Technology Letters, vol. 2, no. 3, March 1990, pp. 200-202

[17] A. Frenkal, J.P. Heritage, M. Stern, "Compensation of Dispersion in Optical Fibers for the 1.3 - 1.6 μm Region with a Grating and a Telescope", IEEE Journal of Quantum Electronics, vol. 25, no. 9, September 1989, pp. 1981-1984

[18] H. Izadpanah, E. Goldstein, C. Lin, "Simultaneous 4-wavelength dispersion compensation over a 20-nm bandwidth near 1550 nm through 1310-nm-optimized single-mode fibers", OFC/IOOC '93 Technical Digest, pp. 134-135

[19] C.D. Poole, "Optical fiber-based dispersion-compensation techniques", OFC/IOOC '93 Technical Digest, pp. 202-203

[20] C.D. Poole, K.T. Nelson, J.M. Wiesenfeld, A.R. McCormick, "Broad-band Dispersion Compensation Using the Higher-order Spatial-mode in a Two-Mode Fiber", Post-deadline paper no. PD13, OFC 1992, pp. 363-366

[21] A.J. Antos, D.W. Hall, D.K. Smith, "Dispersion-compensating fiber for upgrading existing 1310-nm-optimized systems to 1550 nm operation", OFC/IOOC '93 Technical Digest, pp. 204-205

[22] A.M. Vengsarkar, A.M. Miller, W.A. Reed, "Highly efficient single-mode fiber for broadband dispersion compensation", Post-deadline paper no. PD13, OFC 1993, pp. 56-59

[23] F. Ouellette, Y. Duval, "Optical Equalization with Linearly Tapered Two-Dissimilar-Core Fiber", Electronics Letters, vol. 27, no. 18, August 29, 1991, pp. 1668-1670

[24] R.M. Jopson, A.H. Gnauck, R.M. Derosier, "10-Gb/s / 360-km Transmission Over Normal-Dispersion Fiber Using Mid-system Spectral Inversion", Post-deadline paper no. PD13, OFC 1993, pp. 17-20

[25] S. Watanabe, T. Naito, T. Chikama, "Compensation of Chromatic Dispersion in a Single-Mode Fiber by Optical Phase Conjugation", IEEE Photonics Technology Letters, vol. 5, no. 1, January 1993, pp. 92-95

[26] A. Gnauck, et. al., "Dispersion Penalty Reduction Using an Optical Modulator with Adjustable Chirp", IEEE Photonics Technology Letters, vol. 3, no. 10, October 1991, pp. 916-918

[27] T. Saito, N. Henmi, S. Fujita, M. Yamaguchi, M. Shikada, "Prechirp Technique for Dispersion Compensation for High-Speed Long-Span Transmission", IEEE Photonics Technology Letters, vol. 3, no. 1, January 1991, pp. 74-76

[28] J.C. Cartledge, R.G. McKay, "Performance of 10 Gb/s Lightwave Systems Using an Adjustable Chirp Optical Modulator and Linear Equalization", IEEE Photonics Technology Letters, vol. 4, no. 12, December 1992, pp. 1394-1397

[29] A.H. Gnauck, et al., "Dispersion Penalty Reduction using a Optical Modulator with Adjustable Chirp", Post-deadline paper no. PD-17, OFC 1991, pp. 78-81

[30] A.D. Ellis, S.J. Pycock, D.A. Cleland, C.H.F. Sturrock, "Dispersion Compensation in 450 km Transmission System Employing Standard Fibre", Electronics Letters, vol. 28, no. 10, May 1992, pp. 954-955

[31] B. Wedding, "New Method for Optical Transmission Beyond Dispersion", Electronics Letters, vol. 28, no. 14, July 1992, pp. 1298-1300

[32] W.D. Grover, "Forward Error Correction in Dispersion-Limited Lightwave Systems", Journal of Lightwave Technology, vol. 6, no. 5, May 1988, pp. 643-654

[33] P.M. Gabla, et al., "401 km, 622 Mb/s and 357 km, 2.488 Gb/s IM / DD Repeaterless Transmission Experiments Using Erbium-Doped Fiber Amplifiers and Error Correcting Code", IEEE Photonics Technology Letters, vol. 4, no. 10, October 1992, pp. 1148-1151

[34] N.L. Swenson, J.M. Cioffi, "Coding Techniques to Mitigate Dispersion-Induced ISI in Optical data Transmission", Proceedings of IEEE International Conference on Communications ICC '90, paper 307.5, 1990, pp. 468-472

[35] R. Brooks, A. Jessop, "Line Coding for Optical Fibre Systems", International Journal of Electronics, vol. 55, no. 1, 1983, pp. 81-120

[36] T. Ohishi, M. Takahara, "Evaluation of EDB Code in Optical Fiber Communications", Electronics and Communications in Japan, part 1, vol. 70, 1987, pp. 93-101

[37] P. Hill, R. Olshansky, W.K. Burns, "Optical Polarization Multiplexing at 4 Gb/s", IEEE Photonics Technology Letters, vol. 4, no. 5, May 1992, pp. 500-502

[38] P.M. Hill, R. Olshansky, W.K. Burns, "Optical Polarization Division Multiplexing at 8 Gb/s with Novel Clock and Carrier Recovery", Proceedings of European Conference on Communications 1992, pp. 165-168

[39] C. Herard, A. Lacourt, "New multiplexing technique using polarization of light", Applied Optics, vol. 30, no. 2, January 1991, pp. 222-231

[40] S. Kawanishi, et. al., "100 Gb/s, 50 km Optical Transmission Employing All-Optical Multi/Demultiplexing and PLL Timing Extraction, Post-deadline paper no. PD2, OFC 1993, pp. 13-16

[41] A. Lender, "The duobinary technique for high-speed data transmission", IEEE Transactions on Communications Electronics, vol. 82, May 1963, pp. 214-218

[42] P. Kabal, S. Pasupathy, "Partial-Response Signaling", IEEE Transactions on Communications, vol. COM-23, no. 9, Sept. 1975, pp. 921-934

[43] B. P. Lathi, Modern Digital and Analog Communication Systems, 2nd Edition, Holt, Rinehart, and Winston, New York, 1989, pp. 184-188

[44] G. May, "Duobinary Coding to Reduce the Impact of Chromatic Dispersion: BNR Internship Report", TRLabs Report Number TR-93-01, March 1993

[45] A.F. Elrefaie, R.E. Wagner, D.A. Atlas, D.G. Gaut, "Chromatic Dispersion Limitations in Coherent Lightwave Transmission Systems", Journal of Lightwave Technology, vol. 6, no. 8, May 1988, pp.704-709

[46] P.J. Corvini, T.L. Koch, "Computer Simulation of High-Bit-Rate Optical Fiber Transmission Using Single-Frequency Lasers", Journal of Lightwave Technology, vol. LT-5, No. 11, November 1987, pp. 1591-1591

[47] N. Olsson, "Lightwave Systems with Optical Amplifiers", Journal of Lightwave Technology, vol. 7, no. 7, July 1989, pp. 1071-1082

[48] D. Barabash, R. Morris, "Semiconductor Laser Amplifier Noise Generation", TRLabs Interim Report #TR-89-15, December 1989

[49] J. Smith, Modern Communication Circuits, Mc-Graw-Hill Book Company, New York, 1986, p. 68

[50] J. Freeman, Theory, Design, and Characterization of Erbium-Doped Fiber Amplifiers, University of Alberta, Fall 1991, pp. 159-163

[51] C.R. Giles, E. Desurvire, "Propagation of Signal and Noise in Concatenated Erbium-Doped Fiber Amplifiers", Journal of Lightwave Technology, vol. 9, no. 2, February 1991, pp. 147-154

[52] A. Chraplyvy, "Limitations on Lightwave Communications Imposed by Optical-Fiber Nonlinearities", Journal of Lightwave Technology, vol. 8, no. 10, October 1990, pp. 1548-1557

[53] T. Fujiwara, S. Sato, H. Mori, Y. Fujii, "Suppression of Crosstalk Drift in Ti:$LiNbO_3$ Waveguide Switches", Journal of Lightwave Technology, vol. 6, no. 6, June 1988, pp. 909-915

[54] R. Harmon, "Polarisation Stability in Long Lengths of Monomode Fibre", Electronics Letters, vol. 18, no. 25, November 1982, pp. 1058-1060

[55] G.J. Foschini, C.D. Poole, "Statistical Theory of Polarization Dispersion in Single Mode Fibers", Journal of Lightwave Technology, vol. 9, no. 11, November 1991, pp. 1439-1456

[56] B. Saleh, M. Teich, Fundamentals of Photonics, John Wiley & Sons, New York, 1991, pp. 351-352

[57] B.P. Lathi, Modern Digital and Analog Communication Systems, 2nd Edition, Holt, Rinehart, and Winston, New York, 1989, pp. 173-175

[58] B.P. Lathi, Modern Digital and Analog Communication Systems, 2nd Edition, Holt, Rinehart, and Winston, New York, 1989, p. 185

[59] J.G. Proakis, Digital Communications, 2nd Edition, McGraw-Hill Book Company, New York, 1989, p. 193

[60] A. Djupsjobacka, "Time Division Multiplexing Using Optical Switches", IEEE Journal on Selected Areas in Communications, vol. 6, no. 7, August 1988, pp. 1227-1231

[61] D.M. Pozar, Microwave Engineering, Addison-Wesley Publishing Company, New York, 1990, pp. 395-400

[62] T. Izawa, S. Sudo, Optical Fibers: Materials and Fabrication, Kluwar Academic Publishers Group, Holland, 1987, pp. 44-45

[63] R. Gitlin, J. Hayes, S. Weinstein, Data Communication Principles, Plenum Press, New York, 1992, pp. 437-441

Appendix A: Bandwidth Reduction with Duobinary Coding

A.1. Viewpoints

There are two viewpoints that can be taken towards understanding duobinary coding and its reduction in bandwidth compared to binary coding.

A.1.1. Correlation Viewpoint

Correlation arises in duobinary symbols because of their polarity property. Assuming a bipolar ternary signal "-1", "0" and "1", the sequence has the following properties:

- A change between the symbols "-1" and "1" (or "1" and "-1") in a sequence is always separated by an odd number of "0"s.
- A sequence of constant "-1" or "1" symbols is always separated by no "0"s or an even number of "0"s.

To simplify the following derivation, bipolar ternary symbols are assumed. Also, it is assumed that half the information symbols are "0", and the other half are evenly distributed between "-1" and "1".

The duobinary sequence can be expressed as:

$$v(t) = \sum_{n=-\infty}^{\infty} a_n \, p(t - nT) \qquad (A.1)$$

where: a_n is the information symbol ("-1", "0", "1")
$p(t)$ is a pulse of arbitrary shape and duration

The autocorrelation function for the duobinary sequence is defined from the expected value of products of the information symbols as:

$$\phi_{aa}[k] = E[a_n \, a_{n+k}] \qquad (A.2)$$

The polarity restrictions imposed by the duobinary sequence result in the following autocorrelation function values [57]: $\phi[0] = 1/2$, $\phi[1] = \phi[-1] = 1/4$, and $\phi[k] = 0$ for $|k| > 1$.

The power density spectrum of the information sequence is given by [59]:

$$\Phi_{aa}(f) = \sum_{m=-\infty}^{\infty} \phi_{aa}[m] e^{-j2\pi f m T} \qquad \text{(A.3)}$$

where: T is symbol period

Substituting the values for $\phi[k]$ in the above equation and simplifying results in:

$$\Phi_{aa}(f) = \frac{1}{2} + \frac{1}{2}\cos(2\pi f T) = \cos^2(\frac{\pi f}{f_o}) \qquad \text{(A.4)}$$

where: f_o is the bit rate frequency = 1 / T

The average power density of the duobinary sequence is now given by [59]:

$$\Phi_{vv}(f) = \frac{1}{T}|P(f)|^2 \Phi_{aa}(f) \qquad \text{(A.5)}$$

where: P(f) is the Fourier transform of the pulse p(t)

For the duobinary case, this results in:

$$\Phi_{vv}(f) = \frac{1}{T}|P(f)|^2 \cos^2(\frac{\pi f}{f_o}) \qquad \text{(A.6)}$$

If the duobinary sequence is transmitted using Non-Return to Zero (NRZ) pulses, the following spectrum results:

$$\Phi_{vv}(f) = \frac{A^2}{f_o}\left[\frac{\sin^2(\pi f / f_o)}{(\pi f / f_o)^2}\right]\cos^2(\frac{\pi f}{f_o}) \qquad \text{(A.7)}$$

where: A is the amplitude of the pulse

For a random polar binary sequence with symbols "-1" and "1", the autocorrelation function $\phi[k] = 1$ for $k = 0$, and $\phi[k] = 0$ for $k \neq 0$. Thus, the following spectrum results when the sequence is transmitted using NRZ pulses:

$$\Phi_{vv}(f) = \frac{A^2}{f_o}\left[\frac{\sin^2(\pi f / f_o)}{(\pi f / f_o)^2}\right] \qquad \text{(A.8)}$$

Figure A.1 presents a comparison of the duobinary power spectrum and the binary power spectrum for 10 Gb/s NRZ pulses (i.e. f_o = 10 GHz), normalized to a peak value of 1. Note that the bulk of the power in the random duobinary signal is contained in one half the bandwidth of the bulk of the power in the random binary signal. The power above 5 GHz in the duobinary signal is almost negligible. Careful selection of the modulated pulse shape could reduce it even further.

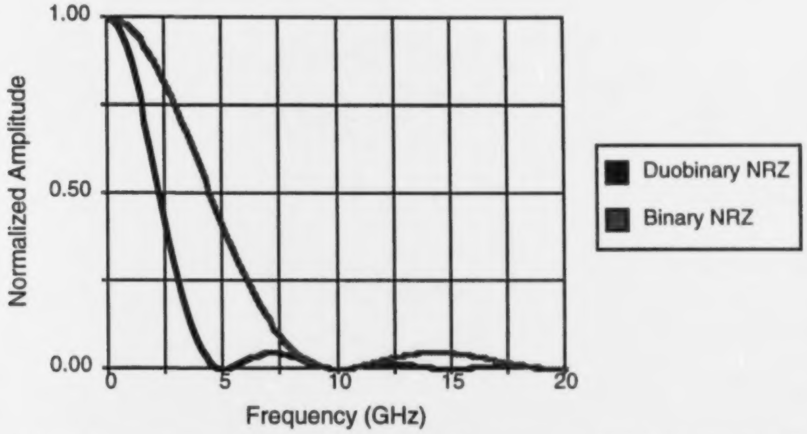

Figure A.1: Comparison of Binary and Duobinary NRZ Power Spectrum

Obviously the correlation in the duobinary signal results in a significant reduction in bandwidth, even without any further low pass filtering. This correlation can conveniently be introduced with a simple delay and add circuit as shown in Figure A.2. Also shown are sample inputs and outputs which have the duobinary polarity property.

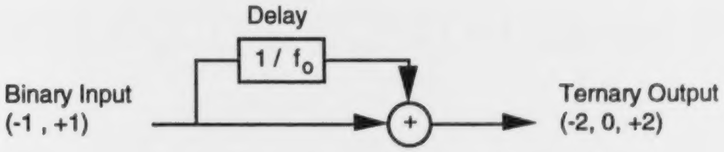

Sample Input Sequence: +1 -1 -1 +1 +1 +1 -1 +1 +1 -1 -1 -1 -1 +1 ...
Corresponding Ouput: 0 -2 0 +2 +2 0 0 +2 0 -2 -2 -2 0 ...

Figure A.2: Delay and Add Circuit

A.1.2. Pulse Shape Viewpoint

Duobinary coding makes use of Nyquist's Second Criterion for Zero Intersymbol Interference which states that controlled intersymbol interference can be used to reduce signal bandwidth. The power spectrum for a duobinary pulse that meets this criterion is:

$$\cos(\pi f / f_o)\, \Pi(f / f_o) \qquad \text{(A.9)}$$

where: the gate function $\Pi(x) = 1$ for $|x| \le 0.5$

$= 0$ for $|x| > 0.5$

This power spectrum can be obtained by passing an impulse through a transfer function with the shape defined in (A.9). This transfer function can be realized with the circuit shown in Figure A.3. The low pass filter following the delay and add provides the gate function.

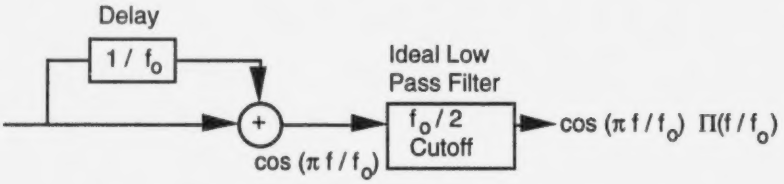

Figure A.3: Duobinary Transfer Function

For a random polar binary sequence ("-1", "1") with the pulse shapes produced by the filter defined in (A.9), the power spectral density of the signal from (A.5) is:

$$\Phi_{vv}(f) = \frac{1}{T} |\cos^2(\frac{\pi f}{f_o})|^2\, \Pi(f / f_o) \qquad \text{(A.10)}$$

Note the similarity of this expression with (A.6) and the filter shape with the correlating delay and add circuit shown in Figure A.2. A reduction in bandwidth compared to binary transmission is realized either by introducing correlation into signals transmitted with an arbitrary pulse shape (correlation viewpoint), or by shaping the pulse to result in controlled intersymbol interference (pulse shape viewpoint). The pulse shaping option has an absolute band limit at $f_o / 2$ with zero distortion, therefore it is the preferred approach.

This circuit shown in Figure A.3 does not sufficiently meet the duobinary transfer function requirements because it is designed for an impulse stream. In a real-world system the transfer function must be modified to factor out the concatenated frequency response of all transmitter and receiver components, as well as the spectral shape of the input pulse itself.

Since it is not possible to design a broadband filter with arbitrary gain and delay to compensate for all path elements as well as the non-impulse signaling format, it is not possible to realize an ideal duobinary filter. One important parameter which is controllable is the hold time in the delay and add circuit. This can be changed to accommodate the roll-off in the spectrum of the input pulse. The 10 Gb/s delay and add circuit with a 100 ps (1 / f_o) delay is designed for impulse signals which have a flat amplitude spectrum to infinity. Return to Zero (RZ) and NRZ signals have a roll off in their spectra. This results in additional roll off within the pass band of the concatenated response. Shortening the hold time in the delay and add circuit results in a null point at a higher frequency in the duobinary transfer function. The combination of this more gradual roll off with the pulse shape roll off results in a concatenated response which more represents the ideal. The impact of changing this delay is shown in Figure A.4. Of course, other components in the path will introduce their own frequency responses, and therefore the delays shown below are not ideal. The delay and add circuit should have a variable delay so maximum eye opening can be achieved in the experimental setup.

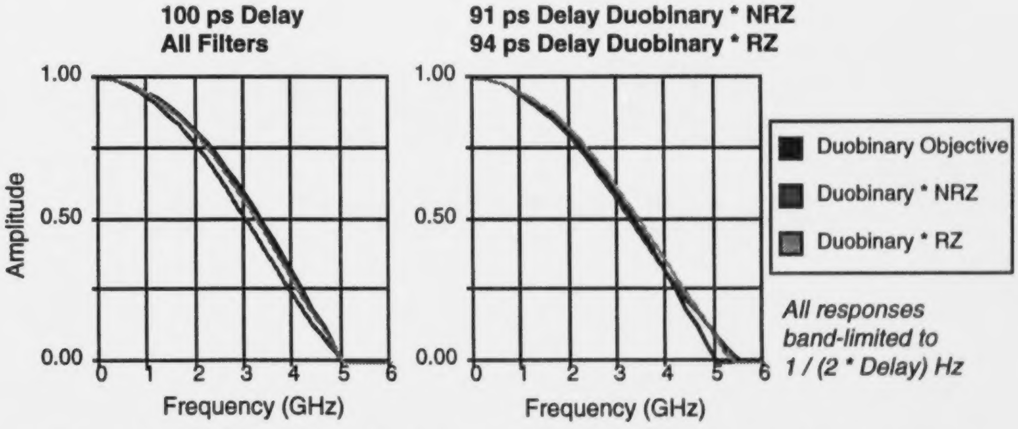

100 ps Delay
All Filters

91 ps Delay Duobinary * NRZ
94 ps Delay Duobinary * RZ

All responses band-limited to 1 / (2 * Delay) Hz

Figure A.4: Pulse Spectrum Combined with Duobinary Filter Response

Appendix B: Electro-optic Switch and Modulator Theory

The electro-optic switches and modulators have a transfer function and chirp characteristics which have a large influence over the performance of the dispersion reduction options tested. All used switches and modulators used were of a Mach-Zehnder form using $LiNbO_3$ electro-optic material. Figure B.1 shows a simple model of a Mach-Zehnder interferometer section (after [1]). Incoming light is symmetrically split between the two branches. Applied voltage on the electrodes causes changes in the refractive index of the material which results in phase shifts. The light is then recombined. The result is an output intensity that can be related to the phase shifts.

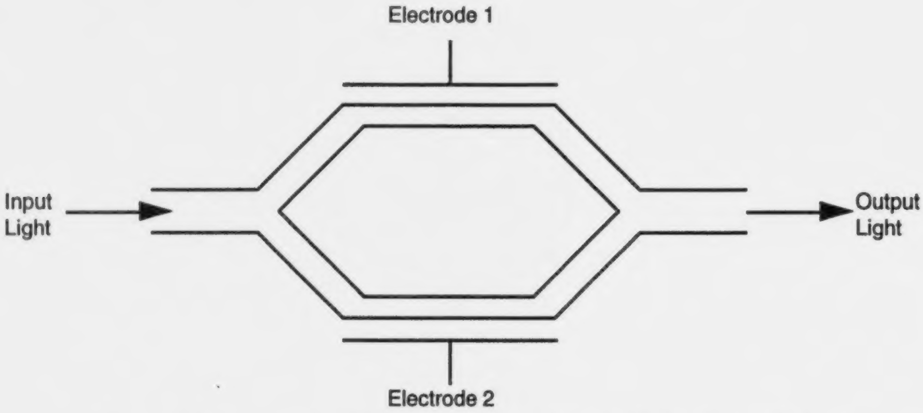

Figure B.1: Basic Structure of a Mach-Zehnder Section

The output electric field at Output 1 is given by [1]:

$$E = \frac{E_o}{2} e^{-j\beta_1 L} + \frac{E_o}{2} e^{-j\beta_2 L} \tag{B.1}$$

where: E_o is the amplitude of the electrical field in the input waveguide

β_i is the propagation constant in waveguide i

L is the device length

This simplifies to:

$$E = E_o \cos(\Delta\beta L) e^{-j\bar{\beta} L} \tag{B.2}$$

$$\Delta\beta = (\beta_1 - \beta_2)/2 \tag{B.3}$$

$$\bar{\beta} = (\beta_1 + \beta_2)/2 \tag{B.4}$$

The intensity of the output is given by the squared magnitude of (B.2):

$$\eta = \cos^2(\Delta\beta L) \tag{B.5}$$

Equation (B.5) is often expressed as a function of applied drive voltage V and the characteristic half-wave voltage of the device V_π.

$$\eta = \cos^2(\frac{\pi V}{2 V_\pi}) \tag{B.6}$$

The RF (radio frequency) signal applied to the modulator is generally centered about 0 Volts. A DC bias is added to position the RF signal in the center of the modulator transfer function:

$$\eta = \cos^2(\frac{\pi}{2 V_\pi}(V_{DC} + V_{RF})) \tag{B.7}$$

This transfer function is repetitive because it is based on a cosine, as shown in Figure B.2. Therefore the same intensity output will be present at a particular V_{DC} or $V_{DC} + 2V_\pi$. Note that the shape of the transfer function changes depending on the input signal level. Close to the center of the transfer function (e.g. $0.5V_\pi$ in Figure B.2), it is almost linear. At the extremes (e.g. V_π in Figure B.2), large variations in the drive signal result in small variations in output intensity. Some degree of distortion in the conversion of electrical signal to optical signal is inevitable with this transfer function. This is especially the case if the DC bias point is not centered properly.

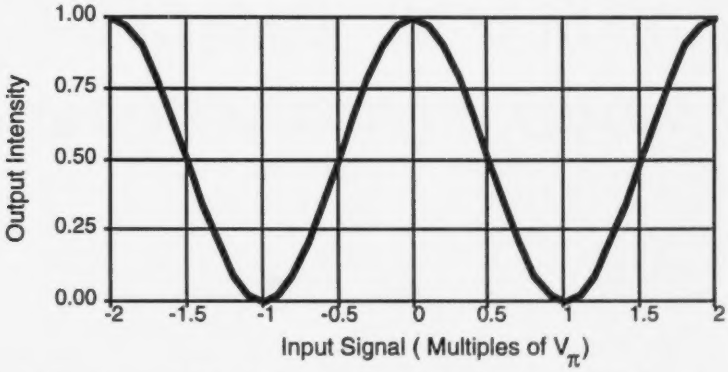

Figure B.2: Output of Mach-Zehnder Modulator as a Function of Input

Equation (B.2) shows that the phase of the electric field will be zero if $\overline{\beta}$ is zero. This is the case if the changes in β_1 and are β_2 exactly opposite. Assuming perfectly matched electrodes, this only occurs if the voltages applied to the electrodes are opposite at all times. In all other cases, $\overline{\beta}$ has a non-zero value. This in turn results in a frequency shift, or chirp on the transmitted signal. Some Mach-Zehnder devices are designed specifically for zero chirp operation with a single drive voltage being evenly distributed to the two phase shift sections. Others have separate electrode drives which allows arbitrary phase shifts.

The modulation chirp parameter represents the ratio of phase modulation to amplitude modulation, and may be expressed as a function of time as [1][26]:

$$\alpha_m(t) = \frac{d\phi / dt}{(1/2I)(dI/dt)} \qquad \text{(B.8)}$$

where: α_m is the modulation chirp parameter
ϕ is the instantaneous phase
I is the instantaneous intensity

In general this is a function of the modulation depth and operating point of the modulator. Assuming a Mach-Zehnder modulator based on the linear electro-optic effect, a DC bias point centered on its switching curve, and the two electrodes are driven with mathematically similar waveforms, α_m is constant in the small signal limit and may be written in terms of peak-to-peak applied voltages ΔV_1 and ΔV_2 [26]:

$$\alpha_m = (\Delta V_1 + \Delta V_2) / (\Delta V_1 - \Delta V_2) \qquad \text{(B.9)}$$

This expression was derived in the small signal regime, but is sufficiently accurate for relatively large modulation depths as well. From (B.9), it is clear that arbitrary chirp values can be realized with the appropriate values of ΔV_1 and ΔV_2. Three chirp values are of particular importance: $\alpha_m = 0$ ($\Delta V_1 = -\Delta V_2$), $\alpha_m = -1$ ($\Delta V_1 = 0$), and $\alpha_m = +1$ ($\Delta V_2 = 0$). In the first case, the modulator is driven to full extinction if $\Delta V_1 - \Delta V_2 = V_\pi$. In the last two cases, the modulator is driven to full extinction if the non-zero voltage peak-to-peak value is V_π. Also, the sign of ΔV_i changes with a V_π shift in DC bias point.

The above expressions for output intensity and chirp were derived for a simple Mach-Zehnder modulator. However, they still apply to other electro-optic switch configurations. A Y-branch switch can be constructed by replacing the output combining stage with a passive 3 dB coupler. The intensity factor η now represents the intensity distribution between the outputs (i.e. the intensity of one output is η, and the other is $1-\eta$). A balanced bridge interferometer has the same output section as a Y-branch switch. Its input splitter is replaced with a 3 dB coupler. It has the same output intensity characteristic if only one input is used.

Another consideration for using Mach-Zehnder modulators and switches is their frequency response. In general, the layout of the design results in a frequency roll-off and an ultimate modulator bandwidth constraint. This modulator frequency response can introduce significant distortion in addition to that caused by its cosine-shaped transfer function.

Appendix C: Optical Time Division Multiplexer

The OTDM to be studied makes extensive use of Mach-Zehnder switches and modulators and RF components. Figure C.1 shows an OTDM capable of generating a 2B Gb/s optical signal using RF components with frequency requirements no higher than B GHz. A simulated evaluation of a similar architecture appears in [60]. This OTDM configuration is also similar to the architecture studied previously at TRLabs and described in [2], which was a 10 Gb/s OTDM with one operational 2.5 Gb/s time slot.

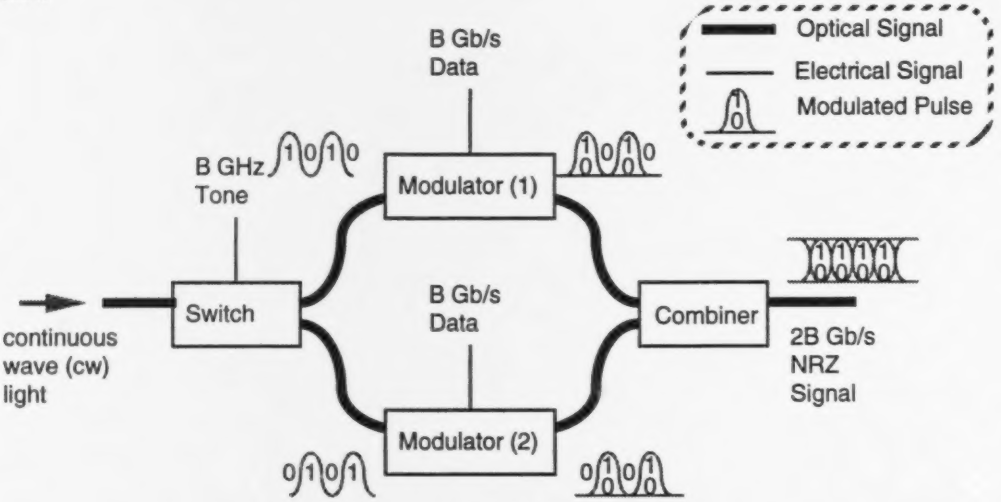
Optical Signal
Electrical Signal
Modulated Pulse
B Gb/s Data
B GHz Tone
1 0 1 0
Modulator (1)
1 0 1 0
continuous wave (cw) light
Switch
B Gb/s Data
Combiner
1 1 1 1 0 0 0 0
2B Gb/s NRZ Signal
Modulator (2)
0 1 0 1
0 1 0 1

Figure C.1: Two Channel OTDM

The main components of this OTDM are the pulse distribution stage, the modulators (1 and 2) and the combiner. The pulse distribution stage is a 1x2 switch driven by a B GHz sinusoidal tone to generate optical "Return to Zero" (RZ) pulses for input into the modulators. These pulses have a sinusoidal appearance. Other pulse shapes are possible with different pulse distribution drive signals, but a high frequency sinusoid is the simplest drive to realize. The RZ pulses alternate between the modulators which impress B Gb/s information on the pulses by either allowing the pulses to propagate through or by blocking them. The modulated RZ pulses are then interleaved at the combiner into a full 2B Gb/s NRZ sequence. This combiner can either be active, using another Mach-Zehnder switch driven by a B GHz sinusoidal tone, or passive, using a fiber optic coupler device. The OTDM system modeled in simulations and evaluated in Chapter 5 used a passive coupler device.

Appendix D: BOSS Block Diagrams

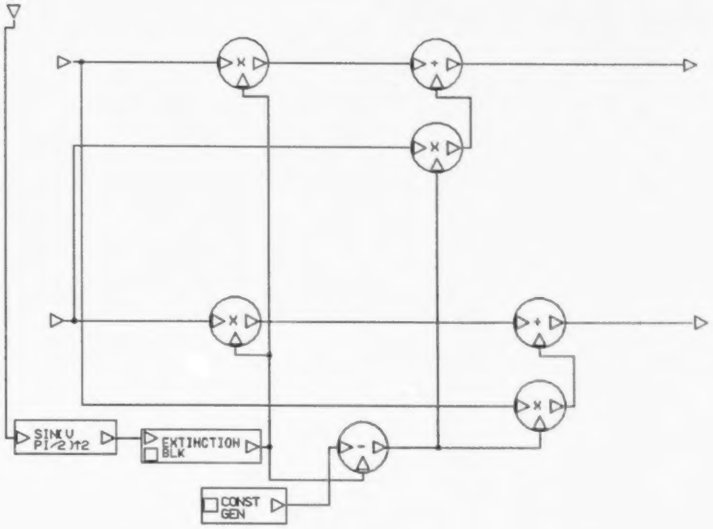
SIN(V PI/2)↑2
EXTINCTION BLK
CONST GEN

Figure D.1: Mach-Zehnder Switch Model

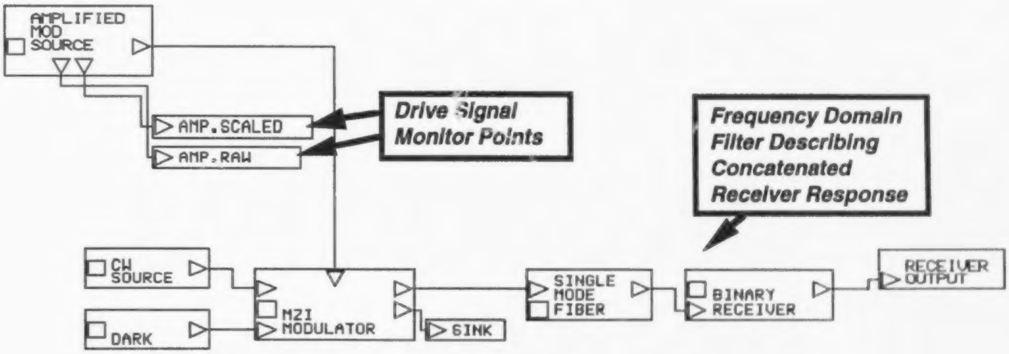
AMPLIFIED MOD SOURCE
AMP.SCALED
AMP.RAW
CW SOURCE
DARK
MZI MODULATOR
SINK
SINGLE MODE FIBER
BINARY RECEIVER
RECEIVER OUTPUT

Drive Signal Monitor Points

Frequency Domain Filter Describing Concatenated Receiver Response

Figure D.2: Binary Transmission with Binary Reception, Electrical Multiplexing

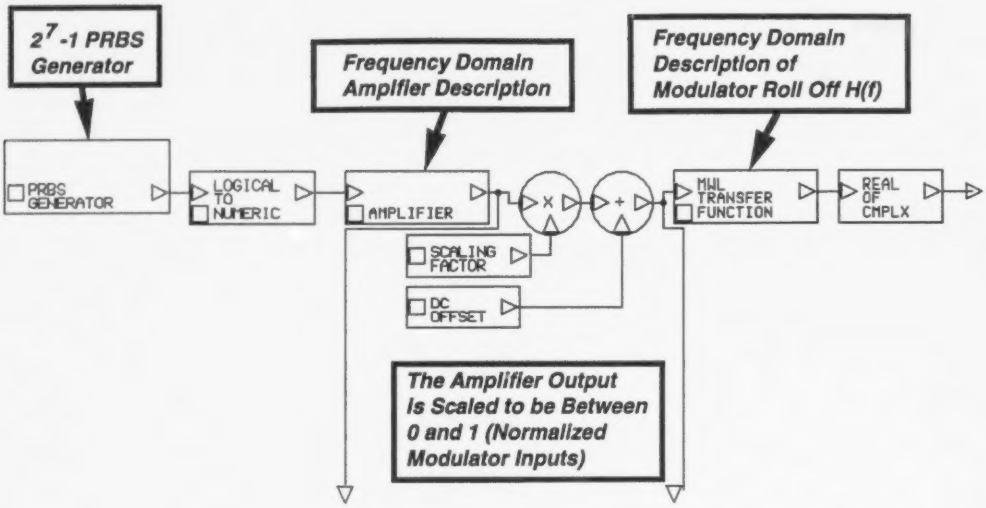
2^7-1 PRBS Generator
Frequency Domain Amplifier Description
Frequency Domain Description of Modulator Roll Off H(f)
PRBS GENERATOR
LOGICAL TO NUMERIC
AMPLIFIER
×
+
SCALING FACTOR
DC OFFSET
MWL TRANSFER FUNCTION
REAL OF CMPLX
The Amplifier Output Is Scaled to be Between 0 and 1 (Normalized Modulator Inputs)

Figure D.3: Drive Circuit for Binary Transmitter, Electrical Multiplexing and OTDM

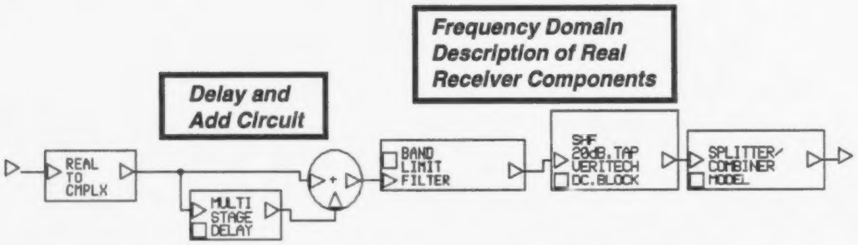
Frequency Domain Description of Real Receiver Components
Delay and Add Circuit
REAL TO CMPLX
MULTI STAGE DELAY
+
BAND LIMIT FILTER
SHF 20dB.TAP VERITECH DC.BLOCK
SPLITTER/ COMBINER MODEL

Figure D.4: Duobinary Receiver for Binary Transmission, Electrical Multiplexing

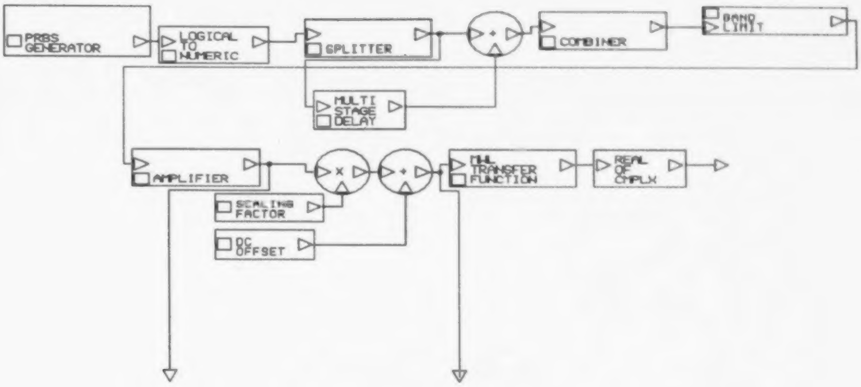
PRBS GENERATOR
LOGICAL TO NUMERIC
SPLITTER
COMBINER
BAND LIMIT
MULTI STAGE DELAY
AMPLIFIER
SCALING FACTOR
DC OFFSET
MWL TRANSFER FUNCTION
REAL OF CMPLX

Figure D.5: Drive Circuit for Duobinary Transmitter, Electrical Multiplexing

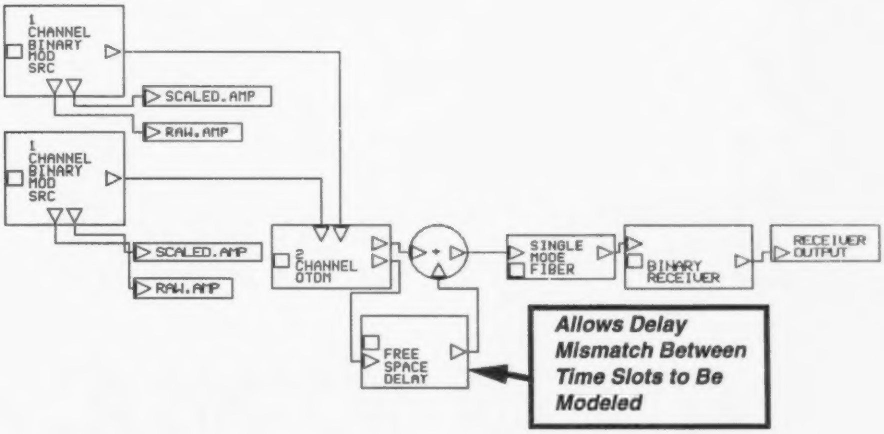
1 CHANNEL BINARY MOD SRC
SCALED.AMP
RAW.AMP
1 CHANNEL BINARY MOD SRC
SCALED.AMP
RAW.AMP
2 CHANNEL OTDM
SINGLE MODE FIBER
BINARY RECEIVER
RECEIVER OUTPUT
FREE SPACE DELAY

Allows Delay Mismatch Between Time Slots to Be Modeled

Figure D.6: Binary Transmission with Binary Reception, OTDM

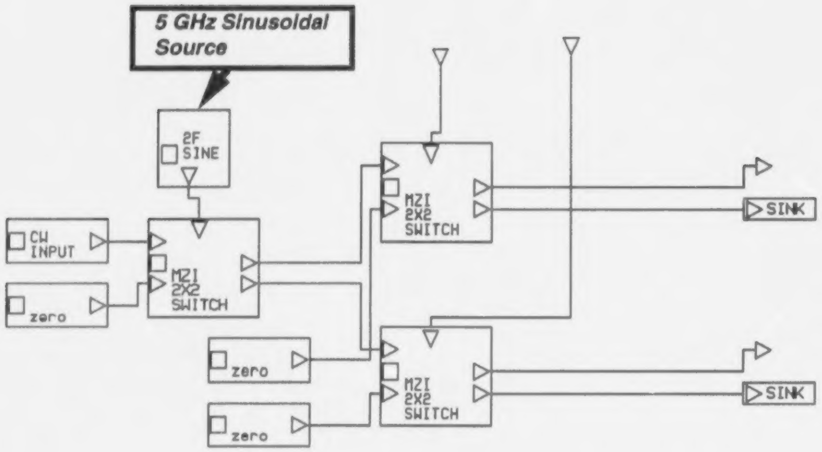
5 GHz Sinusoidal Source
2F SINE
CW INPUT
zero
MZI 2X2 SWITCH
MZI 2X2 SWITCH
zero
zero
MZI 2X2 SWITCH
SINK
SINK

Figure D.7: Two Input OTDM

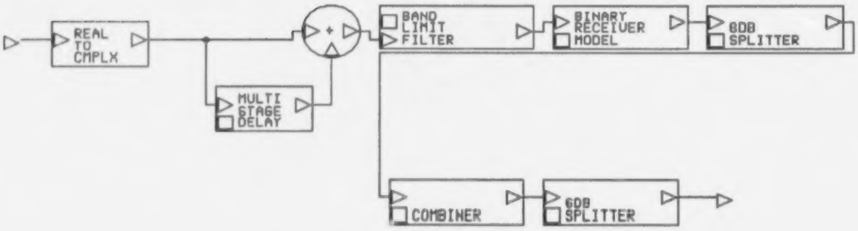
REAL TO CMPLX
+
MULTI STAGE DELAY
BAND LIMIT FILTER
BINARY RECEIVER MODEL
6DB SPLITTER
COMBINER
6DB SPLITTER

Figure D.8: Duobinary Receiver for Binary Transmission, OTDM

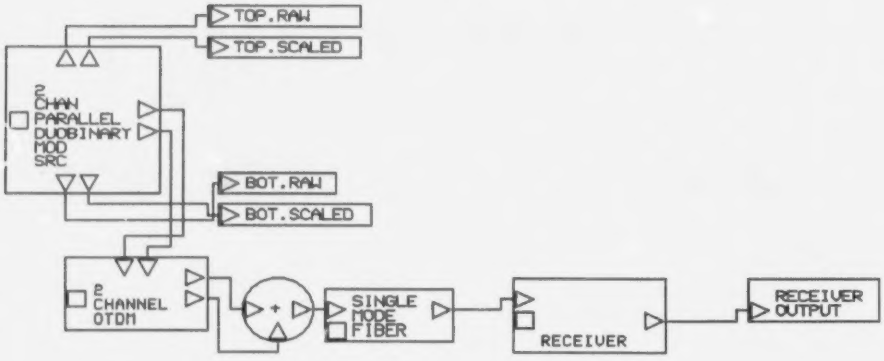
TOP.RAW
TOP.SCALED
2 CHAN PARALLEL DUOBINARY MOD SRC
BOT.RAW
BOT.SCALED
2 CHANNEL OTDM
+
SINGLE MODE FIBER
RECEIVER
RECEIVER OUTPUT

Figure D.9: Duobinary Transmission, OTDM

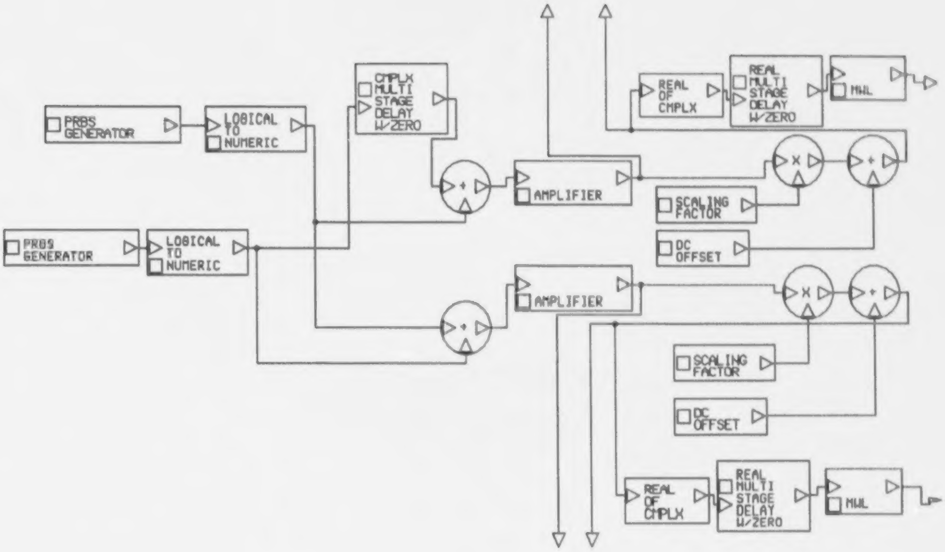
PRBS GENERATOR
LOGICAL TO NUMERIC
CMPLX MULTI STAGE DELAY W/ZERO
PRBS GENERATOR
LOGICAL TO NUMERIC
AMPLIFIER
AMPLIFIER
REAL OF CMPLX
REAL MULTI STAGE DELAY W/ZERO
MWL
SCALING FACTOR
DC OFFSET
SCALING FACTOR
DC OFFSET
REAL OF CMPLX
REAL MULTI STAGE DELAY W/ZERO
MWL

Figure D.10: Parallel Duobinary Drive Circuit for OTDM

Appendix E: Program to Generate Frequency Response of Fiber Transfer Function

```
#include <stdio.h>
#include <math.h>

main() {
        /* This program generates the BOSS fiber transfer function (frequency
        * domain filter) data points.
        *                                   Greg May, May 1992                    */

        int data_rate;                      /* system data rate */
        double dt;                          /* sampling interval */
        int number_of_points;               /* number of data points for file */
        int trials;                         /* number of trials within a loop calculation */
        double alpha;                       /* phase parameter */
        double D;                           /* dispersion parameter (ps / km*nm) */
        double length;                      /* length of fiber (km) */
        double lambda;                      /* wavelength of light (um) */
        double f;                           /* intermediate frequency counter */
        double phase;                       /* fiber transfer function phase */

        dt = 10e-12;
        lambda = 1.55;
        length = 100;

        D = 17.0;
        number_of_points = 1001;                    /* number of data points to take *
        trials = (number_of_points-1 ) /2

        printf("3, %d\n",number_of_points);

        printf("frequency in Hz\n");
        printf("db power magnitude\n");
        printf("phase in degrees\n");

        alpha = (3.14 * D * pow(lambda,2.0) * length *pow(10.0,-15.0)) / 3e8;

        for(f = -0.5 / dt ; f <= 0; f = f + ( 0.5 / (dt * trials )) ) {
                phase = - alpha * pow(f,2.0);
                phase = phase * 360 / (2 * 3.14);   /* convert rads to degrees */
                printf("%20.0f   0    %f\n",f,phase);
                }

        for (f = 0.5/(dt*trials) ; f <= 0.5 / dt; f = f + (0.5 / (dt * trials )) ){
                phase = - alpha * pow(f,2.0);
                phase = phase * 360 / ( 2 * 3.14);
                printf("%20.0f   0    %f\n",f,phase);
                }
}
```

Appendix F: Transmitter and Receiver Electronics

F.1. Microwave Waveguides and Components

All components in high bit rate transmitters and receivers have a non-ideal frequency response. Each introduces its own distortion which in turn reduces signal quality at the transmitter and receiver. The system's performance is maximized only if the concatenated frequency response of all components is as flat in amplitude and delay as possible.

All electronics and passive components in the transmitter and receiver must be capable of signal processing up to at least the GHz frequency range. Therefore, by definition they are microwave band components. Distortion is a major concern when working with these components. This is especially true for high speed digital signals since they have frequency content ranging from very low frequencies (kHz to low MHz) up to very high frequencies and therefore need to be supported by devices with a flat amplitude and group delay response across the same band. In practice, a B Gb/s digital signal has important frequency content up to at least B GHz. Less bandwidth is required for tone (e.g. clock) amplification and distribution.

Connection between components require waveguides. Both coaxial cable and microstrip can be used. The frequency response of coaxial cable varies from poor for most flexible types to very good (flat amplitude and phase response beyond 10 GHz) for semi-rigid types. Microstrip is simply a strip of metal deposited on a grounded substrate. The wave is guided partially in air and partially in the substrate. The thickness and dielectric constant of the substrate as well as the width of the strip control the characteristic impedance of the microstrip line. Discontinuities in the strip due to bends and size changes result in impedance changes which may have a large impact on it frequency response. In many cases, the length of the various waveguides is critically important because centimeter spans of length can represent multiple bit periods of delay.

Assorted microwave components are used for a variety of functions within the transmitter and receiver. Generally, DC blocks, Bias Tees, and power splitters are used. DC blocks are simply broadband capacitors that prevent DC voltage on their inputs from appearing a their outputs. Bias Tees incorporate a DC block and have a connection for DC voltage to be applied to their outputs without affecting their inputs.

Power splitters are available in many different forms, depending on the frequency range of operation required. They can also be used in the reverse direction as power combiners. Almost all splitters are designed for a relatively narrow frequency band of operation. The ultra-broadband splitters are the resistive splitter and certain Wilkinson power dividers.

A broadband resistive splitter is an impedance matched resistive divider network. Figure F.1 shows a 6 dB splitter implementation, which allows the signal to be split equally between two outputs. The power level of each output of this device is down 6 dB from the input (i.e. S-parameters $S_{mn} = -6$ dB, $m \neq n$). Similar resistive splitter devices are also available to divide the signal unequally. An example of this is a 20 dB scope probe, which splits off 10 percent of the signal to a monitoring output.

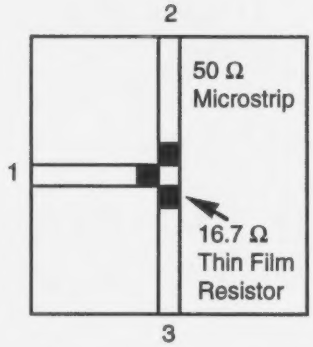

Figure F.1: 6 dB Resistive Splitter

Resistive splitters can be also be used as power combiners with 6 dB isolation between inputs, since their S-parameters are symmetric (i.e. $S_{mn} = S_{nm}$).

Wilkinson power dividers are devices that are impedance matched in such a way that the two output ports (or the two input ports, when the device is used as a combiner) are highly isolated from each other [61]. This can be an advantage compared to the 6 dB splitter / combiner when isolation is critical to a system's performance. A simple Wilkinson Divider implementation is shown in Figure F.2 (after [61]). Because it includes components with lengths tuned to a particular wavelength λ (or frequency), its isolation and reflection characteristics are frequency-specific. As shown in Figure F.3, this power divider has good transmission characteristics within a small band (center frequency $f_c \pm 0.5\ f_c$) (after [61]). By symmetry, these dividers can be used as combiners with identical isolation characteristics. It is possible to increase the bandwidth of the divider across decades of frequency by including more microstrip sections of different impedance (i.e. transformers). Because section lengths are wavelength specific, it is difficult to design a divider that will work across more than a few decades of frequency. This is particularly a problem when the Wilkinson divider / combiner is required for digital signals.

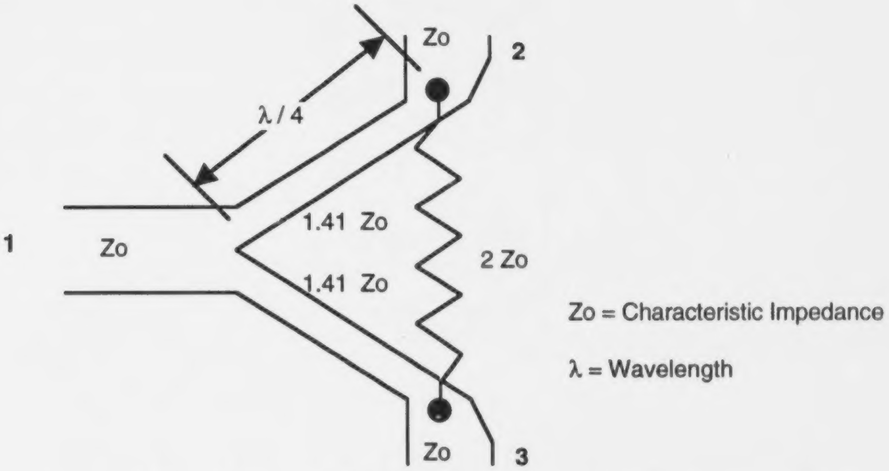

Figure F.2: A Simple Wilkinson Power Divider Implementation

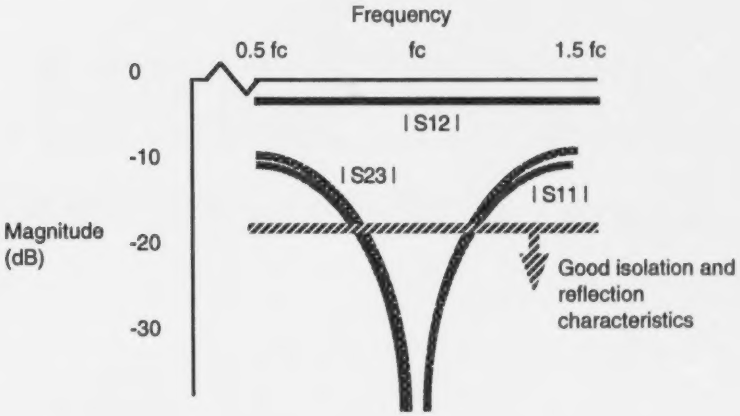

Figure F.3: S-Parameters of a Simple Wilkinson Power Divider

F.2. Integrated Circuits

High speed integrated circuits (ICs) were purchased from NTT Electronics (NEL) and used for clock distribution, decision circuits, and logic gates. Part numbers and descriptions are located in Appendix I. This section describes how the ICs were packaged for use in transmission experiments.

IC packaging is shown in Figure F.4. All of the ICs were designed for use at bit rates up to and beyond 10 Gb/s. Their packaging therefore required microstrip waveguides for RF signals and extensive RF blocking networks for DC supplies. Although the entire digital path of a receiver could be laid out on one substrate, this lacked the flexibility required to test different combinations of components and receiver layouts. Instead, each IC was packaged in its own subassembly. These could be connected to other subassemblies or RF components with standard SMA connectors. These subassemblies consisted of a substrate which supported microstrip and DC tracks, and a mechanical assembly which housed the complete circuit and supported the various connectors to the outside.

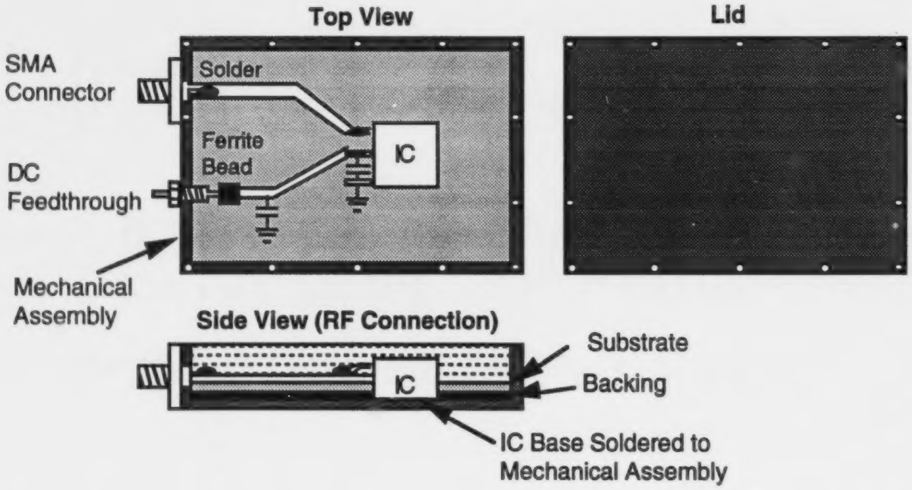
Top View
Lid
SMA Connector
Solder
Ferrite Bead
IC
DC Feedthrough
Mechanical Assembly
Side View (RF Connection)
Substrate
Backing
IC
IC Base Soldered to Mechanical Assembly

Figure F.4: 10 Gb/s Integrated Circuit Packaging

Duroid was selected as the substrate material because it is relatively easy to work with compared to ceramic materials. It is flexible and can be cut with scissors. If necessary, tracks can also be scraped off the substrate and be replaced with lines made from copper tape, although their RF transmission quality will be compromised. All tracks and the back plane of the substrate were gold plated for maximum conductivity. The mechanical assembly box was made out of silver plated aluminum for maximum conductivity and to ensure a high quality ground. Grounds were provided on the substrate where required by plated through via holes. Liberal quantities of these vias were placed as close as possible to the pins to be grounded to minimize path inductance.

All microstrip connections were dimensioned to provide a 50 Ω characteristic impedance. Bends and thickness transitions were made as gradual as possible to minimize impedance discontinuities and subsequent reflections. Where possible, microstrip lines were kept at least three line widths apart from all other conducting materials to minimize the effect of these materials on the strip waveguide properties. Microstrips were run right to the walls of the container, where connectors were soldered on through holes in the container walls. The connectors used have a flat frequency response from DC to beyond 10 GHz.

All DC connections included blocking networks to reduce RF pick-up. Feedthroughs connect the DC connection to the outside supply. These have path inductance which blocks RF. Additional inductance is incorporated by running the feed wire through a ferrite bead. A capacitor to ground is added in parallel to ground any picked up RF signal. Another capacitor to ground is soldered across IC pins to ground any RF seen by the IC. Similar RF blocked tracks were also placed to terminate adjacent to microstrips. A 470 Ω chip resistor could then be soldered across the gap to allow a DC offset to be applied to the RF signal without changing the microstrip impedance significantly. This required a broadband DC block to be connected to the input SMA connector to protect attached devices from the DC voltage.

Appendix G: Binary Filter Selection

Low pass filters are desired for binary receivers because they reduce the noise bandwidth of the receiver and can shape the pulses to reduce intersymbol interference. Nyquist's First Criterion can be applied to determine the frequency domain description of a pulse with zero intersymbol interference [58]. A time domain pulse p(t) is defined to have zero intersymbol interference if it is non-zero at the sampling point (t=0) and zero at all other sampling intervals, i.e. $p(t) = 1$ if $t = 0$, and $p(t) = 0$ at $t = +/- nT$.

This means that:

$$p(t) \bullet \Sigma\, \delta(t - nT) = \delta(t) \qquad \text{(G.1)}$$

The criterion (G.1) corresponds to the following in the frequency domain:

$$\Sigma\, P(\omega - n\,\omega_o) = T \qquad \text{(G.2)}$$

where: $\omega_o = 2\pi / T$

Criterion (G.2) means that the sum of the pulse spectrum and a shifted version of the pulse spectrum add up to T. This is known as a vestigial spectrum.

Clearly from (G.1) and (G.2) many different pulse shapes and spectra meet the criteria. One common vestigial pulse spectrum in literature is the raised cosine characteristic:

$$P_b(f) = \cos^2(\pi f / 2f_o) \qquad \text{(G.3)}$$

where: $f_o = 1 / T$

This pulse can be obtained by passing an input pulse not meeting the criteria through a transfer function which shapes it. In general, the output pulse spectrum $P_o(f)$ is generated by:

$$P_o(f) = P_i(f)\, H(f)\, H_f(f) \tag{G.4}$$

where: $P_i(f)$ is the frequency spectrum of the incident pulse
$H(f)$ is the concatenated frequency response of all transmitter and receiver components
$H_f(f)$ is the frequency response of the lowpass filter in the receiver

The frequency content of the pulse and the concatenated frequency response of all transmitter and receiver components is generally not changeable to any large extent. This leaves the selection of the lowpass filter as the means to control the amount of intersymbol interference in the receiver. The target frequency response of this filter can be obtained from:

$$H_f(f) = P_i(f)\, H(f) \,/\, P_o(f) \tag{G.5}$$

where $P_o(f)$ is set to a target vestigial spectrum, such as the raised cosine response $P_b(f)$. Computer software such as Mathematica can be used to generate the pulse spectrum and to model the concatenated frequency response of transmitter and receiver components. Then a plot of (G.5) provides an objective filter frequency response.

Unfortunately, commercially available lowpass microwave filters generally have too sharp of a roll off to realize a raised cosine response. Real filters can be selected with a trial and error process by including their response in (G.4) and checking the criterion (G.2). This was attempted for 10 Gb/s binary receivers tested with an electrically multiplexed transmitter. A two section (fifth order) 8 GHz Butterworth low pass filter was chosen for 10 Gb/s reception. This filter was used in certain cases where it demonstrated a performance gain over a binary receiver without a low pass filter.

Appendix H: Duobinary Filter Implementation

H.1. Practical options

Figure A.3 in Appendix A shows an ideal duobinary filter for an impulse signal stream. The ideal low pass filter in the figure can be replaced with a high order Butterworth filter with a 3 dB cutoff at (f_o / 2) GHz without significant distortion penalty. This is because as frequency increases, the filter amplitude response does not begin to roll off until the amplitude response of the delay and add circuit is down significantly. Implementation of the delay and add circuit is more complicated because it requires power splitter and combiner components with flat amplitude and delay response across decades of frequencies. This reduces the types of splitter and combiner components that can be used to resistive 6 dB splitters / combiners and broadband Wilkinson splitter / combiners. Two implementations of the delay and add circuit with good frequency characteristics are therefore available: a 6 dB Splitter / Combiner implementation, and a 6 dB Splitter / Wilkinson Combiner implementation.

H.2. 6 dB Splitter / Combiner Implementation

This implementation uses a 6 dB splitter at the head end and a 6 dB combiner at the tail end. A coarse delay setting is made by choosing different path lengths for the two cables run from the splitter to the combiner. A line stretcher can be included as part of the delay path to allow some flexibility in the delay setting. These devices alone are not sufficient because of their poor isolation. Power at the combining end circulates within the delay and add loop and appears at the output and another time interval. This is effectively another delay and add circuit with a significantly longer delay time. The result is unwanted amplitude ripple in the transfer function [44].

The solution to this problem is to introduce additional path loss into the circuit. Figure H.1 shows such the final design. Now power circulating through the circuit is attenuated more than power that goes straight through the circuit. This reduces the amount of ripple. Ripple suppression increases with an increasing attenuation factor x. The penalty is that now the circuit has an additional x dB through loss which has to be compensated for by either optical or electrical amplifiers. This extra amplification reduces receiver sensitivity by introducing more noise and distortion into the circuit.

This circuit could also be implemented in microstrip. In this case, the circulation loop delay may be sufficiently short to move any unwanted ripple towards the stop band of the duobinary filter. An important consideration for this implementation is the type of resistors used at the splitter and combiners. Chip resistors introduce unwanted stray inductance into the transfer function of the duroid implementation of the circuit, which in turn results in an unwanted dip in the frequency response within the pass band of the circuit. Thin film resistors deposited onto the circuit substrate are a better choice because they have negligible inductance, but make fabrication of the circuit more difficult.

H.3. 6 dB Splitter / Wilkinson Power Combiner Implementation

Broadband Wilkinson power combiners can be purchased from some microwave component suppliers. These could be used at the tail end of a delay and add circuit, such as the one shown in Figure H.1. There are no suppliers with a product that has high isolation across the multiple decades of frequency required for DC to multiple GHz response. However, the out of band isolation of some available combiners can still equal or exceed that of the 6 dB combiners. This circuit has a performance comparable to or even better than the best resistive design with a through loss of only 3 to 4 dB, compared to the resistive version's loss of 6 + x dB. The penalty of using this circuit is that very low frequency performance can be worse than the resistive models because of poor low-band isolation. This increases the pattern dependency of the transmission system, since longer pattern strings have lower frequency content than shorter pattern strings.

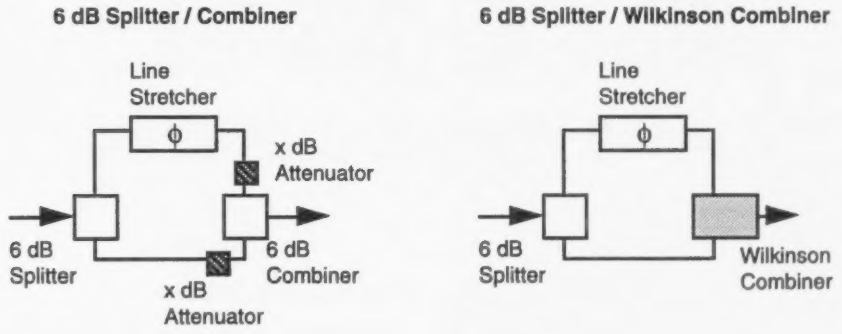

Figure H.1: Delay and Add Circuit Implementations

Appendix I: Description of Components

I.1. Amplifiers

The main operating characteristics of the RF amplifiers used are outlined in Table I.1 and Table I.2.

Manufacturer and Model No.	Application	Frequency Range	Gain (dB) and Gain Ripple (dB)	1 dB Gain Compression Output (dBm)	Noise Figure (dB)
SHF 90P	Receiver	10 kHz - 15 GHz	23 ± 1	10	7
Veritech VMA3K10C-232	Receiver	3 kHz - 10 GHz	32 ± 1	17	8
SHF 75Es	Ext. Mod. Transmitter	10 kHz - 9 GHz (Custom Built)	12 ± 1	24	6
B&H AC80XYH24	Ext. Mod. Transmitter	1 kHz - 7.6 kHz	24 ± 1.1	24	5.5
Mini-Circuits ZHL-42W	OTDM - Modulators	10 MHz - 4.2 GHz	30 ± 1.5	29	7.5

Table I.1: Signal Amplifier Characteristics

Manufacturer and Model No.	Application	Frequency Range	Gain (dB) and Gain Ripple (dB)	1 dB Gain Compression Output (dBm)	Noise Figure (dB)
Avantek AWT-8035	Clock Recovery	2 GHz - 8 GHz	41 ± 1.75	15	4
Avantek LMT12436	Clock Rec. Limiting Amp	7 GHz - 12.4 GHz	35 ± 1.5	14	4.5
Veritech VMA3K10P-124	Ext. Mod. Modified Clock Rec.	3 kHz - 10 GHz	24 ± 1	13	8
CTT APM/080-3036	OTDM - UTP 5 GHz Drive	2 GHz - 8 GHz	36 ± 2	30	5.5
Mini-Circuits ZHL-42W	OTDM - Clock Dist.	10 MHz - 4.2 GHz	30 ± 1.5	29	7.5

Table I.2: Power Amplifier Characteristics

I.2. High Speed Integrated Circuits

Table I.3 provides a list of the high speed integrated circuits used in the experiments.

Manufacturer and Model No.	Description	Application	Maximum Speed of Operation
NTT Electronics NLG4104	D Flip Flop	All Decision Circuits	≥ 10 Gb/s
NTT Electronics NLG4103	Exclusive OR Gate	Duobinary Rec & Zero Chirp Mod.	≥ 10 Gb/s
NTT Electronics NLG4120	Clock Distributor	Receiver & BERT Clock	≥ 10 Gb/s
NTT Electronics NLG4115	2:1 Selector (Multiplexer)	5 Gb/s Data Generation	≥ 18 Gb/s

Table I.3: Integrated Circuit Characteristics

I.3. Optical Bandpass Filter

Figure I.1. provides a monochromator scan of the optical bandpass filter used to filter ASE at the output of the EDFA preamplifier. This scan was used to calculate the normalized optical bandwidth of the filter for subsequent noise calculations. It has been normalized to a peak of 0 dB.

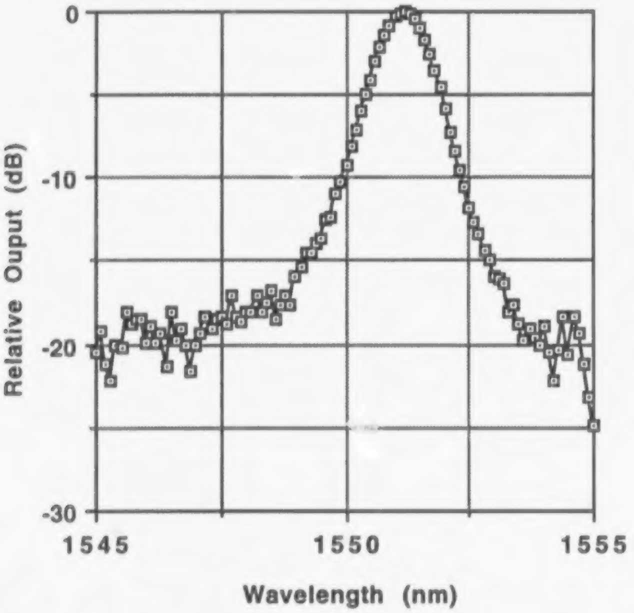

Figure I.1: Monochromator Scan of EDFA Pre-Amplifier Filter

I.4. Electro-Optic Components

I.4.1. AT&T Mach-Zehnder Modulator

Figure I.2 shows a representative frequency response plot for the AT&T m2123AB-2 modulator used for experiments described in Chapter 4.

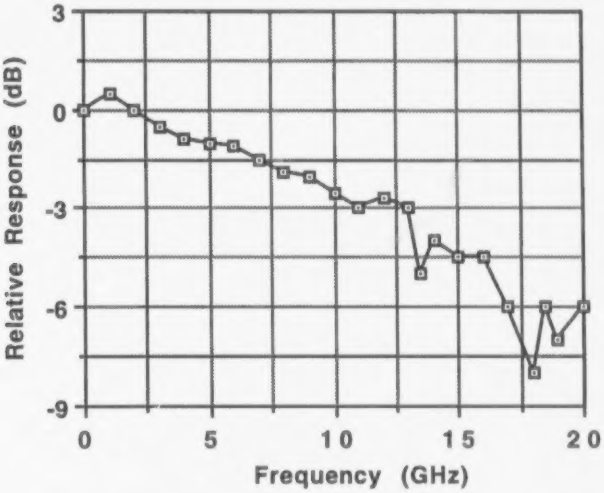

Figure I.2: Representative Frequency Response Plot for AT&T Modulator

I.4.2. ETEK and UTP Mach-Zehnder Switches

The following data sheets on the ETEK and UTP switches have been reprinted from [2].

TR LABS

Test Data Sheet

Device Under Test : United Technologies Photonics 1x2 Modulator
Part Number : APE-YBBM-1.5-12.T-02
Serial Number : 266
Device Length : 8.5 cm
Fiber Lengths : Input 1.60 m
Output 1 2.09 m
Output 2 1.77 m

Performance Data

Insertion Loss Output 1 : 4.5 dB
Insertion Loss Output 2 : 5.0 dB
Extinction Ratio Output 1 : 23.5 dB
Extinction Ratio Output 2 : 32.0 dB

DC V_π Switching Voltage : 5.8 Volts
RF Switching Power (1 GHz) : +27.0 dBm into 50 ohms
RF Frequency Response : See Plot Below

Test Conditions

Optical Source : Fujitsu DFB 4 mW max.
Operation Wavelength : 1551 nm
Detector used in Swept Frequency Response Test : BT&D PDC4310-30 (20 GHz BW)

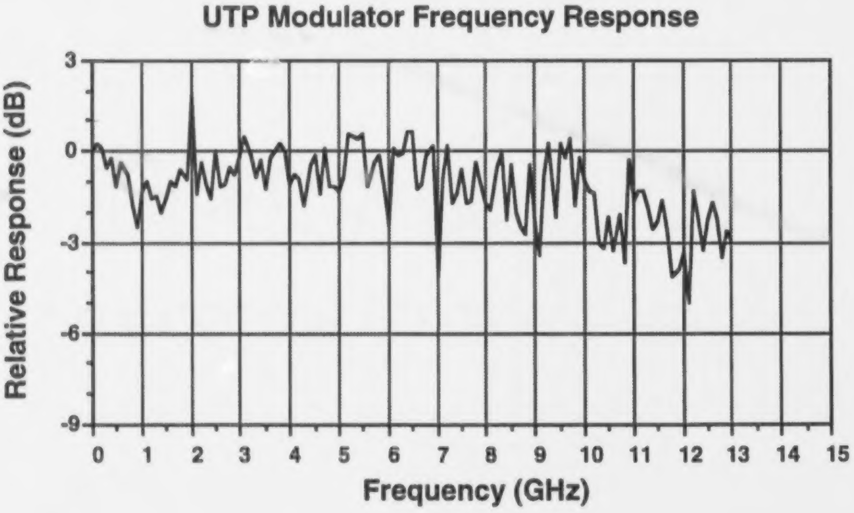

TR LABS

Test Data Sheet

Device Under Test : ETEK 2x2 Electro-Optic Switch (ETEK #2)
Part Number : EOSW-0202-1550
Serial Number : 92101601
Device Length : 8.5 cm
Fiber Lengths : Input 1 (#1) 1.22 m Output 1 (#3) 1.24 m
Input 2 (#2) 1.18 m Output 2 (#4) 1.12 m

Performance Data

Insertion Loss (I1 to O3) : 7.1 dB (Incl. 1.8 dB loss from 2 core mismatches)
Insertion Loss (I1 to O4) : 5.6 dB
Insertion Loss (I2 to O3) : 8.1 dB
Insertion Loss (I2 to O4) : 7.6 dB

Extinction Ratio (I1 to O3) : 32 dB
Extinction Ratio (I1 to O4) : 33 dB
Extinction Ratio (I2 to O3) : 24 dB
Extinction Ratio (I2 to O4) : 22 dB

V_1 Tuning Voltage : 12.5 Volts
V_3 Tuning Voltage : 11.3 Volts
DC V_π (V_2)Switching Voltage : 4.5 Volts
RF Switching Power (1 GHz) : +21.5 dBm into 50 ohms
RF Frequency Response : See Plot Below

Test Conditions

Optical Source : Fujitsu DFB 4 mW max.
Operation Wavelength : 1551 nm
Detector used in Swept
Frequency Response Test : BT&D PDC4310-30 (20 GHz BW)

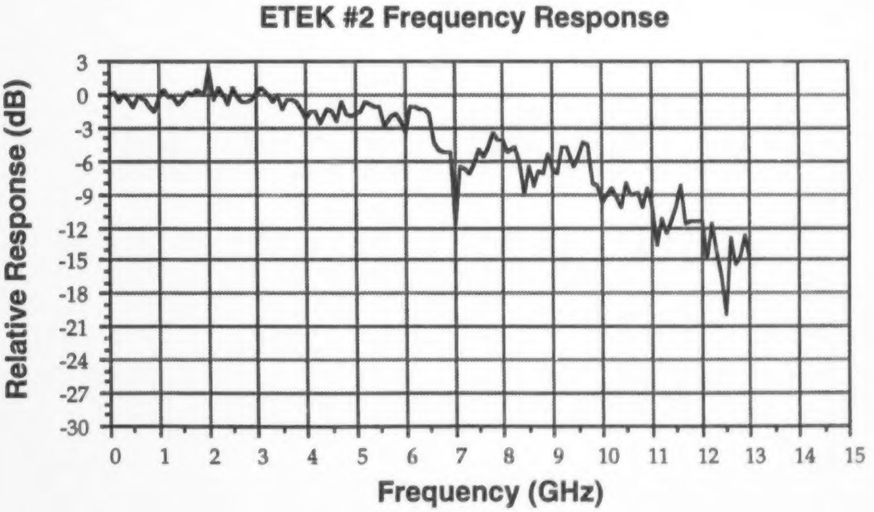

TR LABS

Test Data Sheet

Device Under Test : ETEK 2x2 Electro-Optic Switch (ETEK #3)
Part Number : EOSW-0202-1550
Serial Number : 92111001
Device Length : 8.5 cm
Fiber Lengths : Input 1 (#1) 1.22 m Output 1 (#3) 1.10 m
Input 2 (#2) 1.21 m Output 2 (#4) 1.10 m

Performance Data

Insertion Loss (I1 to O3) : 7.1 dB (Incl. 1.8 dB loss from 2 core mismatches)
Insertion Loss (I1 to O4) : 6.7 dB
Insertion Loss (I2 to O3) : 7.6 dB
Insertion Loss (I2 to O4) : 6.9 dB

Extinction Ratio (I1 to O3) : 26 dB
Extinction Ratio (I1 to O4) : 37 dB
Extinction Ratio (I2 to O3) : 23 dB
Extinction Ratio (I2 to O4) : 27 dB

V_1 Tuning Voltage : 9.9 Volts
V_3 Tuning Voltage : 10.0 Volts
DC V_π (V_2)Switching Voltage : 4.3 Volts
RF Switching Power (1 GHz) : +21.5 dBm into 50 ohms
RF Frequency Response : See Plot Below

Test Conditions

Optical Source : Fujitsu DFB 4 mW max.
Operation Wavelength : 1551 nm
Detector used in Swept
Frequency Response Test : BT&D PDC4310-30 (20 GHz BW)

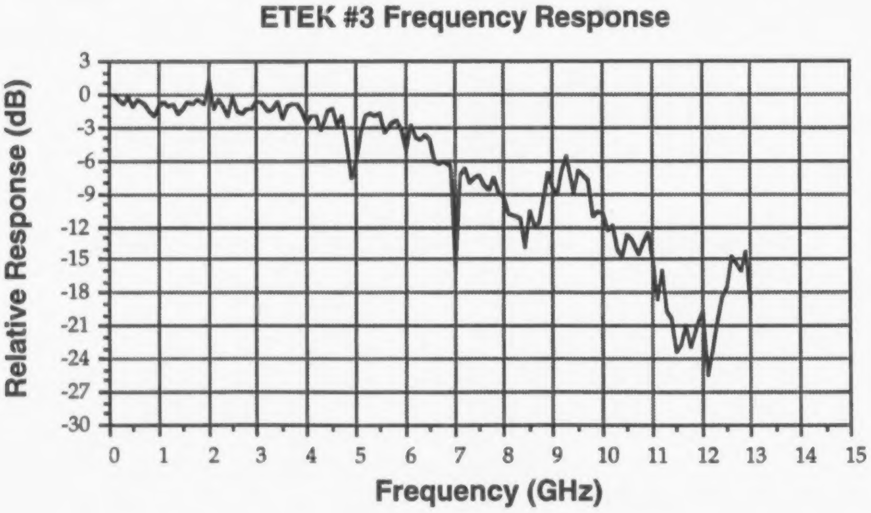

I.4.3. BT&D Photodetector

Figure I.3 shows the frequency response of the BT&D PDC4310 photodetector that was used for experiments described in Chapter 5. It has been reprinted from [2].

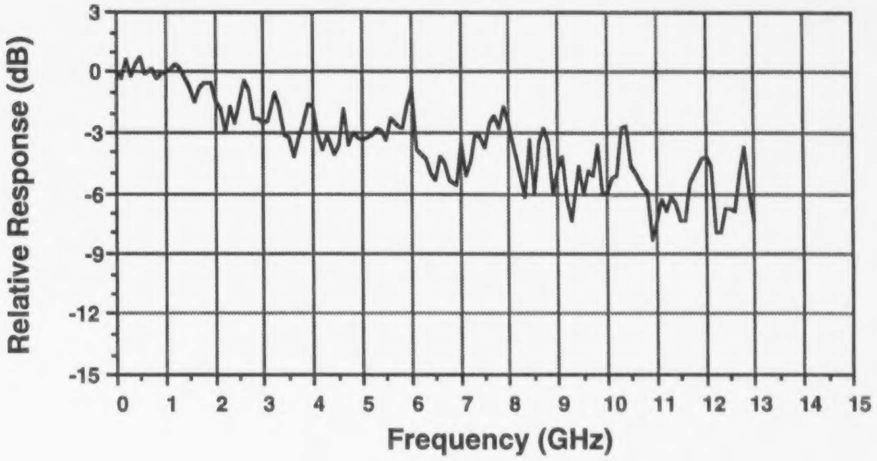

Figure I.3: Frequency Response of BT&D Photodetector

I.5. EDFA Data

I.5.1. Amoco 1.5-AMP-18 EDFA

ASE across bandwidth of EDFA operation = 14.3 dBm

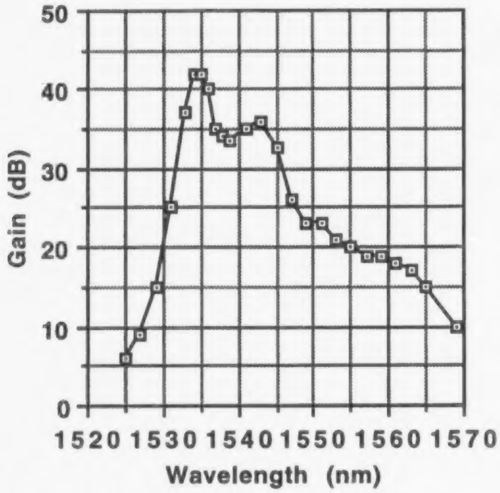

Figure I.4: Gain Bandwidth of Amoco EDFA

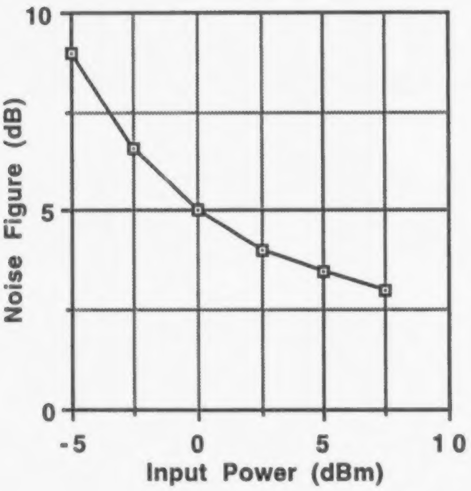

Figure I.5: System Noise Figure versus Input Power for Amoco EDFA

I.5.2. TRLabs Prototype EDFA #303

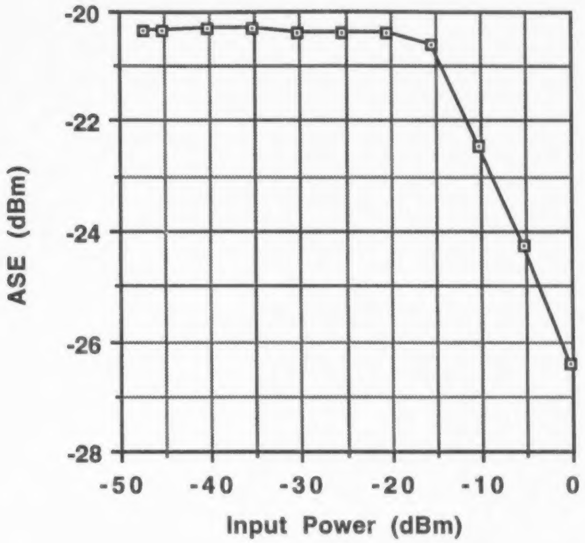

Figure I.6: Filtered ASE from EDFA #303 as a Function of Input Power

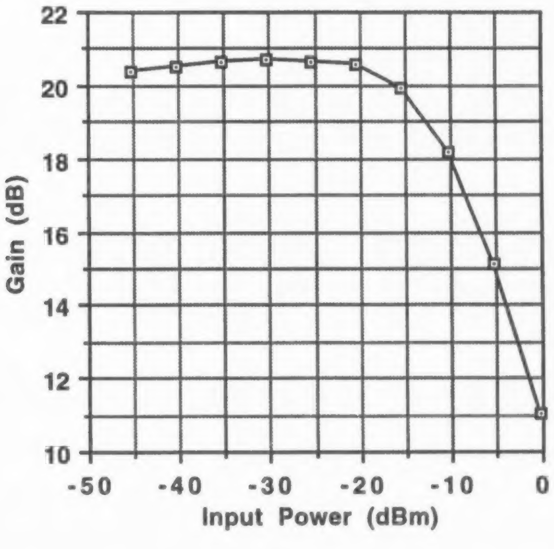

Figure I.7: Gain of EDFA #303 as a Function of Input Power

Appendix J: Parallel Duobinary Code Generation

Figure J.1 shows a general model of an OTDM. There are X independent modulators involved in generating the N * X Gb/s optical signal. The full N * X Gb/s signal is not available anywhere in electrical form, therefore a serial delay and add circuit (described in Appendix A and Appendix H) can not be used to generate the duobinary codes. A different form of delay and add circuit is required. A parallel coding scheme can be envisioned which performs the encoding in parallel across the modulator inputs to the OTDM. This introduces the correlation necessary to reduce the transmission bandwidth of the signal. The theory for this parallel delay and add encoder follows.

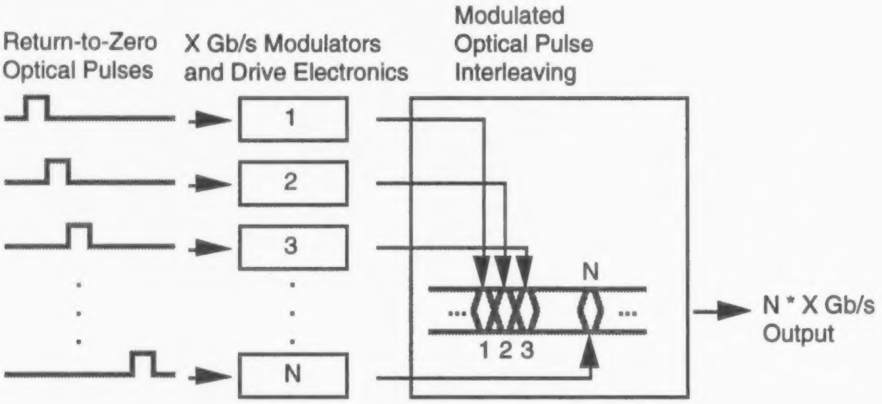

Figure J.1: General Model of an OTDM Transmitter

Duobinary codes in optical form can be a set of positive symbols {"0", "1", "2"}. Let a_k represent an element in a binary sequence ... a_k a_{k+1} a_{k+2} ... transmitted at a line rate B bits per second. A duobinary sequence with elements b_k can be generated from the binary sequence with a delay and add operation as follows:

$$b_k = a_k + a_{k-1} \tag{J.1}$$

Once the code has been generated, the output symbols b_k are then transmitted at the line rate B, resulting in a duobinary sequence ... b_k b_{k+1} b_{k+2} ... . In many cases this sequence can be passed through a low pass filter to reduce its transmission bandwidth further.

Most high speed fiber optic transmission systems will have at least one multiplexing stage incorporated into the transmitter. The signals arrive at the input of the multiplexer as relatively low speed parallel signal. The multiplexer then samples these parallel signals and outputs a high speed serial stream at the system line rate B, as shown in Figure J.2. The multiplexer model discussed below assumes that adjacent channels are mapped into adjacent time slots after multiplexing (bit interleaving).

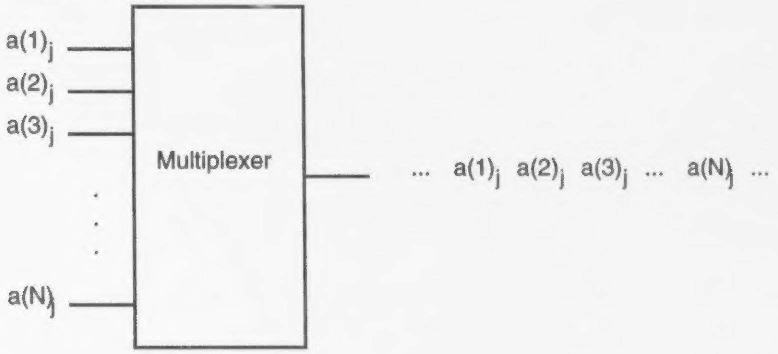

Figure J.2: Bit Interleaved Multiplexer

The bits arrive in parallel at the input of the multiplexer as follows:

$$\ldots[\ a(1)_j\ a(2)_j \ldots a(m)_j \ldots a(N)_j\ ][\ a(1)_{j+1}\ a(2)_{j+1} \ldots a(m)_{j+1} \ldots a(N)_{j+1}\ ] \ldots \qquad (J.2)$$

where the symbol j is the block index, and the individual bits within the block are denoted a(m). Obviously, the block rate is B / N.

The output from the multiplexer is a sequence:

$$\ldots\ a(1)_j\ \ a(2)_j \ldots a(m)_j \ldots a(N)_j\ \ a(1)_{j+1}\ \ a(2)_{j+1} \ldots a(m)_{j+1} \ldots a(N)_{j+1} \ldots \qquad (J.3)$$

The index k can be used to denote a symbol number within the multiplexed stream. The block index j and the bit index m within the block are directly related to the index k by summing them together, i.e. $k = (j-1)N + m$ where m and j vary as shown in (J.2) and (J.3).

This substitution results in the line rate sequence:

$$\ldots\ a_k \quad a_{k+1} \quad a_{k+2}\ \ldots \tag{J.4}$$

Adjacent bits at the input of the multiplexer appear in adjacent time slots at the output of the multiplexer. Therefore, the parallel addition of adjacent bits at the input of the multiplexer will result in a delay and add operation at the output. This principle is incorporated into the parallel duobinary encoder shown in Figure J.3. This encoder operates at a fraction of the line rate B because it processes the signals in parallel at the input block rate B / N.

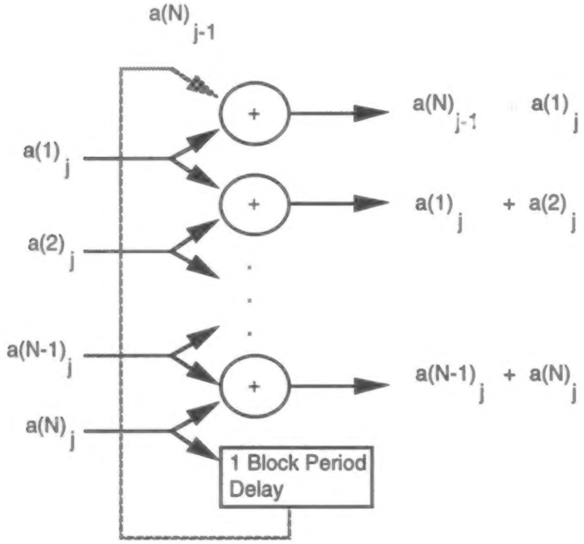

Figure J.3: Parallel Duobinary Encoder

The output blocks j from the encoder are:

$$\ldots\ [\ a(N)_{j-1} + a(1)_j \quad \ldots\ a(m)_j + a(m+1)_j \ldots \quad a(N-1)_j + a(N)_j\ ]\ \ldots \tag{J.5}$$

These blocks are then multiplexed up to the line rate to produce the sequence:

$$\ldots(\ a(N)_{j-1} + a(1)_j\ )\ \ldots\ (\ a(m)_j + a(m+1)_j\ )\ \ldots\ (\ a(N-1)_j + a(N)_j\ )\ \ldots \tag{J.6}$$

Now, substituting the indices m and j with k =(j-1)N + m, this sequence becomes a line rate sequence:

$$\ldots (a_{k-1} + a_k)\ (a_k + a_{k+1})\ (a_{k+1} + a_{k+2}) \ldots \qquad (J.7)$$

By substituting for the duobinary symbol b from the delay and add operation of (J.1), this results in the line rate sequence:

$$\ldots b_k \quad b_{k+1} \quad b_{k+2} \ldots \qquad (J.8)$$

Which is identical to the duobinary sequence which was generated by serially processing the input signal.

The ternary output from the parallel encoder can not be multiplexed with a digital multiplexer since the multiplexer can only accommodate binary signals. An OTDM is ideally suited to the parallel encoder since it is capable of multiplexing light pulses of varying intensity. The outputs from the encoder therefore can be used to modulate the intensity of OTDM light pulses. This parallel technique is the overlay required to achieve duobinary codes at the transmitter.

The implementation of the parallel delay and add circuit must consider the real-world broadband microwave devices that are available. 6 dB splitters / combiners can be used to perform the split and add operations, but have poor isolation. This will result in unwanted crosstalk between ports. For example, in the four input / output implementation shown in Figure J.4, the unwanted crosstalk between ports 1 and 7 is 12 dB below the actual desired signal level (e.g. the coupling from port 1 to port 6). Figure J.4 also shows two potential solutions. The first is to introduce path attenuators. These tend to attenuate crosstalk more than signal. The other option is to introduce broadband amplifiers. Provided that they are high quality and are well matched in gain and delay, these amplifiers will completely eliminate crosstalk with little penalty to the overall signal quality. Another important consideration is the length of the feedback path. For example, a 2.5 Gb/s circuit requires a 400 ps delay, which corresponds to a waveguide section around 8 cm long. This may affect the layout geometry of the design.

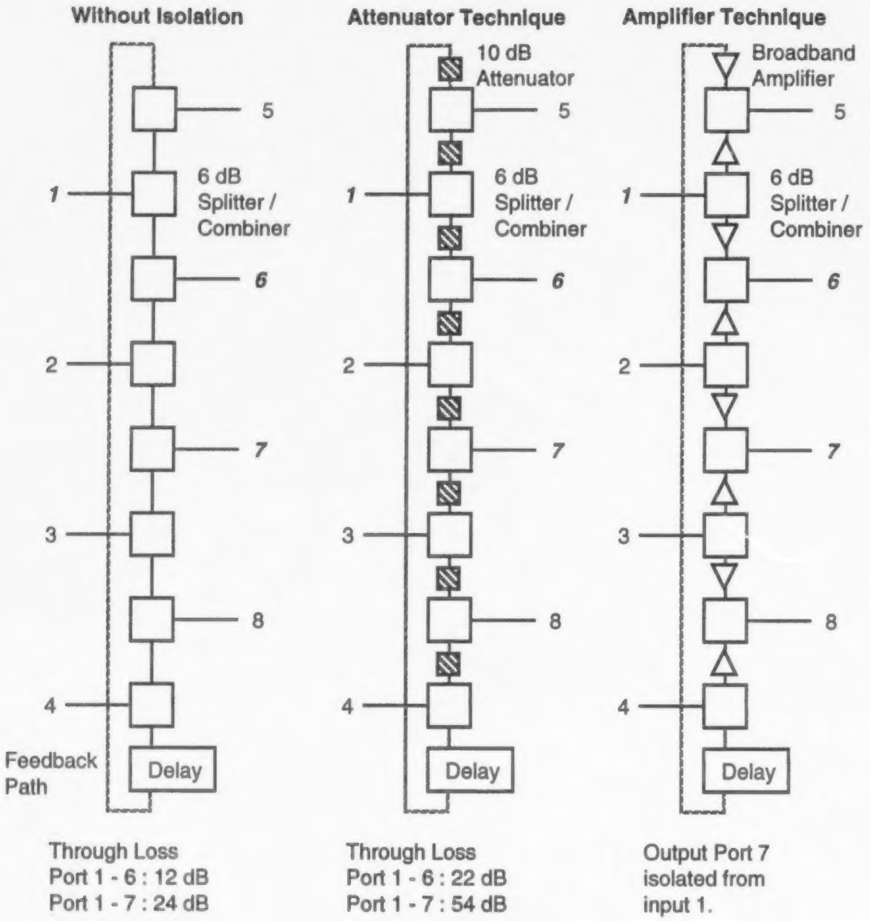
Without Isolation
Attenuator Technique
Amplifier Technique
10 dB Attenuator
Broadband Amplifier
6 dB Splitter / Combiner
6 dB Splitter / Combiner
6 dB Splitter / Combiner
1
2
3
4
5
6
7
8
Feedback Path
Delay
Delay
Delay
Through Loss
Port 1 - 6 : 12 dB
Port 1 - 7 : 24 dB
Through Loss
Port 1 - 6 : 22 dB
Port 1 - 7 : 54 dB
Output Port 7 isolated from input 1.

Figure J.4: Parallel Delay and Add Implementation

Appendix K: Receiver Sensitivity Theory for Binary and Duobinary Signaling

A simplistic assumption about the probability distribution of noise at the input of a binary receiver is that it has a Gaussian distribution with the same characteristics associated with both a "0" symbol and "1" symbol. This is sufficient to provide an estimate of the signal to noise ratio required to obtain a 10^{-9} bit error rate. This theory can be extended to allow similar predictions to be made about a duobinary receiver.

K.1. Binary Receiver Sensitivity

Assuming a Gaussian distribution, the probability density function P(x) of a signal level x is:

$$P(x) = \frac{1}{\sqrt{2\pi\sigma^2}} e^{-(x-m)^2/(2\sigma^2)} \qquad (K.1)$$

where: σ^2 is the variance

m is the mean

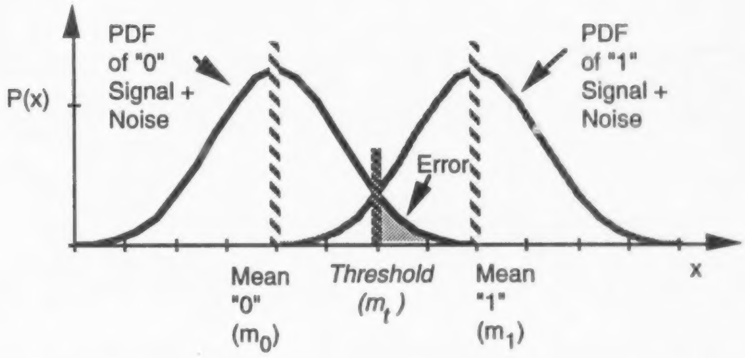

Figure K.1: Probability Density Functions of Gaussian Noise

For Gaussian noise, the variance σ^2 is equivalent to the mean square noise current or voltage.

The probability of error for the binary receiver depends on the placement of decision threshold. The probability of error for a "0" symbol is equivalent to the area under the probability distribution above the decision threshold m_t (as shown in Figure K.1):

$$P_{E0} = \int_{m_t}^{\infty} \frac{1}{\sqrt{2\pi\sigma^2}} e^{-(x-m_0)^2/(2\sigma^2)} dx \qquad (K.2)$$

where: m_0 is the mean "0" level

Similarly, the probability of error for a "1" symbol is equivalent to the area under the probability distribution below the decision threshold m_t:

$$P_{E1} = \int_{-\infty}^{m_t} \frac{1}{\sqrt{2\pi\sigma^2}} e^{-(x-m_1)^2/(2\sigma^2)} dx \qquad (K.3)$$

where: m_1 is the mean "1" level

The optimal threshold setting is located where both probabilities are minimized. This occurs in the center of the mean "0" and "1" levels for identical Gaussian distributions. In general, the optimal threshold occurs where the probability densities P_{E0} and P_{E1} are equal. The average probability of error is then:

$$P_E = \frac{P_{E1} + P_{E0}}{2} = P_{E1} = P_{E0} \qquad (K.4)$$

Both (K.2) and (K.3) simplify to the same form when the threshold setting is optimal:

$$P_{E1} = \frac{1}{2} \mathrm{erfc}\left(\frac{m_1 - m_t}{\sqrt{2\sigma^2}}\right) = \frac{1}{2} \mathrm{erfc}\left(\frac{Q}{\sqrt{2}}\right) \qquad (K.5)$$

$$P_{E0} = \frac{1}{2} \mathrm{erfc}\left(\frac{m_t - m_0}{\sqrt{2\sigma^2}}\right) = \frac{1}{2} \mathrm{erfc}\left(\frac{Q}{\sqrt{2}}\right) \qquad (K.6)$$

where erfc() is the complementary error function

From (K.5) and (K.6), Q is defined as:

$$Q = \frac{(m_1 - m_t)}{\sigma} = \frac{(m_t - m_0)}{\sigma} = \frac{(m_1 - m_0)}{2\sigma} \qquad (K.7)$$

For NRZ signaling, the value for Q is the equivalent of the ratio of average signal $(m_1\text{-}m_2)/2$ to average noise σ. For RZ signaling, the value for Q is twice the ratio of average signal to average noise.

For $Q >> 1$, (K.5) and (K.6) can be approximated with minimal error as:

$$P_{E1} = P_{E0} \approx \frac{1}{Q\sqrt{2\pi}} e^{-Q^2/2} \qquad (K.8)$$

A Q value of 6 is equivalent to a signal to noise power ratio of 15.5 dB at the sampling instant and represents a probability of error of 10^{-9}.

K.2. Duobinary Receiver Sensitivity

In all cases studied, the duobinary symbols were decoded one at a time. Since there is no interdependence between decisions for correctness, a similar Gaussian theory for signal to noise ratio can be applied to a duobinary receiver. Figure K.2. shows a simple model of a duobinary transfer function.

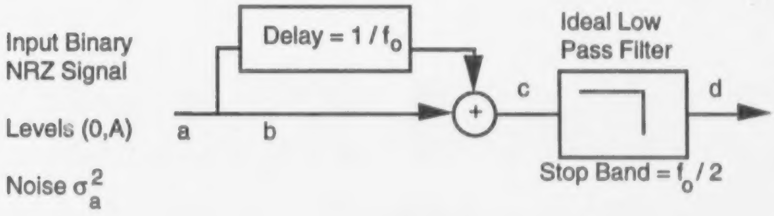

Figure K.2: Duobinary Transfer Function

The split and recombination stage of the delay and add are assumed to be 6 dB splitters and combiners in order to model physically realizable devices. These stages are assumed to have perfect isolation in order to remove additional path attenuators from the analysis. Also, the low pass filter is assumed not to introduce any eye closure. A real filter will result in some intersymbol interference and pulse broadening that will slightly affect the signal to noise ratio at the decision point.

The noise power at point "b" in Figure E is down a factor of 6 dB from the input of the splitter because of its 3 dB insertion loss and because one half the power signal is split to the other output.

$$\sigma_b^2 = \frac{\sigma_a^2}{4} \tag{K.9}$$

Identical copies of this noise are added at the combiner, with another 3 dB insertion loss. The output noise at point "b" is:

$$\sigma_c^2 = \frac{1}{2}\left(\frac{\sigma_a^2}{4} + \frac{\sigma_a^2}{4}\right) = \frac{\sigma_a^2}{4} \tag{K.10}$$

At the output of the band pass filter (point "d"), the noise level is scaled down by another factor of two. This is because the noise bandwidth of the duobinary receiver is approximately half that of a binary receiver, and because all noise terms are directly proportional to noise bandwidth (from Chapter 3).

$$\sigma_d^2 = \left(\frac{\sigma_a^2}{4}\right)\frac{B_{\text{duobinary}}}{B_{\text{binary}}} \approx \frac{\sigma_a^2}{8} \tag{K.11}$$

where: $B_{\text{duobinary}}$ is the noise bandwidth of the duobinary receiver

B_{binary} is the noise bandwidth of the binary receiver

The binary signal at the transmit end is split and recombined with a 6 dB insertion loss at each end. At point "b", the peak signal is A / 2 after a 6 dB loss. At point "c", each of the two input signals is down 6 dB, but then they directly add to give a peak output level of A / 2, a middle level of A/4, and a low level of 0. These are also the signal levels at point "d", assuming that the low pass filter does not introduce significant distortion.

Figure K.3 shows the resulting ternary signal probability density function at point “d”. As with the binary case, the probability of error is equivalent to the tail probabilities above and below the various thresholds. The bit error rate will be dominated by a crossing of a local threshold (e.g. the probability of an error with a “0” symbol will be dominated by the probability of crossing Threshold 1, not both Threshold 1 and Threshold 2) because of the rapid taper off of the probability density functions. The thresholds are centered about the mean levels to minimize the probability of error for all symbols.

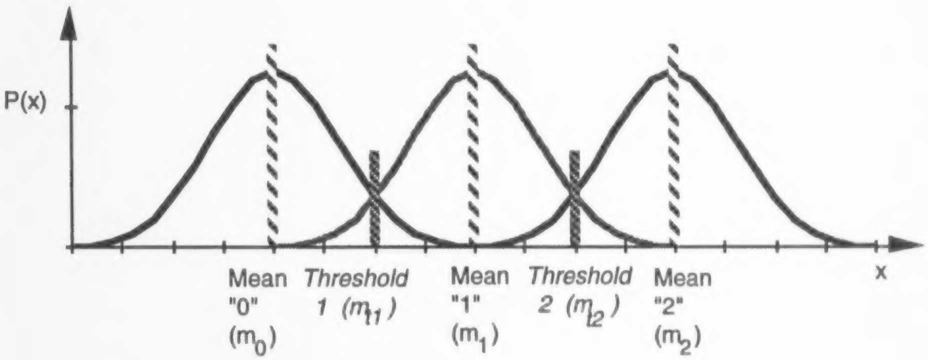

Figure K.3: Ternary Signal Probability Density Function

The probability of error is not the same for each symbol. The probability of an error with a “1” symbol is twice that of a “0” symbol or a “2” symbol because it has two potential threshold crossings (Threshold 1 and Threshold 2) and subsequently two tail probabilities.

For a binary stream with an equal probability of “0”s and “1”s, the average probability of error is:

$$P_{avg} = 0.25 * P_{E0} + 0.5 * P_{E1} + 0.25 * P_{E2} \qquad (K.12)$$

$$P_{avg} = 0.75 \ \mathrm{erfc}(\frac{Q_{duobinary}}{\sqrt{2}}) \qquad (K.13)$$

A $Q_{duobinary}$ value of 6 now provides a bit error probability of $1.5*10^{-9}$, which is identical to a 10^{-9} bit error rate point within experimental error.

Now, the binary signal to noise ratio at point "a" must be related to the duobinary signal to noise ratio at point "d". $Q_{duobinary}$ is related to threshold spacing and noise the same way that Q was defined for binary (Q_{binary}) in (K.5) and (K.6). Selecting the first threshold and the mean value for a "1" symbol, $Q_{duobinary}$ is:

$$Q_{duobinary} = \frac{(m_1 - m_{t1})_d}{\sigma_d} \tag{K.14}$$

But $(m_1\text{-}m_{t1})_d$ is equal to one quarter the peak duobinary signal at point "d". Therefore,

$$(m_1\text{-}m_{t1})_d = A / 8 \tag{K.15}$$

The binary signal at point "a" has a difference between mean value and threshold of:

$$(m_1\text{-}m_t)_a = A / 2 \tag{K.16}$$

Also, the noise at point "d" is related to the noise at point "a" by:

$$\sigma_d^2 \approx \frac{\sigma_a^2}{8} \tag{K.17}$$

Now $Q_{duobinary}$ can be related to the input signal to noise ratio.

$$Q_{duobinary} = \frac{(m_1 - m_t)_a / 4}{\sigma_a / (2\sqrt{2})} = \frac{(m_1 - m_t)_a}{\sigma_a \sqrt{2}} \tag{K.18}$$

And therefore:

$$Q_{duobinary} = Q_{binary} / \sqrt{2} \tag{K.19}$$

For a $Q_{duobinary}$ value of 6 to achieve a 10^{-9} BER, Q_{binary} must be $6\sqrt{2}$. As shown in Chapter 3, optical power is proportional to the square of electrical signal power. Also, thermal noise is independent of signal, and all other noise terms are related to signal. If the receiver is limited by thermal noise, then, Q is directly proportional to optical signal and hence the optical power required to realize a 10^{-9} BER in a duobinary receiver is a factor of $\sqrt{2}$ (1.5 dB) higher than the optical power required to realize the same BER in a binary receiver. If the receiver is noise in signal limited, then the optical power required to realize a 10^{-9} BER in a duobinary receiver is a factor of 2 (3 dB) higher than the optical power required to realize the same BER in a binary receiver.

This is a simplistic model because it assumes identical noise associated with each signal level, Gaussian statistics, a duobinary receiver noise bandwidth of exactly half the binary receiver noise bandwidth, and a distortion-free transfer function that does not affect eye opening. In reality, none of these factors apply. However, the above analysis is sufficient to provide a reasonable estimate of the binary received signal to noise ratio required to get a 10^{-9} bit error rate from a duobinary receiver.

Appendix L: Clock Recovery Technique

Recovered clock is required to drive the receiver components, and in the case of a laboratory test, an oscilloscope and a bit error rate test set receiver. Usually in the laboratory it is possible to use a "cheat" clock, which is simply the clock output provided by the bit error rate test set transmitter. Although this method works, its effectiveness diminishes as the length of fiber between the transmitter and receiver increases. Small clock phase shifts arise because of thermal expansion and contraction in the fiber length, and also because of changes in refractive index due to temperature change. These phase shifts can result in higher bit error rates being reported that would occur if the receiver clocking could track the signal more effectively. For example, pure silica glass has a typical thermal expansion coefficient of $10^{-6}/^{o}C$ [2], a typical refractive index of 1.44 for 1550 nm light [62], and a typical room temperature refractive index variant of $1.1*10^{-5}/^{o}C$ [62]. A 1^{o} C increase in fiber temperature in a 100 km link results in a 10 cm increase in fiber length. The delay caused by length change is around 480 ps and by the refractive index change is around 3600 ps. In practice, temperature variations will not be uniform along the fiber so this change in length could be considerably more or less.

The answer to avoiding problems with length changes is to extract clock from the signal itself and to distribute the recovered clock to the decision circuit and the bit error rate test set receiver. The recovered clock can also be used to trigger an oscilloscope to obtain a clear view of received signals at long distances.

A common clock recovery method is to pass the received binary signal through a squarer, or some form of non-linearity. A microwave doubler can be used for this function. Figure L.1 shows a 9.952 GHz clock recovery circuit which uses this method.

In the first stage, the incoming signal is filtered and amplified. The bandpass filter eliminates the low frequency component of the signal, and at the same time makes the frequency content of the signal symmetric about 5 GHz. This filtering stage can be consolidated into the first amplifier stage by selecting an amplifier with a pass band centered about the appropriate frequency. The doubler then acts as a nonlinear transfer function on the filtered signal. This produces a strong clock tone at the fundamental signal harmonic and additional signal which distorts the clock tone. The clock tone then can be extracted by filtering it with a very narrow band bandpass filter centered at 9.952 GHz. A limiting amplifier follows this filter to reduce variations in the clock signal level.

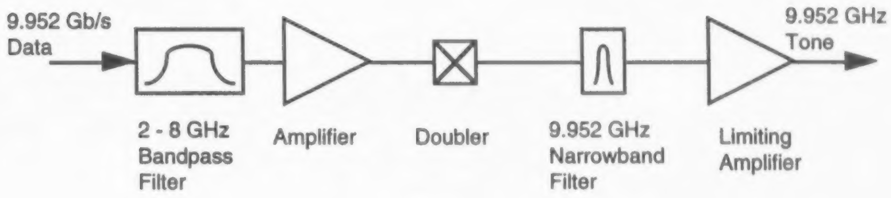
9.952 Gb/s
Data
9.952 GHz
Tone
2 - 8 GHz
Bandpass
Filter
Amplifier
Doubler
9.952 GHz
Narrowband
Filter
Limiting
Amplifier

Figure L.1: Basic Components of a 9.952 GHz Clock Recovery Circuit

This clock recovery technique is based on the cyclostationary nature of the binary signal. Using a derivation from [63], it can be shown that only part of the frequency content of the signal determines the magnitude of the recovered clock tone.

Let x(t) be a baseband pulse amplitude modulated signal [63]:

$$x(t) = \sum_{k=-\infty}^{\infty} a_k \, p(t - kT - \tau) \tag{L.1}$$

where: a_k is a random binary symbol
p is a pulse
T is the signaling interval
τ is a time shift introduced by the channel

The mean of the square of x(t) has a periodic expected (mean) value [63]:

$$E\left[x^2(t)\right] = \bar{a}^2 \sum_k p^2(t - kT - \tau) = E\left[x^2(t + kT)\right] \tag{L.2}$$

This signal can be used for clock recovery if it is properly filtered. The magnitude of the fundamental component in (2.11) can be determined using the Poisson sum formula [63]:

$$\sum_{k=-\infty}^{\infty} h(t-kT) = \frac{1}{T}\sum_{n=-\infty}^{\infty} H(n/T)e^{j2\pi nt/T} \tag{L.3}$$

where: h(t) and H(f) are Fourier transform pairs

Substituting (L.3) into (L.2), the result is [63]:

$$E[x^2(t)] = \bar{a}^2 \operatorname{Re}\sum_{nl} D_n \exp\frac{j2\pi n t}{T} \tag{L.4}$$

where:

$$D_n = \int_{-\infty}^{\infty} P(n/T - f)P(f)\,df \tag{L.5}$$

From (L.4), the clock tone is related to the coefficient D_1. This coefficient is the area under the curve plotted in Figure L.2 (after [63]). It corresponds to the excess bandwidth of the signal beyond the minimum Nyquist bandwidth 1 / 2T. α is the roll off factor.

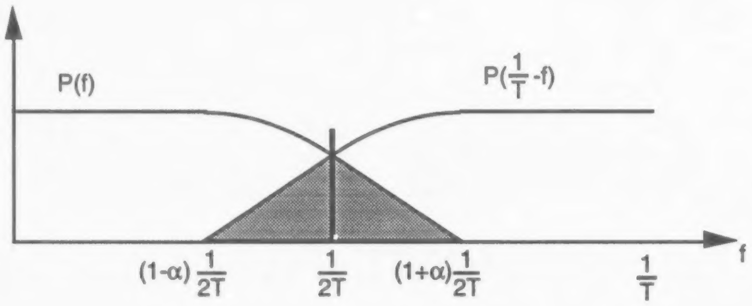

Figure L.2: Computation of Clock Tone Magnitude

The output of the squarer can now be passed through a narrow band filter to extract the recovered clock tone. This recovered waveform is [63]:

$$E[w(t)] = \frac{\bar{a}^2}{T} \mathrm{Re}[D_1 e^{j2\pi(t-\tau)/T}] = \frac{\bar{a}^2}{T} \cos[\frac{2\pi}{T}(t-\tau)] \tag{L.6}$$

Two important considerations arise from this calculation. The first is that only frequency content in the signal about 1 / 2T (5 GHz for a 10 GHz clock recovery circuit) contributes to the clock tone. The remaining content contributes to unwanted jitter which can potentially increase bit error rate. Hence, the signal should be filtered about 1 / 2T (5 GHz for a 10 Gb/s signal) before it is squared. The second important consideration is that severe chromatic dispersion will impact the magnitude of the recovered clock tone. Since dispersion broadens the signal in the time domain, it is narrowed in the frequency domain. In the most severe case, the signal power spectrum could be narrowed within 1 / 2T, resulting in no clock tone being recovered.

Appendix M: Ternary Decision Circuit and Precoder

There are two decision thresholds involved in decoding ternary duobinary signals. This requires two decision circuits: one for the bottom threshold and one for the top threshold of the signal. These circuits can be implemented by using two D flip-flops in the configuration shown in Figure M.1.

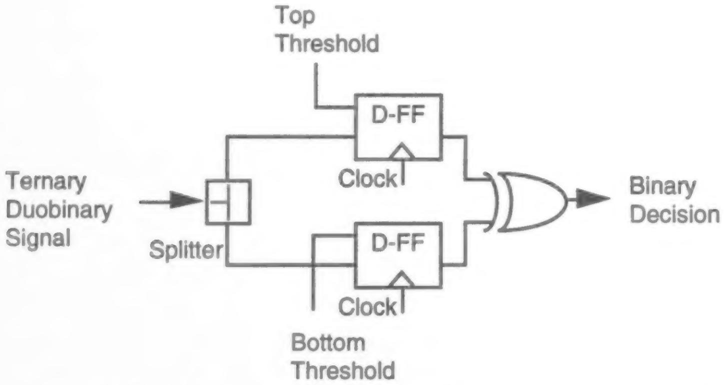

Figure M.1: Ternary Decision Circuit Implementation

The exclusive-OR (XOR) gate following the flip flops is used to convert the ternary decision circuit output into binary form. At the inputs to the XOR, a duobinary "2" level is now represented as "11", a duobinary "1" level is now "01", and a duobinary "0" level is now "00". The outputs from the XOR gate have a 1:1 correspondence to the transmitted signal, providing the transmitted signal has been precoded in advance. A precoding step for a serial duobinary transfer function is the delay and XOR operation shown in Figure M.2. This can be expressed as:

$$p_k = a_k \oplus p_{k-1} \qquad \text{(M.1)}$$

where: $\oplus$ is base-2 addition (identical to Exclusive-OR (XOR))

Figure M.2 also shows the truth table for the circuit, the output from a delay and add operation, and the output from the ternary decision circuit. Note the correspondence between the decision circuit output and the original input bit a_k.

The propagation delay of the XOR gate must be less than the bit period for this circuit to work. It is not currently possible to realize a 10 Gb/s version of this precoder circuit because the propagation delay of commercially available XOR gates is greater than 100 ps (a 10 Gb/s bit period). A commercially available 10 Gb/s Toggle flip-flop can be used instead. This device has the identical truth table as the precoder circuit, provided it is supplied with an RZ signal (Figure M.3). An RZ signal is required to trigger transitions from the flip-flop when multiple "1"s are input.

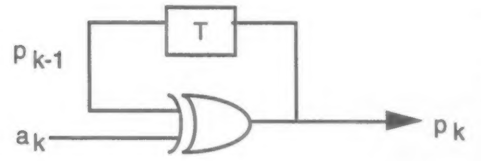

a_k	p_{k-1}	p_k	$p_{k-1} + p_k$	Ternary Decision Circuit Output
0	0	0	0	0
0	1	1	2	0
1	0	1	1	1
1	1	0	1	1

Figure M.2: Precoding Stage for Serial Duobinary Filter

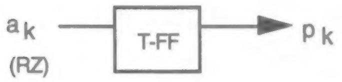

a_k	p_{k-1}	p_k
0	0	0
0	1	1
1	0	1
1	1	0

Figure M.3: Precoding Stage using Toggle Flip-Flop

The serial precoding circuits in Figure M.2 and M.3 do not lend themselves to the parallel duobinary encoder. Precoding must be performed in parallel as well. Such a parallel precoder circuit is described in Appendix Q. This circuit requires a large number of discrete components in order to realize a laboratory prototype.

Fortunately neither the serial precoder or the parallel precoder are required when a programmable bit error rate test set is available. Precoders can conveniently be eliminated by programming the bit error rate test set transmitter with the precoded pseudo-random bit sequence (PRBS) to be used and setting the bit error rate test set receiver to look for the standard PRBS. Alternatively, the transmitter can be set to the PRBS and the receiver can be programmed to look for the PRBS after it has encoded in duobinary form and decoded by the ternary decision circuit. A short program is sufficient to generate the altered sequence.

Appendix N: Comparison of PRBS and Precoded Sequence

It can be shown that the precoded form of the standard 2^7-1 Pseudo-Random Bit Sequence (PRBS) is identical to the PRBS shifted by 6 positions. Figure N.1 shows the shift registers which generate the PRBS, followed by the precoder.

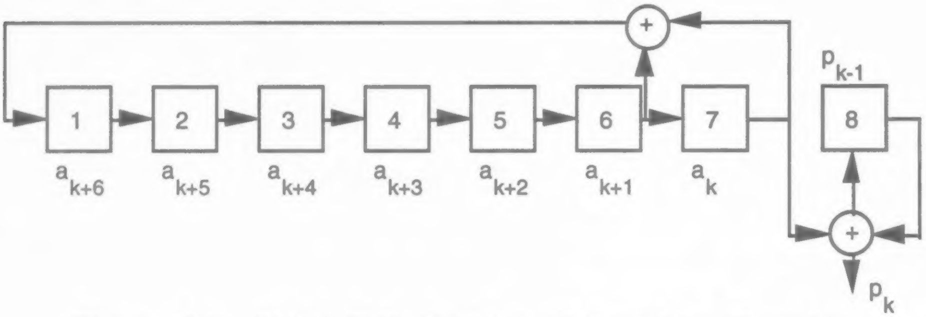

Figure N.1: PRBS Shift Registers Followed by Precoder

Using the symbols presented in Figure N.1, it is clear that bits in the PRBS are related to each other by the following expression:

$$a_{k+7} = a_k \oplus a_{k+1} \qquad \text{(N.1)}$$

where: k = the current sample

$\oplus$ is base-2 addition (identical to Exclusive-OR (XOR))

The precoded value output p_k at time k is:

$$p_k = a_k \oplus p_{k-1} \qquad \text{(N.2)}$$

Starting with sample 1:

$$p_1 = a_1 \oplus p_0 \qquad \text{(N.3)}$$

where: p_0 is the starting value for the precoded sequence

$$p_2 = a_2 \oplus p_1 = a_2 \oplus a_1 \oplus p_0 \qquad \text{(N.4)}$$

$$p_3 = a_3 \oplus p_2 = a_3 \oplus a_2 \oplus a_1 \oplus p_0 \qquad \text{(N.5)}$$

.

.

.

$$p_k = p_0 \oplus \sum_{j=1}^{k} a_j \qquad \text{(N.6)}$$

where: the summation sign indicates base-2 addition

Let p_0 be equal to 1, and a_1 through a_7 be equal to the standard starting values for the 2^7-1 PRBS (a_1 through $a_6 = 0$, $a_7 = 1$). For $k > 7$, the precoded sequence can be arranged in the form:

$$p_k = [a_k \oplus a_{k-1} \oplus \ldots a_8] \oplus a_7 \oplus a_6 \oplus \ldots \oplus a_1 \oplus p_0 \qquad \text{(N.7)}$$

Substituting values for a_7 through to p_0 results in their cancellation from (N.7):

$$p_k = [a_k \oplus a_{k-1} \oplus \ldots a_8] \qquad \text{(N.8)}$$

Substitute the remaining terms using (N.1):

$$p_k = [a_{k-6} \oplus a_{k-7} \oplus a_{k-7} \oplus a_{k-8} \oplus \ldots a_2 \oplus a_1] \qquad \text{(N.9)}$$

All inner addition terms disappear, since $a_j \oplus a_j = 0$. Also, $a_1 = 0$. This leaves:

$$p_k = a_{k-6} \qquad \text{(N.10)}$$

for all $k > 7$.

Since a_k is a sequence that repeats itself after 127 bits, it follows from (N.10) that p_k is also a sequence that repeats itself after 127 bits.

This proves that for all $k > 7$, that $p_k = a_{k-6}$, if the assumed starting value for $p_0 = 1$. If the starting value of $p_0 = 0$, then $p_k = \bar{a}_{k-6}$. In either case, the decoded sequence after the delay and add will be seen by the receiver to be a standard 2^7-1 PRBS since the decoding process is independent of the starting value of the precoded sequence.

Appendix O: Method for Tuning Duobinary Receiver

Optimizing the bit error rate performance of the duobinary receiver was not a trivial task due to the large number of variables which affect is operation. There are two decision thresholds and two timing phases which must be set. These four variables are all inter-dependent, therefore tuning the receiver was a lengthy iterative process.

It was discovered from experience with the duobinary receiver that near-optimal bit error rate performance could often be reached quickly by following the procedure below. Referring to Figure O.1:

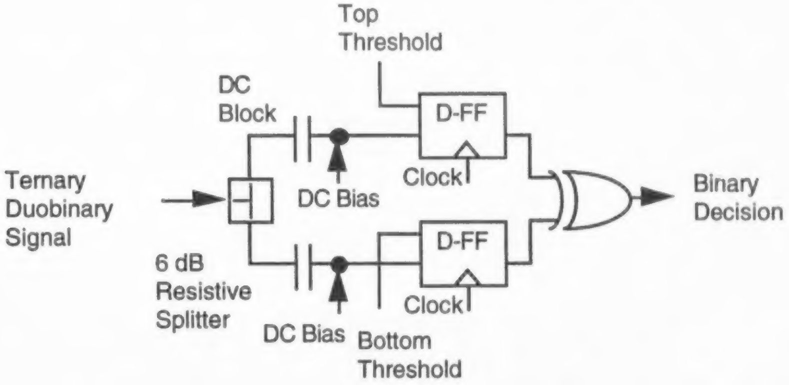
Top
Threshold
DC
Block
D-FF
Clock
Ternary
Duobinary
Signal
DC Bias
Binary
Decision
D-FF
6 dB
Resistive
Splitter
Clock
DC Bias
Bottom
Threshold

Figure O.1: Ternary Decision Circuit

Each D flip-flop has its own DC bias level and decision threshold. This pulls the incoming duobinary eye to within the dynamic range of the flip-flop, and positions either the top or bottom eye within the allowable range of the threshold setting.

1. Set the input power to the receiver at a level where low bit error rate operation is expected.
2. Tie the two D flip-flop DC bias levels together and connect to pull-down voltage for the top eye. Ensure that the input to the D flip-flops is off while doing this step, otherwise the D flip-flops could be exposed to input voltage outside recommended limits.

3. Tie the two D flip-flop decision thresholds together and connect to the top eye threshold setting.
4. Vary the threshold and timing settings, monitoring an eye diagram output of the XOR gate on an oscilloscope. If the output level of the XOR fluctuates, then one or both of the flip-flops are making decision errors. If both D flip-flops are making exactly the same decision at all times, then the Q output of the XOR will be 0 (i.e. 1 XOR 1 = 0, 0 XOR 0 = 0). This means that the thresholds are set at a low bit error rate level and that the timing of the two D flip-flops is close to being synchronized. Stop tuning when this flat line is seen. Double check the threshold level setting to ensure that is in the region where the top eye opening is expected.
5. Repeat steps 2 through 4 for the bottom eye.
6. Power off the input to the D flip-flops. Connect each flip-flop to its own DC bias level and threshold. Power the input back on.

If done properly, this should at least result in the bit error rate test set receiver locking on to the incoming signal. A poorly tuned receiver will result in no bit error rate report.

Significant trial and error effort is required to further tune the receiver to optimal performance. Slight timing and threshold adjustments are required to minimize the bit error rate. Once it appears to be minimized, reduce the input power level and re-tune the receiver. Back up and repeat bit error rate measurements often to increase confidence in the readings.

Appendix P: Polarization Technique for Characterizing an EDFA

Polarization rotators and polarization splitters can be used to measure the gain and ASE characteristics of an EDFA, providing the input signal is highly polarized. Figure P.1 shows the experimental setup that was used to characterize the EDFA preamplifier in the receiver studied at TRLabs (Chapter 5 results).

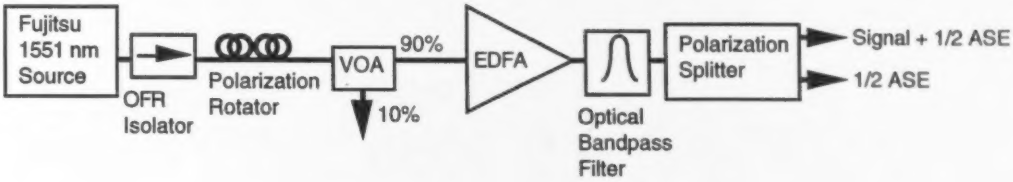

Figure P.1: EDFA Characterization Setup

ASE from the EDFA is not polarized, and therefore will be evenly distributed between the outputs of the polarization splitter. The signal is highly polarized at the output of the isolator and therefore can be set to appear at only one output. The polarization rotator aligns the polarization of the input signal with one of the output axes of the polarization splitter. The input signal was sufficiently polarized and the splitter was high enough quality to achieve a maximum isolation of 30 dB at the splitter outputs. At this setting, half the ASE is coupled to one output of the polarization splitter, and the entire signal plus the other half of the ASE is coupled to the other output.

For a particular input power, the output readings from the polarization splitter provide the EDFA characteristics providing that signal crosstalk into the isolated output is sufficiently below ASE levels. It is simply a matter of doubling the ASE reading at the 1/2 ASE output to get the ASE as a function of input power. The signal output power (and subsequently gain) is measured by subtracting the 1/2 ASE output reading from the Signal + 1/2 ASE output.

Appendix Q: Parallel Precoding Technique

Figure Q.1 shows a four bit wide implementation of a parallel precoder circuit for use with the parallel delay and add circuit described in Appendix M. The combined propagation delays of the D flip-flops and the gates are assumed to be much shorter than the block period T. A parallel array of D flip-flops follows the XOR gate in order to sample the gate's settled output and synchronize the inputs to the next stage.

The design of the feedback path at the output of the precoder represents a very challenging design problem for a high bit rate parallel system. The feedback path at a minimum includes an XOR gate, waveguides to transfer the signal, and taps to split the signal. Amplifiers may also be required to increase the amplitude of the signal after it is split. The feedback path could also include a D flip-flop to synchronize the output. The time to traverse this path must be less than or equal to the block period of the signal. The allowance for this time can be increased by introducing more parallel input streams into the circuit and reducing the block rate.

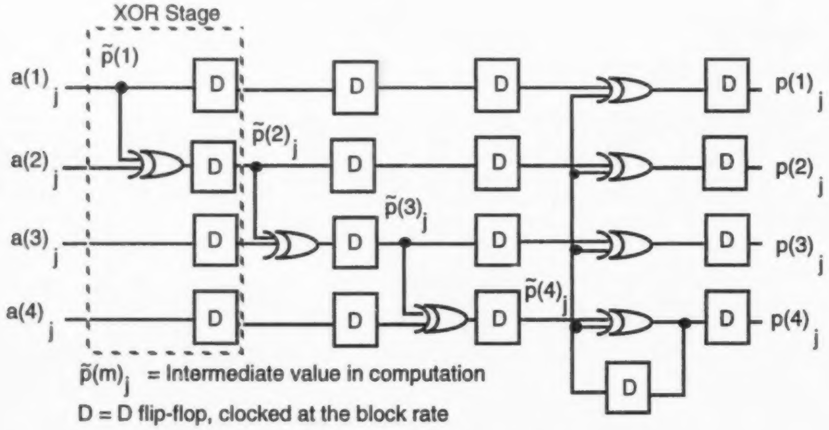

$\tilde{p}(m)_j$ = Intermediate value in computation

D = D flip-flop, clocked at the block rate

Figure Q.1: Parallel Precoder Circuit

An N bit wide parallel precoder circuit has the same basic architecture as the circuit shown in Figure Q.1. Additional XOR computation stages are required to obtain $\tilde{p}(N)_j$, and the feedback path is based on $p(N)_j$. A validation of an N bit wide parallel precoder circuit can be demonstrated in a manner similar to that used to demonstrate the parallel delay and add circuit (Appendix J). Let p_k represent an element in a precoded binary sequence ... p_k p_{k+1} p_{k+2} ... transmitted at a line rate B bits per second. Assume that the bits $p(m)_j$ are multiplexed by bit interleaving.

The precoded bits arrive in parallel at the input of the multiplexer as follows:

$$...[\ p(1)_j\ p(2)_j...p(m)_j...p(N)_j\ ][\ p(1)_{j+1}\ p(2)_{j+1}...p(m)_{j+1}...p(N)_{j+1}\ ]\ ... \qquad (Q.1)$$

where the symbol j is the block index, and the individual bits within the block are denoted p(m). Obviously, the block rate is B / N.

The output from the multiplexer is a sequence:

$$...\ p(1)_j\ \ p(2)_j...p(m)_j...p(N)_j\ \ p(1)_{j+1}\ \ p(2)_{j+1}\ ...p(m)_{j+1}...p(N)_{j+1}\ ... \qquad (Q.2)$$

The index k can be used to denote a symbol number within the multiplexed stream. The block index j and the bit index m within the block are directly related to the index k by summing them together, i.e. $k = (j-1)N+m$ where m and j vary as shown in (Q.1) and (Q.2).

This substitution results in the line rate sequence:

$$\cdots\ p_k\ \ p_{k+1}\ \ p_{k+2}\ \cdots \qquad (Q.3)$$

The outputs of the parallel circuit are processed forms of the raw bits $a(m)_j$ as follows:

$$p(1)_j = a(1)_j \oplus p(N)_{j-1} \qquad (Q.4)$$
$$p(2)_j = [\ a(2)_j \oplus a(1)_j\ ] \oplus p(N)_{j-1} \qquad (Q.5)$$
$$p(3)_j = [\ a(3)_j \oplus [a(2)_j \oplus a(1)_j]\ ] \oplus p(N)_{j-1} \qquad (Q.6)$$

.

.

.

$$p(N)_j = [\sum_{m=1}^{N} a(m)_j] \oplus p(N)_{j-1} \qquad (Q.7)$$

where: $\oplus$ is base-2 addition (identical to Exclusive-OR (XOR))
the summation sign also indicates base-2 addition

Substituting for the k index:

$$p_k = a_k \oplus p_{k-1} \tag{Q.8}$$

$$p_{k+1} = a_{k+1} \oplus a_k \oplus p_{k-1} = a_{k+1} \oplus p_k \tag{Q.9}$$

$$p_{k+2} = a_{k+2} \oplus a_{k+1} \oplus a_k \oplus p_{k-1} = a_{k+2} \oplus p_{k+1} \tag{Q.10}$$

.

.

.

$$p_{k+N-1} = a_{k+N-1} \oplus p_{k+N-2} \tag{Q.11}$$

Or simply, for all k:

$$p_k = a_k \oplus p_{k-1} \tag{Q.12}$$

This is identical to the output from the serial precoder (M.1). Of course, the output from the parallel precoder circuit will not be directly multiplexed, but will be passed on to the parallel delay and add circuit instead. The output of the circuit was shown earlier to be identical to that from a serial delay and add. Therefore, the output from the combination of the parallel precoder and parallel delay and add circuit is identical to the output of a serial precoder followed by a serial delay and add circuit.

With precoding in place, the receiver decision circuit can decode one duobinary symbol at a time. This permits a serial or optical time division demultiplexed ternary decision circuit implementation with minimal complexity.

The above precoding implementation has been presented to demonstrate that parallel precoding is viable. Obviously the parallel precoder circuit is more complex than the parallel delay and add. It would be extremely difficult to implement with discrete components in a laboratory situation because of the large number of gates and delay elements required. This circuit should not present a significant obstacle within a production system, however, since it could be packaged within an Application Specific Integrated Circuit (ASIC) as part of the transmitter electronics.